UNIVERSITY OF CAMBRIDGE

# Recapitulating mammary gland development and breast cancer cell migration in vitro using 3D engineered scaffolds

Robert David Hume

**September 2017**

**Robinson College**

**This dissertation is submitted for the degree of Doctor of Philosophy.**

# Acknowledgements

I would to thank all members of the Watson lab, past and present, which have been there during the completion of my PhD. You have all been there during moments of joy and despair, helping me through the day to day and generally being there as friends.

I would like to specifically thank Jonathan for helping me find my feet with the project, providing additional supervision and being a great presence at many a pub trip; Tim for being a great laugh, rocking to Black Sabbath in tissue culture; Sara for helping extensively with the project being a voice of reason to guide me through; Bethan for always finding the time to hear my problems despite being the busiest person I've ever met; Felicity for her pragmatic approach to science and generally putting up with me as a desk mate; Kate for her massive brain and her helping me understanding histology; Jessie for help with mouse experiments, reading through my thesis and generally being a very cheery member of the lab; Max for his excellent moments of hilarious weirdness; Ala for listening to me every day whether she liked it or not; Livvi for helping with the CUBIC protocol and generally being a microscope aficionado; Henrike for teaching me extensively about the art of fake tanning regardless of whether it fell on deaf ears; Pam for helping with numerous paper edits and being a great inspiration; Mike for his dedication to Friday beers and not wanting to see "the bloody sunset"; and of course Matt for being a massive weirdo who made me laugh throughout (Koffing)!

My supervisor Christine has been instrumental in getting me to this point. She has helped nurture me through this process, pushing me when needed and giving me space to grow as a scientist even when I wasn't aware I was able. Thank you very much for helping me through and giving me this incredible opportunity.

I would also like to thank my funding body, the National Centre for the Refinement, Reduction and Replacement of Animals in Research (NC3Rs), for their student fellowship award. Without this funding opportunity none of the work would have been possible to which I am extremely grateful.

I would like to thank friends and family who have all been there throughout the PhD to listen, or just pretend to listen, to let me get 'science stuff' off my chest. Specifically, I would like to especially thank my Mum and Dad whom without their help over the years I wouldn't be where I am today and for their putting up with me for a few months so that I could write up the PhD.

Last but certainly not least I would like thank Sadé for being the most incredible, supporting, and caring person someone could ask for. Thank you for listening on the phone or in person every step of

the way, no matter how small or insignificant a thing I had to say you were always there to listen and help and I am eternally grateful.

# Abstract

This thesis is focused on recapitulating the *in vivo* processes of mammary gland development and breast cancer progression *in vitro* using engineered collagen scaffolds.

The adult mammary gland is comprised of a bi-layered epithelium of luminal and myoepithelial cells surrounded by an adipocyte-rich fat pad, a highly collagenous extra-cellular matrix (ECM) and a number of other stromal and endothelial cell types. Mammary stem cells (MaSCs) reside within the epithelium and these are capable of repopulating a mammary fat pad that is devoid of epithelium, upon transplantation. It was sought to recapitulate this process of MaSCs repopulating a fat pad using a synthetic fat pad, engineered from a collagen scaffold invested with adipocytes, to provide an *in vitro* 3D model. Fluorescently tagged murine Axin2-expressing cells were obtained from transgenic mice and seeded into these scaffolds and cultured, mimicking the process of fat pad repopulation. Immunohistochemical analysis demonstrated that $Axin2^{+}$ myoepithelial cells were rarely capable of forming bi-layered structures that expressed correct myoepithelial localisation and resemblance to a luminal morphology.

Breast tumours surrounded by anisotropic (directional) collagen fibres running perpendicular to the tumour boundary are more aggressive and associated with poor patient prognosis. To recapitulate this anisotropic collagen phenotype *in vitro*, an ice-templating technique was used to modify the structure of the collagen scaffolds producing both non-directional (isotropic) and anisotropic internal architectures. Tumour cells from various breast cancer cell lines were seeded into both isotropic and anisotropic scaffolds to investigate whether this approach could distinguish cell type-specific migratory ability and whether anisotropy affected migration efficiency. Following analysis by confocal microscopy and ImageJ, anisotropic scaffolds were observed to enhance the migratory potential of MDA-MB-231 breast cancer cells. These results highlight the importance of collagen alignment and provide a reproducible method to quantitatively measure cell migration in 3D for cells derived from different breast cancer subtypes.

Building on these data, the protocol was adapted to permit the direct investigation of tumour biopsy material. Given the heterogeneity of breast tumours, it was considered important to maintain tumour architecture and stromal components. Thus, murine mammary tumour fragments from two different established mammary cancer models were utilised and cultured in anisotropic collagen scaffolds in the presence or absence of adipocytes to allow an investigation of their influence on tumour cell migration. Further experiments included addition of various therapeutic drugs followed by immunofluorescence microscopy coupled with an optical clearing technique. These data

demonstrated the utility of the model in determining both the rate and capacity of tumour cells to migrate through the engineered stroma while shedding light also on the mode of migration. Moreover, the response of different mammary tumour types to chemotherapeutic drugs could be could be readily quantified.

To humanize the fat pad for subsequent human tissue analysis, human mesenchymal stem cells (MSC) were obtained from reduction mammoplasties and immortalised, before differentiating them into adipocytes within anisotropic collagen scaffolds. Human breast cancer cells were fluorescently tagged for tracking using lentiviral methods and were seeded into scaffolds invested with differentiated MSCs. Both cell types were successfully co-cultured for 7 days and imaged using multiphoton methods.

These data demonstrate the utility of novel 3D organotypic *in vitro* models to provide more informative 3D analysis of cancer cells than traditional 2D cell culture models. Future experiments combining human tumour biopsies and chemotherapeutics into the system could provide a screening platform for breast cancer patients. This would provide *in vitro* assays for the delivery of tailor-made personalised medicines and a valuable addition to the oncologist's armamentarium.

# Declaration

This thesis is not substantially the same as any that I have submitted, or, is being concurrently submitted for a degree or diploma or other qualification at the University of Cambridge or any other University or similar institution except as declared in the Preface and specified in the text.

I further state that no substantial part of my thesis has already been submitted, or, is being concurrently submitted for any such degree, diploma or other qualification at the University of Cambridge or any other University or similar institution except as declared in the Preface and specified in the text

This thesis does not exceed the prescribed word limit of 60,000 words excluding bibliography, figures and appendices.

This thesis is the result of my own work and includes nothing which is the outcome of work done in collaboration except as declared below and specified in the text.

As the project was multidisciplinary by design a number of collaborations were essential to its success and are listed below:

**Chapter 3**

Due to the absence of a UK mouse license only schedule 1 procedures were permitted by myself. Hence, mouse technicians in the Gurdon Institute (University of Cambridge) assisted with tamoxifen injections and husbandry protocols for mouse experiments.

**Chapter 4**

Dr. Jonathan Campbell and Dr. Anke Husmann (University of Cambridge, Department of Materials) assisted with experiments in Chapter 4. Contributions are outlined under each figure legend.

**Chapter 5**

Dr. Sara Pensa and Dr. Jessica Hitchcock (University of Cambridge, Departments of Pharmacology and Pathology, respectively) injected TUBO cells into mammary fat pads and harvested established TUBO tumours.

Dr. Peter Kreuzaler (University of Cambridge, Department of Biochemistry) harvested and gifted MMTV-*Wnt1* tumours.

Elizabeth Brown (University of Cambridge, Undergraduate) assisted with therapeutic testing on MMTV-*Wnt1* tumours under my supervision.

**Chapter 6**

Professor Mohammed Bentires-Alj (Friedrich Miescher Institute, Basel, Switzerland) provided human mesenchymal stem cells isolated from reduction mammoplasties.

Dr. Jenny Gomm (Queen Mary University of London (QMUL), Bart's Institute) supplied human tumour biopsies for optical clearing experiments.

# Table of contents

# Table of figures

# List of tables

# Abbreviations

| | |
|---|---|
| AM | Acetoxymethyl |
| AMT | Amoeboid-to-mesenchymal transition |
| BAT | Brown adipose tissue |
| BCA | Bicinchoninic acid assay |
| bFGF | Basic fibroblast growth factor |
| BMP4 | Bone morphogenic protein 4 |
| BSA | Bovine serum albumin |
| CAFs | Cancer-associated fibroblasts |
| CARS | Coherent anti-stokes raman scattering |
| CCL20 | Chemokine (C-C motif) ligand 20 |
| CC3 | Cleaved caspase-3 |
| CSC | Cancer stem cell |
| CUBIC | Cleared unobstructed body imaging cocktails and computational analysis |
| DCIS | Ductal carcinoma *in situ* |
| DMEM | Dulbecco's modified Eagle's medium |
| DMSO | Dimethyl sulfoxide |
| DNA | Deoxyribonucleic acid |
| ECL | Enhanced chemiluminescence |
| EDTA | Ethylenediaminetetraacetic acid |
| EGF | Epidermal growth factor |
| EGFR | Epidermal growth factor receptor |
| EHS | Engelbreth-Holm-Swarm |
| EMT | Epithelial-to-mesenchymal transition |
| ER | Oestrogen receptor |
| ET-SIM | Engineered tumour-stroma interaction model |
| FCS | Foetal calf serum |
| FVB | Friend virus B |
| F-12 | Ham's F-12 nutrient mixture |
| HBSS | Hank's Balanced Salt Solution |
| HEPES | 4-(2-hydroxyethyl)-1-piperazineethanesulfonic acid |
| HER2 | Human epidermal growth factor receptor 2 |

| | |
|---|---|
| hET-SIM | Human engineered tumour-stroma interaction model |
| HF | Hank's Balanced Salt Solution supplemented with 1% foetal calf serum |
| HPV | Human papillomavirus |
| HRP | Horseradish peroxidase |
| iBAT | Beige or induced brown adipose tissue |
| IBMX | 3-isobutyl-1-methylxanthine |
| IDC | Invasive ductal carcinoma |
| IGFBP-2 | Insulin-like growth factor binding protein-2 |
| ILC | Invasive lobular carcinoma |
| iMSC | Immortalised mesenchymal stem cells |
| ITH | Intra-tumour heterogeneity |
| kPa | Kilopascal ($kg \cdot m^{-1} \cdot s^{-2}$) |
| K5, K8, K14, K17, K18 | Cytokeratin-5, -8, -14, -17, -18 |
| lrECM | Laminin rich extra cellular matrices |
| $Lin^-$ | Subset of cells depleted of CD31, CD45 and TER119 cells |
| LM-PCD | Lysosomal-mediated programmed cell death |
| LOX | Lysyl-oxidase |
| MaSC | Mammary stem cell |
| MEFs | Murine embryonic fibroblasts |
| MAT | Mesenchymal-to-amoeboid transition |
| MET | Mesenchymal-to-epithelial transition |
| MGDA | Human mammary gland derived adipocytes |
| MM | Maintenance media |
| MMPs | Matrix metalloproteinases |
| MMTV | Mouse mammary tumour virus |
| MSC | Mesenchymal stem cell |
| Nrg1 | Neuregulin1 |
| NC3Rs | National Centre for the Replacement, Refinement & Reduction of animals in research |
| NSG | Non-obese diabetic-SCID-Gamma |
| PBS | Phosphate buffered saline |
| PBST | Phosphate buffered saline with 0.1% Tween-20 |
| PEI | Polyethylenimine |

| | |
|---|---|
| PFA | Paraformaldehyde |
| PPARγ | Peroxisome proliferation-activated receptor gamma |
| PR | Progesterone receptor |
| pRb | Retinoblastoma protein |
| PRL | Prolactin |
| PRLR | Prolactin receptor |
| Procr | Protein C receptor |
| P/S | Penicillin/streptomycin |
| QMUL | Queen Mary University of London |
| ROCK | Rho-associated protein kinase |
| rpm | Rotations per minute |
| s | Seconds |
| Sdc1 | Syndecan-1 |
| SEM | Scanning electron microscopy |
| SHG | Second harmonic generation |
| TACS | Tumour-associated collagen signature |
| TAM | Tumour-associated macrophage |
| TCP | Tissue culture plastic |
| TERT | Telomerase reverse transcriptase |
| TNBC | Triple negative breast cancer |
| UCP1 | Uncoupling protein-1 |
| V | Volts |
| VEGF | Vascular endothelial growth factor |
| 2D | Two-dimensional |
| 2pf | Two photon fluorescence |
| 3D | Three-dimensional |

# 1 Introduction

# 1.1 The mammary gland

## 1.1.1 Mammary gland development

The mammary gland is a secretory organ that is essential for the feeding of new-born infants through the provision of milk. This nourishment also provides a source of protective factors to boost the infantile immune system during early stages of development post birth. The gland itself comprises a number of different cell types: epithelial cells, that make up a bi-layered ductal network; adipocytes, the main component of the fat pad; endothelial cells, that line the walls of mammary gland vasculature; and a number of other stromal cells, including immune cells and fibroblasts. Mammary epithelium comprises bi-layered structures of basal cells (otherwise known as myoepithelial) and luminal cells (Fig. 1.1). Luminal epithelial cells are located lining the inner layers of alveolar and ductal structures. Surrounding the luminal cells is a layer of thin contractile basal cells, otherwise known as myoepithelial cells, which are responsible for the mechanical expelling of milk from the ducts. Both epithelial subtypes express intermediate filaments known as cytokeratins that form part of their cytoskeletal component. However, in the murine mammary gland, luminal cells exclusively express cytokeratin-8 (K8) and cytokeratin-18 (K18), whilst basal cells express cytokeratin-5 (K5), cytokeratin-14 (K14). Other exclusive luminal markers include epithelial-cadherin (E-cadherin) and membranous β-catenin (Fig. 1.2). Further exclusive basal cell markers include α-smooth muscle actin (αSMA) and the nuclear marker p63 (Glukhova et al., 1995; Reichardt et al., 2001) (Fig. 1.2).

Within the luminal epithelial population there is heterogeneous expression of hormone receptors such as the oestrogen receptor (ER) (Shehata et al., 2012). Additionally, luminal cells are polarised; with an apical cell membrane facing inward toward the lumen in which milk is secreted during lactation and a basolateral surface in contact with basal cells that surround the ducts and alveoli. Both this spatial organisation of the epithelial layers and the communication between the two cell types, is essential for the correct functioning of the gland (Faraldo et al., 2000; Forster et al., 2014).

Development of the mammary gland is complex with extensive remodelling events occurring *in utero*, during puberty and in the adult gland. Formation of placodes on the torso of mice is one of the first indications of embryonic mammary gland development (Hens et al., 2007; Veltmaat et al., 2004). Subsequent invagination of placodes to form mammary buds induces the establishment of a surrounding mammary mesenchyme. Following this, buds sprout and branch into the mesenchyme to form a rudimentary structure that projects into a subdermal fat pad. At this point, growth of the gland in arrested and development does not restart until puberty. During puberty, ducts undergo extensive elongation accompanied with branching morphogenesis to provide secondary ductal

structures that are capped by ‘club-like’ structures known as terminal end buds (Fig. 1.2a). Basal cells aligned in the direction of the duct’s long axis surround the luminal cells in these structures (Lloyd-Lewis et al., 2016) (Fig. 1.2a). Upon pregnancy tertiary branching occurs with the formation of alveoli structures at the ends of branches. Within these structures, differentiated milk-producing luminal alveolar cells are organised in ‘grape-like’ structures surrounded by basal cells with projections in an almost stellate appearance (Fig. 1.2b). During lactation, basal cell contraction enables alveolar cells to eject milk into the ducts to the nipple for suckling by new-born infants. Following weaning, the gland undergoes remodelling via lysosomal-mediated programmed cell death (LM-PCD) of mammary epithelium and subsequent clearing of dead cells by macrophages (Kreuzaler et al., 2011; O’Brien et al., 2012; Sargeant et al., 2014). This post-lactational regression of the gland is known as involution. At this point gland epithelium returns to a pre-pregnant state of primary and secondary ductal branching and an absence of tertiary alveolar structures.

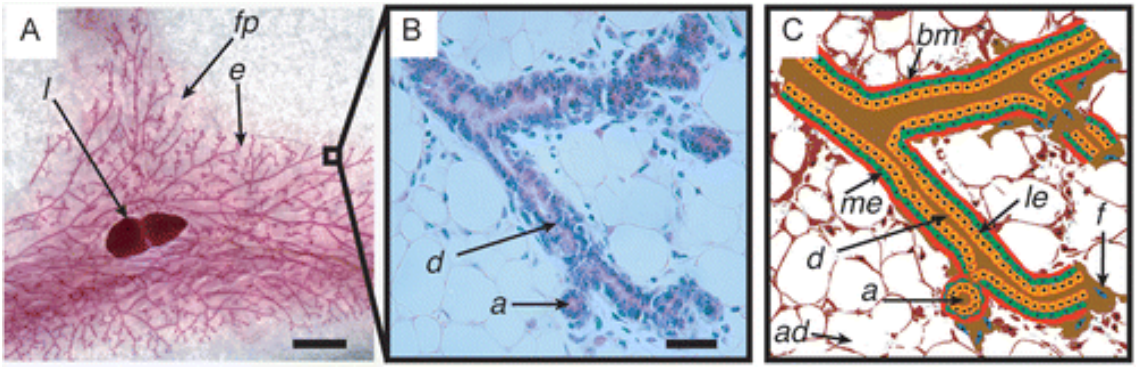


***Figure 1-1: Ultrastructure of the murine mammary gland.***

(**A**) Whole-mount adult murine mammary gland (10 day gestation) stained with carmine showing branched epithelium (*e*) stained pink, a prominent lymph node (*l*) stained dark pink surrounded by an adipocyte-rich fat pad (*fp*) with no staining. Scale bar = 1mm. (**B**) Higher power micrograph of an adult murine mammary gland (10 day gestation), stained with haematoxylin and eosin. Ductal epithelial structures (*d*) and acini epithelial structures (*a*) can be observed within an adipocyte-rich fat pad. Scale bar = 50 µm (**C**) Schematic of the micrograph shown in B, showing a branched epithelium composed of ducts (*d*) and acini (*a*) surrounded by adipocytes (*ad*). Epithelial structures are composed of an inner layer of luminal epithelial cells (*le*) surrounded by myoepithelial cells (*me*) anchored to a basement membrane (*bm*). A number of stromal fibroblasts (*f*) can also be observed surrounding ducts and acini (Campbell et al. 2014).

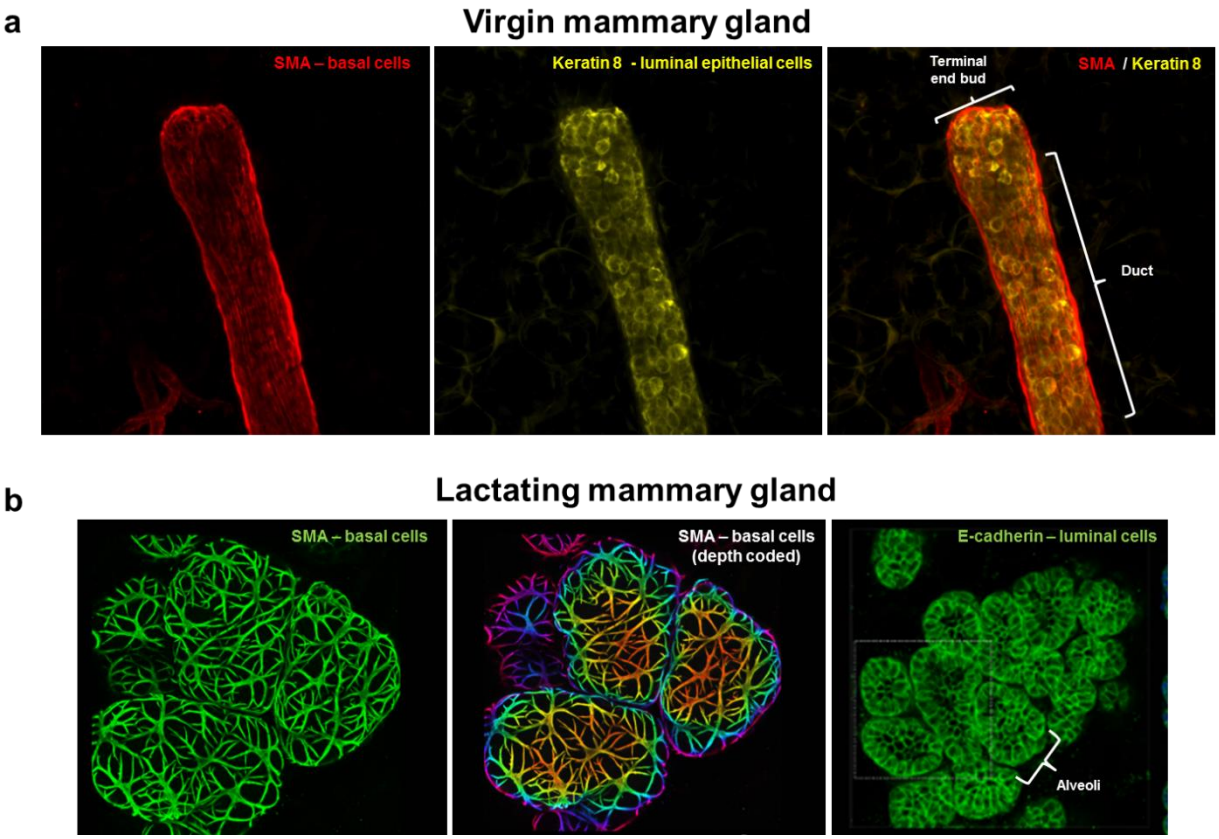


***Figure 1-2: Basal and luminal epithelial markers of the mammary gland***

Virgin murine mammary gland (a) and lactating murine mammary gland (b) were optically cleared using CUBIC and whole mount stained to image the different epithelial lineages of the gland. Smooth muscle actin (SMA) positive basal cells can be seen surrounding Keratin-8/E-cadherin positive luminal cells in (a) ducts and terminal end buds in the virgin mammary gland and (b) alveoli in the lactating mammary gland. Images were provided courtesy of Livvi Harris (Watson laboratory) and adapted with permission (Lloyd-Lewis et al., 2016).

### 1.1.2 Mammary stem cells (MaSC)

The mammary gland is unique in its ability to undergo significant post-natal and post-puberty epithelial proliferation, differentiation and regression. Due to this regenerative potential and also the fact that there are multiple epithelial lineages within the gland, such as basal, luminal and luminal alveolar cells, a multipotent mammary stem cell (MaSC) has long been hypothesised to be implicated in both development and homeostasis of the gland (Daniel et al., 1968; Deome et al., 1959). Historically, this was investigated using the fat pad transplantation assay. This technique required removing the epithelial tree from a developing gland, leaving only stromal cells, injecting epithelial fragments from a donor mouse into the recipient gland and investigating the potential for fragments to repopulate the donor gland's with a replacement epithelial tree. Through combination of this technique and limiting dilution assays, it was shown that a single cell can repopulate an entire gland and regain full functionality (Kordon and Smith, 1998; Shackleton et al., 2006; Stingl et al., 2006). To identify the cellular subset capable of repopulating the gland, fluorescence-activated cell sorting (FACS) protocols were employed. Harvested mammary glands were depleted of $CD31^+$ endothelial and $CD45^+$ / $TER119^+$ haematopoietic cells (the $CD31^-$ $CD45^-$ $TER119^-$ population is termed $Lin^-$ hereafter) using specific cell surface marker antibodies. Following this, epithelial cells were identified using CD24 and CD49f or CD29. Using these markers luminal cells were isolated from the $Lin^-$ $CD24^+$ $CD49f^{low}$ population whilst basal cells were isolated from $Lin^-$ $CD24^+$ $CD49f^{+/high}$ population. Single cells that were able to repopulate an entire gland were identified as $Lin^-$ $CD24^+$ $CD49f^{high}$ and were therefore identified as a subset of the basal cell population. These cells were termed mammary repopulating units (MRUs). These studies also showed that these cells have self-renewal capacity and remain MRUs upon serial fat pad transplantation assays (Shackleton et al., 2006). From these studies it was hypothesised that these MRUs were the source of MaSC and that therefore MaSC were of a basal epithelial origin. More recent studies focussed on further defining the MRUs with cell surface markers, such as protein C receptor (Procr), to identify the characteristics and location of the elusive MaSC (Wang et al., 2014a).

Other studies encouraged the investigation of MaSC using *in vivo* lineage tracing models to reduce the influence of external factors (Davis et al., 2016; Van Keymeulen et al., 2011; Lafkas et al., 2013; Malhotra et al., 2014; Prater et al., 2014; Rios et al., 2014; Scheele et al., 2017; van Amerongen et al., 2012; de Visser et al., 2012; Wuidart et al., 2016). These models enable the tracking of cell progeny *in vivo* to provide valuable information on stem cell biology. In these studies, prospective MaSC were permanently fluorescently tagged at various developmental time points and their progeny traced to reveal their cell fate in a more physiologically relevant setting.

Wnt signalling is required during many different stages of mammary gland development such as embryogenesis, branching morphogenesis and alveolar development during pregnancy (Brisken et al., 2000; Chu et al., 2004; Kim et al., 2009b). With evidence of Wnt signalling involvement in stem cell maintenance of other tissues, one lineage tracing study set out to investigate a subset of Wnt-responsive Axin2$^+$ cells and their contribution to the mammary gland (Batlle et al., 2002; Choi et al., 2013; Pinto et al., 2003). They evidenced that Axin2$^+$ cells contributed variably to both luminal and basal epithelial lineages throughout different stages of mammary development and that Axin2$^+$ cells were capable of repopulating a cleared fat pad (van Amerongen et al., 2012). These data showed that Axin2$^+$ cells are MRUs and are a prospective source of MaSC for further investigation.

In order to determine the progeny of specific epithelial lineages using *in vivo* lineage tracing, one study used transgenic mouse models to fluorescently tag basal or luminal cells by targeting their specific cell markers (Van Keymeulen et al., 2011). Using these methods, this study showed that MaSC in the adult are unipotent lineage restricted cells and that mutipotent MaSC are not present in the adult mammary gland. On the basis of this evidence, they argued that the transplantation assay caused a reprogramming event in transplanted epithelial cells inducing multipotency and that this artefact was not present in the *in vivo* scenario. Another study used a number of lineage tracing models to target specific epithelial lineages as well as a multi-coloured model to fluorescently tag multiple epithelial cells of both lineages and follow their clonal evolution (Rios et al., 2014). During their analyses, they showed conflicting results with earlier studies, and claimed the presence of a multipotent MaSC exists in the adult mammary gland. Recently, one study aimed to solve this controversy by utilising an unbiased approach of fluorescently labelling a single mammary epithelial cell and tracking its progeny (Davis et al., 2016). Findings from this study agreed with earlier literature and evidenced a unipotent MaSC in the adult mammary gland. Despite a plethora of transgenic mouse models the adult MaSC remains a controversial topic, with some arguing for a long lived progenitor that is restricted to either luminal or basal lineages, whilst others claim a bi-potent/multipotent stem cell is present that is able to give rise to both luminal and basal epithelium.

### 1.1.3 Epithelial breast cancers

Breast tumours may arise from a number of different cell sources. Non-epithelial breast tumours include lymphomas, melanomas and sarcomas which relate to lymphatic, melanocyte and connective tissue tumours respectively. Although these tumours are potentially malignant, they account for less than 1% of all cases and this subject area is thus not within the scope of this introduction (reviewed in O'Donnell et al. 2009). Epithelial breast cancers account for the majority of breast cancer diagnoses and vary dramatically in a number of characteristics including phenotype,

prognosis, genetic signature, subtype, invasive potential and treatment. These tumours arise from genetic mutations in epithelial cells that are caused either as a result of environmental factors or due to their genetic inheritance. Consequently, these cells acquire the ability to avoid senescence and apoptosis, continuously proliferate, and also spread to and propagate in other organs of the body.

#### 1.1.3.1 *Classifications of breast cancer*

Commonly, pre-malignant breast cancer is found as a precursor lesion known as a ductal carcinoma *in situ* (DCIS) (Sikandar et al., 2015). DCIS consists of neoplastic cells growing within the ducts of the gland and is classed as a non-invasive subtype. This classification is named so due to its inability to penetrate the basement membrane surrounding the epithelium and spread to other locations in the gland or potentially other organs. DCIS varies in its prognosis ranging from: low risk lesions, that pose little or no threat to the patient throughout their lifetime; to high risk lesions, that may progress with time into a more aggressive tumour known as an invasive ductal carcinoma (IDC) (Virnig et al., 2010). IDCs are the most common invasive breast cancer diagnosed and account for approximately 70-80% of cases (Arps et al., 2013; Balekouzou et al., 2016; Elshof et al., 2016). These lesions invade from within the ducts into the surrounding breast tissue and can potentially metastasize to other sites in the body. An additional breast tumour subset is the invasive lobular carcinoma (ILC) which accounts for approximately 5-15% of cases and differs from IDC in phenotype, morphology, prognosis and treatment (Sastre-Garau et al., 1996). ILC are defined by small, round cells that infiltrate the surrounding stroma in a single file fashion. They are more likely to be ER / progesterone receptor (PR) positive and human epidermal growth factor receptor 2 (HER2) / p53 negative and have an increased incidence in older patients (Arpino et al., 2004).

To further classify breast cancers, studies have analysed the gene expression profiles of breast carcinomas and normal breast tissue samples to define breast cancer subtypes (Perou et al., 2000; Sorlie et al., 2001). In these studies, using hierarchical clustering analysis tumours were grouped into a number of categories: ‘basal-like’ that showed high expression of basal epithelial cell markers K5 and K17; ‘HER2-overexpressing’, that showed high expression of HER2 related genes; and ‘Normal’, that showed the highest expression of non-epithelial cell types such as adipocytes. All of these aforementioned subtypes expressed low to absent levels of ER. Furthermore, two additional categories were also defined: Luminal A, that showed the highest levels of ERα expression, other luminal-enriched genes and has later been defined as having low expression of the proliferation marker Ki67; and Luminal B, that showed low to moderate luminal specific genes and has also been further characterised as exhibiting relatively high Ki67 expression (Inic et al., 2014)

### 1.1.3.2 *Oestrogen receptor (ER) status in breast cancers*

Alternatively, breast cancers can be subdivided based upon their ER, PR and HER2 status. Using this taxonomy, $ER^+$ cancers account for approximately 80% of all breast cancer cases (Lumachi et al., 2015). As these tumours are hormone receptor positive, endocrine therapy, such as a treatment called tamoxifen, is considered for a large proportion of cases. Tamoxifen is the competitive inhibitor of estradiol, the agonist of the ER and is commonly used in the treatment of $ER^+$ breast cancers. This cancer therapeutic reduces the risk of an $ER^+$ tumour becoming invasive in approximately 50% of cases. Consequently, many of these tumours are readily treatable and have a relatively good prognosis compared to other subtypes (Waters et al., 2010).

For post-menopausal women with $ER^+$ breast cancer the first choice of treatment are aromatase inhibitors such as anastrozole, exemestane and letrozole (Breast International Group (BIG) 1-98 Collaborative Group et al., 2005; Gangadhara and Bertelli, 2009; Goss et al., 2011). Aromatase is an enzyme that converts androgen into oestrogen and hence by inhibiting it there are reduced levels of ER stimulation in $ER^+$ breast cancer. As the ovaries are also responsible for generating oestrogen and aromatase inhibitors cannot prevent this, these inhibitors are more effective in treating postmenopausal women whose ovaries have ceased to produce oestrogen.

To study $ER^+$ cancers *in vitro*, groups commonly utilise the $ER^+$ MCF7 human breast cancer cell line. This is because its $ER^+$ status makes it ideal for hormone response studies (Soule et al., 1973). Breast tumours can also be separated on their PR status into $ER^+PR^+$, $ER^+PR^-$, and $ER^-PR^+$ subtypes (Davies et al., 2011). $ER^+PR^+$ tumours are less aggressive and have better prognosis than $ER^+PR^-$ tumours. Interestingly, there is no correlation between how the two different subsets respond to hormonal therapy. Notably, $ER^-PR^+$ tumours are very rare making up 0-4% of cases with some studies claiming that this subtype only exists as a false negative as a result of technical errors (Hefti et al., 2013).

### 1.1.3.3 *HER2-overexpressing breast cancers*

HER2, otherwise known as *neu* or *erbB-2* (the rodent analogue of HER2), is amplified in approximately 15-20% of breast cancer cases and was historically associated with poor prognosis (Slamon et al., 1987). Over amplification of the gene leads to activation of the PI3K pathway and results in up-regulated cellular proliferation and suppression of apoptosis, both classic hallmarks of cancer (Rusnak et al., 2001). Since the discovery of HER2 specific therapies survival rates have significantly improved and it is no longer associated with poor prognosis (Harris et al., 2011). To study HER2 *in vitro* a number of breast cancer cell lines have been utilised. For example, $ER^+$ $PR^{+/-}$ $HER2^+$ cells classified as the "Luminal B" subtype, such as the BT474 human cell line and the $ER^-PR^-$

$HER2^+$ "HER2-enriched" subtype, such as SKBR3 and MDA-MB-453 human cell lines have been used extensively (Neve et al., 2006; Subik et al., 2010).

#### 1.1.3.4 *Triple negative breast cancers (TNBC)*

Breast tumours that lack ER, PR and HER2 receptors are termed triple negative breast cancers (TNBC). This tumour type accounts for approximately 15-20% of all diagnosed invasive breast cancer cases (Kwon et al., 2017). Patients with TNBC have lower relapse free survival, preferential metastasis to the brain and lungs and a poorer overall prognosis (Gogia et al., 2014; Harrell et al., 2012). One cause of such poor survival rates is the lack of potential treatments for TNBC as the three main receptors ER, PR and HER2 usually targeted with therapeutics are not present within the tumour. TNBC can be further subdivided on their molecular signatures into the 'basal-like' and 'claudin-low' subsets (Perou et al., 2000). Basal-like TNBC, as defined in section 1.1.3.1, is characterised by its gene expression of basal epithelial cell markers K5, cytokeratin-17 (K17), integrin-β4 and laminin. For the *in vitro* investigation of basal-like TNBC the MDA-MB-468 and BT20 human breast cancer cell lines have commonly been utilised due to similarities with their gene expression profiles and that of basal-like TNBC (Filmus et al., 1985; Lebeau and Goubin, 1987; Neve et al., 2006). Claudin-low TNBC is typically much rarer and is characterised by a zero to low expression of luminal gene expression markers and epithelial-to-mesenchymal transition (EMT) markers (Perou et al., 2000). EMT is a process defined as the transition of epithelial cells to a similar phenotype to mesenchymal cells, such as the acquisition of long spindle like projections, increased migratory potential, increased expression of markers such as vimentin, N-cadherin, twist and snail and decreased expression of typical epithelial markers such as E-cadherin and cytokeratins (Smith et al., 2014). Interestingly, some cell lines can be induced into an EMT phenotype through chemical or environmental pressures. For example, it has been shown that MDA-MB-468 cells express higher amounts of vimentin and twist upon epidermal growth factor or hypoxia treatment (Davis et al., 2013; Lo et al., 2007). The human breast cancer cell line MDA-MB-231 has been shown to have a similar gene expression profile to the claudin-low TNBC subtype (Neve et al., 2006). It is therefore commonly chosen for *in vitro* experiments modelling the disease. Overall, there are multiple breast cancer subtypes for which a number of human cell lines have been derived for their study *in vitro*.

#### 1.1.3.5 *Intra-tumour heterogeneity (ITH)*

Cancerous epithelial cells residing within the same tumour can have vast differences in their phenotype (Gerlinger et al., 2012; Hernandez et al., 2012; Patani et al., 2011). The resulting intra-tumour heterogeneity (ITH) can have major implications when treating cancers. For example, therapeutics may successfully target and kill one subset of cells whilst other more resistant cells will expand, leading to disease relapse (Ng et al., 2015; Nowell, 1976; Wang et al., 2014b). One source of

ITH is a process known as clonal evolution. This process initiates when cells acquire a threshold number of mutations and become cancerous. As a tumour then progresses some of these cells acquire more mutations that are advantageous to their survival. Consequently, they out-compete one another and thus sub-clones arise resulting in ITH. Notably, cancer cell lines that are often used for *in vitro* studies to increase reproducibility, are relatively homogenous with regards to the phenotype in the cell population and hence often do not address the *in vivo* reality of ITH. Another origin of ITH is cancer stem cells (CSCs). CSCs are defined as tumour initiating cells with stem-cell like properties able to propagate and produce daughter cells that are phenotypically distinct. As it has been shown that claudin-low TNBCs have a similar gene expression to MaSCs, it has been suggested that these tumours may arise as a result of a transforming event in a stem or progenitor (Drobysheva et al., 2015; Lim et al., 2010). Of note, unlike what has been proposed for the differentiation of MaSCs, evidence shows that CSC progression is not necessarily unidirectional or hierarchically organised (Quintana et al., 2010). In xenograft experiments a subset of $Lin^-$ $CD44^+$ $CD24^{-/low}$ human breast cancer cells injected into murine mammary glands have been shown to form tumours with as few as 100 cells (Al-Hajj et al., 2003). These tumorigenic cells have been identified to have stem-cell like properties and believed to be one source of CSCs (Ponti et al., 2005).

#### 1.1.3.6 *Murine tumour models*

To investigate breast cancer *in vivo*, a number of transgenic mouse models have been utilised. For example, HER2-overexpressing tumours have been investigated using a number of models that overexpress different forms of ErbB-2 (rodent HER2) under the mouse mammary tumour virus (MMTV) promoter and result in subsequent mammary tumour formation (Bouchard et al., 1989; Guy et al., 1992, 1996; Muller et al., 1988). The HER2-overexpressing murine mammary cancer cell line named TUBO, was derived from a mammary carcinoma that developed in a MMTV-Her2/*neu* transgenic mouse of a Balb/c strain (Rovero et al. 2000). In one study, TUBO cells were injected into the fat pad of a recipient mouse from a Balb/c background (Koebel et al., 2007). As the recipient mouse was syngeneic to the mouse that the TUBO cells were originally derived, it did not reject the cells through immune surveillance; a process whereby the immune system destroys cells seen to be foreign or a threat. Although the injection did elicit an immune response, TUBO cells were still able to seed and propagate in the gland due to the matching of mouse strains. Subsequent tumour formation occurred in approximately 5 weeks after cells were inoculated allowing the study of Her2-overexpressing mammary cancer *in vivo*. Importantly, as the immune system is implicated in natural tumour progression *in vivo* it is therefore desired to include this feature to accurately model tumorigenesis in mouse models (Chen et al., 2017; Cunningham-Rundles et al., 1981; Levy et al., 1987; Stewart et al., 1995).

Some studies utilise mouse models that are immunocompromised, such as the non-obese diabetic (NOD)-SCID-Gamma (NSG) strain, to overcome the issue of immunosurveillance and therefore permit the injection of human breast cancer cell lines that would otherwise be rejected into the mammary fat pad for human tumour studies (Bondarenko et al., 2015; Puchalapalli et al., 2016; Zhang et al., 2013). NSG is the most immunodeficient mouse strain to date, with depletion of T and B immune cells, low natural killer cell activity and impaired innate immunity. Although these mice ensure high engraftment of a number of different tumour cells, the natural immune response during tumorigenesis is not factored into the model and it therefore disregards an essential aspect of the tumour microenvironment.

The well-established MMTV-*Wnt1* transgenic mouse model has been used extensively to study breast cancer (Cho et al., 2008; Monteiro et al., 2014; Oloumi et al., 2010; Teissedre et al., 2009; Watanabe et al., 2014). The model comprises the overexpression of the *Wnt1* oncogene driven by the murine mammary tumour virus (MMTV) promoter and results in adenocarcinoma in 50% of friend virus B (FVB) mice (Taketo et al., 1991; Tsukamoto et al., 1988). Commonly, these tumours display ductal hyperplasia, mixed basal and luminal characteristics and a reversed bilayer phenotype (Monteiro et al., 2014; Teissedre et al., 2009). They also form ER positive tumours and have been utilised for the study of hormone receptor positive tumours, the most common human breast tumour subtype (Li et al., 2000; Zhang et al., 2005). However, it should be noted that these tumours do not fully recapitulate the $ER^+$ disease as they differ in both morphology and phenotype from the human form. Gene expression profiles MMTV-*Wnt1* tumours show clustering to the aggressive human basal-like tumour subtype (Pfefferle et al., 2013). This model has therefore attracted much attention due to its parallels with human tumour subtypes.

## 1.1.4 The extra-cellular matrix (ECM)

### 1.1.4.1 *The normal mammary gland ECM*

The acellular proportion of tissue within the body is known as the extracellular space. Cells secrete a range of molecules into this space to construct scaffolding structures that give both mechanical support to a tissue and provide an anchorage point on which cells can adhere. Furthermore, these structures provide biophysical cues with which cells interact via cell surface receptors which subsequently can affect cellular phenotype. These 'scaffolds' are known as the extra-cellular matrix (ECM) and are integral to the correct functioning of a tissue. In the mammary gland, the ECM can be separated into two major components: the basement membrane and the interstitial connective tissue. The basement membrane provides an anchorage point for basal cells of the gland and separates the epithelium from the surrounding adipocyte-rich fat pad; the stromal component of the

gland (Dulbecco et al., 1982; Prince et al., 2002; Yurchenco et al., 1986). In contrast, the interstitial connective tissue matrix, otherwise known as stromal ECM, provides a 3D scaffold for the containment of stromal cells which, in the case of the mammary gland, are predominantly adipocytes. The majority of this stromal ECM is comprised of the structural protein, fibrillar collagen I.

Cellular interactions with their surrounding ECM influences cell fate, proliferation, survival and cellular morphology (Benya and Shaffer, 1982; Hadjipanayi et al., 2009; Wang et al., 2000). As the basement membrane surrounds the epithelium, this cell-ECM signalling has important implications on the epithelial component of the gland. Epithelial-basement membrane signalling occurs through a number of receptors and transmembrane proteoglycans such as dystroglycan and syndecan (Hu et al., 2017; Morgan et al., 2007). The basement membrane itself can be further divided into two components: the basal lamina, which is in direct contact with the cell membrane and the external fibrillar reticular lamina (Bowman, 1840). The basal lamina contains heparan sulphate proteoglycans and non-fibrillar polymers of collagen IV and VII (Costell et al., 1999; Ervasti and Campbell, 1991; Murshed et al., 2000; Poschl et al., 2004; Smyth et al., 1999). These collagen polymers provide a scaffold to bind laminins through the glycoprotein, entactin, and to connect the basal lamina to the reticular lamina. Laminins are then able to bind to cell membranes through integrins and dystroglycans. More complexity is added through the inclusion of collagen IV with various proteoglycan species and various isoforms of laminin, allowing the basal lamina to tailor itself to be tissue and function specific. Through this tight control of basal lamina composition, cell signalling can be altered to influence cell fate (Streuli et al., 1991).

#### 1.1.4.2 *Remodelling of the ECM*

Remodelling of the ECM is essential during mammary gland development to allow expansion of the epithelium. Breakdown of ECM proteins during this process is orchestrated by various enzymes, such as collagenase and hyaluronidase, that are involved in the proteolysis of collagen I and hyaluronic acid respectively; two major components of the ECM. One group of enzymes that are known to play a fundamental role in ECM remodelling are matrix metalloproteinases (MMPs). They encompass the proteolysis of a wide range of ECM proteins during various stages of development (Bonnans et al., 2014). For example, during puberty MMP2, MMP3, MMP9 and MMP14 are required for promoting ductal invasion, inhibiting/promoting secondary branching of epithelium and collagen proteolysis (Alcaraz et al., 2011; Mori et al., 2013; Wiseman et al., 2003). The process of remodelling the ECM through the release of MMPs is carried out by stromal cells of the gland such as resident macrophages (Witty et al., 1995). During *de novo* synthesis of the interstitial ECM, collagen-producing stromal cells such as fibroblasts are also required (O'Brien et al., 2010). Contrastingly, *de*

*novo* basement membrane synthesis is orchestrated by epithelial cells in concert with stromal cells to ensure correct positioning and polarisation of the epithelial bi-layer (Jalkanen et al., 1988).

#### 1.1.4.3 *Collagen*

Collagen is the most abundant ECM protein of the breast and is therefore of profound importance when discussing the structure of the gland (Thompson et al., 2017). Fibrillar collagen is observed in the adipocyte-rich interstitial matrix and is formed of three polypeptide α-chains in a triple helix (Francis et al., 1981). During early collagen synthesis, cells produce a soluble precursor chain named procollagen which is secreted into the extra-cellular space for posttranslational modification. Collagen type-specific metalloproteinase enzymes then cleave the propeptide domains at the N and C terminals of the molecule to form mature collagen molecules. At the cell surface initial fibrial polymerisation occurs as collagen molecules begin to self-assemble (Wenstrup et al., 2004). Extracellular lysyl-oxidase (LOX) is then responsible for intermolecular covalent cross-links between microfibrils for formation of the supramolecular collagen structure and collagen fibrils (Pinnell and Martin, 1968; Rucker and Murray, 1978). The resultant structure of fibrillar collagen is able to withstand tensile forces. However, the alignment of a material's fibres is known to affect its tensile strength as well as compressive strength and stiffness (Li et al., 2016; Skedros et al., 2006). If fibres are randomly orientated mechanical properties will be equal in all directions and it is then described as an isotropic structure. Conversely, if fibres are aligned in a one direction material mechanical strength will vary depending on load direction and the structure is termed anisotropic. Collagen anisotropy can influence cellular phenotype and migratory potential (Provenzano et al. 2008; Conklin et al. 2011b; Riching et al. 2014). Furthermore, throughout different stages of development interstitial matrix collagen fibres display localised anisotropy, which suggests that matrix organisation and anisotropy influences epithelial growth (Brownfield et al., 2013; Ingman et al., 2006).

Of critical importance to cellular adherence to the ECM is the integrin family of cell surface receptors. Cells adhere to collagen through these receptors and their interactions can initiate various signalling cascades. In succession this can effect cell phenotype and differentiation status (Jokinen et al., 2004). Integrin signalling can also induce cellular remodelling of collagens by altering the degree of polymerisation and fibril formation within a tissue (Li et al., 2003; Velling et al., 2002). The structure and composition of the ECM is therefore closely controlled not only by the cells that synthesise it but also by the cells that interact and adhere to it.

#### 1.1.4.4 *Collagen density in breast cancer*

ECM composition and structure is tightly regulated in the mammary gland. Incorrect ECM remodelling frequently occurs during tumorigenesis and can lead to a number of implications. For example, increased LOX expression in cancers amplifies collagen cross-linking and causes an increased ECM stiffness (Levental et al., 2009). This increased stiffness during tumour progression amplifies focal adhesions and consequently integrin signalling. The result is an increased deposition of collagen by fibroblasts known as fibrosis and a higher collagen density within the mammary gland (Bonnans et al., 2014). Mammographic density measurements and mouse models indicate that these higher levels of collagen density correlate with an increased risk of breast cancer (Boyd et al. 2011; Erler et al. 2006; Provenzano et al. 2006). Furthermore, ECM stiffening has also been associated with poor patient prognosis. Conversely, inhibition of LOX supresses fibrosis thus decreasing integrin signalling and has been shown to delay tumour onset (Levental et al., 2009). Collectively, these data demonstrate the importance of collagen during breast tumorigenesis.

#### 1.1.4.5 *Anisotropy in stromal ECM of breast tumours*

Previously it has been shown that the ECM surrounding breast tumours can be grouped into 3 different tumour-associated collagen signatures (TACS) (Provenzano et al. 2006). Stromal collagen fibres at the tumour boundary are either orientated into an isotropic TACS-1 structure or two distinct anisotropic structures; TACS-2 and TACS-3. In the anisotropic cases, fibres may either encase the tumour by running parallel to the tumour edge (TACS-2), or run perpendicular to the tumour boundary creating a highway for metastatic cells to migrate into the surrounding tissue (TACS-3). Using a MMTV-*Wnt1* transgenic mouse model that spontaneously forms mammary tumours, Provenzano et al. observed the more aggressive tumours generated from this mouse model displayed a TACS-3 phenotype (Provenzano et al. 2006). A further study investigated the effects of excessive collagen deposition on the TACS phenotype of mammary tumours through use of the Col1a1$^{tmJae}$ mouse model (Provenzano et al. 2008). In this study, this transgenic mouse model harboured mutations in their collagen I protease cleavage site. Consequently, their collagen I was more resistant to degradation and increased collagen deposition and matrix stiffness was observed in a number of organs including the mammary gland. When the Col1a1$^{tmJae}$ mouse was crossed with the murine mammary tumour model MMTV-PyVT (MMTV-PyVT/Col1a1$^{tmJae}$), there was increased collagen deposition around the tumour. Furthermore, increased tumour incidence, invasion, and lung metastasis were observed as well as an increased incidence of the TACS-3 phenotype in these mice, as compared to MMTV-PyVT/Col1a1$^{wildtype}$ mice. Importantly, other studies have also confirmed the presence of the TACS-3 phenotype in human breast tumours and its association with poor patient prognosis (Conklin et al., 2011; Jiang et al., 2016; Kakkad et al., 2016; Yang et al., 2011).

This demonstrates the link between increased collagen deposition and anisotropic collagen fibres enhancing mammary tumour progression.

One culprit of the abnormal ECM deposition seen during tumour progression is the cancer-associated fibroblast (CAFs) (Schor et al., 2003). These are stromal fibroblasts that are located either within or in close proximity to a tumour that are continuously activated. CAFs do not undergo senescence or apoptosis events normally associated with a typical wound healing scenario and aberrantly express a number of proteins involved in ECM signalling such as syndecan-1 (Sdc1) (Desmoulière et al., 1995; Mercier et al., 2008; Yang et al., 2011). Sdc1 expressing CAFs have previously been shown to display a tendency to organise the surrounding ECM into a parallel fibre patterning and increase breast carcinoma cell invasion through increased directional migration (Yang et al., 2011). This suggests Sdc1 expressing CAFs may be responsible for the anisotropic TACS-3 phenotype observed surrounding aggressive breast tumours (Yang et al. 2011; Provenzano et al. 2006). These studies highlight the importance of stromal collagen surrounding breast tumours and the influence of anisotropy on prognosis and metastasis.

#### 1.1.4.6 *Matrix Metalloproteinases (MMPs) in breast cancer*

A crucial component of the aberrant ECM remodelling predominant in breast cancers is the family of MMPs. For example, MMP-1, otherwise known as collagenase 1, is involved in the breakdown of collagen I and its elevated expression is observed clinically in advanced stage breast cancers (Poola et al., 2005). Furthermore, it is a predictive marker for invasive subsets of breast cancers. MMP-3, also known as stromelysin, when upregulated in tumour cells, is another prognostic marker of poor survival in breast cancer (Mehner et al., 2015). MMP-2 and MMP-9 are both found at elevated levels in the circulating plasma of breast cancer patients and are associated with invasion and metastasis – processes responsible for the spread of cancer to other organs (Somiari et al., 2006). These MMPs are type IV collagenases and are therefore able to degrade a portion of the basement membrane as has been previously demonstrated *in vitro* (Mao et al., 2010; Rider et al., 2013). Overall, MMPs play an important role in the regulation of the tumour microenvironment and their dysregulation can lead to tumour progression.

### 1.1.5 Invasion, migration and metastasis of breast cancer cells

Primary breast tumours are rarely responsible for mortality. Predominantly, it is the secondary tumours that have spread to essential organs of the body that are life-threatening and the underlying cause of death (American Cancer Society, 2016). In breast cancer, there is a predilection for secondary tumours to arise in the lymph nodes, bone, brain, lungs and liver (Patanaphan et al., 1988). This process of the spreading and seeding of breast cancer cells preferentially into other

organs was first recognised in Paget's 1889 "seed and soil theory" whereby it was hypothesised that cancer cells (the 'seed') grow and propagate better in certain organs (the 'soil') over others (Paget, 1889). Later, this mechanism by which cancer cells spread and populate other organs was discovered and termed metastasis. In solid tumours, cancer cell spread requires number of processes; invasion through a basement membrane, migration through stromal ECM and stromal tissue to a lymph node or blood vessel, transport through the lymphatic or blood system and eventual seeding and propagation in a target organ. This process of invasion and migration for consequential metastasis is accomplished via a range of different routes. Firstly, cancer cells can degrade their surrounding ECM through MMP expression; in essence carving out their own path of migration (Bremer et al., 2001; Fisher et al., 2009). Secondly, migration can be through following 'leader' cancer or cancer-associated stromal cells along a predefined track or tunnel formed by these leader cells (Fisher et al., 2009; Gaggioli et al., 2007; Patsialou et al., 2013). Thirdly, cells may migrate along a pre-existing structure already present within the tissue such as stromal ECM fibres (Alexander et al., 2008; Weigelin et al., 2012). Lastly, ECM surrounding a breast tumour can undergo remodelling to produce radially aligned anisotropic collagen fibres at the periphery of the tumour (TACS-3). This provides an enhanced migratory phenotype associated with a newly formed ECM structure during tumorigenesis (Provenzano et al. 2006). Notably, these processes are not mutually exclusive and can occur in unison or consecutively (Carey et al., 2015; Wolf et al., 2003).

In order to propel themselves forward during migration, cancer cells must adopt a specific migratory mechanism to permit cell movement. These migratory mechanisms by which cancer cells typically follow is frequently either an adhesive pseudopodal mesenchymal movement or a low-adhesive amoeboidal movement (Gao et al., 2017; Ge et al., 2004; Petrie et al., 2012). Mesenchymal migration of cancerous epithelium requires an EMT so that cells can acquire mesenchymal properties (Saito et al., 2012; Wolf et al., 2003). Following EMT cells display an elongated morphology with projections at the leading edge named pseudopods (from the Greek: "fake feet") that bind to the ECM substrate. Through actin based contraction and the release of the adhesive bonds at the trailing edge, the cell is propelled in a direction of travel. In this mode of migration the adhesion receptors integrin-β1 and integrin-β3 are principally responsible for the traction and interaction with the underlying ECM substrate (Brooks et al., 1996; Palecek et al., 1997; Saito et al., 2012; Wolf et al., 2003).

Amoeboidal migration occurs after a mesenchymal cancer cell acquires amoeboidal properties following a mesenchymal-to-amoeboid transition (MAT) (Gao et al., 2017). Migratory cells of this phenotype often display a rounded morphology with weak ECM interactions and do not rely on ECM

remodelling through protease expression to migrate. Migration occurs either by squeezing through spaces in the ECM, or through deformation of ECM fibres via an enhanced contractility mechanism governed by the Rho/Rho-associated protein kinase (ROCK) pathway (Rosel et al., 2008; Wolf et al., 2003; Wyckoff et al., 2006). During this process the cytoskeleton contracts resulting in tension in cortical actomyosin, causing blebbing and contributing to cellular motility (Keller and Eggli, 1998; Ruprecht et al., 2015). Through use of the broad spectrum MMP inhibitor GM6001 and blocking a range of other proteases, one study has shown that breast cancer cell migration can be protease independent and amoeboidal in mode (Wyckoff et al., 2006). Moreover, another study has shown that MAT can be induced in MDA-MB-231 cells through blocking a number of proteases (Wolf et al., 2003). This suggests that some malignant cells are resistant to protease inhibitor treatments *in vivo* due to their ability to switch migratory mechanism as and when it is required (Liebscher et al., 2017; Shim et al., 2012). Importantly, it should be noted that all of these migratory modes have a degree of plasticity and that both an amoeboid-to-mesenchymal transition (AMT) and a mesenchymal-to-epithelial transition (MET) have also been previously described (Gadea et al., 2008; Pinner and Sahai, 2008; Sanz-Moreno et al., 2008).

## 1.1.6 Adipose tissue

### 1.1.6.1 *Adipocytes of the normal mammary gland*

The murine mammary stroma is predominantly an adipocyte-rich fat pad (Fig. 1.1). Historically, adipocytes were considered solely a structural component of the gland. However, thanks to evidence from previous studies, it is now well appreciated that adipocytes also have a multitude of roles throughout development, such as hormonal signalling (Elias et al., 1973; Marzan et al., 2011; Sakakura et al., 1982). These previous studies have shown that mammary adipocytes are hormone responsive, particularly during postnatal development. Treatment with the hormones oestrogen and relaxin were shown to cause hyperplasia and hypertrophy of adipocytes respectively. Moreover, progesterone-treated glands induced the formation of multilocular adipocytes; adipocytes with numerous lipid droplets found within the cytoplasm of each cell (Bani-Sacchi et al., 1987; Matsumoto et al., 1995). Other studies have further shown that both human and murine adipose tissues are not only hormone responsive, but also able to synthesise hormones (Hugo et al., 2008; Zinger et al., 2003). Prolactin (PRL) is one such hormone produced by adipocytes and, as both mammary epithelium and adipocytes have the prolactin receptor (PRLR), it is not clear whether adipocyte-released PRL has an autocrine or paracrine effect (Ling et al., 2003; Morales et al., 2012). Others report paracrine effects in the mammary gland from a range of other adipocyte derived hormones, such as oestrogen, insulin-like growth factor-I (IGF-I), hepatocyte growth factor (HGF) and

leptin (Grodin et al., 1973; Landskroner-Eiger et al., 2010; Morgan and Forsyth, 1999; Tomimatsu et al., 1997).

Adipose tissue can be stratified into three main subtypes: white adipose tissue (WAT), brown adipose tissue (BAT) and beige/induced brown adipose tissue (iBAT). WAT is unilocular and therefore contains one large lipid droplet within its cytoplasm (Fig. 1B, surrounding epithelial ducts and acini). It is involved in both lipid storage and synthesis of a range of endocrine effectors (Cousin et al., 1992). BAT is characterised as multilocular and is essential for thermogenesis in mammals (Gouon-Evans and Pollard, 2002). It is characterised by numerous mitochondria containing uncoupling protein-1 (UCP1), a protein involved in heat generation (Cypess et al., 2009). Found within WAT, iBAT contains cells that, similar to BAT, have a multilocular lipid content (Cypess et al., 2009; Vitali et al., 2012). Contrastingly, these cells differ in their ability to respond to various stimuli by expressing specific genes, such as *Ucp1*, only under certain environmental pressures. Interestingly, the thoracic murine mammary gland contains BAT whilst the other glands are primarily WAT. However, although different in phenotype to WAT, BAT still supports normal mammary gland development. These studies highlight the importance and varied roles carried out by adipocytes of the mammary gland. Including these cells in the study of the gland is therefore imperative for a fuller understanding of the interactions between epithelium and stroma.

#### 1.1.6.2 *Adipocytes and breast cancer*

It is well documented that adipocytes are implicated in breast cancer progression through paracrine and endocrine signalling. For example, one study shows the influence of human adipocytes on the $ER^+$ MCF7 breast cancer cell line by decreasing both membranous E-cadherin and β-catenin markers of luminal epithelium, upregulating MMP-2 and increasing migratory potential (Wang et al., 2015) . In the aforementioned study, adipocytes were shown to synthesise the cytokine insulin-like growth factor binding protein-2 (IGFBP-2) that was responsible for the increased metastatic ability of MCF-7 cells. However, the paracrine effect of adipocytes and cancer cells is not necessarily unidirectional. Boyden chamber co-cultures have shown that conditioned media from MDA-MB-231 breast cancer cells is able to stimulate the lipolysis of differentiated preadipocyte 3T3-L1 cells (Balaban et al., 2017). This lipolysis then produced a feedback effect on the cancer cells by increasing fatty acid uptake, metabolism and mitochondrial oxidative capacity within MDA-MB-231 cells resulting in higher proliferation and migratory potential.

Notably, one study has shown that adipocytes can reduce certain therapeutic efficacy (Duong et al., 2015). They demonstrated that exposing breast cancer cells to adipocyte conditioned medium reduced specific anti-migratory therapeutic effects, evidencing adipokines can interfere with cancer

treatments. Furthermore, evidence shows adipocytes can increase stem-like marker expression in breast cancer cells when co-cultured *in vitro* (Picon-Ruiz et al., 2016). Importantly, adipocytes do not affect all breast cancers subtypes equally. This was observed in one study through the co-culturing of human mammary gland derived adipocytes (MGDA) and a range of breast cancer cell lines. In this case adipocytes promoted malignancy in some cell lines but had no effect on others (Huang et al., 2017). These data show that adipocytes can induce phenotypic changes in cancer cells within the tumour niche, they can affect therapeutic efficacy and have differential effects on breast cancer subtypes.

#### 1.1.6.3 *Mesenchymal stem cells (MSCs)*

Mesenchymal stem cells (MSCs) are multipotent precursors found in a range of tissues, including adipose tissue of the mammary gland, where MSCs can be isolated following procedures such as reduction mammoplasties (Beltrami et al., 2003; Duss et al., 2014; Trivanović et al., 2013). These cells have the capacity to differentiate into various connective tissues both *in vitro* and *in vivo* (Awad et al., 1999; Desiderio et al., 2013; Pittenger et al., 1999; Takeda and Xu, 2015). Early *in vitro* experiments induced MSC differentiation into chondrocytes, osteoblasts and adipocytes using a range of stimulatory factors (Pittenger et al., 1999). Further *in vivo* experiments also showed differentiation into other tissues such as muscle, tendon and neurons (Awad et al., 1999; Desiderio et al., 2013; Takeda and Xu, 2015). Both the ability to harvest MSCs from a number of locations in the body and the ability to manipulate their downstream phenotype *in vitro* has made them an attractive candidate for regenerative medicine treatments and *in vitro* tissue culture models.

MSCs within the mammary gland are located in WAT and are implicated in adipogenesis (Li et al., 2013). This adipogenic differentiation of MSC is a two-step process. Firstly, MSCs differentiate into adipocyte precursors known as preadipocytes with low levels of peroxisome proliferation-activated receptor gamma (PPARγ). Following this, PPARγ is upregulated allowing differentiation into mature adipocytes (Lee et al., 2014b). *In vitro* differentiation of MSCs to adipocytes requires confluent cells to be treated with an adipogenic cocktail (Pittenger et al., 1999). This relatively simple technique can therefore be utilised as an *in vitro* model of adipose tissue. Similarly, the immortalised murine 3T3-L1 preadipocyte cell line is often used for *in vitro* adipose studies as it also requires comparatively simple adipogenic methods (Zebisch et al., 2012). During *in vitro* adipogenesis of both human MSCs and murine 3T3-L1 cells, collagen IV, entactin and laminin are all synthesized and deposited extra-cellularly, thus evidencing that all the essential structural components of the basal lamina are generated during this process (Aratani and Kitagawa, 1988; Mori et al., 2014; Noro et al., 2013; Sillat et al., 2012). Studies using immunohistochemistry and proteomics have also show that these basal lamina proteins and other ECM proteins are present within human and murine adipose tissue *in vivo*

(Mariman and Wang, 2010; Mori et al., 2014; Vaicik et al., 2014). This demonstrates that the basement membrane deposition during adipogenesis is not just an *in vitro* phenomenon.

# 1.2 In vitro models

## 1.2.1 2-dimensional (2D) *in vitro* models of the mammary gland

### 1.2.1.1 *Primary cell lines*

To investigate mammary gland biology *in vitro*, a number of models have been developed (Campbell et al., 2011, 2014b; Gordon et al., 2000; Montesano et al., 1998; Qu et al., 2015; Romanov et al., 2001). Historically, 2D cell culture on tissue culture plastic (TCP) has been widely utilised for *in vitro* studies due to its high throughput and relative simplicity. This technique requires the use of either primary or immortalised cell lines, both of which have various advantages and limitations. Primary cells are derived from living animal tissue and taken directly into culture. As they have spent little time in *in vitro* culture conditions that are abstract from their natural *in vivo* environment, they have had less time to acquire mutations which may alter them from their original *in vivo* state. They are also naturally heterogeneous populations, especially when comparing across individuals, as the animals they are derived from have genetic differences altering their phenotype. This means that although experimental results are frequently highly variable using primary cell lines, inherent differences between individuals are reasonably well represented and consequently a modestly realistic *in vitro* situation can be observed. However, the main caveat of using primary cells as a model is that they have a finite life time *in vitro* and can only undergo a certain number of passages in culture before they can no longer divide. At this point cells are no longer able to undergo mitosis and enter senescence, a phenomenon known as the Hayflick limit (Hayflick and Moorhead, 1961). In this process, fragments of non-coding deoxyribonucleic acid (DNA) within the telomeres are unable to copy during DNA replication, resulting in their shortening. Once the telomeres are completely depleted the cells are no longer able to divide and the cells enter senescence or undergo apoptosis. As a result, cell culture of a primary cell lines is time-dependent, making it harder to reproduce and compare results across individuals.

### 1.2.1.2 *Immortalised cell lines*

To overcome the Hayflick limit and hence surpass senescence, cells can become immortalised to permit indefinite cell divisions. Immortalisation can occur through a range of genetic mutations that allow cells to avoid apoptosis and continue to proliferate. These mutations may arise spontaneously under *in vitro* culture conditions, 'naturally' within cancerous cells or introduced through viral insertion of specific genes (Gillio-Meina et al., 2000; Runnebaum et al., 1991; Zhu et al., 1991). As a

result, mutations cause the loss of cell cycle checkpoint pathways via inactivation of retinoblastoma protein (pRb), p53 or p16 and cells are subsequently immortalised (Hawley-Nelson et al., 1989; Tsutsui et al., 2002; Zhu et al., 1991). For example, introduction of the human papillomavirus oncogenes E6 and E7, or simian virus 40 into primary cells can lead to inactivation of pRb and p53, resulting in the generation of an immortalised cell line. Alternatively, indefinite cell division can also be obtained through maintenance or extension of the telomeres. Lengthening of the telomeres increases the stability of the chromosomes and therefore induces immortalisation (Morales et al., 1999). This can be achieved through introduction of either the enzyme telomerase or the catalytic subunit of telomerase, telomerase reverse transcriptase (TERT) (Tsai et al., 2010).

Immortalised cell lines hold a number of advantages as an investigate tool. As the use of primary cells limits the time and number of experiments that can be carried out *in vitro*, immortalisation can overcome these hurdles and potentially allow indefinite study. Furthermore, although an immortalised cell line can obtain more spontaneous genetic mutations *in vitro* over time, they are frequently more homogeneous than primary cell lines. This allows multiple experiments across a number of laboratories to be performed and compared. However, if these genetic mutations are significant and undetected, then comparisons across experiments using the same cell line may lead to inconsistent results. Another limitation of immortalised cell lines is that through decreasing heterogeneity important phenotypic differences present in the *in vivo* population may also be excluded.

#### 1.2.1.3 *Mono-cultures versus co-cultures*

Routine *in vitro* cell cultures are commonly carried out as 2D mono-cultures in culture flasks or petri dishes. Mono-cultures are chosen because different cell types proliferate at different rates and thus co-cultures frequently result in one dominant cell type. However, mono-cultures do not address the fact that individual cell types *in vivo* exist alongside multiple other cell types with which they interact. Furthermore, cell cultures in flasks or petri-dishes propagate as monolayers as there is no ECM present to provide a 3D substrate to which to adhere. Likewise, this contrasts with the *in vivo* scenario whereby cells are located in multi-layered structures surrounded by 3D ECM rather than TCP.

As different cell types communicate with one another through paracrine and endocrine signalling and this is not accounted for in mono-cultures, groups have designed methods to investigate signalling events between different cell types *in vitro* (Boyden, 1962; Faber et al., 2012; Hongisto et al., 2012; Prater et al., 2014). One such example is through the use of conditioned media experiments; this requires the culturing of one cell type, collecting its media (conditioned media)

and using this media to culture a target cell type (Faber et al., 2012). Through this method any growth factors and signalling molecules that have been secreted into the extra-cellular space and therefore into the media, will be passed onto the target cell type. Furthermore, the target cell phenotype and the conditioned medium itself can be analysed to provide insight into the signalling molecules released. Alternatively, cells can be separated by a microporous membrane that allows diffusion of molecules between both cell types, allowing two monolayers of cells to grow on separate surfaces but still communicate through the media (Boyden, 1962). This culture apparatus is known as a transwell membrane or Boyden chamber. Although these methods hold significant advantages over mono-cultures, neither the use of conditioned media nor using Boyden chamber assays takes into account communication through cell-to-cell contact from two different cell types and they therefore do not truly replicate this aspect of the *in vivo* reality. Moreover, they do not recapitulate the 3D ECM in which cells reside *in vivo*.

Another co-culture method is the use of irradiated feeder cells. In this protocol one cell type is irradiated to induce senescence and produce cells that enable another cell type to proliferate without competing with it, permitting the co-culture of two different cell types in a 2D mono-layer without selective growth issues (Prater et al. 2014). Despite the irradiated feeder cells becoming growth arrested they still remain viable and provide growth factors for the maintenance and propagation of the other cell type by acting as a 'feeder layer'. Commonly, the cell lines chosen as a feeder layer are the 3T3 murine fibroblast cell line or murine embryonic fibroblasts (MEFs). Using this technique studies have shown that embryonic stem cells are more likely to retain their differentiation capacity, have increased survival and have increased proliferation *in vitro* when in the presence of irradiated MEFs (Hongisto et al., 2012). Another study has demonstrated that mammary basal epithelial cells can be cultured and passaged in the presence of 3T3 feeder cells whilst retaining MRU potential (Prater et al. 2014). This technique is therefore advantageous for the expansion of stem cell populations.

#### 1.2.1.4 *Additional limitations of 2D cell cultures*

Mammary luminal epithelial cells are polarized *in vivo* with an apical membrane orientated towards the lumen and a basolateral membrane in contact with the basal cells of the gland (Li et al., 2009; Liu et al., 2015). This is imperative to the correct functioning of the cell and the secretion of milk into the ducts, as both the location of the internal trafficking machinery and the external cell receptors are influenced by this cellular polarization (Druso et al., 2016). One limitation associated with the 2D cell culture of epithelial cells is potential incorrect polarization. The hormone receptor PRLR is essential for milk production. One study reported that during 2D culture of murine luminal cells the PRLR was basolaterally orientated towards the TCP to which they were adhered (Xu et al., 2009).

This meant PRLR was not exposed for ligation and consequently the cells could not form milk proteins when stimulated. When murine luminal cells were cultured in a 3D laminin rich environment polarity and function was restored, highlighting the importance of 3D culture techniques (Xu et al., 2009).

As cells *in vivo* are not adhered to TCP, studies have investigated the influence of coating TCP with ECM proteins to improve the physiological relevance of 2D cell culture (Prater et al. 2014; Wang & Rosenberg 1999; Hannink et al. 2013). For example, coating TCP with collagen I promotes the survival, adhesion and proliferation of mesenchymal stem cells (Somaiah et al., 2015). Although this can improve 2D culture techniques, cells often still do not conform to the correct phenotype, signalling or morphology as seen *in vivo*. In an effort to control cellular morphology, the 2D substrata can be engineered to introduce surface micro-patterning (Kim et al., 2014). This process alters the surface topography on which the cells adhere. As surface modifications can influence cellular alignment, migration and phenotype, engineering this component may provide more insight into mammary gland development and more accurately represent the true *in vivo* environment (Frohlich et al., 2012).

Cell signalling in 2D culture does not necessarily reflect the *in vivo* reality. For example, Fak, a protein involved in integrin signalling, is required for the proliferation of mammary epithelial cells in 2D cultures but not within *in vivo* mammary tissue (Wang et al., 2011). Moreover, cell motility, morphology and adhesions within a 2D environment often bear little similitude to the 3D scenario (Grinnell et al., 2003; Meshel et al., 2005). This phenotype has previously been observed in fibroblasts that displayed significantly different morphologies and migratory mechanisms on 2D collagen coated surfaces compared to 3D collagen matrices. Moreover, embryonic stem cells differentiated into hepatocytes form more physiologically relevant morphologies and gene expression profiles when cultured in 3D collagen scaffolds compared to 2D collagen coated surfaces (Baharvand et al., 2006). Differentiation status can also be incorrectly altered through 2D culture. This was previously shown by a study with chondrocytes in 2D culture synthesising ECM proteins analogous to their dedifferentiated state and upon 3D culture in agarose, returning to their original differentiated phenotype (Benya and Shaffer, 1982). Furthermore, 2D culture can contribute to a flattened cell morphology that is not observed *in vivo* (Soares et al., 2012). It has also been shown that altered cell morphology has implications on growth, nutrient uptake and gene expression (Bissell et al., 1977; Folkman and Moscona, 1978). From these data it is shown that 2D culture systems exhibit distinct limitations to which 3D culture systems may alleviate.

### 1.2.2 2-dimensional *in vitro* models of cell migration

Breast cancer cells become lethal when they are able to metastasize to essential organs of the body. To do this they must first have the ability to migrate in, along or around obstacles within a tissue. In order to facilitate the study of cell migration a number of *in vitro* culture models have been developed, all of which have defined utility (de Both et al., 1999; Boyden, 1962; Chaudhuri et al., 2014; Poujade et al., 2007; Ray et al., 2017a; Todaro et al., 1965; Wang et al., 2015). One such model is the scratch assay (Liang et al., 2007). This involves scratching a line through a monolayer of cultured cells using a pipette tip or other apparatus and monitoring the time required for cells to migrate or proliferate across the gap. Although this is an inexpensive and simple technique to perform it holds a number of caveats. Repeatability is a key concern, as providing the same sized scratch between experiments can be difficult to control. Furthermore, scratching removes cells from the gap and leaves cell debris and damaged cells at the scratch edge. This can elicit damage response pathways, rupturing of cell membranes and the emptying of cellular contents. It therefore specifically resembles a healing wound and may not translate to other migratory processes. To alleviate these issues a 'gap closure assay' was developed which entails the seeding of cells around a reproducible virgin surface for the cells to traverse (Poujade et al., 2007). However, the overlying limitation with this and other 2D migration studies is that it only encompasses the movement of cells in the X and Y axes directions. Boyden chamber/transwell assays have been utilised to overcome this issue. Migratory cells are seeded on one side of the chamber and migration to the other side of a porous membrane is analysed. Additionally, the Boyden chamber membrane can be coated in ECM gels, including the basement membrane rich Matrigel, to more closely mimic *in vivo* migration/invasion through ECM proteins (de Both et al., 1999; Boyden, 1962).

### 1.2.3 3-dimensional (3D) *in vitro* models of the mammary gland

To better mimic the native environment of the mammary gland a number of 3D models have been developed. Cells are cultured in a 3D ECM gels or scaffolds generated from synthetic or naturally occurring materials. Synthetic materials must be biocompatible and therefore non-toxic to the cells intended to be cultured. Furthermore, they must also be bioinert and not affect cellular phenotype or be bioactive and hence encourage cellular growth. For 3D *in vitro* models, studies often opt for the use of naturally occurring ECM polymers so that they can recapitulate the *in vivo* ECM and cellular phenotype more appropriately. Many current 3D epithelial culture models commonly use the laminin-rich basement membrane substitute Matrigel (Boj et al., 2015; Drost et al., 2016; Kleinman and Martin, 2005; Kleinman et al., 1982). As most epithelia are in contact with a basement membrane, Matrigel provides a physiologically relevant environment for the propagation of many epithelial cell types *in vitro*. Therefore, Matrigel is intended to provide the correct structural cues for

the propagation of complex epithelial structures in a more organotypic manner (Kleinman et al., 1982). However, Matrigel has a number of caveats as an ECM substrate. As Matrigel is generated from the Engelbreth-Holm-Swarm (EHS) mouse sarcoma cell line, exact synthesis machinery cannot be completely controlled and therefore it has substantial batch-to-batch variation and a complex protein content (Hughes et al., 2010). To overcome this issue a growth factor reduced variation of Matrigel has been manufactured. However, this can still contain over 400 unique protein identifications with only 50% matching protein content across different suppliers (Hughes et al., 2010). This uncertainty associated with its exact composition can cause experimental variation with undesired and unquantifiable consequences and a reduced rate of reproducibility. Matrigel also poses as a conflicting model when attempting to model the normal mammary gland ECM due to its tumour origin.

Collagen I is often used in 3D culture models due to its relatively high abundance in the majority of tissues. It can be easily isolated and processed from a number of species and, because it is a major component of the mammary gland ECM, it is highly relevant in the context of 3D *in vitro* cell culture (Hashim et al., 2014; Nagai et al., 2000; Senaratne et al., 2006). Furthermore, because it can be extracted from the tissue of animals due for slaughter, such as from bovine Achilles tendon or rat tails, it is relatively cheap in comparison to more complex ECM substitutes such as Matrigel (Lam and Longaker, 2012). Moreover, the exact protein content can be more tightly controlled compared to Matrigel as it does not rely on the EHS cell line to produce the protein. After extraction collagen I can be processed into a viscoelastic hydrogel or a scaffold. Processing occurs through the self-assembly of collagen monomers and is affected by pH, temperature, ionic strength and the addition of chemical or enzymatic cross-linkers (Zhu and Kaufman, 2014). Some studies have utilized a freeze drying protocol that uses an ice templating technique to form collagen scaffolds (Davidenko et al. 2010; Davidenko et al. 2012; Campbell et al. 2011). In these studies, collagen was dissolved and homogenised before freezing and sublimation; the process by which a material transitions from a solid to a gaseous state, or in this case ice to steam. The ice provided a template which when sublimed created a porous collagen internal architecture that was then retained via chemical cross linking. In one study the ECM protein hyaluronic acid was also added to the process and 3T3-L1 cells were cultured and differentiated in 3D to create a ‘synthetic fat pad’ to mimic the mammary gland stroma (Davidenko et al. 2010). In this study, to model the epithelial component of the mammary gland an immortalised murine cell line named KIM-2 was added to the cultures. KIM-2 cells are capable of generating both luminal and basal epithelial layers making them morphologically relevant for investigating mammary gland biology (Gordon et al., 2000). When in the 3D cultures, KIM-2 cells formed correctly polarised acini and ductal structures and were able to undergo lactogenesis to

produce milk proteins (Campbell et al. 2011). This system was then further developed as a model of involution; a developmental process involving post-lactational remodelling of the mammary epithelium to a structure similar to the pre-pregnant state. In this study macrophages were also added to the model as another stromal component that is implicated in the process of involution (Campbell et al. 2014). These data evidence the potential for collagen scaffolds to recapitulate complex 3D epithelial structures within stromal ECM and adipose tissue in a physiologically relevant setting to study the mammary gland *in vitro*.

To improve translatability of 3D models of the mammary gland a number of human *in vitro* models have been generated. One such model uses the human mammary epithelial cell line MCF10A seeded in Matrigel (Debnath et al., 2003). In this study cells form single layered acini structures with polarized golgi structures similar to luminal acini morphology. However, the use of MCF10A cells as a model of breast epithelium comes with limitations. For example, they lack an epithelial bilayer comprising both basal cell and luminal cells typical of breast epithelium. Furthermore, despite being intended as a luminal epithelial model the cells are positive for a number of basal cell markers (Qu et al., 2015). In this way they are luminal in both morphology and in the polarization of internal structures but not necessarily with regards to markers and gene expression.

Another model of the human breast aimed to further improve the aforementioned MCF10A model by using primary breast epithelial cell clusters in a tailored ECM hydrogel (Sokol et al., 2016). In this study, the aforementioned hydrogel contained fibronectin, laminin and hyaluronic acid loaded with growth factors. This was then seeded as cell clusters into the hydrogel and surrounded by a collagen I gel. The resulting composite was then detached from the surface to form a floating gel. Structures formed by the cell clusters were bi-layered complex branching epithelium that bared similar morphology to that of human tissue. Additionally, they also demonstrated significant organoid formation and alveolar formation upon PRL stimulation compared to both a pure collagen I gel and Matrigel cultures.

One model of the human breast incorporated a tri-culture of immortalised myoepithelial and fibroblast cells obtained from a reduction mammoplasty and the luminal cell line HB2, all seeded within a collagen I gel (Nash et al., 2015). After 3 weeks culture, and only when in tri-culture, these cells formed correctly polarised bi-layered epithelial structures with hollow lumen and loosely distributed fibroblasts throughout the gel. They also formed a layer of basement membrane surrounding the myoepithelial cells in a manner that was comparable to human breast tissue *in vivo*.

Carter et al. employed techniques to develop the aforementioned model of the human breast previously described by Nash and colleagues, using dissociated primary cells (Carter et al., 2017; Nash et al., 2015). Human myoepithelial and luminal breast epithelial cells from reduction mammoplasties were FACS sorted based on their cell surface markers CD10 and EpCAM respectively. These were taken into culture where they could proliferate and were fluorescently tagged. Through recombination of the two cell types in a 1:1 ratio and culture in a collagen gel, complex ductal and spheroid structures were formed after 21 days. Immunostaining of a number of basal/luminal cell markers and comparison with human breast sections showed the correct positioning of each cell type as an epithelial bilayer. Interestingly, the correct polarisation was only achieved in collagen I and not Matrigel cultures whereby only spheroid structures were formed. As basal cells are attached to basement membrane, one might assume that an ECM containing high amounts of these proteins, such as Matrigel, may be most appropriate, however this was not achieved in this case. This may suggest that Matrigel bears little resemblance to the *in vivo* basement membrane surrounding epithelium within the human breast.

Collectively, these studies have highlighted the importance of the choice of ECM for 3D cultures and its influence on cell phenotype. Although more complex and requiring more skill than 2D cultures, these 3D culture techniques have shown a dramatic improvement with respect to enhanced mimicking of *in vivo* cell morphology, phenotype and particularly epithelial polarisation.

## 1.2.4 3-dimensional *in vitro* models of cancer and migration

### 1.2.4.1 *Matrigel*

3D cultures of cancerous epithelial cells demonstrate a higher degree of similarities in morphology, signalling pathways, gene expression and phenotype to the *in vivo* reality when compared with 2D culture methods (Baharvand et al., 2006; Benya and Shaffer, 1982; Weaver et al., 1997; Zietarska et al., 2007). Many studies have utilised Matrigel for such 3D cancer cultures (Boj et al., 2015; Debnath et al., 2003; Drost et al., 2015, 2016; Lee et al., 2007). Although Matrigel has proven incredibly important for the advancement of 3D cell culture systems, it comes with a number of caveats as outlined in section 1.2.3. Of note, Matrigel is considered a basement membrane ECM and whilst initial tumour invasion begins through a basement membrane, it is followed by migration through a collagen-rich interstitial matrix ECM (Kaushik et al., 2016). Therefore this latter form of cancer cell migration is not truly represented in Matrigel cultures. To address this point, Matrigel has often been substituted with collagen gels.

### 1.2.4.2 *Collagen*

Using collagen gels for the 3D culture of cancer cells comes with advantages and limitations. For example, a limitation of collagen gels is that increased contraction with increased cell seeding numbers correlates with effects on overall elasticity and ultimate stress (Chieh et al., 2010). This makes the morphology and interior structure of the gel difficult to control and predict. However, an advantage to collagen gels is that by adjusting their collagen concentration their overall stiffness can be controlled. As there is an association between increased collagen density and breast cancer this factor can be manipulated for its study *in vitro* (Paszek et al., 2005).

### 1.2.4.3 *Anisotropy*

Previously it has been shown that cells can exhibit an enhanced migratory potential on anisotropic collagen fibres *in vivo* (Provenzano et al., 2006). Multiple studies have investigated this phenomenon using various 3D *in vitro* models (Riching et al. 2014; Provenzano et al. 2008; Ray et al. 2017; Thomopoulos et al. 2005; Thomopoulos et al. 2007; Dickinson et al. 1994; Ray et al. 2017). By employing different protocols to align collagen gels these studies provided anisotropic collagen *in vitro*. One technique involved seeding fibroblasts to remodel collagen gels along the axis of the cell body (Ray et al. 2017; Thomopoulos et al. 2005). Although this may have relevance to the *in vivo* setting, fibroblast remodelling is difficult to control and requires an extra step of decellularisation. Therefore these factors reduce reproducibility and are somewhat time consuming. Others used magnets to pre-align gels along the axis of a magnetic field (Provenzano et al. 2008; Riching et al. 2014). However, as with all collagen gels, this system was subject to contraction issues. Nonetheless,

these systems have allowed the study of anisotropic collagen *in vitro* and provided insight into how this effects cell migration.

## 1.3 3-dimensional imaging techniques

### 1.3.1 Confocal microscopy

To image tissues in 3D there are a number of techniques available. One such technique is confocal fluorescence microscopy which obtains z-sectioning capabilities using a single photon laser and the inclusion of a spatial pinhole to remove out of focus light (Minsky, 1988). Fluorophores within a sample are excited by photons at the wavelength of the incoming laser light. This is followed by vibrational relaxation in the system and emission of a photon at a longer wavelength. Although confocal microscopy sufficient for imaging thin samples (approximately 100 µm), imaging depths are limited due to the scattering of photons in thicker samples.

### 1.3.2 Two-photon fluorescence (2pf) microscopy

To increase imaging depths a number of multi-photon techniques have been developed. Two-photon fluorescence (2pf) microscopy relies on the two-photon excitation of a fluorophore in a single event (Denk et al., 1990). The two photons contain half the energy required for excitation to occur and are therefore approximately double the wavelength. Consequently, following vibrational relaxation in the system as a by-product of fluorescence, the emitted photons are not at a longer wavelength than the incoming two excitation photons. As the event is highly unlikely to occur anywhere else other than the illuminated plane of interest, a pinhole to remove out of focus light is not required. Therefore more light can be captured and deeper imaging can be carried out. Additionally, longer wavelengths are less toxic to tissues and produce less scattering than shorter wavelengths also allowing deeper imaging.

### 1.3.3 Second harmonic generation (SHG) microscopy

Another multiphoton microscopy technique is second harmonic generation (SHG) (Heinz et al., 1982). This is a nonlinear optical technique that enables the imaging of non-centrosymmetric structures such as collagen I. As with 2pf, SHG requires two-photon excitation of a structure but because there is not vibrational relaxation in the system the emitted photon is exactly half the wavelength of the two excitation photons. This provides direct imaging of collagen without the requirement of a fluorophore. Moreover, because SHG allows imaging of unlabelled, unaltered collagen there are no effects on collagen structure. Furthermore, without the requirement for fluorescent dyes there are no issues with photobleaching of samples (Theodossiou et al., 2006).

### 1.3.4 Coherent anti-Stokes Raman scattering (CARS) microscopy

Like SHG, Coherent anti-Stokes Raman scattering (CARS) microscopy enables dye-free imaging of structures and allows samples to remain unaffected (Begley et al., 1974; Jungst et al., 2011; Li et al., 2011; Zumbusch et al., 1999). It is also a nonlinear technique and allows imaging of structures according to their vibrational contrast. For CARS to occur two lasers at different frequencies are required; a pump beam with frequency $\omega_p$ and a Stokes beam with frequency $\omega_s$. The vibrational contrast from the CARS signal is only detectable when the difference in frequency ($\omega_p$- $\omega_s$=$\Delta\omega$) is equivalent to molecular vibrational frequency of a particular chemical bond. CARS microscopy can be used to image lipids and can be combined with SHG and 2pf to image multiple structures simultaneously.

### 1.3.5 Cleared unobstructed body imaging cocktails and computational analysis (CUBIC)

Deeper imaging can also be achieved through optical clearing techniques. Through reduction of the opacity of a tissue, clearing permits deeper laser penetration for confocal or multi-photon laser microscopy. Cleared unobstructed body imaging cocktails and computational analysis (CUBIC) is one such clearing protocol that relies on matching refractive indices to increase tissue transparency (Lloyd-Lewis et al., 2016; Susaki et al., 2014, 2015). It also allows immunostaining *in situ* to fluorescently tag and image proteins using specific antibodies. Furthermore, it has reduced quenching of fluorescent proteins compared to other clearing techniques allowing 3D localisation of fluorescently tagged proteins. As it is a relatively simple technique it is useful for an increased depth of imaging of 3D structures.

## 1.4 Aims and objectives of the study

### 1.4.1 National Centre for the Replacement, Refinement & Reduction of animals in research (NC3Rs)

According to the National Centre for the Replacement, Refinement and Reduction of animals in research (NC3Rs) review it is estimated that >100 million rodents per year are culled worldwide for experimentation (Burden et al., 2015). With a paradigm shift in opinions on animal testing alongside obvious financial incentives, scientists are being encouraged to minimise *in vivo* animal experimentation. Furthermore, there is a push to use 3D cell cultures as *in vitro* models as they more accurately resemble the *in vivo* environment in comparison with their 2D counterparts (Baharvand et al., 2006; Benya and Shaffer, 1982; Bissell et al., 1977; Campbell et al., 2011; Folkman and Moscona, 1978; Kleinman et al., 1982; Soares et al., 2012; Weaver et al., 1997; Zietarska et al.,

2007). This improvement in mimicking the *in vivo* environment through 3D culture systems inherently improves *in vitro* data validity, which in turn is informative for the choice of further *in vivo* experiments and consequently reduces unnecessary animal testing. Using this ideology it was sought to model mammary gland development and breast cancer cell migration using 3D *in vitro* systems to reduce animal numbers culled in these areas of research.

### 1.4.2 Recapitulating the mammary gland *in vitro*

This project aimed to develop a bi-layered murine mammary model of both basal and luminal epithelial cells derived from a basal epithelial cell subset in a relevant *in vitro* setting. This intended to recapitulate MaSCs potential and the fat pad transplantation assay *ex vivo*. Additionally, this model aimed to provide researchers with a more malleable system than an *in vivo* mouse model and a more relevant system than 2D cell cultures. Furthermore, it aimed to reduce the number of mice required experimentally and therefore the burden on animal testing for mammary gland research. To achieve this goal, a previously established synthetic fat pad protocol was utilised for culturing adipocytes in a 3D collagen I scaffold. This intended to mimic the adipocyte-rich fat pad of the mammary gland and the highly collagenous ECM in which it resides. Subsequently, it was sought to harvest and FACS fluorescently tagged prospective MaSCs from the mammary glands of transgenic mice. After seeding and culturing MaSCs within synthetic fat pads, immunostaining methods would be utilised to conclude whether MaSCs could produce relevant bi-layered epithelium and 3D structures.

### 1.4.3 Recapitulating breast cancer cell migration *in vitro*

This project also aimed to recapitulate the anisotropic collagenous tumour stroma and TACS-3 phenotype frequently found surrounding breast tumours associated with poor prognosis and investigate how this anisotropy effects cancer cell migration. Through modifying a previously established ice-templating technique, this project aimed to synthesise collagen scaffolds with an anisotropic internal structure to mimic the anisotropic ECM (Davidenko et al. 2010). Following this, it was sought to investigate the effects of anisotropy on three breast cancer cell lines and their migratory potential using immunohistochemical and ImageJ analysis techniques.

### 1.4.4 Mammary tumour cell migration analysis and therapeutic testing

Subsequent experiments intended to culture mammary tumour fragments from two different mouse models with or without murine adipocytes in anisotropic collagen scaffolds in the presence of a number of inhibitors. This would elucidate whether adipocytes influence migration in an organotypic environment and ascertain if the system is a valid therapeutic testing tool. Through culture of tumour fragments it also aimed to model the ITH that is not present in breast cancer cell lines. Using

complex culture techniques, IHC, optical clearing in conjunction with whole mount IHC and 2pf/SHG microscopy, and ImageJ analysis, it was sought to analyse tumour cell migration in the model.

### 1.4.5 Humanising the synthetic fat pad

Lastly, it was intended to humanise the synthetic fat pad and investigate whether human breast cancer cells could be co-cultured within them. This would be achieved through immortalising human MSCs, seeding them in anisotropic scaffolds, differentiating into adipocytes and analysing their lipid content using immunostaining and 2pf, SHG and CARS microscopy techniques. Following this, MDA-MB-231 cells would be fluorescently tagged and seeded into the human adipocyte invested scaffolds and their migration imaged using 2fp and SHG. Through future inclusion of human biopsy material this model intends to provide a therapeutic testing tool for personalised medicine strategies to benefit both patients and oncologists alike.

# 2 Experimental methods

# 2.1 Animals

All experimental animal work was performed in accordance to the Animals (Scientific Procedures) Act 1986, UK and local ethical committee approval.

## 2.1.1 Animal models

K14-cre$^{ERT2}$/ROSA26-tdTomato transgenic mice were developed in the Watson laboratory and were genotyped by Dr. Sara Pensa (University of Cambridge, Department of Pharmacology) before commencing the project. Axin2-cre$^{ERT2}$/ROSA26-tdTomato transgenic mice were gifted by Dr. Emma Rawlins (University of Cambridge, Gurdon Institute). Mouse ear biopsies from Axin2-cre$^{ERT2}$/ROSA26-tdTomato transgenic mice were obtained by animal technicians at the Gurdon Institute, University of Cambridge.

Both models contain the Cre recombinase enzyme expressed downstream of either a Cytokeratin-14 (K14) or Axin2 promoter in cells expressing K14 or Axin2 respectively. Upon tamoxifen administration, Cre is activated in target cells resulting in the removal of the floxed STOP cassette. The STOP cassette is located flanking tdTomato coding sequences on the Rosa26 locus and its removal permits subsequent constituent expression of the fluorescent protein tdTomato in target cells.

## 2.1.2 Genotyping

### 2.1.2.1 *DNA extraction*

100 µL of chelex solution (0.1 g/mL chelex resin (biorad #142-1253), 0.001% tween-20 (Sigma P1379), 100 µg/mL proteinase K (Roche #3115836001), 9.9 mL dd$H_2O$) was added to each ear biopsy and incubated at 50°C for 45 mins. Samples were then incubated at 95°C for 30 mins to inactivate Proteinase K, followed by vortexing for 5 seconds. The biopsy and chelex were then pelleted by centrifugation at 2000 rpm for 2 mins. 1 µL of the supernatant was used for each PCR reaction.

### 2.1.2.2 *PCR reactions*

See Tables 2.1, 2.2 and 2.3.

| Primer | Sequence |
|---|---|
| Cre Forward | 5'-TGCTGTTTCACTGGTTATGCGG-3' |
| Cre Reverse | 5'-TTGCCCCTGTTTCACTATCCAG-3' |
| tdTomato wildtype forward | 5'-AAGGGAGCTGCAGTGGAGTA-3' |
| tdTomato wildtype reverse | 5'-CCGAAAATCTGTGGGAAGTC-3' |
| tdTomato mutant forward | 5'-CTGTTCCTGTACGGCATGG-3' |
| tdTomato mutant reverse | 5'-GGCATTAAAGCAGCGTATCC-3' |

***Table 2-1: Primer sequences for genotyping PCR***

(All PCR reaction mixture reagents were from the Qiagen kit #201205)

| **Reaction mixture component** | **Volume (µL) per 50 µL reaction (Cre allele)** | **Volume (µL) per 21 µL reaction (tdTomato allele)** |
|---|---|---|
| 10x buffer | 5 | 2 |
| 50mM MgCl2 | 2.5 | 0.5 |
| 10mM dNTPs | 1 | 1 |
| Primer CreF | 1 | 1 µL of 4 primer mix (10 µM each) |
| Primer CreR | 1 | NA |
| Taq | 0.25 | 0.1 |
| $dH_2O$ | 38.5 | 15.4 |
| DNA | 1 | 1 |

***Table 2-2: Reaction mixture concentrations for genotyping PCR***

| Cycle number | Cycle temp ($^{o}$C) (Cre allele) | Cycle time (min:seconds) (Cre allele) | Cycle temp ($^{o}$C) (tdTomato allele) | Cycle time (min:seconds) (tdTomato allele) |
|---|---|---|---|---|
| 1 | 94 | 5:00 | 94 | 3:00 |
| 2* | 94 | 0:30 | 94 | 0:20 |
| 3* | 55 | 0:30 | 61 | 0:30 |
| 4* | 72 | 1:00 | 72 | 0:30 |
| 5 | 72 | 8:00 | 72 | 2:00 |
| 6 | 4 | Hold | 4 | Hold |

***Repeat cycles 2-4, 35 times, for both Cre and tdTomato alleles**

***Table 2-3: Cycle temperatures and times for genotyping PCR***

#### 2.1.2.3 *Agarose gel*

10 µL of each PCR reaction was mixed with 2 µL loading dye, run on a 1% agarose gel at 100 V and imaged on a Bio-Rad Gel Doc.

### 2.1.3 Tamoxifen preparation and injection

200 mg of tamoxifen (Sigma #T5648) was added to 1mL of ethanol under sterile conditions, vortexed for 5 seconds and heated to 50°C for 10-30 min until fully dissolved. 9 mL of sterile sunflower oil was added to dilute the solution and vortexed for 5 seconds. 250 µL aliquots (20mg/mL) were then frozen at -20°C until required. Tamoxifen solution was thawed and administered to mice via intravenous injection of 200 µL (4mg tamoxifen) every 48 hours a total of 3 times. All tamoxifen injections were carried out by animal technicians at the Gurdon Institute, University of Cambridge.

### 2.1.4 Harvesting of mammary glands

72 hours after the final tamoxifen injection, mice were euthanized by dislocation of the neck and mammary glands were harvested into 5 mL of Dulbecco's Modified Eagle's Media / Ham's F-12 nutrient mixture GlutaMAX (DMEM/F-12) (Gibco #41965-039) supplemented with 10% foetal calf serum (FCS) (Gibco #10500064) 10 mM 4-(2-hydroxyethyl)-1-piperazineethanesulfonic acid (HEPES) (Gibco #15630080), 1 mg/mL Collagenase A (Roche, #11088793001), 100 U/mL Hyaluronidase (Sigma, #H3506), 100 U/mL penicillin/streptomycin (Invitrogen, #15140122), 5 µg/mL bovine insulin (Sigma #11882) and 10 µg/mL murine epidermal growth factor (EGF) (Sigma #E4127). Mammary glands were then digested overnight at 37°C in 5% $CO_2$ before processing for fluorescence activated cell sorting (FACS).

### 2.1.5 Tumour models

Syngeneic TUBO mammary tumours were established by injection of $5 \times 10^3$ TUBO cells into the abdominal mammary gland of BALB/c females. Injections were carried out by Dr. Sara Pensa or Dr. Jessica Hitchcock (University of Cambridge, Watson Laboratory). The TUBO cloned cell line was established from a mammary carcinoma that spontaneously arose in a BALB-*neu*T mouse and carries the Her-2/*neu* oncogene driven by the MMTV promoter (Rovero et al. 2000; Guy et al. 1992). Tumours were harvested before exceeding humane end points (4–5 weeks) and frozen for future use. MMTV-*Wnt1* mice were crossed onto an FVB background for quicker tumour onset. Tumours were harvested at humane end points (2-12 months). Mice were euthanized by dislocation of the neck.

### 2.1.6 Tumour freezing

MMTV-*Wnt1* and TUBO tumours were placed in cryovials, covered with freezing medium (DMEM/F12 supplemented with 40% FCS and 6% dimethyl sulfoxide (DMSO) (Sigma #276855)), placed immediately into a Mr. Frosty freezing container (ThermoFisher #5100-0001) followed by overnight incubation at -80$^{o}$C. Cryovials were then stored in liquid nitrogen until required.

## 2.2 Fluorescent activated cell sorting (FACS)

### 2.2.1 tdTomato$^+$ primary mammary basal epithelial cells

FACS was carried out using a modified previously published method (Stingl et al., 2006). Harvested and digested mammary glands from either K14-cre$^{ERT2}$/ROSA26-tdTomato or Axin2-cre$^{ERT2}$/ROSA26-tdTomato transgenic mice, were vortexed for 5 seconds. Hank's Balanced Salt Solution (HBSS) (Gibco #24020) supplemented with 1% FCS (termed HF hereafter) was added to samples to a total volume of 10 mL. Samples were then centrifuged at 1000 rpm for 5 mins and resuspended in 1 mL HF and 4 mL ammonium chloride solution (Stemcell technologies #07800). All subsequent centrifugations mentioned in this protocol were at 1000 rpm for 5 mins. The samples were then centrifuged and resuspended in 1 mL trypsin-EDTA (Sigma #T4174). Samples were pipetted up and down 20 times, incubated for 1 min at room temperature, when this step was repeated. 9 ml of HF was then added, followed by centrifugation. Pellets were then resuspended in 1 mL (5 mg/mL) dispase (Sigma #D4693), 100 µL (1 mg/mL) DNase (Sigma #D4513) and 10 mL HF, followed by filtration through a 40 µm cell strainer and subsequent centrifugation. Cells were then either resuspended in Primary Complete media (DMEM supplemented with 10% FCS, 100 U/mL P/S, 5 µg/mL bovine insulin and 10 µg/mL EGF) and plated for tamoxifen titration experiments (see section 2.9.3.2) or processed for FACS.

For FACS, cells were blocked in DMEM supplemented with 10% normal rat serum (500 µL per sample) (Thermofisher Scientific #10710C) and incubated for 30 mins on ice. Antibodies recognising blood lineage and epithelial cell types were then added to samples followed by incubation on ice for 10 mins. For antibody concentrations see Table 2.4. 3 mL of HF was then added to the samples followed by centrifugation. Samples were resuspended in 500 µL HF and streptavidin-PE-Cy7 (1:500) (BDBioscience #557598) followed by incubation on ice for 10 min. Finally, 3 mL of HF was added to samples, followed by centrifugation and resuspension in 500 µL HF, ready for FACS. FACS was carried out using the MoJo cell sorter with the assistance of Nigel Miller (University of Cambridge, Pathology Department). Single colour controls were used to calibrate the machine. tdTomato$^+$ basal epithelial cells were isolated from the entire mammary cell population based on their CD24$^+$ CD49f$^{med/hi}$ CD45$^-$ CD31$^-$ Ter119$^-$ surface marker expression.

| Antibody | Cell recognition | Conc. | Company | Catalogue no. |
|---|---|---|---|---|
| CD45-biotinylated | Blood lineage | 1:500 | eBioscience | #13-0451-82 |
| CD31-biotinylated | Blood lineage | 1:500 | eBioscience | #13-0311-82 |
| Ter119-biotinylated | Blood lineage | 1:500 | eBioscience | #13-5921-82 |
| CD24-AlexaFluor488 | Epithelial | 1:500 | Biolegend | #101816 |
| CD49f-AlexaFluor647 | Epithelial | 1:100 | Biolegend | #313610 |

***Table 2-4: Fluorescence activated cell sorting (FACS) antibodies***

### 2.2.2 tdTomato$^+$ MDA-MB-231 cells

tdTomato MDA-MB-231 cells were FACS using the MoJo cell sorter with the assistance of Nigel Miller based on their tdTomato expression. Uninfected MDA-MB-231 cells were used as a negative control.

## 2.3 Collagen scaffold synthesis

Scaffolds were prepared according to a modified previously published method (Pawelec et al., 2014). Collagen from bovine Achilles tendon (Sigma #C4387) was dispersed overnight in 0.05 M acetic acid (Sigma #71521) at 4°C to make 1wt% collagen slurry. The slurry was homogenised at 10,000 rpm for 30 mins using an overhead homogeniser, keeping the container in an ice water bath, followed by centrifugation at 2500 rpm for 5 mins to remove air bubbles. The slurry was carefully aspirated into scaffold moulds (Fig. 2.1), taking care to completely cover the copper pins with minimal bubble formation. A glass cover slide was then placed on top of the mould chamber (Fig. 2.1). To alter the seeding funnel morphology, either a cylindrical (Fig. 2.1b) or conical copper pin (Fig. 2.1c) was used in moulds. For anisotropic scaffolds (Fig. 2.1b,c, Table 2.5), the freeze dryer shelf was pre-cooled prior to use, ensuring a shelf temperature of -40°C and moulds were placed so that the copper pins were in direct contact with the metal shelf (Fig. 2.1b,c). For isotropic scaffolds, the freeze dryer shelf was cooled from 20°C to -40°C over a 1h period with the moulds *in situ*. In this case the copper pins were thermally insulated with a thin rubber foam mat of less than 1 mm thickness, so that they were not in direct thermal contact with the metal shelf (Fig. 2.1d). The freezing protocol was chosen to produce pore sizes of around 100 µm away from the funnel (Husmann et al., 2015).

Following freeze-drying, scaffolds were removed from the mould by carefully lifting the glass cover slide to which the collagen scaffolds stuck to. Using a scalpel blade and forceps, scaffolds were carefully removed from the glass slide ensuring not to crush or compromise their structure. Scaffolds were then immediately submerged in cross-linking solution (70% ethanol, 33 mM 1-ethyl-3-(3-dimethylaminopropyl)-carbodiimide hydrochloride (Sigma #E6383) and 6 mM *N*-hydroxysuccinimide (Sigma #130672)) for 30 mins with constant agitation on a rotating plate. Following cross-linking, the scaffolds were removed to fresh 70% ethanol and degassed under vacuum (approximately 10 kPa) for 5 mins. Samples were stored in 70% ethanol to ensure sterility until required.

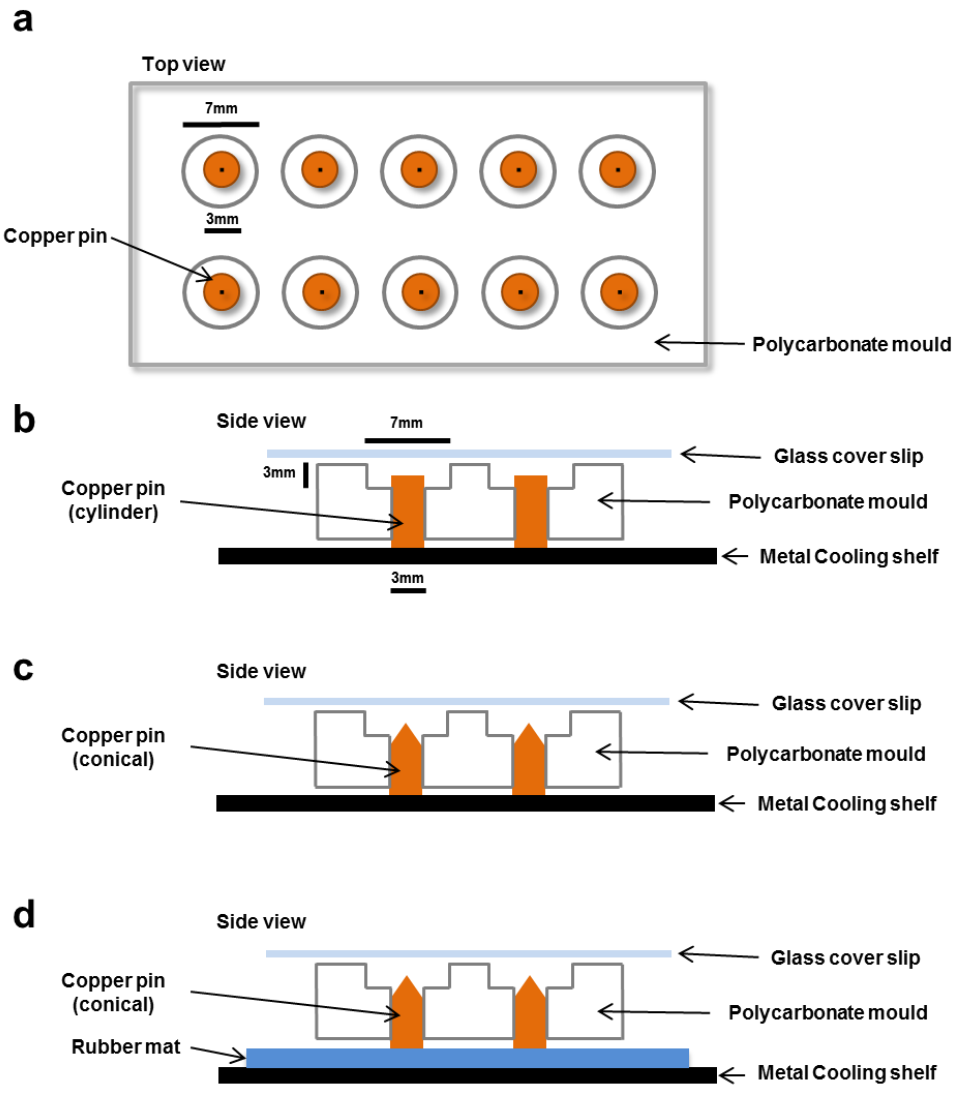


***Figure 2-1: Mould design for collagen I scaffolds***

To produce collagen I scaffolds with different geometries and different internal architectures a number of mould designs were generated. These were filled with collagen I slurry and placed in a freeze drier for thermal cycling. The main body of the mould was machined from 9.6 mm thick polycarbonate sheet with evenly spaced 7 mm diameter by 3 mm deep troughs. In the centre of each trough, a 3 mm diameter hole was added in which a copper pin with a conical or cylindrical tip was inserted. The tip was covered by PTFE tape to prevent contact with the slurry. (a) Mould shown as a top down view. (b) Mould side view with cylindrical tipped pin set up for anisotropic scaffolds. Copper pin is in thermal contact with the thermal cooling shelf. (c) Mould side view for conical tipped pin set up for anisotropic scaffolds. Copper pin is in thermal contact with the thermal cooling shelf. (d) Mould side view for conical tipped pin set up for isotropic scaffolds. Copper pin is not in thermal contact with the thermal cooling shelf and is thermally insulated by a rubber mat.

| Scaffold type | Cooling procedure | Freezing procedure | Subliming procedure |
|---|---|---|---|
| Anisotropic | Cooling shelf quenched to -40°C, moulds added when shelf was cold. Copper pins were in thermal contact with the cooling shelf. | Moulds were kept at -40°C for 2 hours to ensure complete freezing. | Ice was subliming for 18 hours. |
| Isotropic | Cooling shelf cooled from 20°C to -40°C in 1 hour with moulds *in situ*, Copper pins were thermally insulated from the cooling shelf. | Moulds were kept at -40°C for 2 hours to ensure complete freezing. | Ice was subliming for 18 hours. |

***Table 2-5: Two distinct freeze-drying protocols used to synthesise scaffolds with either anisotropic or isotropic internal architectures***

Two different freeze drier cooling procedures of collagen slurries within moulds were required to produce the two scaffold types. In the anisotropic case, ice nucleated at the pins from which it grew in directional channels. In the isotropic case, the slurry was cooled evenly throughout, resulting in random locations of ice crystal nucleation points. After ice was nucleated, it grew in a dendritic form throughout the slurry (Husmann et al., 2015).

# 2.4 Cell culture

All cell culture was carried out under sterile conditions in either a laminar flow cell culture hood or in a humid incubator at 37°C in 5% $CO_2$.

## 2.4.1 3T3-L1 cells

### 2.4.1.1 *3T3-L1 maintenance*

Cells were passaged when cells were at approximately 70% confluency ensuring cells did not reach total confluency. 3T3-L1 Maintenance Media (3T3-L1 MM) comprised DMEM supplemented with 10% FCS. Cells were maintained up to but not beyond passage 20.

### 2.4.1.2 *Adipogenesis*

Once cells had reached confluency, maintenance media was removed and replaced with adipogenic media (3T3-L1 MM supplemented with 1 µg/ml insulin (Sigma I6634), 0.25 µM dexamethasone (Sigma #D4902) and 0.5 mM 3-isobutyl-1-methylxanthine (IBMX) (Sigma #I5879)) replacing every 48 hours for 1 week. Lipid filled vesicles could be observed under phase contrast light microscopy.

## 2.4.2 3T3 cells

### 2.4.2.1 *Maintenance*

3T3 cells were passaged at approximately 70% confluency. 3T3 Maintenance Media (3T3 MM) comprised DMEM supplemented with 10% FCS.

### 2.4.2.2 *Irradiation*

3T3 cells were trypsinized from sub-confluent (<60%) cultures, resuspended at $10^6$ cells/mL in HF and irradiated 220 KV, 14.0 mA on an X-ray machine for 12 mins. Cells were frozen at 2 x $10^6$ cells/ml/vial in freezing media (DMEM supplemented with 20% FCS and 10% DMSO) until required.

## 2.4.3 tdTomato$^+$ primary basal mammary epithelial cells

### 2.4.3.1 *Maintenance of tdTomato$^+$ basal epithelial cells isolated by FACS of K14-cre$^{ERT2}$/ROSA26-tdTomato transgenic mouse mammary glands*

tdTomato$^+$ basal cells were maintained in Primary Complete Media (DMEM supplemented with 10% FCS, 100 U/ml P/S, 5 µg/ml bovine insulin and 10 µg/ml EGF) and seeded onto tissue culture plastic plates no lower than 50% confluency to ensure viability.

#### 2.4.3.2 *Tamoxifen titration of tdTomato$^+$ basal epithelial cells isolated by FACS of K14-cre$^{ERT2}$/ROSA26-tdTomato transgenic mouse mammary glands*

tdTomato$^+$ basal cells were titrated in Primary Complete Media supplemented with 0.1-500 µM tamoxifen *in vitro*, to determine the optimal dosage required for *in vitro* Cre recombination.

#### 2.4.3.3 *Expansion of tdTomato$^+$ basal epithelial cells isolated by FACS of Axin2-cre$^{ERT2}$/ROSA26-tdTomato transgenic mouse mammary glands*

tdTomato$^+$ basal cells were expanded in 2D cultures according to a previously published protocol (Prater et al., 2014). Growth factor reduced Matrigel (Corning, #CB-40230A) was defrosted overnight at 4$^o$C. PBS, petri dishes, pipettes and pipette tips were all cooled to 4$^o$C prior to the handling of Matrigel. Matrigel was mixed with PBS at 1:60 ratio and pipetted evenly onto a cold petri dish at a volume that ensured complete covering of the dish surface. This was performed as quickly as possible to minimise any warming of Matrigel to room temperature. The dish was then incubated at 37$^o$C for 1 hour followed by aspirating the remaining liquid to leave a Matrigel coating on the surface of the dish. FACS sorted tdTomato$^+$ cells from an Axin2$^+$ basal cell origin were seeded on Matrigel coated dishes at 10-20$^4$ cells/cm$^2$ mixed with 10$^4$/cm$^2$ irradiated 3T3 feeder cells in FAD media (DMEM :Ham's F12 (3:1) supplemented with 10% FCS, 1.8x10$^{-4}$ M adenine, 100 IU/mL P/S, 0.5 µg/mL hydrocortisone, 8.47 ng/mL cholera enterotoxin (Sigma #C8052), 10 ng/mL EGF, 5 µg/mL insulin and 10 µM Y-27632 (Cambridge Bioscience #SM02-10)). Prior to passaging, fresh petri dishes were pre-coated with Matrigel according to the aforementioned protocol. Cells were then washed three times with PBS followed by the addition of trypsin-EDTA. Following 60 seconds incubation, 3T3 feeder cells detached and were discarded. Additional trypsin was then added to detach tdTomato$^+$ cells and left on no more than 5 mins. The cells that had detached in this time period were neutralized in fresh FAD media. For any remaining cells that had not detached by this point, more trypsin-EDTA was added, incubated and neutralized following detachment. The tdTomato$^+$ cells were then centrifuged at 200*G* for pelleting, resuspended in fresh FAD media and seeded on pre-coated Matrigel petri dishes at 10-20$^4$ cells/cm$^2$ mixed with 10$^4$/cm$^2$ irradiated 3T3 cells.

### 2.4.4 Human breast cancer cell lines

#### 2.4.4.1 *Maintenance*

All cell lines were maintained between passages 5 to 15 in their respective maintenance media (MM): MCF7 cells were cultured in DMEM media (Gibco #41965) supplemented with 10% FCS in a humidified 5% $CO_2$ incubator at 37°C. MDA-MB-468 and MDA-MB-231 were cultured in Leibovitz L-15 media (Gibco, #11415-064) supplemented with 10% FCS in a humidified air incubator at 37°C.

#### 2.4.4.2 *Epithelial-to-mesenchymal transition (EMT) induction of MDA-MB-468 cells*

MDA-MB-468 cells were serum starved and treated with epidermal growth factor (EGF) (Leibovitz L-15 media supplemented with 0.5% FCS and 50 ng/ml EGF) for 12h as previously described (Davis et al., 2013). EGF treatment continued for 10 days in normal serum conditions (Leibovitz L-15 supplemented with 10% FCS and 50 ng/ml EGF). Following this cells were either collected for western blotting, fixed for immunocytochemistry, or seeded into anisotropic scaffolds for migration assays.

### 2.4.5 Human primary mesenchymal stem cells (MSC)

#### 2.4.5.1 *Maintenance*

Human mesenchymal stem cells (MSC) isolated from routine breast reduction mammoplasty surgery (passage 0) were gifted by Dr. Mohammed Bentirez-Alj (Friedrich Miescher Institute, Basel, Switzerland). MSC were maintained in the following MSC Maintenance media (MSC MM): DMEM/F12 supplemented with 20% FCS, 15 mM HEPES (Sigma #83264), 1 nM 17-β-estradiol (Sigma #E2758), 100 U/ml P/S, 50 µg/ml gentamicin (Sigma #G1397), 10 ng/ml EGF, 10 ng/ml basic fibroblast growth factor (bFGF) (Peprotech #100-18B). Cells were passaged at approximately 70% confluency, ensuring 100% confluency was not reached during passage steps.

#### 2.4.5.2 *Adipogenesis*

100% confluent cells had their MSC MM removed and replaced with MSC adipogenic media (DMEM/F12 supplemented with 10% FCS, 15 mM HEPES (Sigma #83264), 10 nM 17-β-estradiol (Sigma #E2758), 100 U/ml P/S, 50 µg/ml gentamicin (Sigma #G1397), 5 µg/mL insulin, 1 µM dexamethasone, 0.5 mM IBMX, 60 µM indomethacin (Sigma #I7378)). Media was replaced with fresh MSC adipogenic media every 48 hours for 11 days.

#### 2.4.5.3 *Antibiotic titration*

Primary MSCs were treated with 0-1 µg/mL puromycin (Gibco #A11138), 0-600 µg/mL geneticin (Gibco #10131) and 0-1 mg/mL zeocin (Melford Labs #20186) in MSC MM for 7 days to determine the minimum concentration of each antibiotic required to kill 100% of primary MSCs.

### 2.4.6 Human embryonic kidney 293T (HEK293T) cells

HEK293T cell maintenance media (HEK293T MM) comprised DMEM supplemented with 10% FCS. Cells were passaged at 70-100% confluency.

# 2.5 Viral transductions

All plasmids were amplified using Qiagen miniprep (#27104) and Quiagen maxiprep (#12362) kits according to the supplier's instructions.

## 2.5.1 Lentiviral transduction of MDA-MB-231 cells

The following protocol is for lentiviral transfection of one 10 cm petri dish of 60% confluent HEK293T cells. 1.5 ml of buffered saline (150 mM NaCl, 20 mM HEPES (pH 7.4)) was added into a bijou with 32.8 µg of DNA (5.84 µg pMD2.G packaging vector, 11.68 µg p8.91 packaging vector and 18.25 µg pCDH-EF1-MCS-T2A-tdTomato lentivector (cloned from the pCDH-EF1-MCS-T2A-copGFP lentivector (System Biosciences #CD521A-1) by Dr. Michael D'Angelo, University of Cambridge, Watson laboratory)) and incubated for 5 mins room temperature. Following this, 82 µL of polyethylenimine (PEI) was added dropwise to the mixture followed by a 5 second vortex and incubation for 10 mins at room temperature. 4 mL of Opti-MEM media (Gibco #51985) was then added, inverted twice and left at room temperature for 10 mins. HEK293T MM was then aspirated from a 10 cm dish of 60% confluent HEK293T cells and replaced with the transfection mixture, followed by incubation at 37°C for 6 hours in 5% $CO_2$. The transfection mixture was then replaced with 6 mL fresh HEK293T MM and left for 48 hours to collect viral particles. Meanwhile, 12 hours before collection of viral particles, two wells of a six well plate were seeded with $5x10^5$ MDA-MB-231 cells. HEK293T viral media was collected, passed through a 0.45 µm filter and stored briefly in a 50 mL tube. Transfected HEK293T cells were replenished with fresh HEK293T MM for further viral particle collection. 8 µg/ml polybrene (Sigma #107689) was then added dropwise to filtered HEK293T viral media and dispensed onto MDA-MB-231 cells (3 mL per well) to replace their MM. Plates of MDA-MB-231 cells were then spin transduced for 80 mins at 173 *G* and returned to the incubator. After 48 hours the process was repeated: viral HEK293T media removed, filtered, ejected onto MDA-MB-231 cells with polybrene and spin transduced. 24 hours following this, viral media from MDA-MB-231 cells was aspirated and replaced with fresh maintenance media for subculture. Viral transduction of the tdTomato gene was assessed with immunofluorescence and FACS analysis (Hsu and Uludag, 2012).

## 2.5.2 Retroviral transduction of human mesenchymal stem cells (MSC) for immortalisation

HEK293T cells were transfected using the aforementioned PEI method for lentiviral transfection with the exception of using 3 µg of viral DNA (retroviral plasmids used for transfection were the pLXSN-neo-E6E7 and pBABE-puro-hTERT gifted by Dr. Heike Laman (University of Cambridge, Department of Pathology)) and 2 µg of packaging vector pMDG.2. Viral particle collection was also according to

aforementioned lentiviral methods with the exception that viral collection media for HEK293T cells was MSC MM so that it was compatible with MSC during viral infections.

Following transduction MSCs were passaged to avoid 100% confluency and cell differentiation. They were then treated with 600 µg/ml geneticin (pLXSN-neo-E6E7) or 1 µg/ml puromycin (pBABE-puro-hTERT) for 5 days. Surviving cells were then pooled into smaller wells to increase confluency to around 50% and to avoid sparse populations dying out. Cells were then expanded and frozen down for future use. MSCs that were transduced with pLXSN-neo-E6E7 were named E6E7-MSC and MSCs transduced with pBABE-puro-hTERT were named hTERT-MSC.

# 2.6 Mammary stem cell (MaSC) culture assay

## 2.6.1 'Synthetic fat pad' set up

3T3-L1 cells were cultured in 3T3-L1 MM between passages 4-20. 3T3-L1 cells were seeded and differentiated in isotropic collagen scaffolds using a modified previously published method (Davidenko et al. 2010). Briefly, $1x10^6$ 3T3-L1 cells were seeded into scaffolds, left to proliferate for 7 days and differentiated using an adipogenic cocktail (3T3-L1 MM supplemented with 1 µg/ml insulin, 0.25 µM dexamethasone and 0.5 mM IBMX) for 7 days, changing media every other day. At this point scaffolds were moved into 6 well plates ready for tdTomato$^+$ primary cell seeding. All cell cultures were in 5% $CO_2$ at 37$^o$C in a humid incubator.

## 2.6.2 MaSC culture assay – tdTomato$^+$ cells from K14-cre$^{ERT2}$/ROSA26-tdTomato transgenic mice

tdTomato$^+$ primary basal epithelial cells were isolated by FACS of K14-cre$^{ERT2}$/ROSA26-tdTomato mouse mammary glands. tdTomato$^+$ cells were seeded in 'synthetic fat pads' at a density of 500 cells per scaffold. Cultures were maintained for 2 weeks in Primary Complete Media (DMEM supplemented with 10% FCS, 100 U/ml P/S, 5 µg/ml bovine insulin and 10 µg/ml EGF) before 4% paraformaldehyde (PFA) (Sigma #P6148) fixation overnight for subsequent immunolocalisation analysis.

## 2.6.3 MaSC culture assay - tdTomato$^+$ cells from Axin2-cre$^{ERT2}$/ROSA26-tdTomato transgenic mice

tdTomato$^+$ primary basal epithelial cells were isolated by FACS of Axin2-cre$^{ERT2}$/ROSA26-tdTomato mouse mammary glands, followed by expansion in 2D on Matrigel covered petri dishes with 3T3 feeder cells. tdTomato$^+$ cells were seeded in 'synthetic fat pads' at a density of $5x10^5$ cells per scaffold. Cultures were maintained for 2 weeks in Primary Complete Media before 4% PFA fixation overnight for subsequent immunolocalisation analysis.

# 2.7 Human breast cancer cell line migration assay

## 2.7.1 Human breast cancer cell line migration assay setup

Collagen scaffolds were washed twice with sterile PBS followed by soaking overnight in the appropriate MM for each cell line, as detailed in section 2.4.4, supplemented with 50 µg/ml gentamicin to ensure contamination free conditions. Using sterile forceps, scaffolds were moved into the upper wells of 6 mm diameter Boyden chambers (0.4 µm pore size, Costar #3470) with upward facing seeding funnels. Care was taken to eliminate residual media from the scaffold. Migration assays were established under both serum gradient (upper chamber 1%/lower chamber 10%, Fig. 2.2a) and non-gradient (upper chamber 10%/ lower chamber 10%, Fig. 2.2b) conditions for all cell types (MDA-MB-231, MDA-MB-468 and MCF7 cells) and scaffold types (isotropic and anisotropic), using maintenance media appropriate for each cell line as detailed in section 2.4.4.

Cells were trypsinized, checked for viability by Trypan blue exclusion assay (>90% in all cases) and resuspended in the appropriate fresh MM for each cell line (1% FCS for gradient samples or 10% FCS for non-gradient samples (Fig. 2.2)) at a concentration of $5 \times 10^6$ cells/ml. Cells were pipette aspirated 5x to minimise cell clumping on suspension. To characterise cell spreading at seeding, Countbright microbeads (Life technologies #C36950) were suspended alongside cells at a concentration of $5 \times 10^3$ /mL. 10 µl ($5 \times 10^4$ cells) of this cell/bead suspension was then pipetted into the nucleation point of each scaffold (Fig. 2.2). The bottom chamber of the Boyden was then filled with 750µl MM (10% FCS in all cases) and the cells were left for 4 hours to attach. The upper chamber was then filled with 250µl media containing either 1% FCS for gradient samples or 10% FCS for non-gradient samples. Samples were left to incubate for either 24 hours or 10 days, with media changed every 48 hours in the latter condition (Fig. 2.2). In 10 day samples, media was substituted for complete media containing 10 µM EdU for the final 24 hours, in order to quantify cells divided over that time period. The provision of a serum gradient was provided to a subset of samples to test if a chemokine differential between upper and lower chambers of the supporting transwell plate was required to force cell migration within the scaffold depth. Following incubation, scaffolds were fixed for analysis in 4% PFA overnight at 4 °C, washed in PBS and segmented in half through the nucleation point using a scalpel blade. One scaffold half was processed to paraffin for immunohistochemical (IHC) analysis.

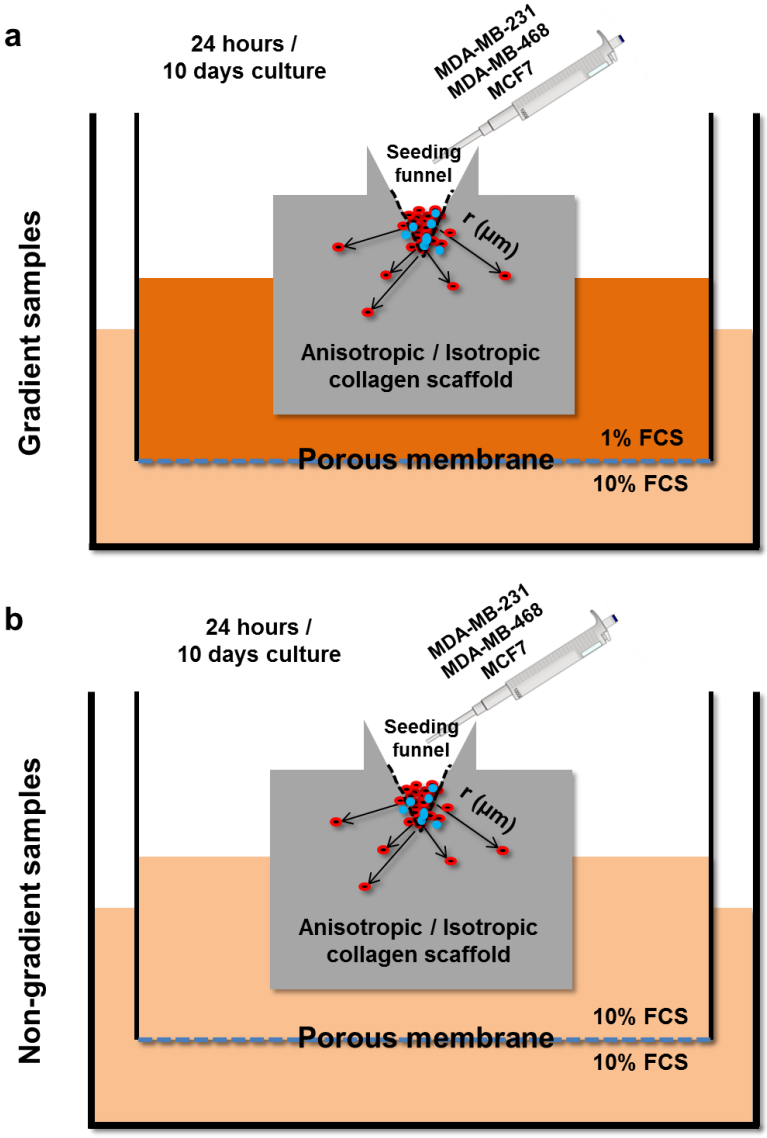


***Figure 2-2: Human breast cancer cell line migration assay schematic***

To test human breast cancer cell line migratory potential within both isotropic and anisotropic collagen I scaffolds, an assay was devised. Scaffold seeding procedure consisted of adding a mixture of cells (red) and beads (blue) into the funnel of anisotropic and isotropic collagen scaffolds placed within a Boyden chamber. (a) For gradient samples, media supplemented with 1% FCS was placed into the upper chamber and 10% FCS in the lower chamber. (b) For non-gradient samples media supplemented with 10% FCS was placed in both the upper and lower chambers. Scaffolds were cultured for 24 hours or 10 days followed by fixation and measurement of the cell migration distance from the seeding funnel - r (µm). This was measured as the shortest distance between the cell or bead with the line (dotted black line) drawn along the funnel as seen under the microscope.

### 2.7.2 Migration analysis – breast cancer cell line migration

Using microscopy images of bisected scaffolds or IHC sections and ImageJ image analysis, the scaffold nucleation point was marked and segmented into 50 separate points which were then saved as individual coordinates. Migratory cells and beads were then marked and saved as coordinates. Using Microsoft Excel formulae, the shortest distance of each cell/bead to the closest point on the segmented nucleation point, also known as the Euclidian distance, (or r(μm) Fig. 2.2) was calculated. Using distance measurements for every migratory cells/bead in one sample, the median distance travelled by cells/beads, $r_{median}$(μm), was calculated.

### 2.7.3 Statistical analysis – breast cancer cell line migration

A Wilcoxon rank-test (otherwise known as a Mann-Whitney U test) on unpaired data of median distances, $r_{median}$(μm), for each set-up was performed with a confidence value of 95% to check for statistically significant results. Relevant parameters were cell line type, scaffold type, serum gradient and vimentin expression.

# 2.8 Engineered Tumour-Stroma Interaction Model (ET-SIM) cancer therapeutic migration assay

## 2.8.1 Engineered Tumour-Stroma Interaction Model (ET-SIM)

3T3-L1 cells were cultured in MM between passages 4-20. 3T3-L1 cells were seeded and differentiated in anisotropic collagen scaffolds using a modified previously published method (Davidenko et al. 2010). Briefly, $1x10^6$ 3T3-L1 cells were seeded into scaffolds, cultured for 7 days to allow proliferation/filling of the scaffold and differentiated using an adipogenic cocktail (MM supplemented with 1 µg/mL insulin, 0.25 µM dexamethasone and 0.5 mM IBMX) for 7 days, replenishing adipogenic media every other day. At this point scaffolds were moved into 6 well plates ready for tumour fragment seeding. All cell cultures were in 5% $CO_2$ at 37°C in a humid incubator. Murine adipocytes derived from 3T3-L1 preadipocytes invested in anisotropic collagen scaffolds were named ET-SIM, hereafter.

## 2.8.2 Tumour fragment seeding and ET-SIM culture

For resuscitation, cryovials containing frozen MMTV-*Wnt1* or TUBO tumours were initially warmed by hand. Once thawing was first observed, room temperature medium was added. Tumours were decanted into tubes containing fresh tumour medium (DMEM/F12 supplemented with 10% FCS, 1x Penicillin/Streptomycin, 5 µg/ml Insulin and 10 ng/ml EGF) making sure not to carry across any freezing medium. Decanting was repeated to wash away any remaining freezing medium. Tumours were mechanically fragmented using a scalpel into approximately 3 $mm^3$ pieces. Tumour fragments were placed into the seeding funnel (vertically facing) of empty scaffolds or ET-SIM using sterile forceps and cultured in 6 well plates (Fig. 2.3). 1 mL of tumour media was carefully added so as not to dislodge the tumour fragment and left for 4 hours to attach (Fig. 2.3). Following this, an additional 4 mL of tumour media was added slowly to again avoid displacement of the fragment, covering both the scaffold and fragment (Fig. 2.3). A fresh 5 mL of tumour media was replaced each day and scaffolds were removed after 72 hours or 10 days, fixed in 4% paraformaldehyde (PFA) and either paraffin embedded for immunohistochemistry or the CUBIC whole mount immunostaining protocol was applied (see section 2.13.4).

## 2.8.3 Therapeutic testing

After 24 hours of tumour fragment culture as mentioned above, the media was replaced with 5 ml of tumour media supplemented with either 35.2 µM DMSO (Sigma Aldrich #D8418), 10 µM Y-27632 (ROCKi)(Cell Guidance Systems #SM02-10), 10 µM GM6001 (Merck Millipore #364205) or 10 µM

Canertinib (Selleckchem, #S1019) (Fig. 2.3). Media was replaced with fresh 5 ml tumour media plus an inhibitor every 24 hours until fixation endpoint in 4% PFA.

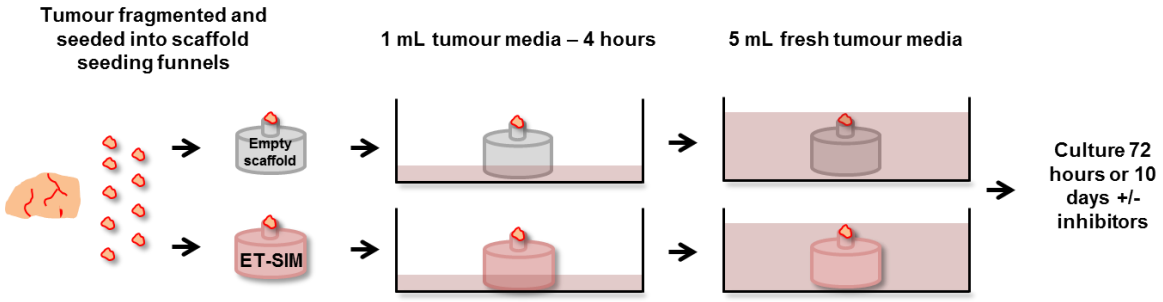


***Figure 2-3: Illustration of tumour fragment culture in ET-SIM and therapeutic testing***

In order to test whether collagen I scaffolds were able to support the culture of primary tumour fragments, tumours were fragmented and seeded into scaffold funnels before culturing *in vitro*. A schematic of MMTV-*Wnt1* and TUBO tumour culture in anisotropic collagen scaffolds is detailed above. Prior to tumour seeding scaffolds were either empty prior or filled with mature adipocytes (ET-SIM). For therapeutic testing tumour media was then supplemented with DMSO (vehicle control), ROCKi, GM6001 or Canertinib and changed daily for 72 hours or 10 days.

### 2.8.4 Migration analysis - ET-SIM cancer therapeutic migration assay

Tumour cell migration was analysed using a modified version of the migration analysis protocol used for the human breast cancer cell line migration assay (section 2.7.2). Using tile scans generated from IHC, cell nuclei of migratory cells were marked using Fiji and their coordinates collected. MMTV-*Wnt1* tumour cell nuclei were distinguished from stromal cells using the markers αSMA and β-catenin and were defined as migratory when found in or on any part of the scaffold away from the tumour fragment. The scaffold nucleation point was marked, segmented and saved as coordinates. The closest distance from the nucleation point to each migratory nucleus (Euclidian distance) was measured using formulae in Microsoft Excel and these results were then combined in GraphPad.

Along with migration distance, the frequency of cell migration was also recorded. Any αSMA and β-catenin positive cell that was found within the scaffold was identified as migratory and added to the total frequency for that sample.

### 2.8.5 Statistical analysis – ET-SIM cancer therapeutic migration assay

Migration distances and migratory cell frequencies of multiple therapeutics regimes were compared to DMSO vehicle controls using the non-parametric unpaired/matching Kruskal-Wallis ANOVA with a Geisser-greenhouse correction combined with a Dunn's multiple comparison test. Migration distances and migratory cell frequencies comparing with/without 3T3-L1 for an individual therapeutic regime were compared using the non-parametric unpaired Mann-Whitney test using a confidence level of 95%. All statistical analyses were carried out using the software GraphPad Prism 6.

# 2.9 Human Engineered Tumour-Stroma Interaction Model (hET-SIM)

## 2.9.1 E6E7-MSC seeding and differentiation

$1x10^6$ E6E7-MSC cells were seeded into anisotropic collagen scaffolds, cultured for 7 days to allow proliferation/filling of the scaffold and differentiated using MSC adipogenic media (DMEM/F12 supplemented with 10% FCS, 15 mM HEPES (Sigma #83264), 10 nM 17-β-estradiol (Sigma #E2758), 100 U/ml P/S, 50 µg/ml gentamicin (Sigma #G1397), 5 µg/mL insulin, 1 µM dexamethasone, 0.5 mM IBMX, 60 µM indomethacin (Sigma #I7378)), for 11 days, replenishing MSC adipogenic media every other day. At this point scaffolds were moved into Boyden chambers ready for MDA-MB-231 migration assays. All cell cultures were in 5% $CO_2$ at 37$^oC$ in a humid incubator. Human adipocytes (derived from E6E7-MSC) invested in anisotropic collagen scaffolds were named hET-SIM hereafter.

## 2.9.2 tdTomato MDA-MB-231 migration assay

Using sterile forceps, empty anisotropic collagen scaffolds and hET-SIM cultures were moved into the upper wells of 6mm diameter Boyden chambers (0.4µm pore size, Costar #3470) with upward facing seeding funnels. Care was taken to eliminate residual media from the scaffold. Migration assays were established with no serum gradient applied (upper chamber 10% FCS/ lower chamber 10% FCS, Fig. 2.2b) using MSC MM.

MDA-MB-231 cells that had been lentivirally transduced to express the tdTomato fluorescent protein (tdTomato$^+$ MDA-MB-231 cells) were trypsinized, checked for viability by Trypan blue exclusion assay (>90% in all cases) and resuspended in the fresh MSC MM at a concentration of $5 \times 10^6$ cells/ml. Cells were pipette aspirated 5 times to minimise cell clumping on suspension. 10 µl ($5 \times 10^4$ cells) of tdTomato$^+$ MDA-MB-231 cell suspension was then pipetted into the nucleation point of each scaffold. The bottom chamber of the Boyden was then filled with 750µl MSC MM and the cells were left for 4 hours to attach. The upper chamber was then filled with 250µl MSC MM. Samples were left to incubate for 7 days, with media changed every 48 hours. Following incubation, scaffolds were fixed for analysis in 4% PFA overnight at 4°C, washed in PBS and segmented in half through the nucleation point using a scalpel blade. Cell nuclei were marked with the green fluorescent DNA dye, SYTO 16 (ThermoFisher #S7578) and samples were then imaged using multi-photon microscopy.

## 2.10 Sodium dodecyl sulphate - polyacrylamide gel electrophoresis (SDS-PAGE) and western blotting

### 2.10.1 Epithelial-to-mesenchymal transition (EMT) induction of MDA-MB-468 cells

EpH4 cells (vimentin negative control), MDA-MB-231 cells (vimentin positive control), MDA-MB-468 cells and MDA-MB-468 cells treated with EGF, were collected in radio immunoprecipitation assay (RIPA) buffer. A bicinchoninic acid assay (BCA) assay was then performed and 20 µg of protein was added per lane. Blots were blocked in 5% bovine serum albumin (BSA) (Acros organics #240405000) in phosphate buffered saline-0.1% Tween-20 (PBST) for 1 hour. Primary antibodies anti-vimentin (cell signalling #5741, 1:1000) and loading control anti-tubulin (Abcam #ab6160, 1:10000) were diluted in 5% BSA-PBST and left rocking overnight 4$^{o}$C. Blots were washed 3 times for 5 min in PBST, moved into 5% BSA-PBST containing the secondary antibodies horseradish peroxidase (HRP)-anti-rabbit (Dako #PO448, 1:4000) and HRP-anti-rat (Dako #PO450, 1:2000) and were left rocking at room temperature for 1 hour. Blots were then developed using enhanced chemiluminescence (ECL) (GE Healthcare #RPN2109) substrate and photographic film.

### 2.10.2 Adipogenesis of mesenchymal stem cells (MSC)

Differentiated MSCs were collected and processed as above with the following exceptions: blots were probed with primary antibody perilipin (Cell signalling #3470, 1:1000) and the secondary antibody HRP-anti-rabbit (Dako #PO448, 1:4000).

# 2.11 Histology

## 2.11.1 Sectioning of scaffolds

Scaffolds were fixed in 4% PFA and incubated at 4°C overnight. For human breast cancer cell line invasion assays, scaffolds were bisected through the nucleation point, dehydrated, infiltrated with paraffin wax, placed freshly cut face faced-down and embedded in a paraffin wax block. Resulting sections provided a longitudinal profile through the centre of the scaffold and included the nucleation point (Fig. 2.4).

For tumour scaffold cultures, scaffolds with tumour fragments seeded in their nucleation point were not chopped in half due to the risk of tumour fragments falling out of the nucleation point. Whole tumour/scaffolds were dehydrated, infiltrated with paraffin wax, placed with the side face of the scaffold facing down and embedded in a paraffin wax block. The scaffold was then continuously chopped in the block until the centre of the tumour fragment, scaffold and nucleation point were visible. At this point sections were taken and provided a longitudinal profile through the centre of the scaffold and included the nucleation point (Fig. 2.4).

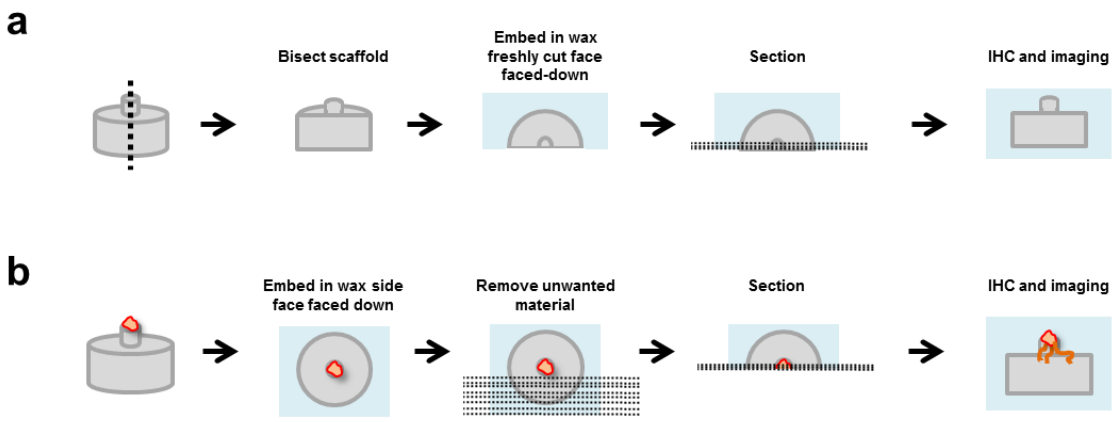


***Figure 2-4: Embedding and sectioning of collagen scaffolds for histological sections***

Following migration assays of human breast cancer cell lines or tumour cultures in collagen scaffolds, sectioning methods were devised to provide longitudinal sections through the centre of the scaffold. This required two different paraffin embedding protocols outlined schematically above. (a) Scaffolds from human breast cancer cell line migration assays were bisected and embedded in paraffin wax with the freshly cut face faced-down to provide longitudinal cross sections through the centre of the scaffold. (b) Scaffold / tumour fragment cultures were embedded in paraffin wax with the side face faced-down. Unwanted material was removed using a microtome. Sections were taken from the centre of the tumour fragment to provide longitudinal cross sections through the centre of the scaffold.

### 2.11.2 H&E

Sections were bathed in the following reagents for the following lengths of time: dewaxing Xylene 6 mins (100% Xylene) twice, 100% ethanol 3 mins, 95% methylated spirit 2 mins, 70% methylated spirit, running tap water 5 mins, Harris' haematoxylin 3-6 mins , running tap water 5 mins, 1% hydrochloric acid in 70% ethanol (acid alcohol) 1 min, running tap water 10 mins, 20% Eosin Y in ethanol 1 min, running tap water 40 seconds, 70% methylated spirit 40 seconds, 95% methylated spirit 1 min, 100% ethanol 3 mins and 100% Xylene 3 mins. Sections were then mounted in DPX and left to dry.

### 2.11.3 Masson's Trichrome

Sections were bathed in the following reagents for the following lengths of time: dewaxing Xylene 6 mins (100% Xylene) twice, 100% ethanol 3 mins, 95% methylated spirit 2 mins, 70% methylated spirit, running tap water 5 mins, Weigerts haematoxylin 15 mins, running tap water 5 mins, 1% hydrochloric acid in 70% ethanol (acid alcohol) 5 seconds, running tap water 5 mins, red mixture 5mins, rinse in 0.2% glacial acetic acid, filtered orange mixture 5 mins, rinse in 0.2% glacial acetic acid, 0.5 g aniline blue in 0.2% glacial acetic acid 2 mins, rinse in 0.2% glacial acetic acid 70% methylated spirit 40 seconds, 95% methylated spirit 1 min, 100% ethanol 3 mins and 100% Xylene 3 mins. Sections were then mounted in Sub-x and left to dry.

### 2.11.4 Oil Red O

To prepare a stock Oil Red O solution, 0.5g Oil Red O (Sigma #O0625) was dissolved in 100mL isopropanol (5 mg/mL). The stock solution was incubated at room temperature for 1h, filtered through a 0.2-mm filter and stored at room temperature for up to 1 year. To prepare a working solution of Oil Red O , 6 mL of stock solution was mixed with 4 mL distilled water. This was incubated at room temperature for 1 hour and filtered through a 0.2 mm filter. This working solution is stable for approximately 3 hours.

Differentiated 3T3-L1 cells or MSCs had their adipogenic media removed and gently washed twice in PBS. Cells were fixed in 4% PFA at 4°C for 1 hour followed by two more gentle washes in PBS. Oil Red O working solution was added, ensuring the entire cell surface was covered and incubated for 15 mins at room temperature. Cells were then rinsed with distilled water approximately 5 times (until the solution is clear) and left in distilled water for light microscope imaging analysis.

### 2.11.5 Senescence-associated β-Galactosidase staining

Mesenchymal stem cells (MSC) were seeded in 6 well culture plates and cultured until approximately 70% confluent. Media was removed and cells were washed with PBS before fixing with 4% PFA at

room temperature for 15 mins. Cells were then washed twice with PBS and covered with β-galactosidase staining solution (930 µl 1X Staining Solution (dissolve 10X Staining Solution at 37$^{o}$C with agitation and dilute in dH2O to a 1X solution), 10 µl 100X Solution A, 10 µl 100X Solution B, 50 µl 20 mg/ml X-gal stock solution (20 mg X-gal dissolved in 1 ml DMSO in a polypropylene tube)). Plates were then sealed with parafilm and incubated at 37°C in a dry incubator overnight. Cells were imaged under a light microscope. Senescent cells stained positive for β-galactosidase and appeared a blue/green colour.

All reagents for this protocol were provided in the β-Galactosidase staining kit (Cell Signalling #9680). The protocol and the reagents list are available from the Cell Signalling website (https://media.cellsignal.com/pdf/9860.pdf). 10X Staining Solution from this kit contains 5-10wt% citric acid, 7-13wt% sodium chloride and 7-13wt% trisodium orthophosphate. 100X Solution A contains 10-30wt% tetrapotassium iron (2+) hexacyanide trihydrate. 100X Solution B contains 10-30wt% tripotassium hexacyanoferrate.

## 2.12 Immunocytochemistry (ICC)

MDA-MB-231 (control), MDA-MB-468 (control) and MDA-MB-468 + EGF were cultured on glass coverslips and fixed in 4% PFA for 10 mins. Permeabilization was carried out for 15 mins in 0.5% Triton-X (VWR chemicals #28817.295) / PBS followed by 1 hour blocking in normal goat serum (NGS). Primary antibody anti-vimentin (cell signalling, #5741, 1:100) and negative control anti-rabbit IgG (Dako, XO936, 1:100) were diluted in blocking buffer and left overnight at 4°C. Secondary goat anti-rabbit AlexaFluor488 (life technologies, A11008, 1:500) was applied to all samples for 1 hour. DNA was marked using Hoechst and cells were visualized using epi-fluorescence. Using 3 separate fields of view from three technical repeats, the total number of MDA-MB-468 (+/− EGF) cells were counted using ImageJ. Following this the number of vimentin positive cells were also counted and plotted as a ratio of vimentin positive to the entire cell population. A statistical comparison was made using an unpaired t-test.

# 2.13 Immunohistochemistry (IHC)

## 2.13.1 Paraffin embedded slides (IHC-P)

For immunohistochemical analysis of paraffin embedded samples, sections were deparaffinised, rehydrated and boiled under pressure for 11 mins in 10 mM sodium citrate for antigen retrieval before blocking in 10% normal goat serum (Sigma) 0.05% triton-X PBS for 1 hour. Primary antibodies were incubated overnight at 4°C in a humidified chamber. For primary antibody specifications see Table 2.6. Signal was detected with conjugated secondary antibodies (1:500) and incubated for 1 hour at room temperature. For secondary antibody specifications see Table 2.7. DNA was marked using Hoechst 33342 2 µg/mL (Thermofisher Scientific) for 10 mins. Slides were mounted in PBS-glycerol 50:50 and viewed using fluorescence microscopy.

## 2.13.2 Bisected scaffolds for human breast cancer cell line migration assay (not sectioned)

Scaffolds were fixed overnight in 4% PFA at 4°C and bisected through the nucleation point. Bisected scaffolds were washed in PBS and bathed directly in 2 µg/mL bisbenzimide-Hoechst 33342 (Thermofisher Scientific #H1399) in PBS for 10 mins or for an assessment of cell proliferation stained for EdU incorporation according to the supplier's protocol (Click-iT, Thermofisher Scientific #C10337) before proceeding to Hoechst staining. The scaffolds were then washed in PBS three times and placed cut face down on a glass slide for epifluorescence imaging.

## 2.13.3 Whole scaffold staining (WSS)

Scaffolds filled with either 3T3-L1s or MSCs were fixed overnight in 4% PFA at 4°C followed by overnight permeabilization in 1% Triton-X - 10% BSA - PBS (blocking solution) at 4°C. Primary antibodies (see Table 2.6) were diluted in blocking solution, added to samples and agitated on a rocker for 4 days at 4°C. Scaffolds were washed thrice for 1 hour in PBS on a rocker at room temperature, moved into secondary antibodies (see Table 2.7) diluted in blocking solution and agitated on a rocker for 2 days at 4°C. Following this scaffolds were washed sequentially for 1 hour in PBS, 1 hour in 10 µM DAPI and 1 hour in PBS, before being moved into fresh PBS for storage. Scaffolds were imaged in ibidi petri dishes with a coverslip thickness bottom (ibidi #81158) for inverted imaging.

## 2.13.4 Whole scaffold/tumour staining using Cleared Unobstructed Body Imaging Cocktails (CUBIC)

Two reagents were required for CUBIC: Reagent 1a (modified from Reagent 1, unpublished, available at http://cubic.riken.jp/) and Reagent 2 (Susaki et al., 2015). Reagent 1a was prepared with the

following ingredients mixed at room temperature in the order they are written: 10wt% Triton-X, 5wt% NNNN-tetrakis (2-HP) ethylenediamine (Sigma), 10wt% Urea (Sigma) and 25 mM NaCl in $dH_2O$. The cocktail was then mixed on a heated magnetic stirrer at 60$^{o}$C until dissolved. Reagent 2 was prepared with the following ingredients: 50wt% Sucrose (Sigma), 25wt% Urea, 10wt% Triethanolamine (Sigma), 0.1wt% Triton-X and $dH_2O$ followed by mixing on a heated magnetic stirrer at 60$^{o}$C until dissolved.

Experiments involving human tumour biopsies, murine MMTV-*Wnt1* tumours, murine TUBO tumours, scaffolds with murine TUBO tumours and scaffolds seeded with tdTomato MDA-MB-231 cells/E6E7-MSCs were fixed overnight in 4% PFA at 4°C followed by immersion in Reagent 1a at 37°C for three days changing into fresh Reagent 1a each day. Samples were blocked overnight in 0.5% Triton-X - 10% NGS - PBS (blocking solution). Primary antibodies (see Table 2.6) were diluted in blocking solution and agitated on a rocker for 5 days at 4°C. Samples were washed in PBS briefly followed by three 1 hour washes in fresh PBS. Secondary antibodies (see Table 2.7) were diluted in blocking solution and agitated on a rocker for 2 days at 4°C. Samples were washed in PBS briefly followed by a 1 hour wash in fresh PBS. Nuclei were marked with a 2 hour wash in either 10 µM DAPI or 1 µM SYTO 16 green fluorescent nuclear stain (Thermofisher Scientific #S7578). Samples were washed in PBS briefly followed by a 1 hour wash in fresh PBS and immersed in Reagent 2 at 37°C in a dry incubator for 24 hours before imaging (Lloyd-Lewis et al., 2016; Susaki et al., 2014, 2015).

| Primary antibody | Application | Conc. | Company | Catalogue no. |
|---|---|---|---|---|
| anti-Ki67 | IHC-P | 1:100 | Abcam | #ab15580 |
| anti-K18 | IHC-P | 1:600 | Abcam | #ab181597 |
| anti-K14 | IHC-P | 1:200 | Abcam | #ab7800 |
| anti-αSMA | IHC-P/CUBIC | 1:500/1:50 | Abcam | #ab7817 |
| anti-β-catenin | IHC-P/CUBIC | 1:100/1:200 | Cell Signalling | #8480S |
| anti-E-cadherin | IHC-P/CUBIC | 1:500/1:100 | Cell Signalling | #3195 |
| anti-p63 | IHC-P | 1:50 | Abcam | #ab375 |
| anti-integrin β1 | IHC-P | 1:35 | Abcam | #ab3167 |
| anti-vimentin | ICC | 1:100 | Cell Signalling | #5741 |
| anti-collagen IV | ICC/WSS | 1:500/1:100 | Abcam | #ab6586 |
| anti-laminin | ICC/WSS | 1:500/1:100 | Abcam | #ab11575 |
| anti-perilipin | WSS | 1:50 | Cell Signalling | #3470S |
| anti-K8 | CUBIC | 1:150 | DSHB | #TROMA-1 |
| anti-Her2 | CUBIC | 1:300 | Dako | #A0485 |

***Table 2-6: Primary antibody concentrations for immunolocalisation***

A range of immunolocalisation methods were used throughout the thesis. Concentrations and company sources are outlined above. IHC-P = immunohistochemistry paraffin embedded, ICC = immunocytochemistry, WSS = whole scaffold immunostaining, CUBIC = whole scaffold immunostaining in conjunction with CUBIC optical clearing,

| Secondary antibody | Company | Catalogue no. |
|---|---|---|
| goat anti-rabbit AlexaFluor-488 | Thermofisher | #A-11008 |
| goat anti-mouse AlexaFluor-488 | Invitrogen | #A11001 |
| goat anti-rabbit AlexaFluor-647 | Lifetech | #A21245 |
| goat anti-Mouse AlexaFluor-647 | Lifetech | #A21237 |
| goat anti-rabbit-594 | Thermofisher | #A-11037 |
| goat anti-rat AlexaFluor647 | Lifetech | #A21247) |

***Table 2-7: Secondary antibody concentrations for immunolocalisation***

For fluorescent labelling of primary antibodies during immunolocalisation methods, complementary fluorescent secondary antibodies were required. Company sources are listed above. All secondary antibodies were used at a concentration of 1:500 for all immunolocalisation methods.

# 2.14 Microscopy

## 2.14.1 Epifluorescence

Automated epifluorescent microscopy was carried out using a Zeiss Observer with 20× objective. Tile scans of 10 × 8 × 0.5 mm (x,y,z dimensions) were performed to capture cells within the entire cut face of the scaffold presented to the slide.

## 2.14.2 Confocal

Confocal microscopy was carried out on confocal laser scanning Leica TCS SP8 microscope.

## 2.14.3 Multiphoton microscopy – Two-photon fluorescence (2pf), Second harmonic generation (SHG) and Coherent Anti Raman Spectroscopy (CARS)

2pf and SHG was carried out on the LaVision BioTec TriM Scope II upright 2-photon scanning fluorescence microscope using a 25x water dipping objective with a fixed 1040 nm laser and a tuneable laser. SHG was excited at 836 nm. CARS microscopy was carried out on the LaVision BioTec TriMscope with the assistance of Dr. Lorraine Berry (University of Cambridge, CRUK Cancer Institute). To produce a CARS signal a stokes beam from a TiSa laser (835 nm) was generated in conjunction with as a pump beam from an OPO laser (1104 nm). Both lasers were collinearly focused to provide a strong anti-stokes beam producing a CARS signal for the imaging of lipids.

## 2.14.4 Scanning electron microscopy (SEM)

All SEM images were taken by Dr. Anke Husmann. Scanning electron microscopy micrographs were used to visualise the pore structure of the scaffolds at various magnifications. Prior to imaging, collagen scaffolds were sputter coated with gold for 2 mins at a current of 20 mA. All micrographs were taken on a JEOL 5800, with a tungsten source, operated at 10 kV.

## 2.14.5 X-ray micro-computed tomography (µCT)

All µCT images were taken by Dr. Anke Husmann. Skyscan 1172 µCT scans were taken of the whole scaffolds (25 kV, 140µA). Reconstructions were performed with the software program NRecon (Skyscan), with a resolution of 6 µm.

# 3 Culture of primary mammary epithelial cells from a basal cell origin in adipocyte-invested collagen scaffolds

# 3.1 Introduction

A mammary gland divested of its epithelium can be repopulated and regain full functionality upon transplantation of a single cell (Kordon and Smith, 1998; Shackleton et al., 2006; Stingl et al., 2006). These cells, named mammary stem cells (MaSCs) or mammary repopulating units (MRUs) are presumed to be located within the basal epithelial population of the gland and therefore express basal cell markers such as K14 and αSMA. Upon transplantation they form an epithelial bilayer of both basal and luminal cells, demonstrating their bipotency during this transplantation procedure. However, transplantation has been shown to produce a regenerative response and so may not reflect the true potential of basal cells in the mammary gland *in situ*. Further study of MRUs has identified other markers to distinguish them from luminal epithelial cells (van Amerongen et al., 2012; Wang et al., 2014a). Notably, Wnt responsive Axin2-expressing cells are capable of repopulating a cleared fat pad and generating both luminal and basal epithelium (van Amerongen et al., 2012). The work in this chapter aimed to recapitulate aspects of the process of epithelial cell repopulation of the mammary gland in a 3D *in vitro* cell culture model. Should this model be successful it would facilitate future studies of MaSC/MRU potential in a 3D *in vitro* environment that is more amenable to molecular analysis than a murine model.

Previously it has been shown that 3T3-L1 preadipocytes can be seeded into collagen I scaffolds and differentiated into mature adipocytes to synthesise a synthetic fat pad (Davidenko et al. 2010). Moreover, this synthetic fat pad has been shown to support 3D culture of the KIM-2 murine mammary epithelial cell line that accurately mimics the epithelial and stromal features of the mammary gland (Campbell et al., 2011). Using a synthetic fat pad, these experiments aimed to seed basal epithelial cells and assess whether they could populate the scaffold with both basal and luminal epithelial cells to form bi-layered structures, as obtained with KIM-2 cells, to recapitulate the potential of MaSCs/MRUs observed *in vivo*.

For these experiments, two mouse models were utilised: K14-cre$^{ERT2}$/ROSA26-tdTomato and Axin2-cre$^{ERT2}$/ROSA26-tdTomato transgenic mice. FACS sorted fluorescent basal cells were isolated from the mammary glands of these mice and then seeded into synthetic collagen fat pads. Their ability to generate both basal and epithelial lineages in a polarized bilayer was then assessed by IHC methods.

# 3.2 Results

## 3.2.1 Fluorescence activated cell sorting (FACS) strategy to isolate tdTomato$^+$ primary murine basal cells

The K14-cre$^{ERT2}$/Rosa26-tdTomato mouse model is a tamoxifen inducible system (Van Keymeulen et al., 2011; Wright et al., 2015). In this model, the enzyme Cre recombinase is expressed downstream of the K14 promoter in K14-expressing cells. Upon tamoxifen administration via injection or ingestion, Cre is activated in K14$^+$ cells. This results in removal of the floxed STOP cassette flanking tdTomato coding sequences inserted at the 'safe harbor' Rosa26 locus and subsequent constituent expression of the fluorescent protein tdTomato. Consequently, the progeny of K14$^+$ cells are permanently fluorescently tagged and their lineage can be traced. As K14 is exclusively expressed in basal mammary epithelial cells, fluorescently tagged daughter cells can be assumed to have arisen from a basal cell.

To isolate tdTomato$^+$ cells and to ensure they were from a basal epithelial origin, an established FACS protocol was utilized (Stingl et al., 2006). Initially, mice were injected with tamoxifen dissolved in sunflower oil to induce Cre-mediated recombination and tdTomato expression in K14$^+$ cells. Tamoxifen injections were carried out by Dr. Sara Pensa, University of Cambridge (Department of Pharmacology). Glands were then harvested, digested overnight, fat tissue removed, separated into single cells and stained for various cell surface markers before FACS.

Cells were first separated using FACS based on their size and granularity through analysis of their forward scatter and side scatter properties, respectively (Fig. 3.1a). As the cells of the mammary gland are highly heterogeneous in both size and granularity, no distinct populations of cells could be distinguished using this approach. However, cells (Fig. 3.1a, gate i) were able to be discerned from cell debris through gating at a minimum forward scatter and side scatter threshold and only sorting cells above that threshold. This purified the entire cell population from contaminating and possibly cytotoxic cellular debris.

Different mammary epithelial cell populations can be distinguished based upon their CD24 and CD49f cell surface marker expression (Stingl et al., 2006). Luminal cells can be demarcated by their CD24$^{hi}$ / CD49f$^{lo}$ expression and basal cells based by their CD24$^+$ / CD49f$^{med/hi}$ expression. Using these parameters, basal cells were then sorted from the general cell population (Fig. 3.1b, gate ii).

For the removal of contaminating blood lineage cells (Lin) and to ensure purity of the basal epithelial population, cells were stained for CD31, CD45 and TER119 to mark endothelial cells, leukocytes and erythrocytes, respectively (Stingl et al., 2006). The antibodies used for this process were biotinylated

and were all conjugated to a secondary PE-Cy7 antibody. This particular antibody was selected to avoid spectral overlap, as the Cy7 fluorophore emits in the far red spectra, at 767 nm, well beyond the emission spectra of tdTomato, at 581nm. Using this strategy, all cells that were negative for PE-Cy7 were classified as $Lin^-$ and were therefore sorted to enrich the epithelial population (Fig. 3.1c, gate iii). Furthermore, $tdTomato^+$ cells were isolated from the $Lin^-$ $CD24^+$ $CD49f^{med/hi}$ basal population based on their tdTomato expression (Fig. 3.1d, gate iv). All the aforementioned gating strategies were applied simultaneously (Fig. 3.1, gates i-iv) in a single FACS protocol to obtain $tdTomato^+$ $Lin^-$ $CD24^+$ $CD49f^{med/hi}$ basal cells from the entire mammary gland cell population.

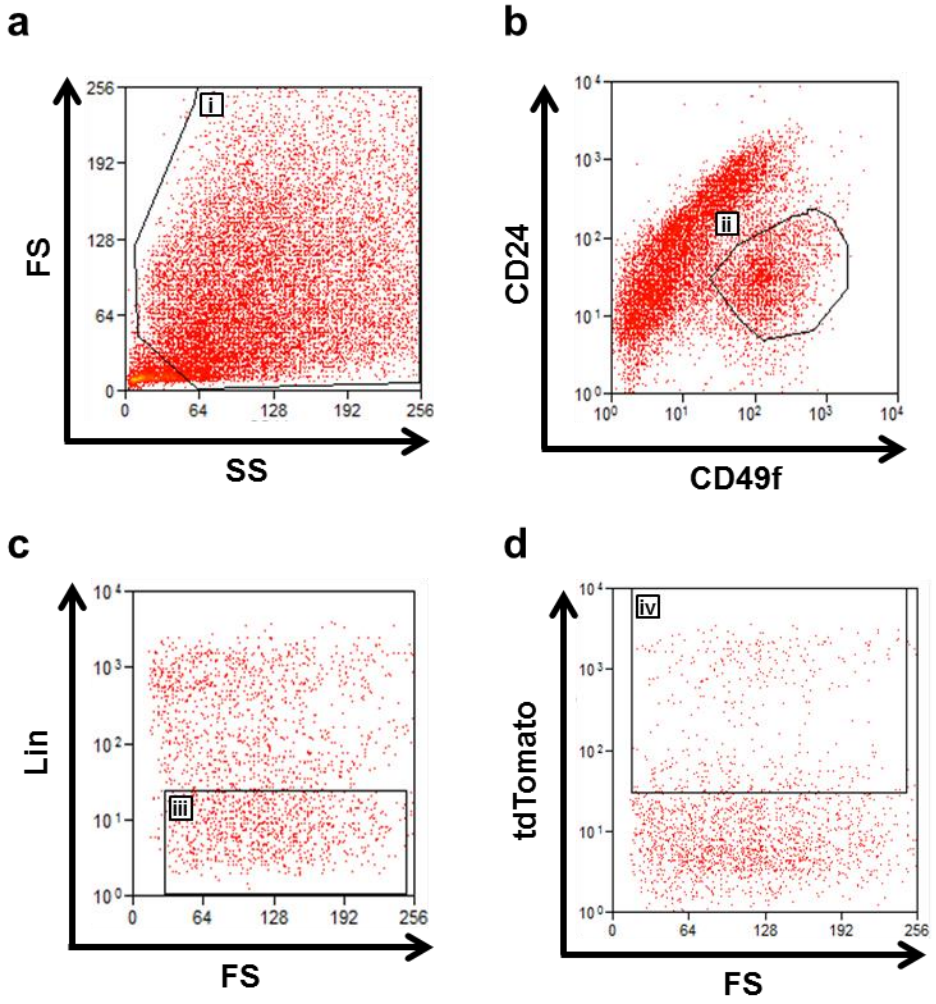


***Figure 3-1: Fluorescent activated cell sorting (FACS) of tdTomato$^+$ primary murine basal mammary epithelial cells***

Harvested and digested mammary glands from tamoxifen induced K14-cre$^{ERT2}$/Rosa26-tdTomato mice were FACS sorted to (a) remove cell debris, (b) separate basal epithelial cells from luminal epithelial cells, (c) remove hematopoietic lineage cells and (d) separate tdTomato$^+$ cells. (a) Entire cell population was gated (i) according to forward scatter and side scatter of incoming FACS laser light to remove cell debris. (b) Basal cells were gated (ii) according to their CD24$^+$/CD49f$^{hi}$ expression. (c) Blood lineage CD31/CD45/TER119 negative cells (Lin$^-$) cells were gated (iii). (d) tdTomato$^+$ cells were gated (iv) according to their tdTomato expression. tdTomato$^+$ Lin$^-$ CD24$^+$ CD49f$^{hi}$ primary murine basal epithelial cells were collected from the mammary gland population by applying gates i, ii, iii and iv simultaneously.

### 3.2.2 Optimising tdTomato$^+$ primary basal epithelial cell yields

FACS of mammary epithelium obtained from the glands of K14-cre$^{ERT2}$/Rosa26-tdTomato mice yielded approximately 300 tdTomato$^+$ basal epithelial cells per mouse (Fig. 3.2a). This low yield meant low cell numbers were available for 3D culture experiments. In an attempt to resolve this, subsequent experiments sought to optimise Cre recombination and therefore the number of tdTomato expressing cells in K14-cre$^{ERT2}$/Rosa26-tdTomato mice to produce higher yields.

Initial steps of the protocol to induce Cre recombinase activity *in vivo* involved dissolving tamoxifen in sunflower oil before administering to mice via intraperitoneal injection. Some studies follow this protocol whilst others opt for dissolving tamoxifen in corn oil as an alternative (Cellurale et al., 2012; Malhotra et al., 2014; Shehata et al., 2014; Wang et al., 2014a). It was therefore investigated whether this alternative method could increase yields. Unfortunately, this yielded similar results to sunflower oil with approximately 300 tdTomato$^+$ basal cells per mouse (Fig. 3.2b).

It was then hypothesised that taking the cells into 2D culture and treating *in vitro* would increase tdTomato$^+$ yields as tamoxifen would not have to pass through the murine bloodstream to reach target cells. Tamoxifen was therefore titrated *in vitro* following tamoxifen-sunflower oil injections, tamoxifen-corn oil injections or without any previous injections in mice, ranging from 0.1-500 µM for 24 or 48 hours (Fig. 3.2c, Table 3.1). IHC and FACS analysis all concluded that 10 µM for 48 hours was the optimal *in vitro* treatment regime. However, this only increased yields minimally from approximately 300 to 500 tdTomato$^+$ cells per mouse.

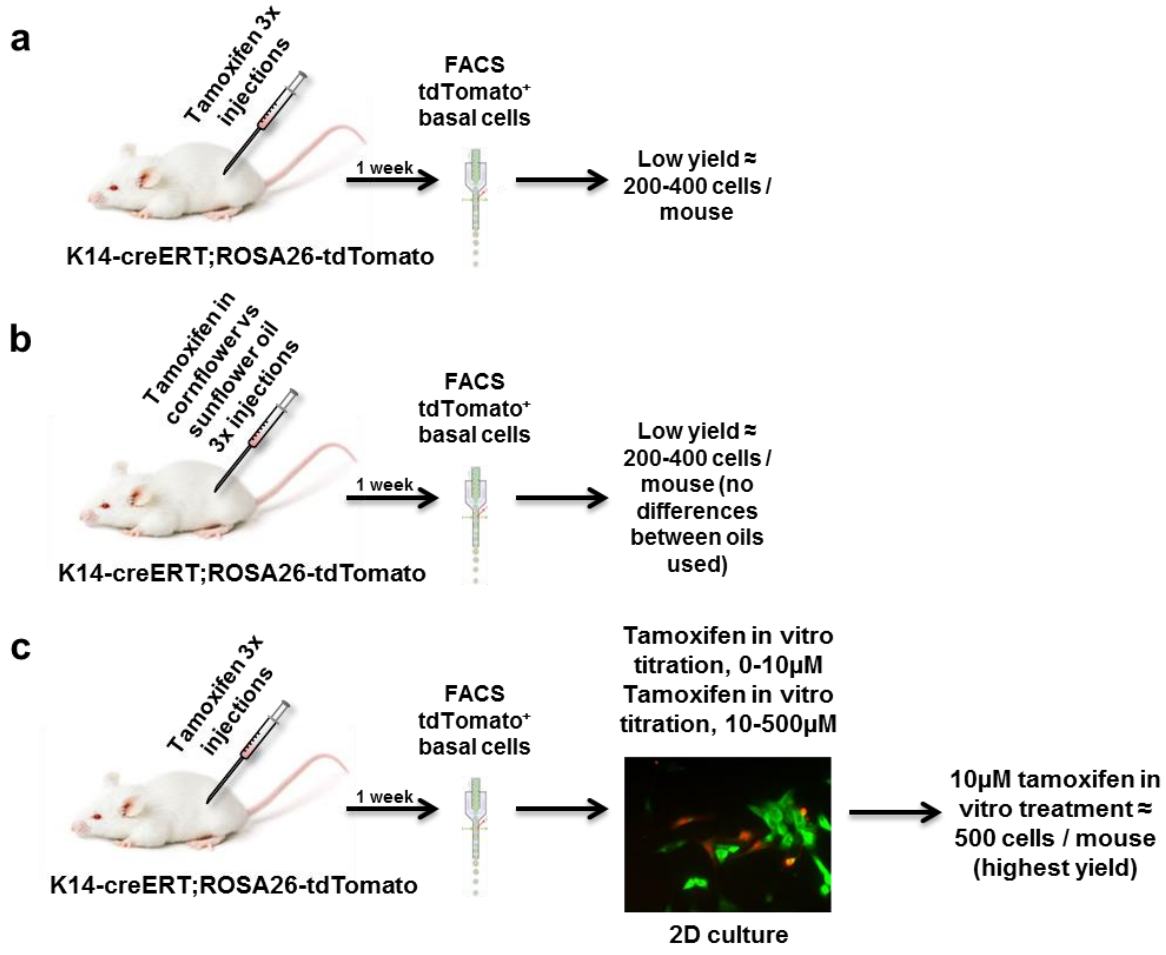


***Figure 3-2: Optimisation of tamoxifen administration in vivo and in vitro***

K14-cre$^{ERT2}$/Rosa26-tdTomato mice were injected with tamoxifen to induce Cre recombination and tdTomato expression in K14$^{+}$ basal mammary epithelial cells. K14$^{+}$tdTomato$^{+}$ cells were then separated from the mammary gland population by FACS. Above are schematics illustrating the different techniques involving the optimisation of tamoxifen administration. (a) Initial experiments show low yields of tdTomato$^{+}$ cells from FACS. (b) Comparison of tamoxifen dissolved in cornflower oil versus sunflower oil showed no differences in yields. (c) *In vitro* tamoxifen titration and fluorescence microscopy imaging of tdTomato (red) expression and anti-K14 antibody staining (green) showed small increase in yields.

| **In vivo tamoxifen treatment** | **In vitro tamoxifen treatment (µM)** | **Time of tamoxifen treatment *in vitro* (hours)** | **IHC** | **Flow Cytometry** | **Optimal tamoxifen treatment** |
|---|---|---|---|---|---|
| Corn Oil* | Vehicle, 0.1, 0.25, 0.5, 1.0, 2.5, 5.0, 10.0 | 24, 48 | Yes | No | 10 µM, 48 hours |
| Sunflower Oil* | Vehicle, 0.1, 0.25, 0.5, 1.0, 2.5, 5.0, 10.0 | 24, 48 | Yes | No | 10 µM, 48 hours |
| None | Vehicle, 10, 50, 100, 150, 200, 500 | 24, 48 | No | Yes | 10 µM, 48 hours |

***Table 3-1: Tamoxifen titration of primary mammary epithelial cells from K14-cre$^{ERT2}$/Rosa26-tdTomato mammary glands in vitro***

Table representing the various *in vivo* tamoxifen treatments (*3 injections, 4 mg/injection over the course of 7 days) of K14-cre$^{ERT2}$/Rosa26-tdTomato mice and the corresponding *in vitro* tamoxifen titration to optimise tdTomato$^{+}$ cell yields following FACS.

### 3.2.3 tdTomato$^+$ basal cells in collagen scaffolds invested with adipocytes

Using a previously published protocol in combination with fluorescently tagged copGFP 3T3-L1 preadipocytes, synthetic fat pads were synthesised (Fig. 3.3, bottom, Fig. 3.4a, green) (Campbell et al., 2011; Davidenko et al., 2010). Following this, Lin$^-$ CD24$^+$ CD49f$^{med/hi}$ tdTomato$^+$ basal cells were isolated from the glands of K14-cre$^{ERT2}$/Rosa26-tdTomato mice by FACS after *in vivo* tamoxifen injections and tamoxifen treatment *in vitro* (Fig. 3.3, top). These tdTomato$^+$ cells were then seeded into the synthetic fat pad, cultured for 2 weeks, fixed and whole mount immunostained for analysis (Fig. 3.3, top).

Confocal microscopy z-stacks revealed that tdTomato$^+$ basal cells were able to form 3D ring-like structures (Fig. 3.4a, red) within the synthetic fat pad (Fig. 3.4a, green). The long thin morphology of these cells was typical of basal mammary epithelial cells *in vivo*. However, no cells observed exhibited a columnar luminal cell morphology. Interestingly, although cells did not have a luminal morphology some tdTomato$^+$ cells (Fig. 3.4b, red) did express the luminal cell marker K18 (Fig. 3.4b, green, white arrows). Due to low cell yields and an incomplete epithelial bilayer formation it was decided to discontinue experiments involving the K14-cre$^{ERT2}$/Rosa26-tdTomato mice.

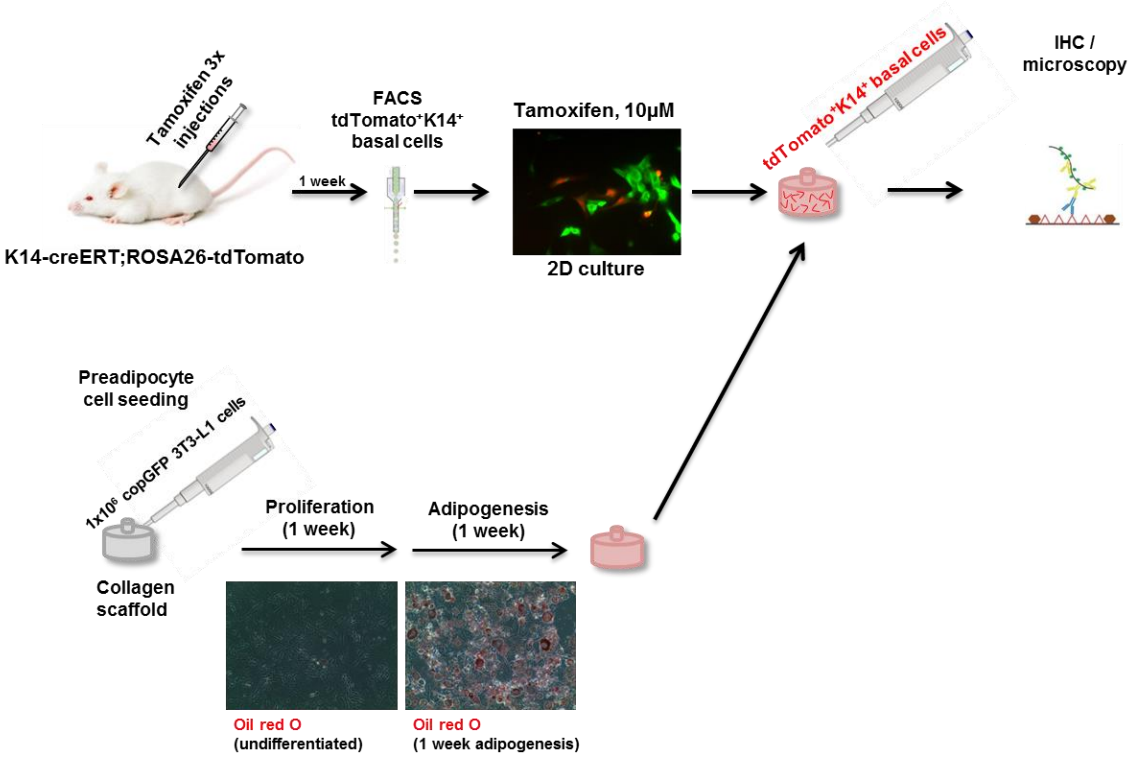


***Figure 3-3: Schematic of tdTomato+ basal cell culture in adipocyte invested collagen scaffolds***

K14-cre$^{ERT2}$/Rosa26-tdTomato mice were injected with tamoxifen to induce Cre recombination and tdTomato expression in K14$^{+}$ basal mammary epithelial cells. tdTomato$^{+}$ cells were then separated from the mammary gland population by FACS and treated *in vitro* with 10 µM tamoxifen (top left). A synthetic fat pad was generated via seeding of 3T3-L1 preadipocyte cells into collagen scaffolds and differentiation into mature adipocytes (bottom left). Oil red O lipid soluble dye shows increased lipid content in differentiated 3T3-L1 cells during 2D culture (bottom left). tdTomato$^{+}$ cells were then seeded into synthetic fat pads followed by confocal microscopy analysis (top right).

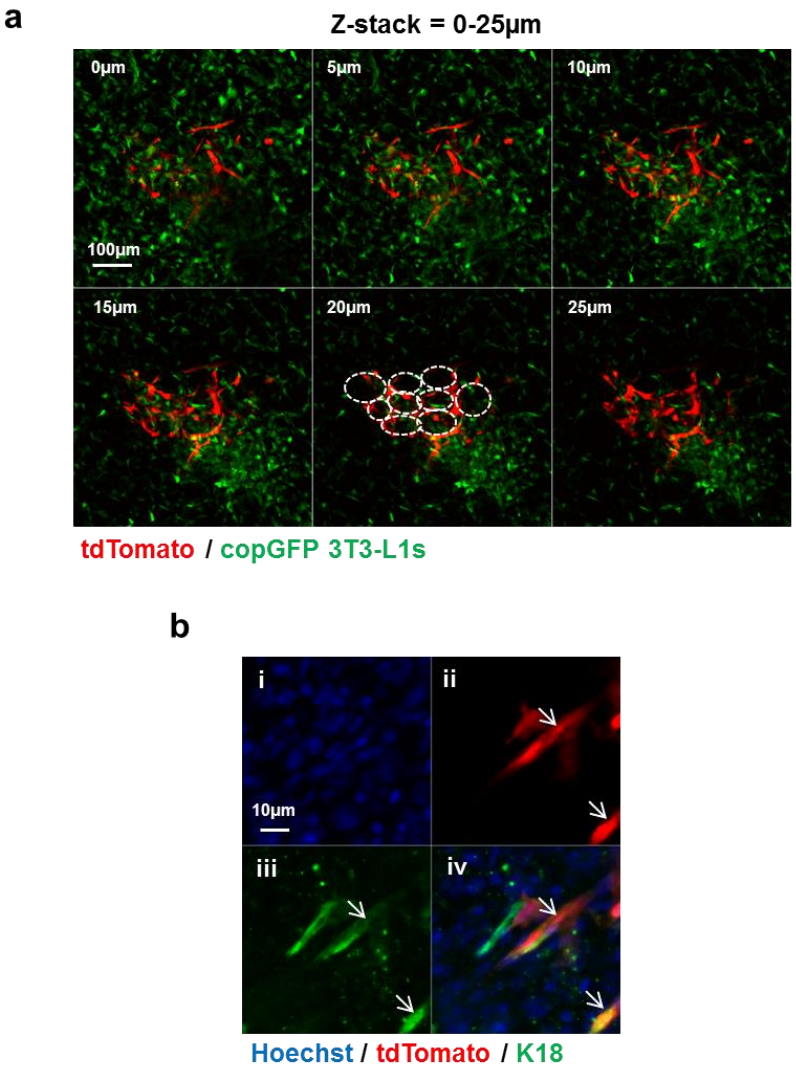


***Figure 3-4: tdTomato$^{+}$ basal cells form rings in synthetic fat pads and can express the luminal marker cytokeratin-18 (K18)***

tdTomato$^{+}$ basal cells that had been FACS sorted from tamoxifen induced K14-cre$^{ERT2}$/Rosa26-tdTomato murine mammary glands, were seeded into collagen scaffolds invested with differentiated 3T3-L1 cells (adipocytes) and showed varying structures during confocal microscopy analysis. (a) Confocal microscopy z-stacks show tdTomato$^{+}$ basal cells (red) with fluorescently labelled copGFP 3T3-L1 adipocytes (green) formed ring-like structures (dotted white lines). (b) Whole mount immunofluorescence on these scaffolds for luminal marker cytokeratin-18 (K18, green) and confocal analysis shows dual positive tdTomato$^{+}$ (red) K18$^{+}$ (green) cells (marked with white arrows). (a,b) DNA is marked with Hoechst dye (blue).

### 3.2.4 Expansion of tdTomato$^+$ cells from an Axin2$^+$ basal mammary epithelial cell origin

During both development and in adult homeostasis, Wnt signalling has been shown to be involved in regulating stem cell maintenance and differentiation in a range of tissues (Bowman et al., 2013; Choi et al., 2013; Chu et al., 2004; Pinto et al., 2003; Zhang et al., 2008). Previously, lineage tracing has shown that Wnt/β-catenin-responsive Axin2$^+$ cells within the mammary gland have a varied contribution to both basal and luminal epithelial lineages, that is dependent on developmental stage (van Amerongen et al., 2012). Furthermore, it was shown that upon fat pad transplantation, Wnt/β-catenin responsive Axin2$^+$ cells behave as multipotent MaSC/MRUs, capable of repopulating the gland with an epithelial bilayer comprising both basal and luminal cells.

Subsequent experiments involved the isolation and culture of Wnt-responsive Axin2$^+$ basal epithelial cells in synthetic fat pads to assess whether they could provide higher yields during FACS and generate bi-layered epithelial structures from a basal cell population. Furthermore, it was intended that these cells would be expanded in 2D culture to increase the potential for further 3D experiments. For this purpose, the Axin2-cre$^{ERT2}$/Rosa26-tdTomato mouse model was utilized (van Amerongen et al., 2012; Yan et al., 2017). Upon tamoxifen administration to these mice, Cre recombinase was activated in Axin2$^+$ cells resulting in the expression of tdTomato from the Rosa26 locus. Consequently, tdTomato$^+$ cells and their progeny were permanently fluorescently tagged and lineage traced.

Following intraperitoneal tamoxifen injections, mammary glands from Axin2-cre$^{ERT2}$/Rosa26-tdTomato mice were harvested and Lin$^-$ CD24$^+$ CD49f$^{med/hi}$ tdTomato$^+$ basal cells were sorted using the same FACS protocol outlined in Figure 3.1. FACS analysis revealed that yields were improved from the 300 cells per mouse observed in K14-cre$^{ERT2}$/Rosa26-tdTomato mice (without *in vitro* treatment), to approximately 10,000 cells per mouse in Axin2-cre$^{ERT2}$/Rosa26-tdTomato (Fig. 3.5a).

To expand cells in culture a previously published protocol was utilized (Prater et al., 2014). This involved culturing cells on Matrigel coated plates with feeder cells and media containing the rho-associated protein kinase inhibitor (ROCKi), Y-27632 (Fig. 3.5b). In this study, Matrigel was used to increase cell attachment whilst feeder cells provided growth factors to help cells survive and proliferate (Hongisto et al., 2012). Media was supplemented with ROCKi because it has previously been shown to increase cellular proliferation, reduce apoptosis and maintain stemness in cell cultures (Koyanagi et al., 2008; Piltti et al., 2015; Prater et al., 2014; Yu et al., 2012). Using this method, cells from 3 mice were expanded and passaged to increase cell numbers 805 times from 31,068 to 25,020,800 tdTomato$^+$ cells (Fig. 3.5c). Successful expansion of cells permitted

considerably higher numbers of cells to be used in 3D cultures to increase the likelihood of organoid formation. Moreover, a higher number of repeats could therefore be carried out and vials of tdTomato$^{+}$ cells were frozen for future experiments.

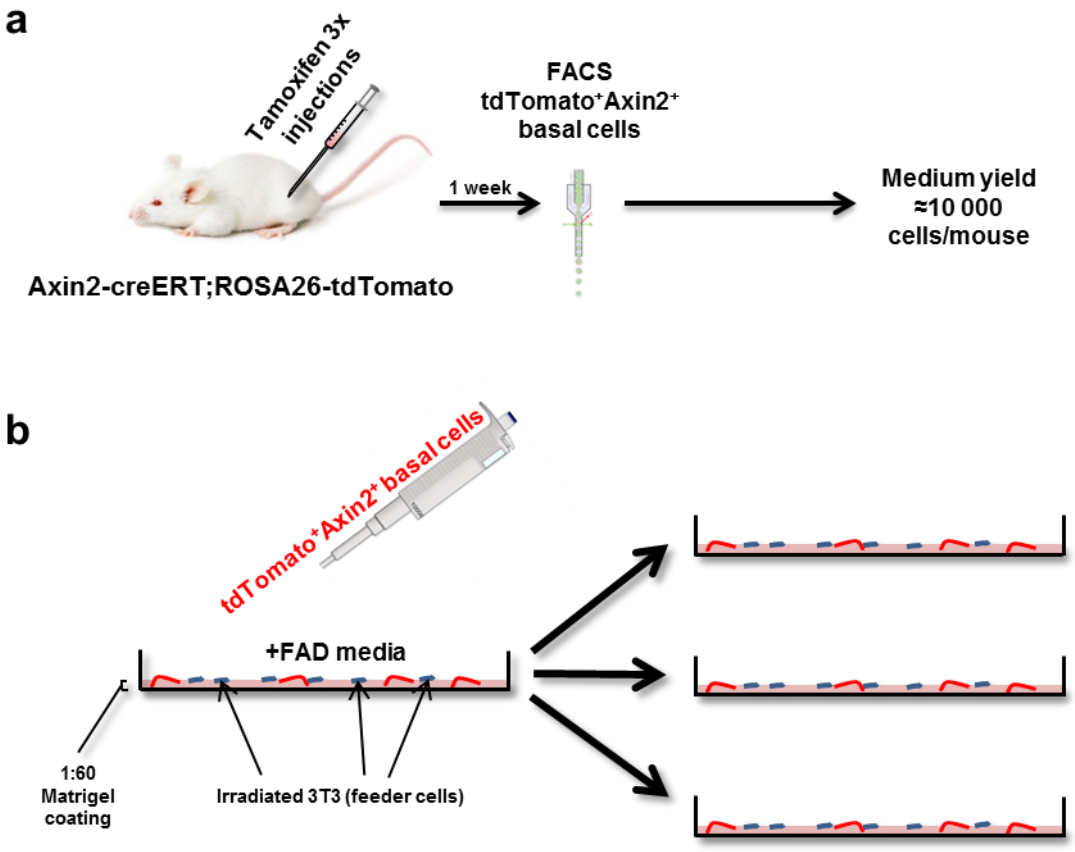


c

| Number of mice | Number of FACS tdT⁺Axin2⁺Lin⁻ cells | Number of tdT⁺Axin2⁺Lin⁻ cells after expansion |
|---|---|---|
| 3 | 31,068 | 25,020,800 |

***Figure 3-5: Expansion of tdTomato⁺ basal cells from Axin2-cre$^{ERT2}$/Rosa26-tdTomato mice in vitro***

(a) Axin2-cre$^{ERT2}$/Rosa26-tdTomato mice were injected with tamoxifen to induce Cre recombination in Wnt-responsive Axin2$^{+}$ cells and tdTomato expression in this cell population. Mammary glands were harvested, digested and FACS sorted for tdTomato$^{+}$ basal cells, providing yields of approximately 10,000 cells per mouse. (b) Schematic showing *in vitro* expansion of FACS sorted tdTomato$^{+}$ basal cells using a feeder layer, Matrigel coating and FAD media. (c) Number of tdTomato$^{+}$ basal cells following *in vitro* expansion.

### 3.2.5 tdTomato$^+$ primary cells from Axin2-cre$^{ERT2}$/Rosa26-tdTomato mice rarely form bi-layered structures in adipocyte invested collagen scaffolds

As tdTomato$^+$ cells were successfully FACS sorted from the basal population of the Axin2-cre$^{ERT2}$/Rosa26-tdTomato glands, this section focussed on investigating whether tdTomato$^+$ cells from an Axin2$^+$ basal cell origin could generate bi-layered epithelial structures in our 3D model. To assess this, expanded cells were seeded and cultured in synthetic fat pads. Whole mount immunostaining was then applied to fixed scaffolds and imaged using confocal microscopy. The basal marker αSMA was used to delineate basal epithelial cells from other cell types (Fig. 3.6-3.11).

Using the aforementioned 3D culture protocol a number of different structures were formed (Fig. 3.6-3.11). Notably, tdTomato$^+$ structures that morphologically resembled aspects of *in vivo* ductal structures were observed (Fig. 3.6-3.9). These were relatively infrequent events and were discovered approximately 0-1 times per scaffold imaged. Within these structures two cell types emerged: long thin cells resembling a basal cell morphology that were dual positive for tdTomato and the basal marker αSMA (Fig. 3.6, white arrows) and rounder cells single positive for tdTomato that more closely resembled a luminal morphology (Fig. 3.6, white arrowheads). Z-stacks revealed tdTomato$^+$ αSMA$^+$ cells were located surrounding single positive tdTomato$^+$ cells in a similar manner to αSMA$^+$ basal cells surrounding luminal cells in ductal structures *in vivo* (Fig. 3.7, Fig. 3.8). A depth colour coded z-projection of the tdTomato channel from Figure 3.8 demonstrates tdTomato$^+$ structures could reach sizes of >400 µm long, >100 µm wide and >130 µm deep (Fig. 3.9).

Another notable structure that was observed, although also infrequently at approximately 1 in 5 scaffolds, was a "terminal end bud" structure. This resembled some aspects of the *in vivo* morphology of a terminal end bud, a structure located at the ends of ductal structures in the virgin pubertal gland (Fig. 3.10). Dual positive thin long tdTomato$^+$ αSMA$^+$ cells were observed wrapped around single positive tdTomato$^+$ cells in a spherical structure, similar to αSMA$^+$ basal cells wrapped around luminal cells at the end of a duct in a terminal end bud (Fig. 3.10).

The majority of structures formed by tdTomato$^+$ cells from an Axin2$^+$ basal cell origin in synthetic fat pads appeared to be disorganised with no visible epithelial bilayer (Fig. 3.11). Long thin tdTomato$^+$ cells with a basal morphology were often observed to be single positive and did not express the basal marker αSMA (Fig. 3.11a,b). Additionally, long thin dual positive tdTomato$^+$ αSMA$^+$ cells often formed long thin structures with no single positive tdTomato$^+$ cells nor any cells resembling a luminal morphology (Fig. 3.11c,d). Moreover, disorganised masses of cells were also observed with no specific localisation of tdTomato or αSMA expression (Fig. 3.11e-h).

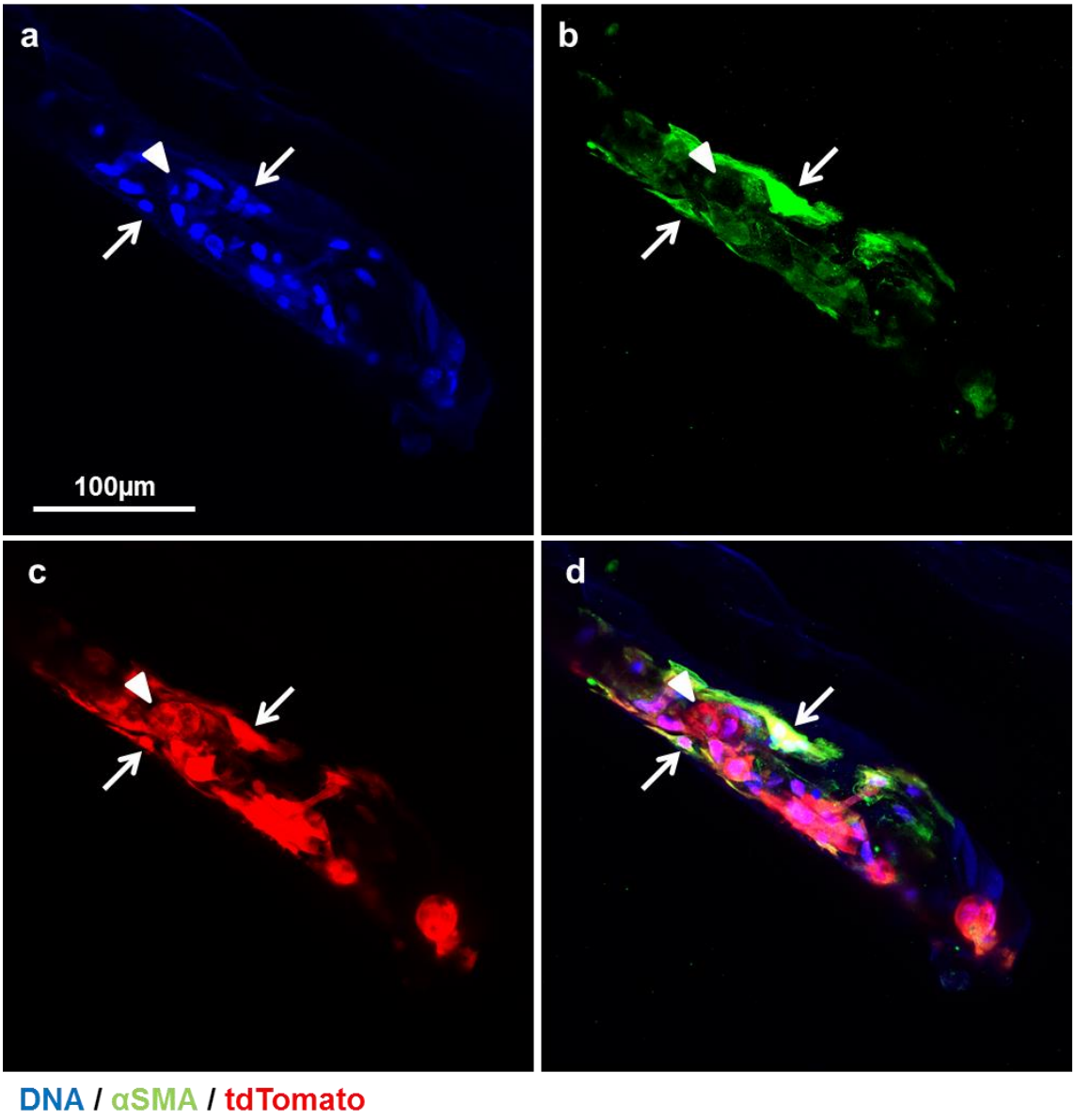


***Figure 3-6: Bilayered tdTomato$^{+}$ "ductal-like" structure in adipocyte invested scaffold***

Axin2-cre$^{ERT2}$/Rosa26-tdTomato mice were injected with tamoxifen to induce Cre recombination in Wnt-responsive Axin2$^{+}$ cells and tdTomato expression in this cell population. Mammary glands were harvested, digested and FACS sorted for tdTomato$^{+}$ basal cells. These cells were then seeded into collagen scaffolds invested with differentiated 3T3-L1 cells, fixed and whole mount immunofluorescence stained. Images shown are confocal image channels of (a) DNA marked with Hoechst - blue, (b) α-smooth muscle actin (αSMA) - green, (c) tdTomato - red and (d) merged image. Dual positive tdTomato$^{+}$ αSMA$^{+}$ cells are marked with white arrows. Single positive tdTomato$^{+}$ cells are marked with a white arrowhead.

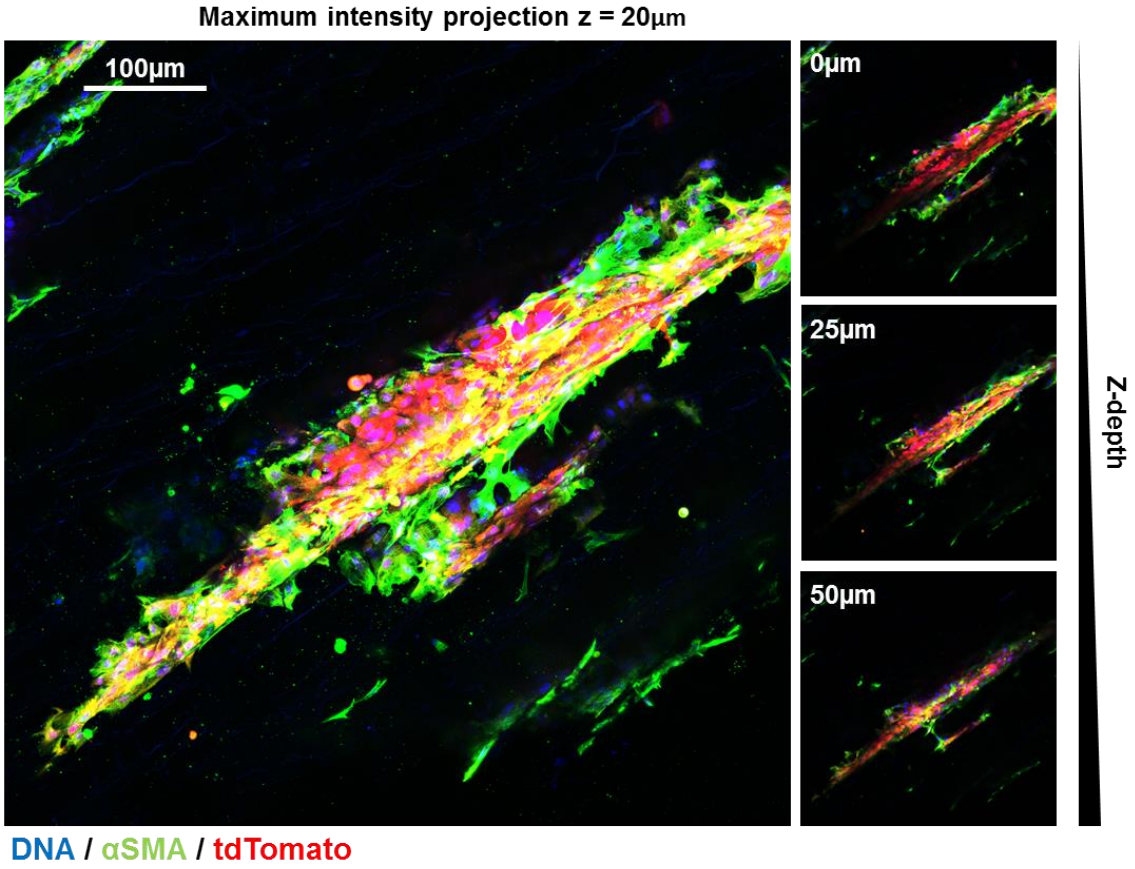


***Figure 3-7: Bilayered tdTomato$^{+}$ "ductal-like" structure in adipocyte invested scaffold – z-stack***

Axin2-cre$^{ERT2}$/Rosa26-tdTomato mice were injected with tamoxifen to induce Cre recombination in Wnt-responsive Axin2$^{+}$ cells and tdTomato expression in this cell population. Mammary glands were harvested, digested and FACS sorted for tdTomato$^{+}$ basal cells. These tdTomato$^{+}$ cells (red) were then seeded into collagen scaffolds invested with differentiated 3T3-L1 cells, fixed, whole mount immunofluorescence stained for α-smooth muscle actin (αSMA) – green and imaged using confocal microscopy. DNA is marked with Hoechst in blue. A 50 µm z stack is represented as a maximum intensity projection (left) and individual z-sections from the top (0 µm), middle (25 µm) and bottom (50 µm) of the z-stack (right).

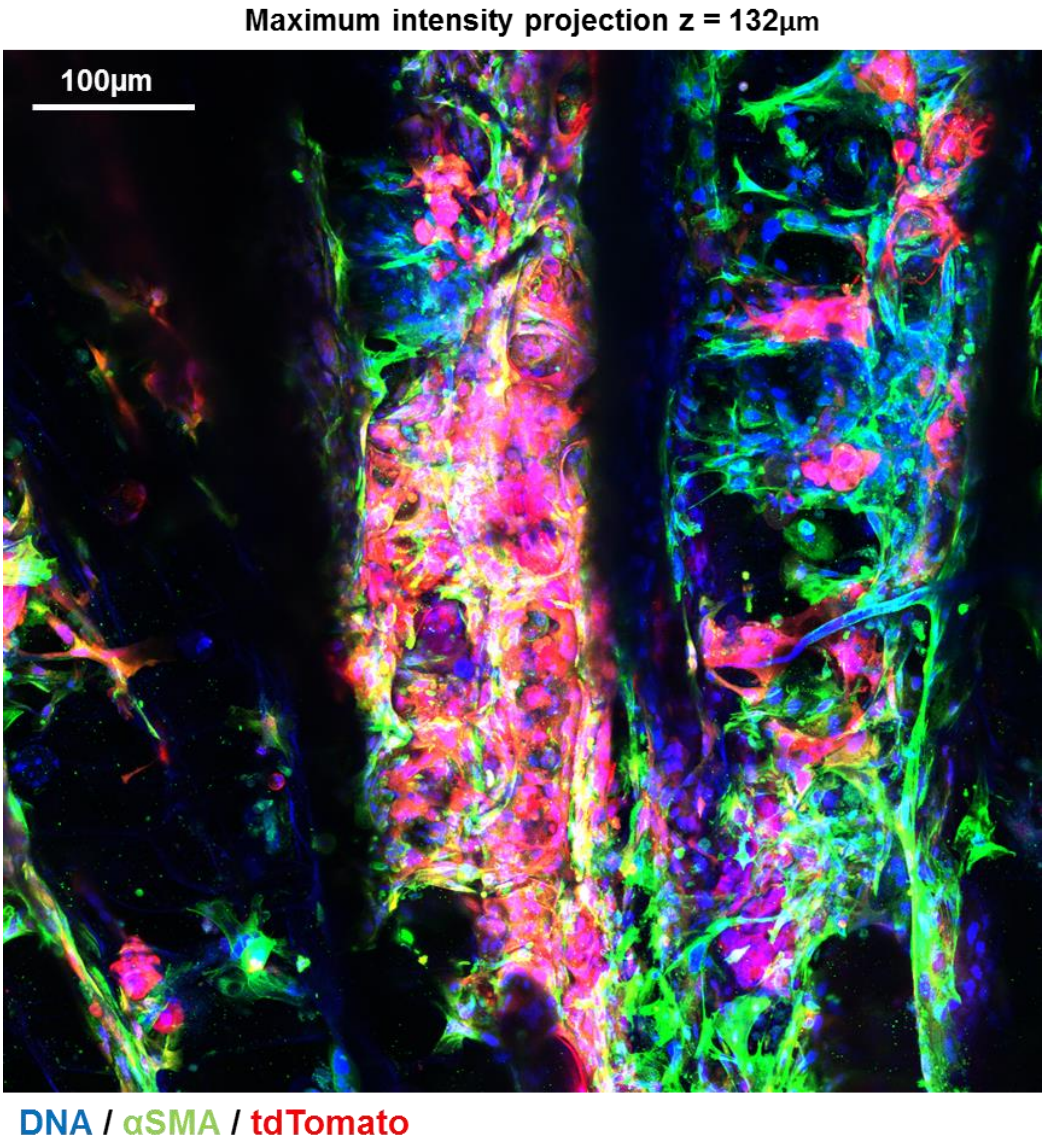


***Figure 3-8: Bilayered tdTomato$^{+}$ structure in adipocyte invested scaffold – z-stack 2***

Axin2-cre$^{ERT2}$/Rosa26-tdTomato mice were injected with tamoxifen to induce Cre recombination in Wnt-responsive Axin2$^{+}$ cells and tdTomato expression in this cell population. Mammary glands were harvested, digested and FACS sorted for tdTomato$^{+}$ basal cells. These tdTomato$^{+}$ cells (red) were then seeded into collagen scaffolds invested with differentiated 3T3-L1 cells, fixed, whole mount immunofluorescence stained for α-smooth muscle actin (αSMA) (green) and imaged using confocal microscopy. DNA is marked with Hoechst (blue). A 132 µm z stack is represented as a maximum intensity projection.

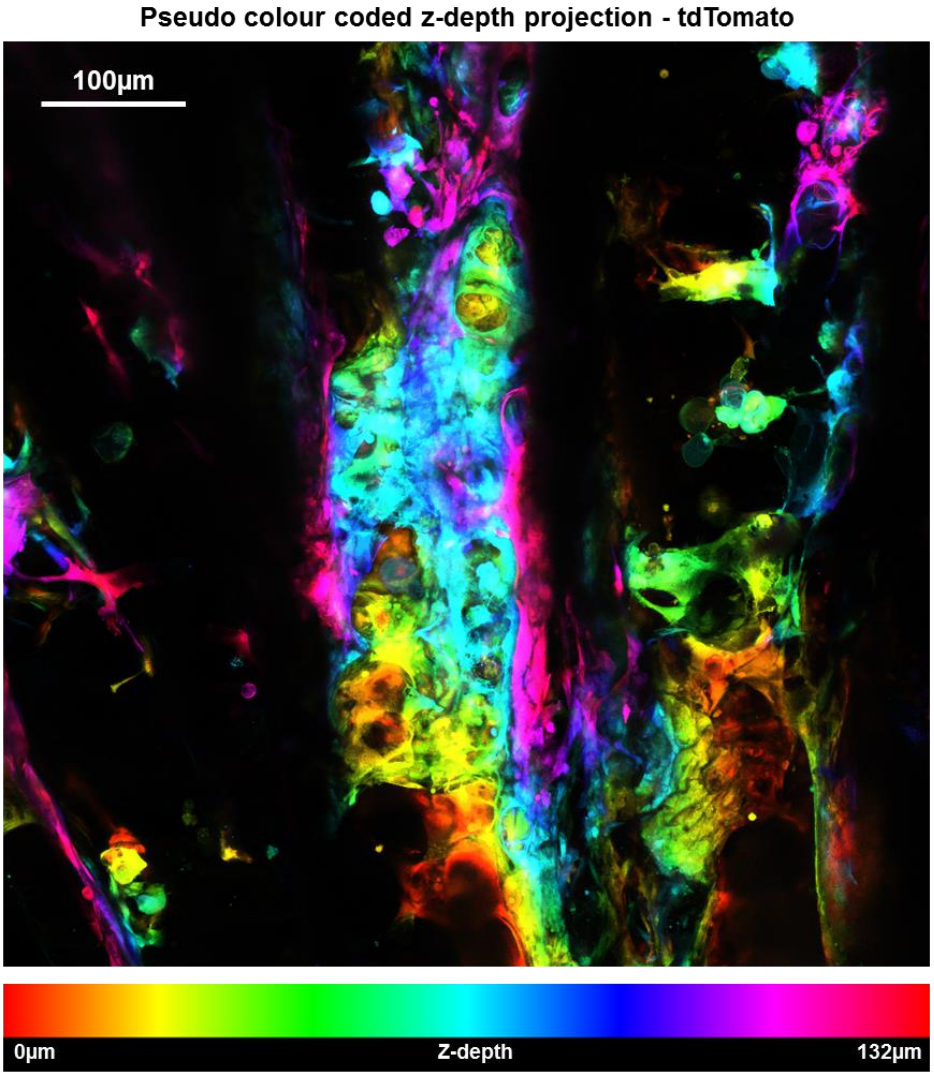


***Figure 3-9: Bilayered tdTomato$^{+}$ structure in adipocyte invested scaffold – pseudo-coloured z-depth projection***

The tdTomato channel from Figure 3.8 has been projected alone with its z-depth projected as a colour spectrum ranging from 0-132 µm (see colour coded key at the bottom of the image).

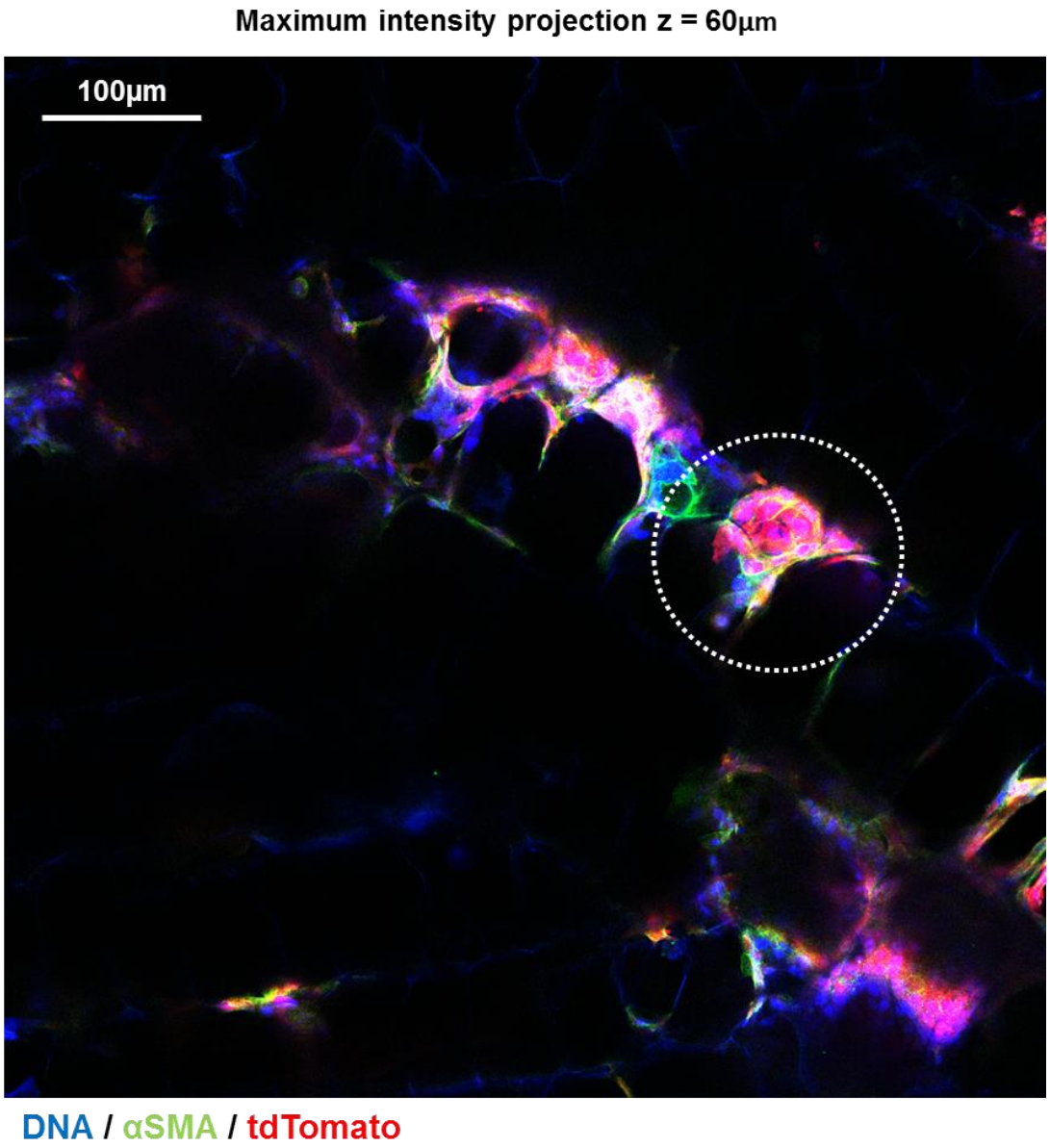


***Figure 3-10: Bilayered tdTomato$^{+}$ "terminal end bud" structure in adipocyte invested scaffold – z-stack***

Axin2-cre$^{ERT2}$/Rosa26-tdTomato mice were injected with tamoxifen to induce Cre recombination in Wnt-responsive Axin2$^{+}$ cells and tdTomato expression in this cell population. Mammary glands were harvested, digested and FACS sorted for tdTomato$^{+}$ basal cells. These tdTomato$^{+}$ cells (red) were then seeded into collagen scaffolds invested with differentiated 3T3-L1 cells, fixed, whole mount immunofluorescence stained for α-smooth muscle actin (αSMA) (green) and imaged using confocal microscopy. DNA is marked with Hoechst (blue). A "terminal end bud" structure is marked with a white dotted line. 60 µm z-stack is represented as a maximum intensity projection.

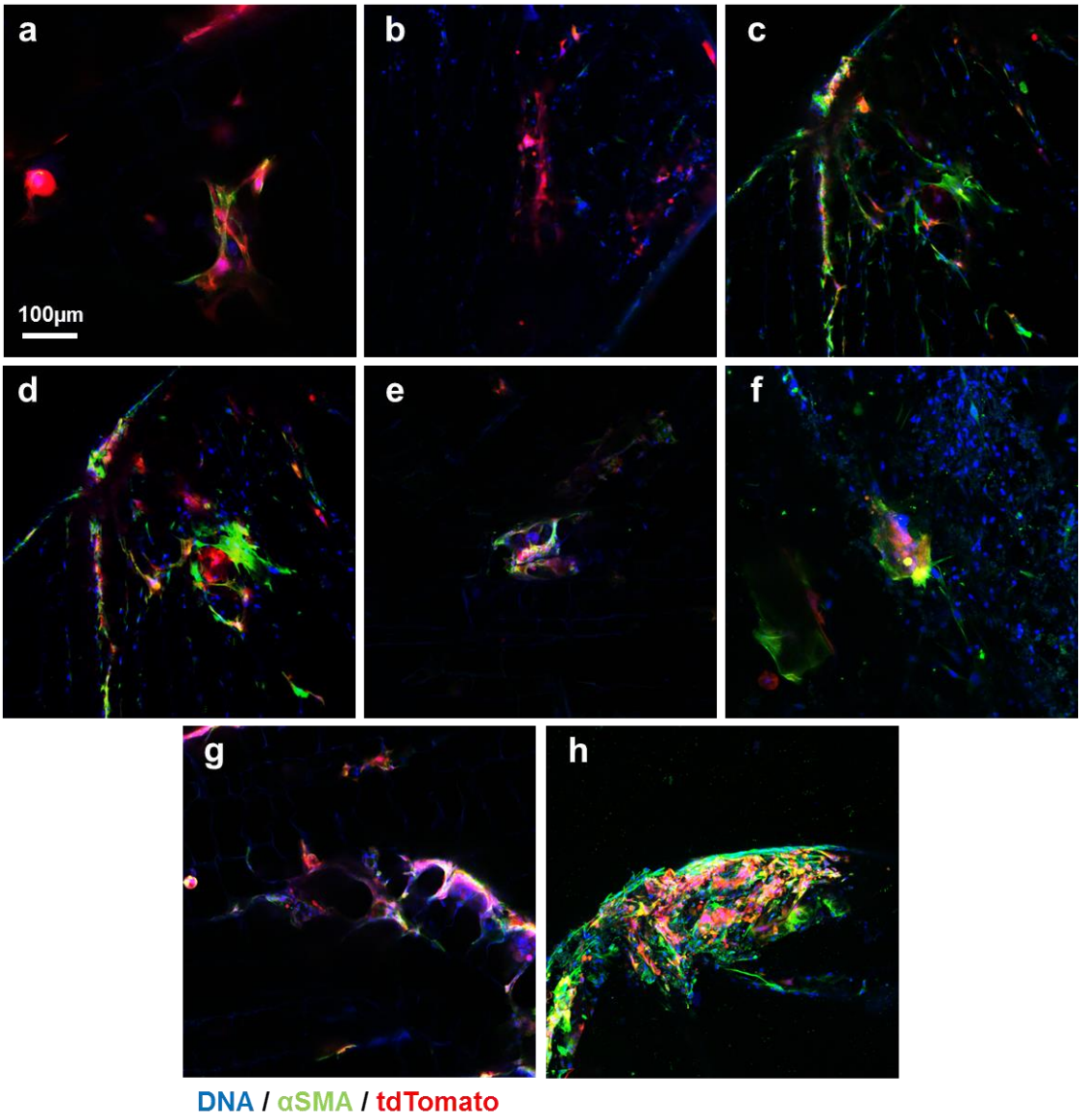


***Figure 3-11: tdTomato$^{+}$ cells from an Axin2$^{+}$ basal cell origin frequently form non-polarized disorganised structures in adipocyte invested collagen scaffolds***

Axin2-cre$^{ERT2}$/Rosa26-tdTomato mice were injected with tamoxifen to induce Cre recombination in Wnt-responsive Axin2$^{+}$ cells and tdTomato expression in this cell population. Mammary glands were harvested, digested and FACS sorted for tdTomato$^{+}$ basal cells. These tdTomato$^{+}$ cells (red) were then seeded into collagen scaffolds invested with differentiated 3T3-L1 cells, fixed, whole mount immunofluorescence stained for α-smooth muscle actin (αSMA) (green) and imaged using confocal microscopy. DNA is marked with Hoechst (blue). (a-h) represent various disorganised tdTomato$^{+}$ structures observed during confocal microscopy.

### 3.2.6 Structures formed tdTomato$^+$ cells from an Axin2$^+$ basal cell origin do not express luminal cell markers

Some structures formed by tdTomato$^+$ cells from an Axin2$^+$ basal cell origin comprised cells resembling a luminal epithelial morphology and did not express the basal marker αSMA. To verify if they were in fact luminal cells that had differentiated from an Axin2$^+$ basal cell origin, samples were stained with the luminal markers K18 and β-catenin. Expression of these proteins was expected to be located in the cytoplasm and cell membranes of luminal cells for K18 and β-catenin staining, respectively.

Unfortunately, K18 expression was not observed in any sample containing tdTomato$^+$ cells upon IHC analysis (Fig. 3.12). In contrast, β-catenin was observed in tdTomato$^+$ structures with some anticipated membranous expression (Fig. 3.13). However, this expression was not restricted to cells with a luminal morphology and was also observed in cells with a basal morphology (Fig. 3.13). Furthermore, there was some cytoplasmic β-catenin expression and no distinct pattern was discerned (Fig. 3.13). These data demonstrate that Axin2$^+$ cells from a basal epithelial origin within our 3D model were unable to correctly form a bi-layered epithelium with the accurate localisation of basal and luminal cell markers.

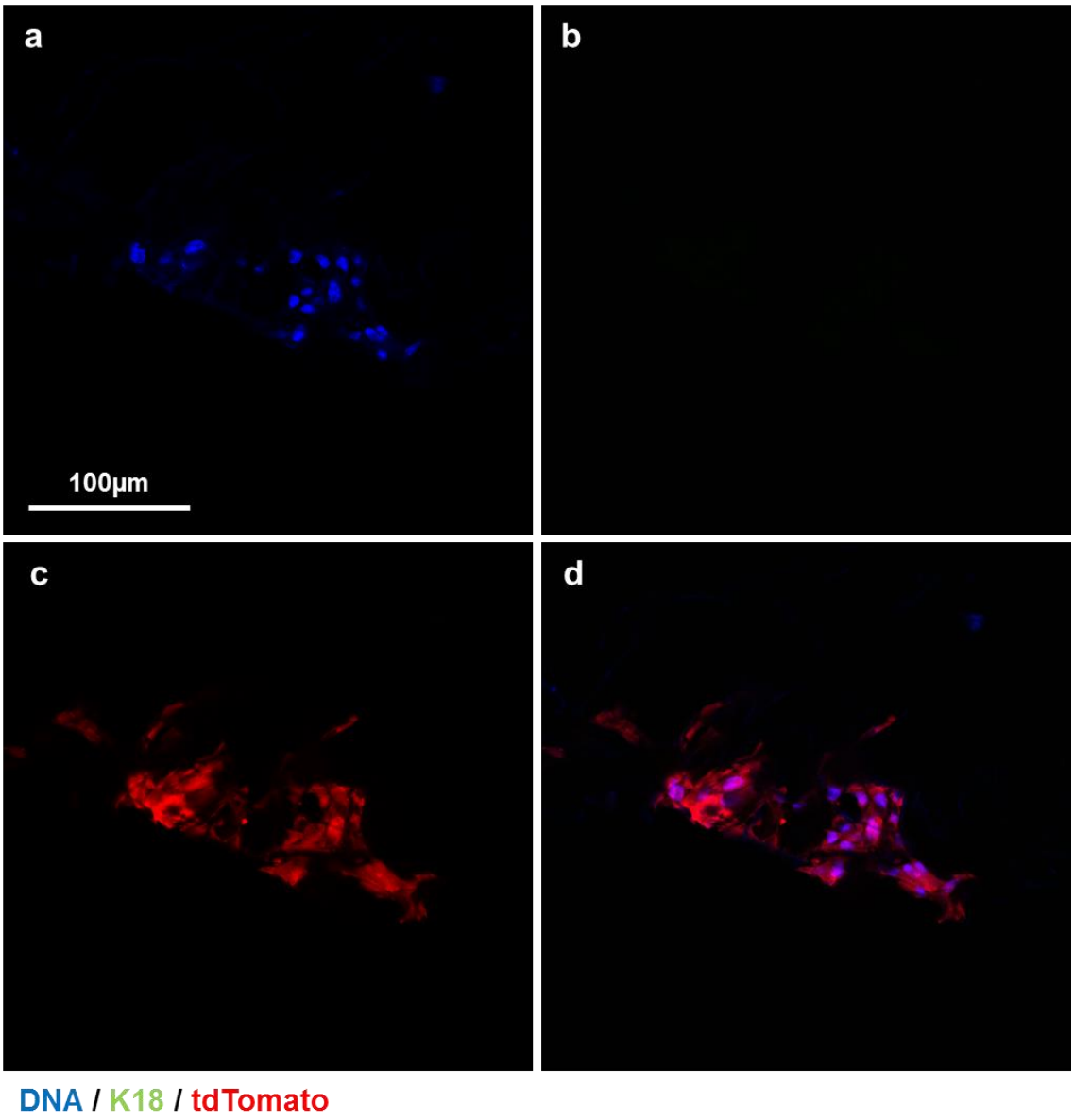


***Figure 3-12: tdTomato$^{+}$ structures do not express luminal marker cytokeratin-18 (K18)***

Axin2-cre$^{ERT2}$/Rosa26-tdTomato mice were injected with tamoxifen to induce Cre recombination in Wnt-responsive Axin2$^{+}$ cells and tdTomato expression in this cell population. Mammary glands were harvested, digested and FACS sorted for tdTomato$^{+}$ basal cells. These tdTomato$^{+}$ cells (red) were then seeded into collagen scaffolds invested with differentiated 3T3-L1 cells, fixed, whole mount immunofluorescence stained for Cytokeratin-18 (K18, green) and imaged using confocal microscopy. DNA is marked with Hoechst (blue). Confocal microscopy images shown are (a) DNA marked with Hoechst - blue, (b) K18 - green, (c) tdTomato - red and (d) merged image. No K18$^{+}$ cells were detected.

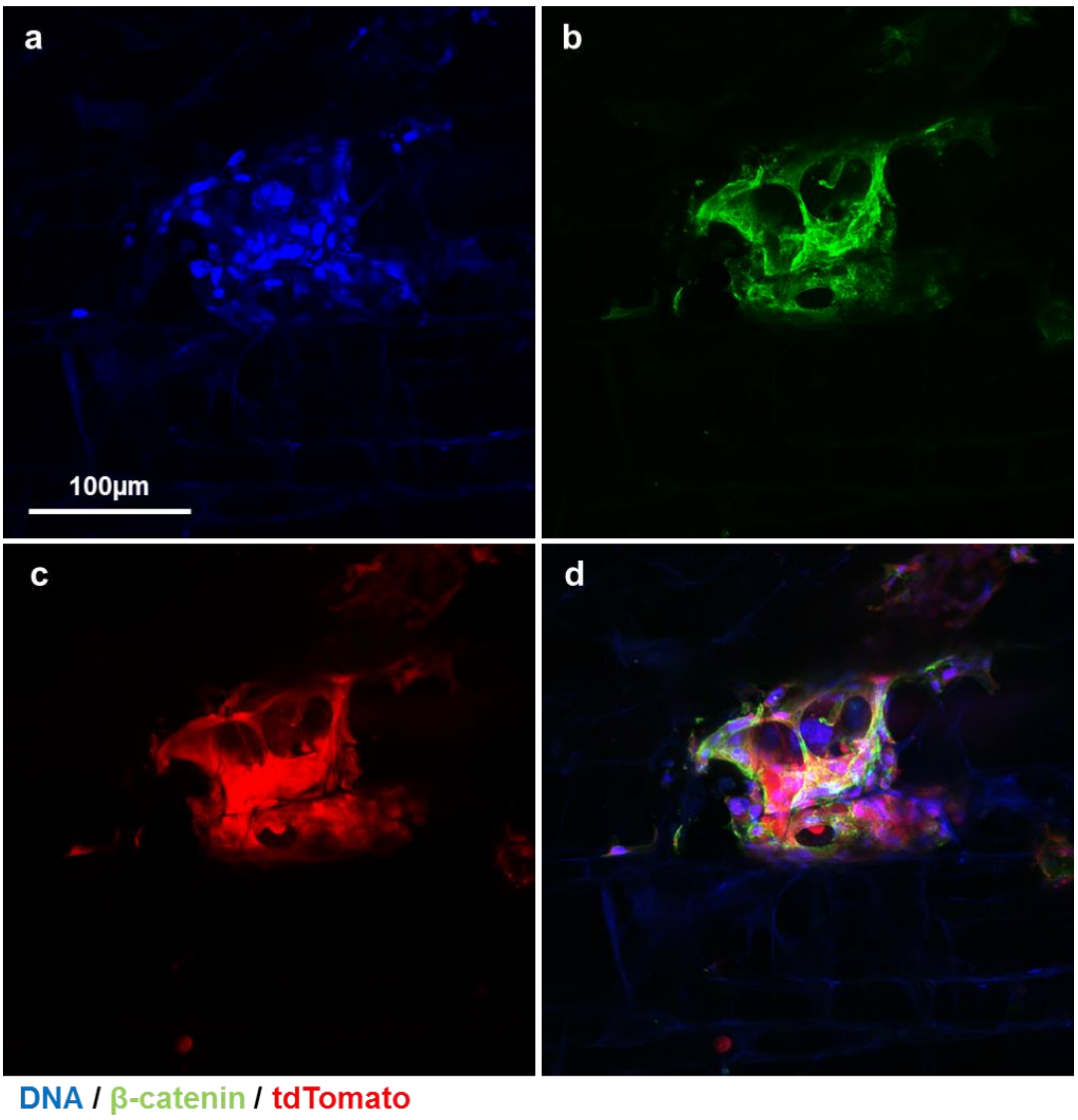


***Figure 3-13: tdTomato$^{+}$ structures do not express β-catenin in a typical luminal location***

Axin2-cre$^{ERT2}$/Rosa26-tdTomato mice were injected with tamoxifen to induce Cre recombination in Wnt-responsive Axin2$^{+}$ cells and tdTomato expression in this cell population. Mammary glands were harvested, digested and FACS sorted for tdTomato$^{+}$ basal cells. These tdTomato$^{+}$ cells (red) were then seeded into collagen scaffolds invested with differentiated 3T3-L1 cells, fixed, whole mount immunofluorescence stained for β-catenin (green) and imaged using confocal microscopy. DNA is marked with Hoechst (blue). Confocal microscopy images shown are (a) DNA marked with Hoechst in blue, (b) β-catenin in green, (c) tdTomato in red and (d) merged image.

# 3.3 Discussion

## 3.3.1 The K14-Cre$^{ERT2}$/Rosa26-tdTomato mouse model

To determine whether basal epithelial cells seeded into collagen scaffolds invested with adipocytes could produce epithelial cells of both basal and epithelial lineages, tdTomato$^+$ K14$^+$ basal cells were isolated by FACS sorting glands from tamoxifen-induced K14-cre$^{ERT2}$/Rosa26-tdTomato mice (Fig. 3.1). Unfortunately, the yield of tdTomato$^+$ K14$^+$ cells was extremely low, differing from other reports that utilize K14-Cre mouse models crossed with fluorescent reporter strains (Van Keymeulen et al., 2011; Rios et al., 2014; Wuidart et al., 2016). Importantly, these previously studied models all yielded a greater number of fluorescently tagged basal cells than the K14-Cre$^{ERT2}$/Rosa26-tdTomato mouse model used in this study. Furthermore, it was not possible to substantially increase fluorescent cell numbers following *in vitro* optimization (Fig. 3.2), suggesting that there were underlying issues with that the cells did not cope well with the sorting process and were not sufficiently viable.

Others have shown that upon fat pad transplantation of K14$^+$ basal epithelial cells into a mammary gland devoid of its epithelium, a proportion of cells can form both K14$^+$ basal and K18$^+$ luminal cells to fully repopulate the gland (Shackleton et al., 2006; Stingl et al., 2006). To test whether this process could be modelled *in vitro*, tdTomato$^+$ K14$^+$ basal cells from K14-cre$^{ERT2}$/Rosa26-tdTomato mice were FACS sorted and seeded into a 'synthetic fat pad' (Fig. 3.3). tdTomato$^+$ ring structures formed with cells exhibiting a long thin basal morphology and some cells expressing the luminal marker Cytokeratin-18 (K18) (Fig. 3.4). However, K18$^+$ cells observed in tdTomato$^+$ structures did not display a luminal morphology, suggesting they may have been cells in the process of transitioning between cell types (de Visser et al., 2012). Alternatively, tdTomato$^+$ cells may maintain a degree of stemness but were unable to complete correct differentiation into a luminal state within the model and remained in a dual luminal/basal-like state (Chakrabarti et al., 2012). Potentially, the cellular plasticity exhibited by tdTomato$^+$ cells from a K14$^+$ basal cell origin exhibited could be an artefact of the FACS process and/or 3D culture conditions. Ductal and terminal end bud structures typical of mammary epithelia were not formed by tdTomato$^+$ cells and hence fat pad repopulation was not recapitulated *in vitro*. These data provided an understanding of the possibilities and limitations of the K14-cre$^{ERT2}$/Rosa26-tdTomato system; however, this model was not pursued further due to the low yield of basal cells obtained.

## 3.3.2 The Axin2-Cre$^{ERT2}$/Rosa26-tdTomato mouse model

Previously it has been shown that Axin2$^+$ mammary epithelial cells contribute to both luminal and basal cells upon fat pad transplantation (van Amerongen et al., 2012). Therefore it was investigated

whether tdTomato$^+$ Axin2$^+$ basal cells isolated from Axin2-cre$^{ERT2}$/Rosa26-tdTomato mice would have the same potential *in vitro*. Following results from K14-cre$^{ERT2}$/Rosa26-tdTomato mice, the Axin2-Cre$^{ERT2}$/Rosa26-tdTomato mouse was utilized with the aim of improving cell yields and epithelial bilayer formation within synthetic fat pads. tdTomato$^+$ Axin2$^+$ basal epithelial cells were successfully isolated using the same FACS protocol used for tdTomato$^+$ K14$^+$ cells. This method provided tdTomato$^+$ basal cell yields approximately 30 times higher than tdTomato$^+$ K14$^+$ FACS.

To increase yields further, cells were expanded in 2D culture for subsequent 3D culture experiments. Expansion conditions on a layer of Matrigel and feeder cells increased cell numbers sufficiently for multiple experiments to be performed (Fig. 3.5). Although this process was effective in increasing fluorescent cell yields, it is important to note that it added a further layer of complexity and cost to the model. Moreover, *in vitro* factors such as 2D culture, culture medium and feeder cells have been previously associated with cellular reprogramming and altered cell stemness (Liu et al., 2012; Prater et al., 2014; Takahashi and Yamanaka, 2006). These factors may have influenced the potency of any MaSC present in the system, potentially explaining the absence of properly polarised Axin2 organoids within collagen scaffolds.

During 3D culture of of tdTomato$^+$ cells from an Axin2$^+$ basal cell origin in synthetic fat pads, a number of structures were formed. Rarely, structures partially resembling the ducts and terminal end buds of an *in vivo* mammary gland were observed with the correct positioning and morphology of αSMA$^+$ basal cells (Fig. 3.6-3.10). Cells with a luminal morphology were also observed within these structures, however, they did not correctly express luminal markers K18 or β-catenin (Fig. 3.11 – 3.13). Notably, the vast majority of tdTomato$^+$ structures formed in scaffolds were disorganised and did not exhibit a similar morphology to epithelium of the *in vivo* mammary gland. Collectively, these data demonstrated that the model was unable to recapitulate the *in vivo* fat pad transplantation assay *in vitro*.

### 3.3.3 Limitations of the *in vitro* primary cell seeding assay

There are multiple factors that could have contributed to the aberrant polarisation of *in vitro* organoids. One such factor may have been the population of Lin$^-$ CD24$^+$ CD49f$^{med/hi}$ basal cells that were selected for scaffold experiments. Although a proportion of these cells have been shown to form a fully functioning mammary gland upon fat pad transplantation, *in vitro* manipulation may have reduced their repopulating capacity (Shackleton et al., 2006). Future studies could incorporate other MaSC markers, such as Procr, to more efficiently purify the MaSC population and therefore increase the probability of bi-layered organoid formation (Wang et al., 2014a).

In order to retain stemness, MaSCs reside within a niche tightly regulated by multiple signalling molecules, receptors and growth factors. These signalling pathways orchestrate quiescence and differentiation and an imbalance can lead to incorrect gland formation (Lane and Leder, 1997; Naylor et al., 2005; Sang et al., 2008; Seagroves et al., 2010; Teissedre et al., 2009). *In vitro* systems such as scaffold cultures rely on the supplementation of the culture medium. Neuregulin1 (Nrg1) is a member of the epidermal growth factor (EGF) family of ligands. Supplementation with Nrg1 instead of EGF has recently been shown to increase cell viability, extend culture periods, permitting formation of complex lobular mammary structures in Matrigel culture (Jardé et al., 2016). Addition of fibroblast growth factor 2 (FGF2) has been shown to increase branching formation during organoid cultures (Zhang et al., 2014). In the current study, scaffold culture media was supplemented with EGF. Hence, future replacement of EGF with Nrg1 and the inclusion of FGF2 in culture media may permit increased mammary organoid formation.

Mammary organoid polarisation and formation is also effected by the ECM composition and supramolecular organisation in which cells or tissue fragments are cultured (Carter et al., 2017; Nguyen-Ngoc and Ewald, 2013; Sokol et al., 2016). Studies involving organoid cultures have shown conflicting evidence over preference to either Matrigel or collagen I as the substrate of choice (Carter et al., 2017; Gudjonsson et al., 2002; Krause et al., 2008). Accordingly, the use of collagen I to synthesise scaffolds, rather than an ECM containing basement membrane proteins such as Matrigel, may have been a contributing factor to the absence of organoid formation in the systems used here.

In both the K14-cre$^{ERT2}$/Rosa26-tdTomato and Axin2-cre$^{ERT2}$/Rosa26-tdTomato mouse models, Cre recombination was induced by tamoxifen administration. However, tamoxifen inducible systems come with an important caveat: tamoxifen is an anti-oestrogen prodrug which forms metabolites that block the oestrogen receptor (ER) and prevent transcription of oestrogen-responsive genes (Wang et al., 2004). It is therefore used in the treatment of ER$^+$ breast cancer by targeting ER$^+$ epithelial cells of the gland (Fisher et al., 2005). Hence, using tamoxifen to fluorescently tag mammary epithelia may have deleterious effects on the gland and may unintentionally influence the population that is to be studied. Accordingly, tamoxifen may have altered the stem cell potential of cells isolated from both mouse models used in these scaffold cultures. Whilst tamoxifen dosages used in Cre recombination experiments are much lower than those therapeutically, many studies opt for alternative models such as the tetracycline inducible system to avoid this issue (Kaanta et al., 2013; Van Keymeulen et al., 2011; Rios et al., 2014; dos Santos et al., 2013).

### 3.3.4 Conclusion

Overall, these data show that the process of repopulating a fat pad to form an epithelial bilayer with MaSC/MRU cells could not be achieved using basal cells derived from K14-cre$^{ERT2}$/Rosa26-tdTomato or Axin2-cre$^{ERT2}$/Rosa26-tdTomato mice with the synthetic fat pad model. This suggests that additional components are present in the mammary fat pad *in vivo* that cannot presently be recapitulated in our scaffold model and further work is required to optimize it for stem cells studies.

# 4 Development of three-dimensional collagen scaffolds with controlled internal architecture for cell migration studies with breast cancer cell lines

# 4.1 Introduction

The work presented in this chapter was a collaborative effort between this author and materials scientists (Professor Ruth Cameron and Dr. Anke Husmann) and Dr. Jonathan Campbell, a postdoctoral scientist in the laboratory of the supervisor Professor Christine Watson. Collaborative contributions that were not solely the work of this author are clarified in each figure legend and marked as †.

A variety of 3D *in vitro* culture models have been generated for studies of both the normal and malignant breast epithelium, all of which have defined utility (Bissell et al., 2002; de Both et al., 1999; Boyden, 1962; Chaudhuri et al., 2014; Daniel et al., 1984; Debnath et al., 2003; Lee et al., 2007; Paszek et al., 2005; Poujade et al., 2007; Ray et al., 2017a; Todaro et al., 1965; Wang et al., 2015). The majority of these consist of cells traversing an isotropic (non-directional) lattice. However, the directional migration of breast tumour cells has been shown to be strongly influenced by chemical gradients and/or directional cues provided by the organisational structure of extracellular matrix (ECM). Notably, stromal collagen is aligned perpendicular to the tumour edge in an anisotropic phenotype that has been named TACS-3, for Tumour Associated Collagen Signature-3 (Provenzano et al. 2006). Furthermore, this phenotype has been observed frequently in aggressive breast tumours and is associated with poor patient prognosis (Jiang et al. 2016; Kakkad et al. 2016; Provenzano et al. 2006; Conklin et al. 2011). As collagen is a major structural component of the breast stroma, and breast cancer cells must migrate through this stroma, it is of significant interest to recapitulate this anisotropic ECM structure *in vitro* to study cancer cell migration in as realistic a context as possible.

For this purpose, engineered anisotropic collagen I scaffolds were synthesized through modification of a previously published freeze drying technique (Davidenko et al. 2010). These structures were intended not only to mimic the anisotropic ECM surrounding breast tumours but also increase model tractability by providing a controlled internal architecture. The effect of collagen anisotropy on the migratory behaviour of three human breast cancer cell lines (MDA-MB-231, MDA-MB-468 and MCF-7) was then investigated. Furthermore, the influence of collagen anisotropy on cellular proliferation was investigated using EdU incorporation combined with IHC analysis for the proliferation marker Ki67 (Gerdes et al., 1983). To elucidate whether this collagen model could distinguish more aggressive subtypes of the same tumour cell line, an epithelial-mesenchymal transition (EMT) was induced in MDA-MB-468 cells and migratory behaviour analysed.

# 4.2 Results

## 4.2.1 Synthesis of anisotropic collagen scaffolds

To synthesize anisotropic collagen I scaffolds, previously established freeze drying techniques were adopted and modified (Davidenko et al., 2010, 2012; Pawelec et al., 2014). The original technique involved dissolving collagen in acetic acid, homogenising it into a slurry, pouring this slurry into polycarbonate moulds then freezing and subsequently subliming ice within the slurry using a freeze drier. During the gradual freezing process, ice crystals nucleated at random throughout the slurry and an isotropic porous structure was formed within the collagen scaffolds. Through modification of this method, the nucleation point was altered in order to manipulate ice crystal growth and generate an anisotropic internal architecture (Methods, Fig. 2.1, Table 2.1). This was achieved by pre-chilling the freeze drier to -40°C before the moulds were added for the purpose of quenching the slurry (Methods, Table 2.1). Additionally, a copper pin was placed within the mould that was in thermal contact with the cooling shelf (Methods, Fig 2.1b,c). As copper has a lower specific heat capacity than that of the polycarbonate mould and the collagen slurry, the pins cool down more quickly than the surrounding materials (Giauque and Meads, 1941; Narijauskaitė et al., 2013; Pawelec et al., 2014). As a result, ice crystals within the slurry nucleated in the area adjacent to the copper pin and grew progressively to the outside of the mould (Fig. 4.1a). Following sublimation of the ice to steam, the resulting directional anisotropic collagen pores that were formed during ice crystal growth were observed throughout the scaffold using scanning electron microscopy (SEM) and micro-computed tomography (µCT) (Fig. 4.2). The presence of the copper pins within the mould also provided a funnel at the top of the scaffolds into which cells could be seeded in subsequent experiments (Fig. 4.2a-f). Two different pin shapes were used in the moulds to synthesise two different shapes of seeding funnels: cylindrical and conical tipped pins (Methods, Fig 2.1b,c, Fig. 4.3).

Photographic images of anisotropic collagen I scaffolds following freeze drying but before cross linking, show the two scaffold types with different funnel geometries (Fig. 4.3). For scaffolds moulded with conical pins, excess slurry that had flowed out of the moulds onto the surrounding glass cover slips was observed (Fig. 4.3b). In this case directional collagen pores were observed macroscopically within the excess collagen, emanating from the base of the scaffold (Fig. 4.3b). This provided an indication that anisotropic pore growth had occurred internally and was removed and discarded using a scalpel blade before cross linking. Photographs also revealed the successful formation of the different seeding funnel types moulded from the two copper types of pin within the moulds (Fig. 4.3).

To produce isotropic, i.e. non-directional collagen scaffolds, the cooling shelf was cooled from 20°C to -40°C over a period of 1hr with the moulds *in situ* and copper pins were thermally insulated from the cooling shelf using a rubber mat (Methods, Fig. 2.1, Table 2.1). As a result, ice crystals nucleated at random throughout the scaffolds producing an isotropic porous structure (Fig. 4.1b). Consequently, anisotropic and isotropic scaffolds were synthesized with the same external dimensions but with an altered internal architecture (Fig. 4.2).

For both anisotropic and isotropic scaffold types, pore size increased with distance from the scaffold funnel (Fig. 4.2e-j), with small isotropic pores observed at the funnel edge (Fig. 4.2i-j). Beyond the initial funnel region, anisotropic scaffolds exhibited a continuous elongated micro-porous structure that was radially orientated from the funnel and extended to the base of the scaffolds (Fig. 4.2a,c,e,g). In contrast, isotropic scaffolds exhibited a randomly orientated porous structure with a more spherical pore morphology (Fig. 4.2b,d,f,h). In both scaffold types finer connections were observed in the macro-porous regions demonstrating an inter-communicated structure (Fig. 4.2g,h).

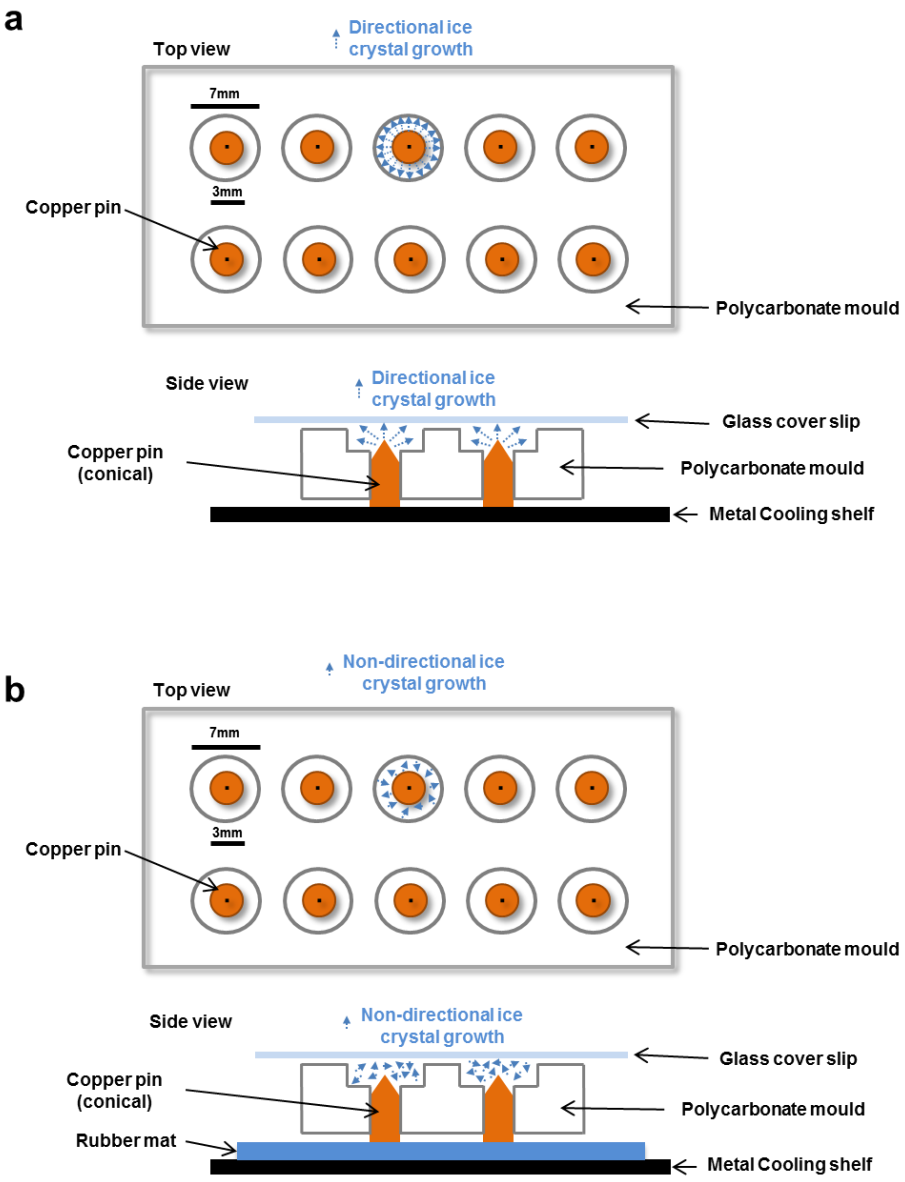


***Figure 4-1: Schematic illustrating ice crystal growth in collagen scaffolds***

Ice crystal nucleation and growth direction (blue arrows) during freeze drying of collagen I slurries in polycarbonate moulds for (a) anisotropic and (b) isotropic collagen scaffolds. (a) Thermal contact with a precooled (-40°C) metal freeze dryer shelf cooling shelf cools the copper pin first, allowing freezing to first occur in the slurry in proximity to the copper pin. Consequently, ice crystals nucleate from this point and propagate in a direction towards the edge of the mould (blue arrows). (b) Copper pin is insulated from the freeze dryer shelf using a rubber mat. The freeze dryer is cooled gradually with the moulds *in situ* from room temperature to -40°C. The collagen slurry is cooled evenly and random ice crystal nucleation occurs throughout. Ice crystals then propagate in random directions (blue arrows).

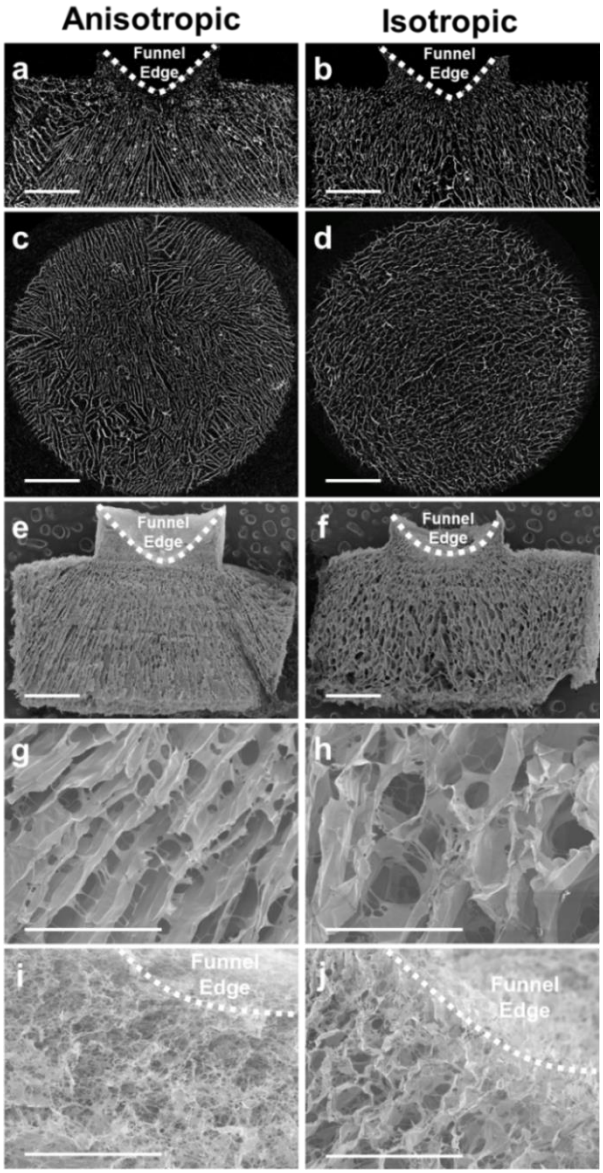


***Figure 4-2: Anisotropic and isotropic collagen scaffolds have different internal architectures***

Anisotropic (left) and isotropic (right) collagen I scaffold architectures, synthesised using conical-tipped copper pins (Methods, Fig. 2.1c), were visualized using micro–computed tomography (µCT) and scanning electron microscopy (SEM). (a–d) Show reconstructed µCT pictures of transversal and horizontal cuts through an anisotropic and an isotropic scaffold. (e–j) Show SEM pictures of the whole scaffold as well as a zoomed area showing the different architectures and regions around the funnel. †Scaffolds were synthesised by Dr. Anke Husmann and Rob Hume, images were taken by Dr. Anke Husmann. (a,c,e,f) have had their brightness increased to allow better visualisation. Scale bars (a-f) 1mm, (g-j) 200µm.

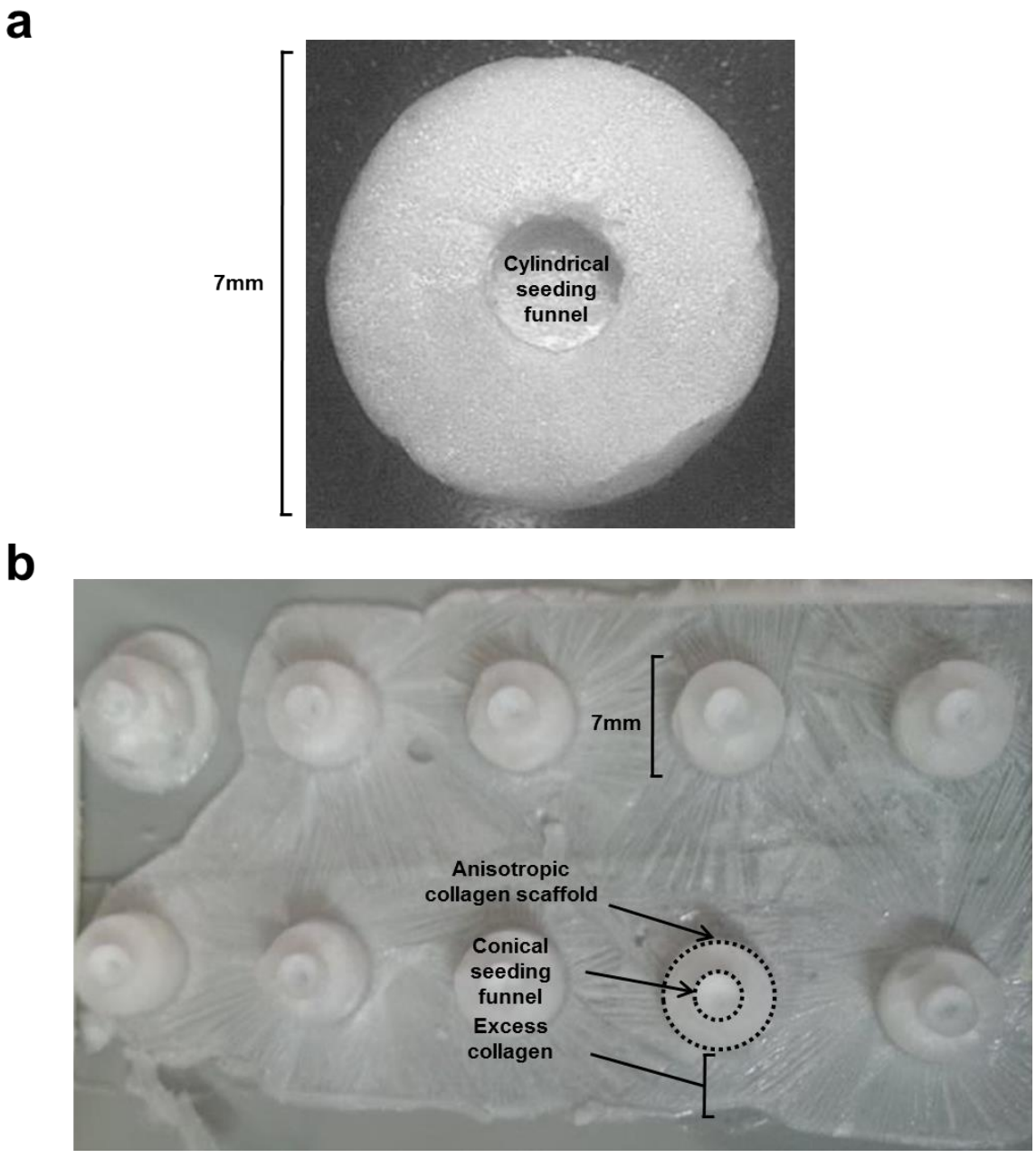


***Figure 4-3: Photograph of anisotropic collagen I scaffolds***

(a) Photograph of anisotropic collagen I scaffold synthesised with cylindrical pin heads. (b) Photograph of anisotropic collagen I scaffolds synthesised with conical pin heads attached to glass slides following freeze drying and their removal from polycarbonate moulds. Excess collagen is observed attached to glass slides due to overflow of collagen slurry during the filling of moulds. Seeding funnels formed by copper pins within the mould are also observed.

### 4.2.2 Seeding of breast cancer cell lines into anisotropic collagen scaffolds

To investigate whether breast cancer cell migration could be assessed in anisotropic collagen scaffolds, and if spatial directionality enhanced cell migration, three human breast cancer cell lines were selected as candidates for these migration assays. Firstly, the aggressive claudin-low triple negative breast cancer (TNBC) cell line MDA-MB-231 was chosen. These cells often exhibit a mesenchymal morphology and highly migratory phenotype *in vitro* (Lundgren et al., 2009; Nurcombe et al., 2000; Timoshenko et al., 2003). Secondly, the basal-like TNBC cell line MDA-MB-468 was selected, as this cell line is characterised by a lower migratory potential compared to MDA-MB-231 cells *in vitro* (Gordon et al., 2003). The third line selected was the $ER^+$ MCF7 cell line, which displays little or no migratory potential *in vitro* in the absence of chemical induction (Prest et al., 1999; Rosman et al., 2008; Walsh and Damjanovski, 2011).

The first scaffolds synthesised were with a cylindrical copper pin in the mould. Preliminary cell experiments used these scaffolds with cylindrical seeding funnels (Methods, Fig. 2.1b) to assess whether cell migration could be observed (Fig. 4.3a, Fig. 4.4, Fig. 4.5). MDA-MB-231 cells were marked with a fluorescent cell dye, seeded into scaffold funnels and after 12 hours the funnels imaged (Fig. 4.4a). From a top down view of the funnels, all of the cells imaged were confined to the funnel region (Fig. 4.4a). Using a further time point of 48 hours and combining confocal with brightfield microscopy to image the cells and scaffold, respectively, a group of migratory MDA-MB-231 cells were observed at a distance from the nucleation point (Fig. 4.4b, white arrow).

In subsequent experiments, anisotropic scaffolds moulded with conical funnels were synthesised (Methods, Fig. 2.1c, Fig. 4.1, Fig. 4.2, Fig. 4.3), providing a more consistent formation and radial distribution of pores around the nucleation point. To investigate whether this scaffold type would also permit migration, cells were seeded in funnels (Methods, Fig. 2.1c), cultured for 7 days and bisected in half before imaging (Fig. 4.5). Bisected scaffolds permitted the investigation of migration below the surface region and the scaffold, thereby allowing for an enhanced analysis of individual cell's migratory response. Additionally, calcein acetoxymethyl (AM), a cell permeant dye that marks only viable cells, was added to the cultures to allow the visualisation of viable migratory cells (Fig. 4.5, white arrows). DAPI was used to mark DNA and hence the cell nuclei of migratory cells (Fig. 4.5, blue). Both calcein AM and DAPI non-specifically stained the collagen scaffold (Fig. 4.5, blue/green scaffold pores). Serendipitously, this enabled the visualisation of the anisotropic internal architecture to which adherent MDA-MB-231 cells migrated (Fig. 4.5, white arrows). As the conical funnel type provided a more consistent internal architecture and allowed visible migration in anisotropic scaffolds, it was selected for further study. Moreover, using one funnel type also reduced

the number of experimental variables to assess and control for, providing a more streamlined analysis. In this, and all subsequent chapters of this thesis, scaffolds were synthesised with conical funnels.

Following this, scaffolds were placed in Boyden chambers, with the cell seeding funnel placed vertically and cultured with or without a FCS serum gradient (Methods, Fig 2.2). This chemical gradient was added to cultures in an attempt to encourage cell migration via chemotaxis. In order to control for migration, scaffold funnels were then seeded with MDA-MB-231, MDA-MB-468 and MCF7 cells mixed with fluorescent countbright beads (Methods, Fig 2.2). As it was anticipated that the fluorescent beads could only be motile if influenced by gravity or agitation of the media, beads could therefore be utilised to assess the variability of a dropwise cell seeding method and provide a control for migration measurements. Furthermore, if the beads were located predominantly in or near the funnel after seeding, then it would indicate an accurate seeding methodology had been achieved.

For migration analysis, bisected scaffolds or IHC sections stained with DAPI were imaged and migration was measured using ImageJ and Microsoft Excel analysis (Fig. 4.6). Firstly, the nucleation point at the edge of the funnel was marked and segmented to produce a number of individual X, Y coordinates along the nucleation point vector (Fig. 4.6b) which was then entered into Excel. Cells were then marked, saved as X, Y coordinates (Fig. 4.6c) and also entered into Excel. Using Excel, the Euclidian distance, otherwise known as the shortest distance between two points, of each cell from its location to the nearest nucleation point segmented coordinate was then calculated.

Each cell's Euclidian distance data was then binned into 50 or 100 µm distance intervals. This was intended to display the frequency of cells at the varying distances into the scaffold and thus represent the complexity of the data. A high variability in the data caused high standard deviations in each distance interval and thus this method was deemed unusable to compare samples. As an alternative, a more simplistic approach was required whereby the median distance for all migratory cells was calculated and plotted graphically (Fig. 4.7, Fig. 4.8). The median was selected over the mean due to the relatively high sample sizes of >100 cells per scaffold and its resistance to the influence of statistical outliers.

Following 24hrs post-seeding, cells and fluorescent beads were measured for their median Euclidian distance travelled from the nucleation point into the scaffolds ($\mathbf{r_{median}}$) (Methods, Fig 2.2) (Fig. 4.6, Fig. 4.7). Both cells and beads exhibited a similar distribution within 100 µm of the nucleation point in both isotropic and anisotropic scaffold types (Fig. 4.7). This indicated that both cell – scaffold and

bead – scaffold interactions were comparable and that beads could be useful for normalisation purposes. When distinguishing between cell types it was observed that MDA-MB-231 cells migrated further from the initial funnel region within this 24hr period when compared to MDA-MB-468 cells which were observed to have a more compact localisation to the funnel region (Fig. 4.7).

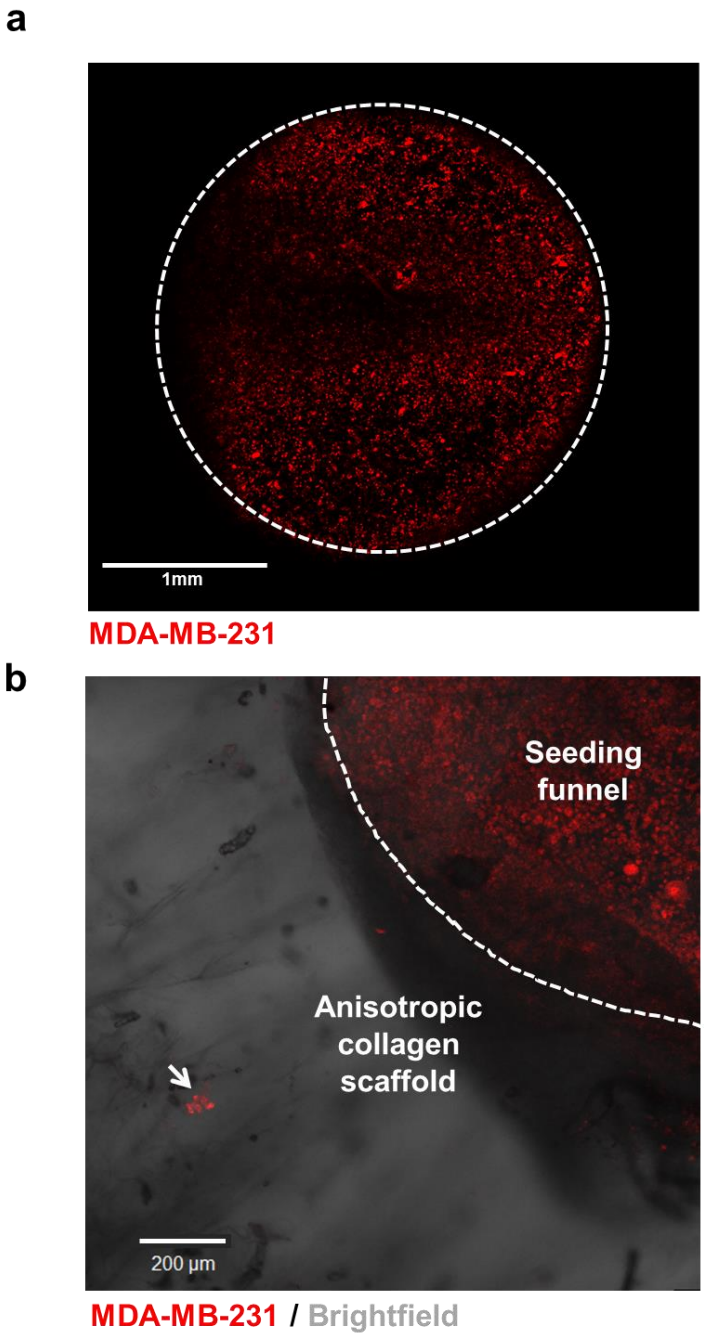


***Figure 4-4: Migration of MDA-MB-231 cells in anisotropic collagen scaffolds***

MDA-MB-231 breast cancer cells fluorescently marked using CellTracker™ Orange were seeded into the seeding funnel of anisotropic collagen I scaffolds containing a cylindrical seeding funnel. (a) MDA-MB-231 cells (red) were cultured for 12 hours and the seeding funnel region (white dotted line) imaged using confocal microscopy. (b) MDA-MB-231 cells (red) were cultured for 48 hours. Confocal and brightfield microscopy were combined to image the cells and scaffold, respectively. A group of cells that have migrated away from the seeding funnel are marked with a white arrow.

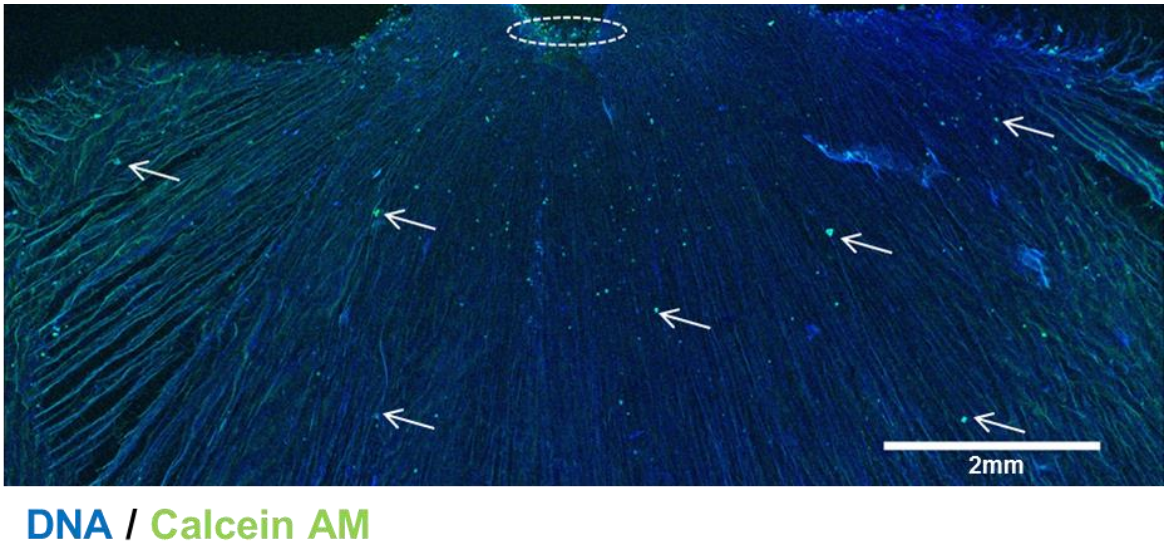


***Figure 4-5: MDA-MB-231 cells migrate along orientated fibres of anisotropic collagen scaffolds***

MDA-MB-231 breast cancer cells were seeded into the funnel (white dotted line) of an anisotropic collagen scaffold synthesized from conical pins, and then cultured for 7 days. Cell viability was assessed via the addition of calcein AM dye (green). DNA was marked with DAPI (blue). Scaffolds were bisected and imaged freshly cut face down using confocal microscopy. White arrows mark viable (calcein $AM^{+}$) migratory cells.

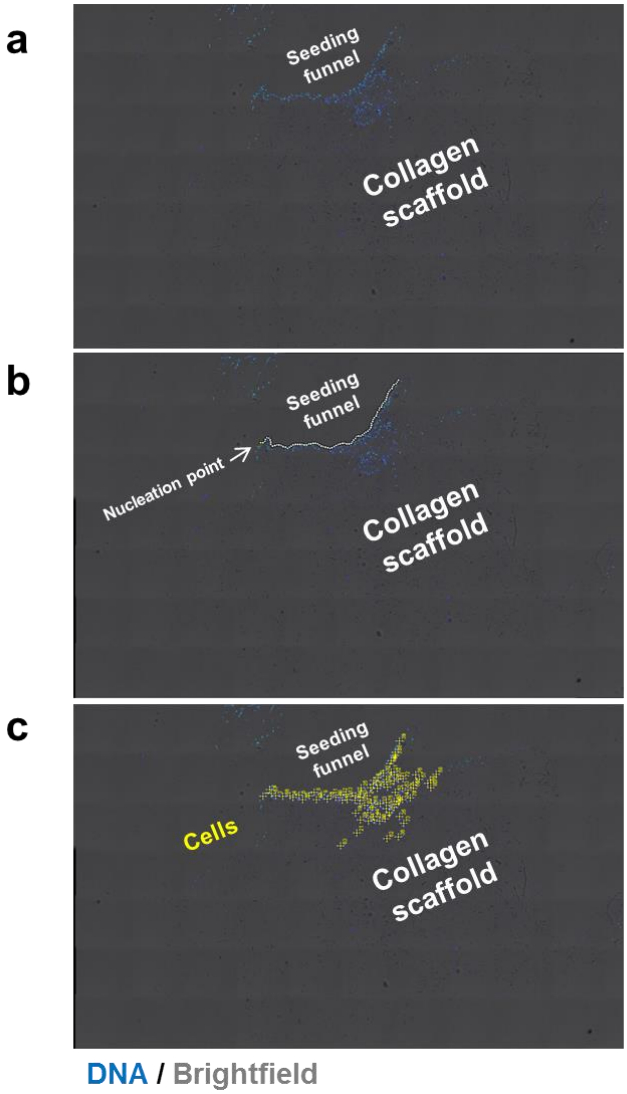


***Figure 4-6: Schematic illustrating cell migration measurements (Euclidian distance)***

Breast cancer cells seeded into the seeding funnel of collagen scaffolds were cultured for either 24 hours or 10 days. To assess migration distances at these time points, a measurement method was devised using immunohistochemistry and ImageJ analysis: (a) Paraffin embedded longitudinal sections of scaffolds (or bisected scaffolds) were imaged and opened on ImageJ software. (b) The edge of the seeding funnel in the scaffold, the nucleation point (white dotted line), was marked and segmented into individual points. The coordinates for these points were then saved into an excel file. (c) Cell nuclei marked with Hoechst (blue) were then marked individually on ImageJ (yellow). These were saved as coordinates and saved into an excel file. The distance for each cell coordinate from the nearest coordinate on the segmented nucleation point was then calculated on excel. This is defined as the Euclidian distance of each cell to the nucleation point.

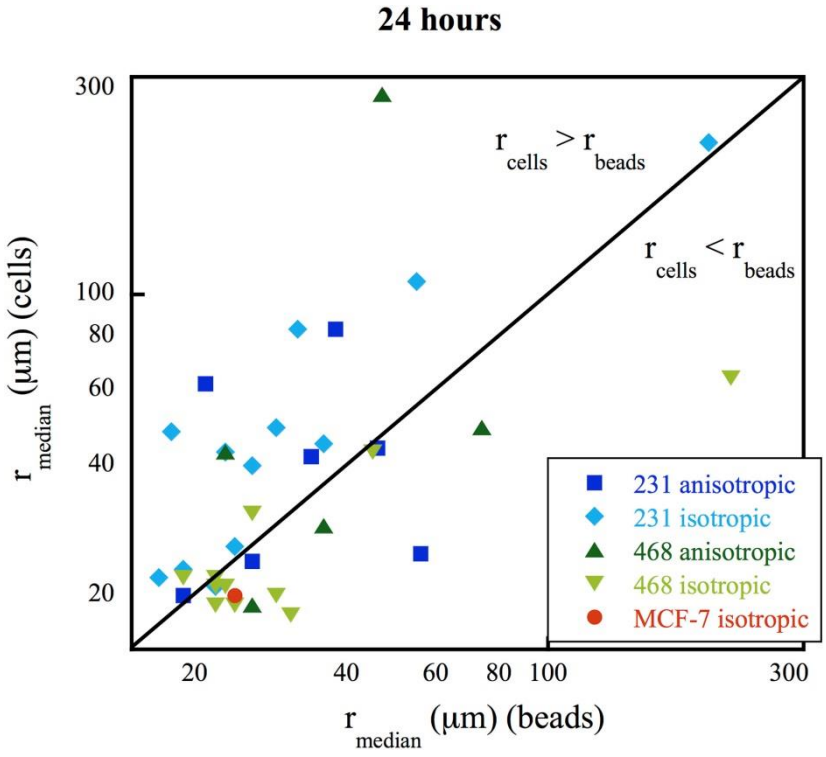


***Figure 4-7: The majority of samples and beads remain within 100 µm distance of the seeding funnel in both isotropic and anisotropic collagen scaffolds following 24 hours culture***

MDA-MB-231, MDA-MB-468 and MCF-7 breast cancer cells and countbright beads (non-migratory control) were seeded into the seeding funnel of collagen scaffolds, cultured for 24 hours, fixed and imaged. The Euclidian distance for each cell/bead was calculated on ImageJ and the median Euclidian distance for each scaffold calculated from this data. The median Euclidian distance $\mathbf{r_{median}}$ (µm) travelled by MDA-MB-231, MDA-MB-468 and MCF-7 breast cancer cells with respect to the median Euclidian distance travelled by countbright beads (non-migratory control) following 24 hours culture was then plotted (above). Each point represents one sample. †Scaffold synthesis, cell seeding and culturing were carried out by Dr. Jonathan Campbell and Rob Hume. Analysis was carried out by Dr. Anke Husmann.

### 4.2.3 Anisotropic collagen scaffolds as a breast cancer cell line migration assay

At longer time points it was predicted that the more migratory breast cancer cells would have migrated further from the cell seeding funnel into the bulk of the scaffolds. Therefore, in an attempt to capture the extent of migration in scaffolds, a time point of 10 days post-seeding was selected and analysed (Fig. 4.8). As anticipated, MDA-MB-231 cells migrated significantly further than MDA-MB-468 and MCF7 cells when all sample types (anisotropic/isotropic, gradient/non-gradient) were pooled and the cell lines compared (Fig. 4.8, significance bars below x-axis). This validated the model's ability to distinguish cell type based on their migratory potential.

As a TACS-3 phenotype is associated with more aggressive breast cancer subtypes and poor prognosis it was also predicted that anisotropic scaffolds would better support the migratory profile of these aggressive tumour types (Provenzano et al. 2006; Provenzano et al. 2008; Conklin et al. 2011b). In order to compare the influence of collagen architecture on cell migration, breast cancer cells seeded in anisotropic scaffolds and isotropic scaffolds were analysed and compared for their migration distance. Notably, MDA-MB-231 cells exhibited an enhanced migratory phenotype in anisotropic scaffolds when compared to isotropic scaffolds, in both gradient and non-gradient samples (Fig. 4.8, significance bars above graph). Indeed, migration of MDA-MB-231 cells under a serum gradient in anisotropic scaffolds was often observed at all depths of the scaffolds showing the large extent of migration (Fig. 4.9a). In contrast, few MDA-MB-468 and MCF-7 cells migrated into the body of the scaffold regardless of scaffold type (Fig. 4.8, Fig. 4.9). As neither cell line is highly migratory in other *in vitro* studies this result is not unexpected and any differences that are due to anisotropy may therefore be difficult to distinguish (Gordon et al., 2003; Prest et al., 1999; Rosman et al., 2008; Walsh and Damjanovski, 2011).

Through immunohistochemical (IHC) analysis of anisotropic scaffolds, it was observed that the different cell lines displayed different morphologies (Fig. 4.10). MDA-MB-231 cells migrated often as singular cells with an elongated mesenchymal morphology whereas MDA-MB-468 cells, although also often singular, exhibited a rounded morphology. Few migratory MCF7 cells were observed with the majority of cells remaining within a cell mass located at or near the top of the scaffold (Fig. 4.10).

To investigate the effects of migration and anisotropy on cellular proliferation, EdU was added in the final 24 hours of culture for 10 day samples. This nucleotide analogue is incorporated into newly synthesised DNA and thus enables measurement of proliferating cells within a specified time frame. Through combination with a fluorophore, EdU labels replicating cells and can be detected with fluorescence microscopy (Salic and Mitchison, 2008). Visual observation of $EdU^+$ cells in scaffolds

provided no obvious correlations between depth of migration and proliferation or anisotropy and proliferation and further analysis was required (Fig. 4.9).

In order to further study proliferation effects, paraffin embedded sections were probed for the proliferation marker Ki67 by IHC analysis. For both EdU and Ki67, the expression of the marker as a ratio of the entire cell population was then analysed and plotted graphically (Fig. 4.11). From these data it was observed that anisotropic scaffold culture had no significant effect on proliferation compared to isotropic scaffold culture, in any of the breast cancer cell lines (Fig. 4.11). When comparing proliferation between cell lines, it was observed that the number of $EdU^+$ and $Ki67^+$ MDA-MB-231 cells as a ratio of the total cells was lower than for MDA-MB-468 and MCF7 cell ratios (Fig. 4.11). These data and previous migration distance data, demonstrated that MDA-MB-231 cells migrated the furthest of the three breast cancer cell lines but exhibited the lowest levels of proliferation. Furthermore, all cell types cultured in 2D tended to proliferate at a higher rate compared to 3D scaffold cultures (Fig. 4.11). However, as with scaffold cultures MDA-MB-231 cells in 2D proliferated at the slowest rate of the three cell lines with approximately 30% of cells expressing Ki67. In contrast, MDA-MB-468 and MCF7 cells in 2D displayed higher proliferation rates with 85% and 70% expressing Ki67, respectively (Fig. 4.11).

Previously it has been shown that the cell surface adhesion receptor integrin β1 is involved in the binding of cells to collagen (Jokinen et al., 2004; Staatz et al., 1990). Moreover, its expression has been shown to reduce proliferation, increase survival and enhance the migration of MDA-MB-231 cells (Hou et al., 2016). As discussed above, MDA-MB-231 cells exhibited higher levels of migration and lower levels of proliferation compared to MDA-MB-468 and MCF7 cells. To examine whether an increased expression of integrin β1 was present in MDA-MB-231 cells compared to MDA-MB-468 and MCF7 cells within our scaffolds, samples were probed for integrin β1 expression by IHC analysis (Fig. 4.12). Due to the high concentration required for the antibody staining and the matching of this concentration in IgG controls, high levels of background were observed (Fig. 4.12, IgG negative controls). Nonetheless, an increase in fluorescent signal was observed in MDA-MB-231 cells compared to MDA-MB-468 cells, MCF7 cells and negative controls (Fig. 4.12) suggesting that integrin β1 expression was increased in this cell line within scaffolds. This is one possible explanation for the migratory and proliferative phenotype of MDA-MB-231 cells in the system. However, further confirmation is required as high background levels highlight concerns into the validity of these results.

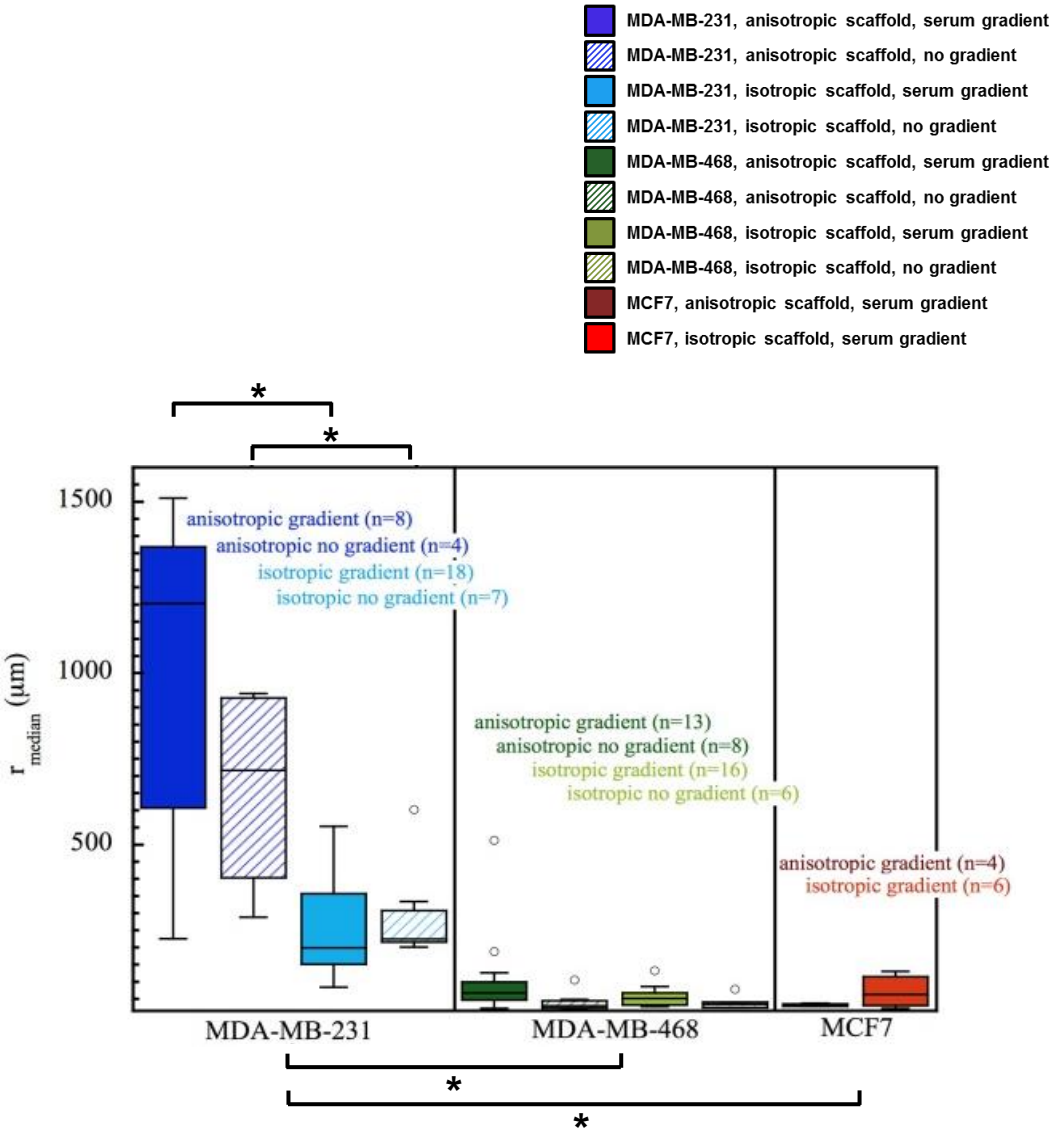


***Figure 4-8: Migration distance $r_{median}$ of human breast cancer cell lines in anisotropic/isotropic scaffolds with/without a serum gradient after 10 days***

MDA-MB-231, MDA-MB-468 and MCF-7 breast cancer cells were seeded into the seeding funnel of collagen scaffolds, cultured for 10 days, fixed and imaged. The distribution of cells by their median Euclidian distance migrated ($r_{median}$) after 10 days was plotted and separated by their cell type (MDA-MB-231, MDA-MB-468 or MCF-7), scaffold type (isotropic/anisotropic) and serum gradient status (see key above graph). Significance bars above x-axis represent MDA-MB-231 anisotropic compared with MDA-MB-231 isotropic samples. Significance bars below x-axis represent MDA-MB-231 cells versus MDA-MB-468 and MCF7 cells with all scaffold types pooled. †Scaffold synthesis, cell seeding and culturing were carried out by Dr. Jonathan Campbell and Rob Hume. Analysis was carried out by Dr. Jonathan Campbell, Rob Hume and Dr. Anke Husmann. *$p<0.05$.

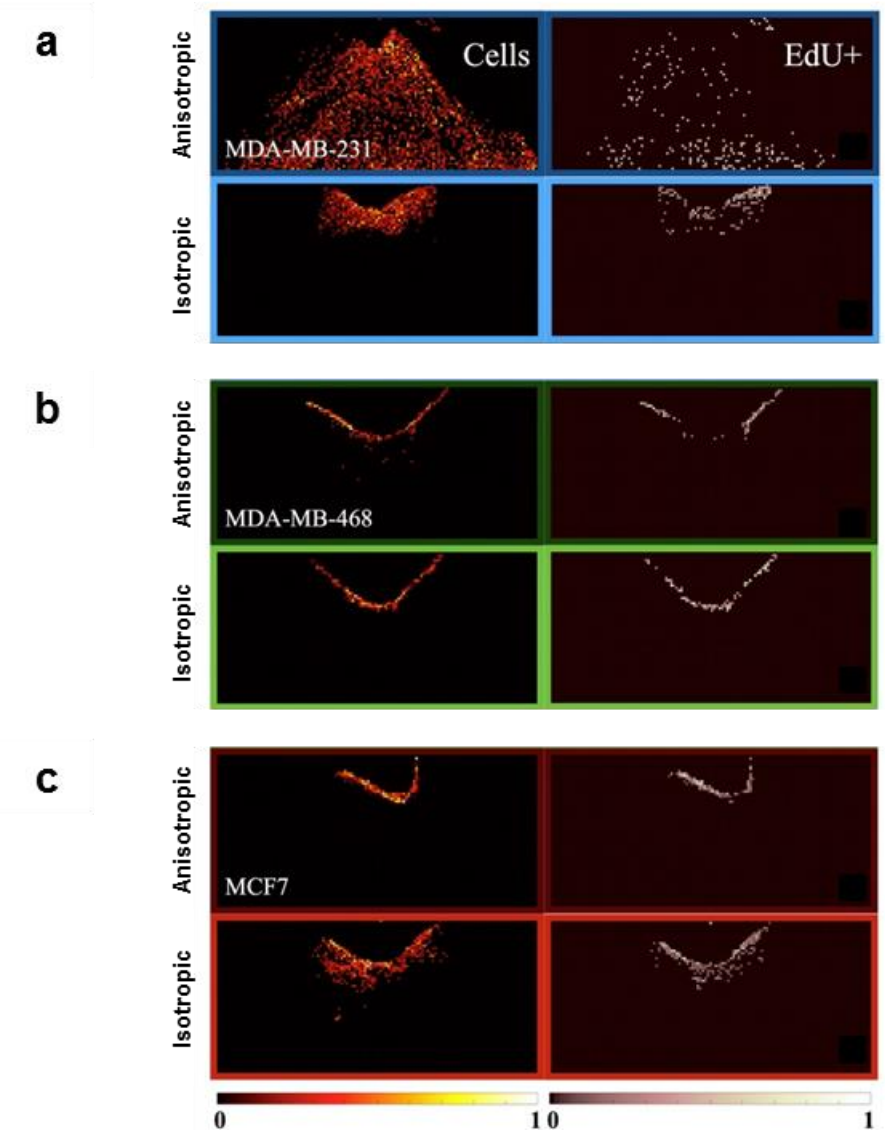


***Figure 4-9: Heat maps representing the migration and proliferation of human breast cancer cell lines in anisotropic/isotropic scaffolds after 10 days***

MDA-MB-231, MDA-MB-468 and MCF-7 breast cancer cells were seeded into the seeding funnel of collagen scaffolds, cultured for 10 days, fixed, imaged and converted into heat maps. Heat maps show representative images of the distribution of cells and the proliferation marker EdU throughout scaffolds with a serum gradient applied for (a) MDA-MB-231, (b) MDA-MB-468 and (c) MCF7 cells. †Scaffold synthesis, cell seeding and culturing was carried out by Dr. Jonathan Campbell and Rob Hume. Imaging was carried out by Dr. Jonathan Campbell, Rob Hume and Anke Husmann. Heat maps were generated by Dr. Anke Husmann.

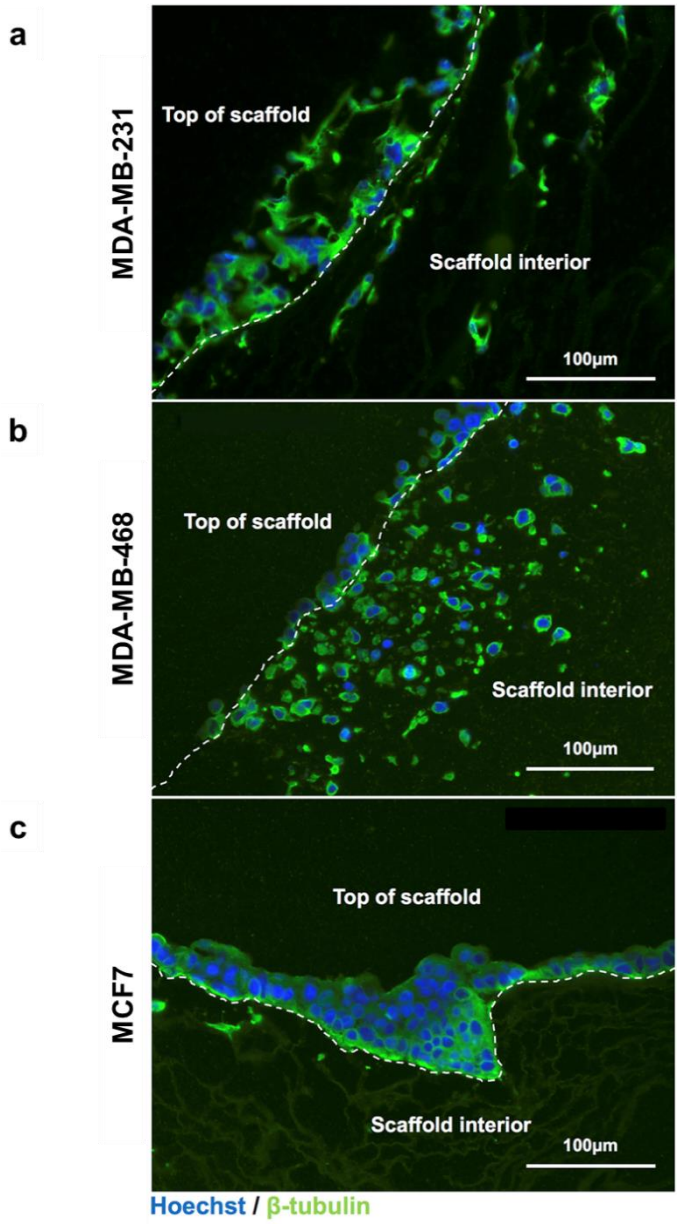


***Figure 4-10: Anisotropic collagen scaffolds reveal different cell morphologies***

MDA-MB-231, MDA-MB-468 and MCF7 cells seeded and cultured in anisotropic collagen scaffolds show different morphologies. (a) MDA-MB-231 cells migrate into the scaffold from the cell mass and have a thin spindle-like morphology. (b) MDA-MB-468 cells migrate into the scaffold, disseminating from the cell mass as single cells/small cell clusters whilst maintaining a round morphology. (c) MCF7 cells are primarily retained as a cell mass on top of the scaffold with few cells showing migration into the scaffold. Hoechst (blue) stains cell nuclei whilst β-tubulin (green) stains cell cytoskeleton.

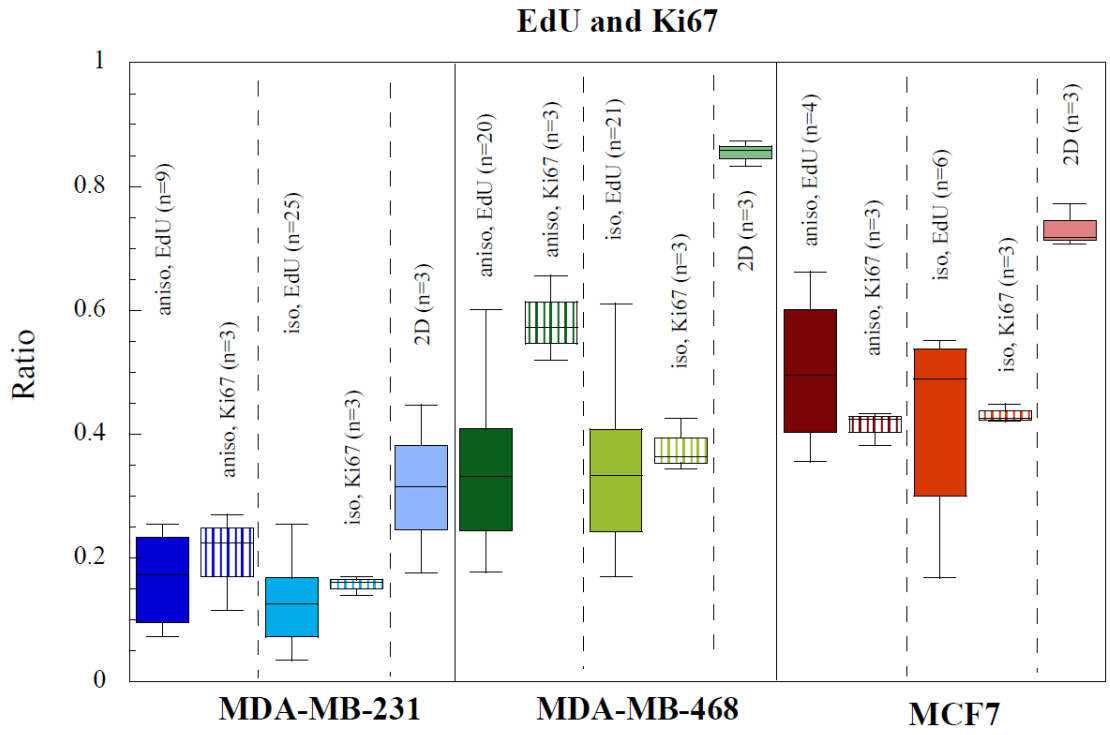


***Figure 4-11: Anisotropy does not affect the proliferation of MDA-MB-231, MDA-MB-468 or MCF-7 cells***

Proliferation of seeded cell lines within 3D collagen scaffolds (EdU and Ki67, paraffin sections, immunohistochemical analysis) that are either anisotropic (aniso) or isotropic (iso) and cell lines on 2D adherent culture on glass cover slips (Ki67, immunocytochemical analysis). Exposure of cell lines to EdU during the final 24 hours of culture (total 10 days) during scaffold cultures recorded the number of proliferating cells during this period by fluorescence microscopy. Proliferation marker Ki67 was measured by IHC analysis following 10 days culture, with counts for the number of $Ki67^{+}$ nuclei on ImageJ. Active mitotic cell frequency recorded by enumeration of $EdU^{+}$ or $Ki67^{+}$ cells, are expressed as a ratio to total cell number. No statistically significant differences could be recorded between scaffold culture analyses between cell lines. †EdU addition to cultures was carried out by Dr. Jonathan Campbell. EdU staining was carried out by Dr. Jonathan Campbell and Rob Hume. Ki67 immunohistochemistry was carried out by Rob Hume. Analysis was carried out by Dr. Jonathan Campbell and Rob Hume.

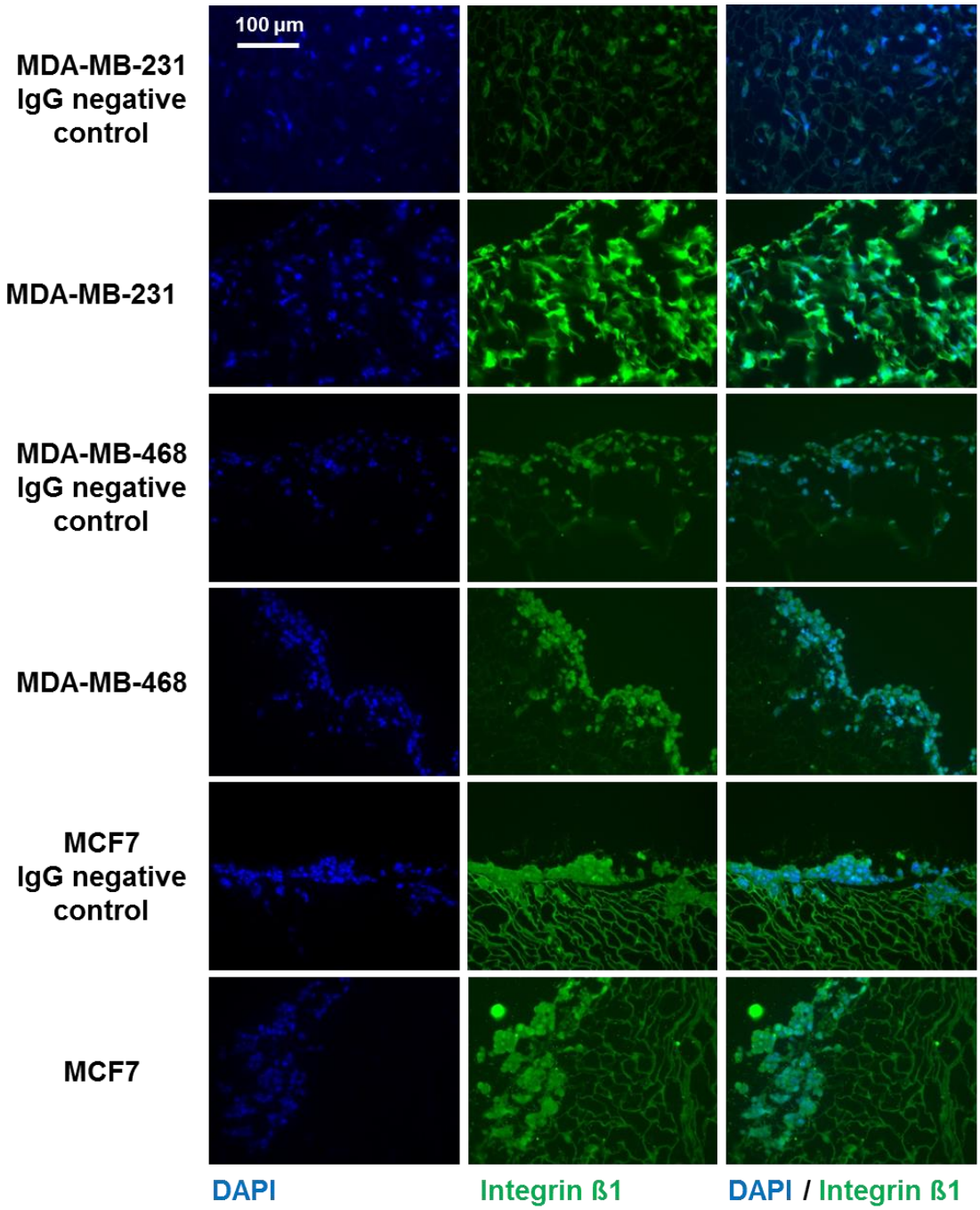


***Figure 4-12: IHC of integrin ß1 suggests expression is increased in MDA-MB-231 cells***

Immunohistochemical analysis of integrin β1 (green) expression in MDA-MB-231, MDA-MB-468 and MCF7 when cultured in anisotropic collagen scaffolds. DNA was marked with DAPI (blue). High levels of background affected the validity of these results as observed in IgG negative controls.

### 4.2.4 Epithelial-to-mesenchymal transition (EMT) of MDA-MB-468 cells and their migration in anisotropic scaffolds

EMT is a process associated with transformation of normal cells to a malignant phenotype and facilitates invasion and metastasis through down-regulation of E-cadherin mediated adhesion and a mesenchymal mode of migration (Wang et al., 2016). Additionally, epithelial cells that have undergone an EMT frequently have an increased migratory potential (Chakrabarti et al., 2012; Davis et al., 2013; Lo et al., 2007; Smith et al., 2014). As MDA-MB-468 cells showed minimal migration in the scaffold model, and to further validate the model's ability to distinguish migratory phenotypes, EMT was induced in MDA-MB-468 cells. This was carried out according to a previously published protocol using EGF treatment and serum starvation (Davis et al., 2013). EMT was identified by a spindle-shaped cell morphology (Fig. 4.13a), upregulated expression of the EMT marker vimentin as confirmed by western blotting (Fig. 4.13b) and IHC analysis (Fig. 4.13c,d).

Following successful EMT induction, EGF-treated MDA-MB-468 cells were seeded and cultured for 10 days in anisotropic collagen scaffolds to investigate whether this would influence migration distances. From these data it was observed that EMT enhanced migration by a small but significant distance in anisotropic collagen scaffolds compared to untreated MDA-MB-468 cells (Fig. 4.14).

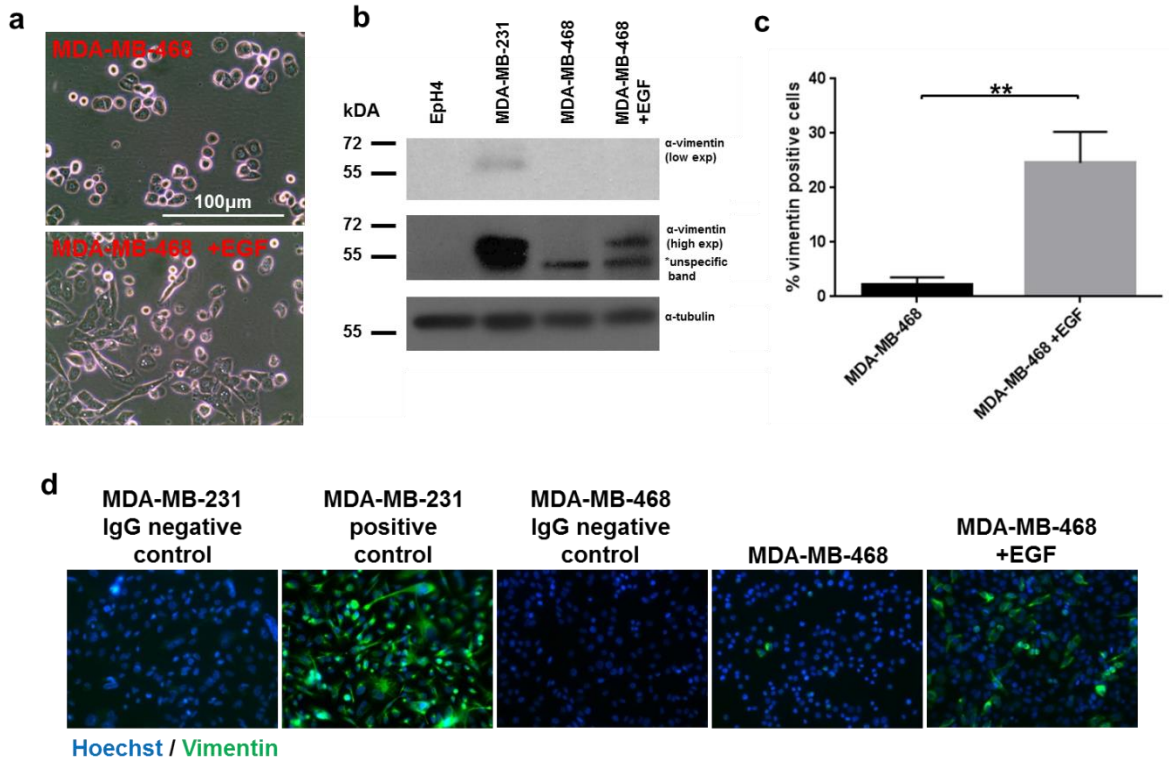


***Figure 4-13: Epidermal growth factor (EGF) induced epithelial-to-mesenchymal transition (EMT) of MDA-MB-468 cells***

MDA-MB-468 breast cancer cells were chemically induced to undergo an epithelial-to-mesenchymal transition (EMT) via epidermal growth factor addition during 2D culture. a) Phase contrast microscopy images of MDA-MB-468 cells +/- EGF treatment. b) Western blotting for EMT marker vimentin (57kDa) showing higher expression in MDA-MB-468 cells when treated with EGF. A non-specific band* was observed in the three human cell lines upon higher exposure. EpH4 murine mammary epithelial cells were used as a negative control, MDA-MB-231 as a positive control and tubulin as a loading control. c) ImageJ analysis of immunocytochemistry for vimentin positive cells as shown in d. d) Immunocytochemistry observation of vimentin expression. **$p<0.01$.

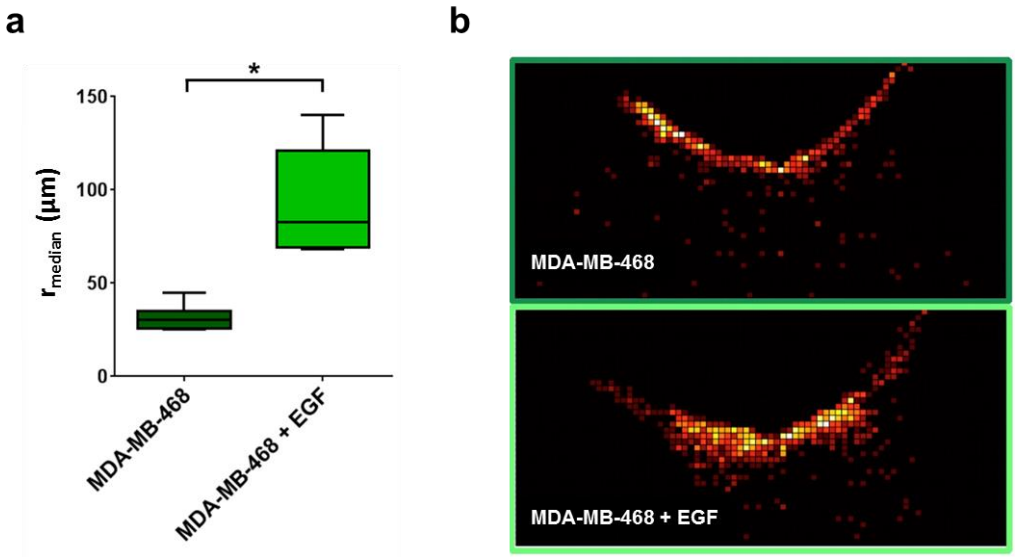


***Figure 4-14: EGF induced EMT enhances migration of MDA-MB-468 cells in anisotropic collagen scaffolds***

a) Median Euclidian cell migration distance ($r_{median}$) after 10 days culture of MDA-MD-468 cells ± EGF in anisotropic collagen I scaffolds. There is a statistically significant difference between the two distributions by Wilcoxon/Mann-Whitney U test, n=7. b) Detailed heat maps of the distribution of cells within representative scaffolds show a more pronounced migration into the scaffold when EGF is present. Each heat map shows an area around the scaffold seeding funnel of 2mm × 4mm. †Scaffold synthesis, cell seeding, culturing, imaging and analysis were carried out by Rob Hume. Heat maps representing images taken by Rob Hume were generated by Dr. Anke Husmann. *p<0.01

# 4.3 Discussion

## 4.3.1 Anisotropic collagen scaffold development

Directional control of the porous architecture of collagen scaffolds has recently been achieved using ice templating techniques (Davidenko et al., 2012; Husmann et al., 2015; Pawelec et al., 2014). Through the manipulation of ice crystal nucleation and growth described in these studies, and novel mould design, whereby a funnel was incorporated to act as a nucleation point for ice crystals to initiate, anisotropic collagen I cross-linked scaffolds were synthesised. Moreover, the funnel generated an ideal location through which cells could be seeded. The resultant internal architecture of these scaffolds was anisotropic collagen pores, radially orientated from the nucleation point that provided tracks for cells to migrate. By controlling pore shape and direction, scaffold reproducibility and tractability was significantly enhanced, which is vital if the model is to be adopted commercially as a future drug discovery platform.

Others have shown that during the freeze drying process of collagen slurries in polymethyl methacrylate moulds, the base of the slurry closest to the freeze drier shelf has a smaller porosity compared to that of the top of the slurry (Pawelec et al., 2014). This is due to an increased initial cooling rate at the base of the moulds, which was caused by a closer proximity to the freeze drier cooling shelf. A similar phenomenon was observed in the scaffolds synthesised in this thesis; pore size was smaller at the base of the slurry and increased proportionally with distance to the top and edges of the slurry. As the funnel-shape was located at the base of the moulds during freeze drying, it was therefore at the funnel edge where the smallest pore sizes were observed (Fig. 4.1, Fig. 4.2). This effect was further enhanced by the presence of the copper pin and its contact with the freeze drier cooling shelf. As copper has a lower specific heat capacity than that of the polycarbonate mould and collagen, slurry adjacent to it had an increased initial cooling rate and hence pore size was reduced in this region (Giauque and Meads, 1941; Narijauskaitė et al., 2013; Pawelec et al., 2014).

During the setup of scaffolds in the freeze drier, moulds were over-filled with collagen slurry to ensure moulds were completely filled. As a result, slurry overflowed onto the glass slips that covered the mould and underwent freeze drying, as photographed in Figure 4.3. This excess collagen displayed a macroscopically visible anisotropic radially orientated structure on anisotropic scaffolds but not isotropic scaffolds. An advantage of this is that it was used as a metric for quality control. For example, on occasions that the freeze drier would malfunction and not complete it cycle correctly, an absence of visible anisotropy on the excess collagen would provide the first indication that there was error during the process and anisotropy had not been achieved. For future development of the

protocol to provide high-throughput production of the scaffolds, these extra quality control measures would be extremely useful. Additionally, excess collagen around the base of scaffolds was not completely removed during tumour culture experiments for two reasons. Firstly, scaffold orientation could easily be identified when placing the funnel vertically. Secondly, it enabled extra stability in this vertical position to reduce the likelihood of tumour fragments falling out of the scaffolds following fragment seeding in later experiments.

### 4.3.2 The effects of ECM components on cell migration

Anisotropic collagen scaffolds were designed to mimic the TACS-3 phenotype described by Provenzano et al. surrounding aggressive breast tumours (Provenzano et al., 2006). In this previous study, TACS-3 was defined as stromal collagen fibres orientated perpendicular to the tumour edge. In Chapter 4, scaffolds recapitulated this ECM characteristic of the tumour microenvironment through the radial distribution of collagen perpendicular to the funnel edge. As breast cancer cell lines were seeded in these funnels, the scaffolds mimicked the migration of tumour cells from the tumour edge into stromal collagen fibres (Provenzano et al., 2006). However, one limitation of the anisotropic scaffolds is that they were comprised of elongated collagen pores rather than, as *in vivo*, collagen fibres. Therefore, although they mimic *in vivo* directionality, they differ in their geometry. For example, orientated collagen fibres surrounding breast tumours range between 1-2 µm thickness and have a rod-like morphology (Perry et al., 2013; Provenzano et al., 2006) . In contrast, the walls of collagen pores ranged between 2 µm thickness at the funnel edge and 5 µm at the edge of the scaffold and had a shell-like morphology. Furthermore, the elongated geometry of pores varied from micro to macro porous regions dependent on distance from the funnel. This is important because cell shape, and subsequently cell phenotype and migration, can be influenced by ECM geometry (Bhadriraju et al., 2007; Bissell et al., 1977; McWhorter et al., 2013; Wolf et al., 2013). Consequently, the porous structure may influence the migratory potential within scaffolds and should be appropriately investigated in future experiments.

### 4.3.3 Collagen scaffolds versus hydrogels

3D *in vitro* migration studies that utilise collagen as an ECM substrate commonly use collagen hydrogels as their model system (Fukuda et al., 2014; Kikuchi et al., 2011; Lee et al., 2014a; Riching et al., 2014; Truong et al., 2016). Throughout this thesis, cross-linked collagen scaffolds were used instead of collagen hydrogels, as they have a number of advantages. The chemical composition of cross-linked scaffolds can be easily manipulated by the addition of other proteins during the homogenisation process (Davidenko et al., 2010). For example, proteoglycans, such as heparin sulphate or hyaluronic acid, can be added into the collagen slurry and have been shown to effect

cellular phenotype (Campbell et al., 2011). Furthermore, by altering the ratios and timing of cross-linking, the mechanical properties of scaffolds can be manipulated (Grover et al., 2012). These tuneable parameters present opportunities for further development of the scaffolds and their potential application recapitulating alternative stromal ECM subtypes *in vitro*.

Unlike scaffolds, hydrogels can undergo shrinkage upon cross-linking which can result in unpredictable cellular remodelling subsequently effecting the mechanical properties of the bulk material (Fernandez and Bausch, 2009). Considering the mechanical properties, influenced by collagen density, can alter a cell's migratory phenotype, it is imperative that these material properties are controlled for assay robustness (Levental et al., 2009; Paszek et al., 2005).

Having access to a freeze drier meant that scaffold synthesis was considerably cheaper than commercially bought ECM products such as Matrigel (Lam and Longaker, 2012). In-house synthesis also meant that quality could be tightly controlled and fresh batches of scaffolds were synthesised on demand, rather than being reliant on commercial ordering. The dried collagen I from bovine Achilles tendon was out-sourced commercially and may be subject to batch variation and therefore future *in vitro* derivation of collagen I could also be generated in-house tested to ensure absolute purity. Furthermore, if anisotropic scaffolds were to become commercially available, the understanding of the synthesis process would be valuable intellectual property that may be of considerable interest to commercial partners.

In summary, both isotropic and anisotropic collagen scaffolds were engineered through mould design and freeze drying techniques. Equivalent external geometries were achieved for both scaffold types with altered internal architectures governed by the manipulation of ice crystal growth. With an increasing frequency of publications on collagen anisotropy and its influence in tumours, these scaffolds represent an important alternative system to investigate the phenotype *in vitro* (Conklin et al., 2011; Kakkad et al., 2016; Provenzano et al., 2006, 2008a, Ray et al., 2017a, 2017b; Riching et al., 2014; Stylianopoulos et al., 2010).

### 4.3.4 Breast cancer cell lines

Cancer cell lines adopt specific morphologies in 3D that correlate with their migratory profile (Kenny et al., 2007). Monitoring cell migration in this 3D state using collagen scaffolds, rather than relying on 2D culture enables an approach which is more reflective of both the *in vivo* scenario and migratory potential of cancer cells. Generating a novel assay for investigating breast cancer cell migration in a 3D environment was achieved using engineered anisotropic collagen scaffolds and cell lines combined with migration distance analyses.

To investigate breast cancer cell migration, three different breast cancer cell lines seeded within anisotropic and isotropic collagen scaffold. These cell lines (MDA-MB-231, MDA-MB-468 and MCF7) have similar gene expression profiles to human claudin-low triple negative breast cancer (TNBC), basal-like TNBC and $ER^+$ breast cancer, respectively (Neve et al., 2006). Previous reports have shown that these cell lines exhibit a range of migratory potential; MDA-MB-231 the most aggressive and MCF7 the least aggressive (Gordon et al., 2003; Sun et al., 2016). Utilising cell lines associated with differing breast cancer subtypes, with a range of invasive potentials, enabled the assay to model an assortment of *in vivo* scenarios *in vitro*. This study did not aim to investigate all human breast cancer subtypes; for example, $HER2^+$ breast cancers were not addressed (Neve et al., 2006; Subik et al., 2010).

The use of human cell lines, originally derived from breast cancer patient samples, infers more validity and translation of the assay to human breast cancer than if murine cell lines were used. However, breast cancer cell lines are generally considered more homogenous than the *in vivo* tumours they model, due to intra-tumour heterogeneity (ITH). Utilising a larger collection of cell lines in breast cancer studies has been shown to better represent inter-tumour heterogeneity (between different tumours). Nevertheless this still does not address the ITH (within the same tumour) that is frequently observed *in vivo* (Keller et al., 2010).

The MDA-MB-231 cell line is associated with the claudin-low TNBC and exhibits mesenchymal characteristics when cultured in 2D (Neve et al., 2006). This mesenchymal phenotype was also observed during migration assays in collagen scaffolds (Fig. 4.10). Furthermore, anisotropic scaffolds frequently supported full depth migration of MDA-MB-231 cells to the edges of the scaffold (Fig. 4.8-4.11). Although traditionally the MDA-MB-468 cell line is considered an invasive cell line, it did not migrate significantly further than the MCF7 cell line in migration assays (Fig. 4.8-4.11) (Gordon et al., 2003; Sun et al., 2016). It is reported that under 'normal' culture conditions, MDA-MB-468 cells retain epithelial characteristics (Davis et al., 2013; Jo et al., 2009). However, these same studies showed that following EGF treatment MDA-MB-468 cells undergo an epithelial-to-mesenchymal transition (EMT) and display an enhanced migratory phenotype. This EGF-mediated EMT in MDA-MB-468 was demonstrated in Chapter 4 successfully in 2D cultures by an altered cell morphology and increased vimentin expression (Fig. 4.15). Furthermore, EGF treated MDA-MB-468 cells also exhibited an enhanced migratory phenotype in anisotropic collagen scaffolds (Fig. 4.16). Potentially, the enhanced migration of mesenchymal MDA-MB-231 and EMT-MDA-MB-468 cell lines over epithelial MCF7 and 'normal' MDA-MB-468 cell lines, suggest that anisotropic collagen scaffolds support the migration of mesenchymal over epithelial cancer cell types.

Tissue disorganisation is a hallmark of cancer and can be regulated by cell-ECM signalling via transmembrane receptors, such as integrins (Lee and Vasioukhin, 2008). Integrin signalling is dependent on the ECM substrate to which a cell is adhered. Hence, accurate modelling of tissue within *in vitro* 3D models is dependent on the ECM substrate utilised and its spatial organisation (Du et al., 2011; Levental et al., 2009). Of note, integrin β1 is required for the correct polarity of epithelium in the normal mammary gland *in vivo* and *in vitro* 3D cultures (Akhtar and Streuli, 2012). Increased integrin β1 signalling can induce tissue disorganisation *in vitro* and *in vivo* and is a prognostic marker for poor survival (Park et al., 2006; dos Santos et al., 2012; Yao et al., 2007). Within anisotropic collagen scaffolds, MDA-MB-231 cells exhibited considerable migration over both MDA-MB-468 and MCF7 cell lines (Fig. 4.8, Fig. 11). Interestingly, increased integrin β1 expression was also observed in MDA-MB-231 cells as compared to the other two cell lines (Fig. 4.12). However, this data should be interpreted with caution due to high background levels present during microscopic analysis. It is plausible to hypothesise that the increased integrin β1 signalling of MDA-MB-231 cells correlates with their increased migration in anisotropic collagen scaffolds. Using western blotting techniques or an alternative antibody for IHC, increased integrin β1 expression in MDA-MB-231 cells could be confirmed in future experiments. Subsequent experiments could then involve genetic manipulation of the cell lines to either increase or decrease integrin expression to investigate its effects on migration within scaffolds. A comparison of migration distances, as used in Chapter 4, could then confirm any effects of integrin expression within the system.

Scaffold architecture can affect the biochemical and physical cues that cells respond to in a given environment. For example, nutrient diffusion and dissolved oxygen concentration can fluctuate in 3D cultures and are dependent on the distance from scaffold edges, scaffold shape, cell density, pore size and pore shape (Bian et al., 2009; Bidan et al., 2013; Kasten et al., 2008; Radisic et al., 2006; Schwan et al., 2016). Differences in the internal architecture of anisotropic and isotropic collagen scaffolds are therefore likely to have played a role in the extent of diffusion observed with different scaffold types. Furthermore, any potential compromised diffusion observed in either scaffold type is likely to be further compounded by the static nature of the culture system. This therefore adds complexity to the influence of anisotropy within the system. It has previously been shown that the migratory potential of MDA-MB-231 cells is modulated by fluctuations in nutrient diffusion and dissolved oxygen concentration (Nagelkerke et al., 2013). Interestingly, during migration assays, MDA-MB-231 cells exhibited an enhanced migratory potential in anisotropic versus isotropic scaffolds. Nonetheless, the degree to which enhanced migration in anisotropic scaffolds was a direct consequence of altered diffusion characteristics has not been quantified and would require extensive testing.

### 4.3.5 Migration distance analysis

During migration distance analysis of breast cancer cell lines, large data sets were generated measuring the Euclidian distance of every migratory cell within each scaffold from the nucleation point. Despite the use of cell lines, which are relatively homogeneous compared to primary tumours, the data still exhibited a large degree of variation (Fig. 4.8, Fig. 4.9a). Thus, even within a relatively homogenous population of cells, there are a range of migratory potentials. Further study of these subpopulations may enable investigation of the mechanisms that enhance/supress migration. For instance, IHC analysis could determine whether expression of markers of interest differ between cells closest to the nucleation point and cells found deep within the scaffolds. In addition, laser capture microdissection could be used to investigate varying migratory phenotypes between spatially separated cell populations (Espina et al., 2006). This technique can laser-dissect small groups of cells or single cells from tissue samples for downstream analysis. For example, changes in gene expression can be subsequently analysed using single cell sequencing to detect differences in migratory subpopulations (Navin et al., 2011; Wang et al., 2014b; Xu et al., 2012). Moreover, laser capture microdissection can be combined with histological or immunocytochemical analysis to identify target populations before cell capture (Vincent et al., 2002).

Collagen scaffolds were 3 mm deep by 7mm in diameter (Fig. 4.2). In contrast, conventional 3D culture is frequently confined to droplets of hydrogel approximately 50-500 µm thick (Casey et al., 2017; Cavo et al., 2016; Shih and Yamada, 2011; Singh et al., 2015). Initial attempts to use live imaging and CellTracker to visualise cells within scaffolds exposed the limitations of imaging techniques in relatively thick samples. Confocal lasers could not penetrate far below the funnel and scaffold surface and therefore only small depth of view was achieved (Fig. 4.4). Imaging to the full scaffold depth was achieved but required fixation and bisecting of scaffolds or embedding in paraffin wax, preventing live imaging from being carried out (Fig. 4.5, Fig. 4.9, Fig. 4.10, Fig. 4.12, Fig. 4.14).

The Euclidian distance ($r_{median}$) was used to quantify cell migration despite not being an exact representation of the migratory path travelled. This was done to normalise the data; the same metric was applied to all cells in all scaffold types. Distance measurements were collected through end-point analysis of fixed samples at either 24 hour or 10 day time points. Hence, exact migratory pathways could not be measured with this methodology, as live cell imaging techniques are required, another rationale for the use of the Euclidian distance metric (Shih and Yamada, 2011).

Although Euclidian distance may not be the true distance travelled, it may hold increased validity in anisotropic scaffolds. This is because collagen alignment encourages the unidirectional/bidirectional movement of cells along the axis of alignment (Ray et al., 2017b). The Euclidian distance from the

segmented nucleation point to each migratory cell approximately followed the long axis of the radially distributed directional collagen pores orientated from the nucleation point to the edge of anisotropic scaffolds. Accordingly, this may have increased the accuracy of the Euclidian distance metric to measure the migratory pathway in anisotropic scaffolds and thus showed increased tractability within this model.

In contrast, unidirectional/bidirectional restricted movement cannot be presumed in isotropic scaffolds due to the absence of pore directionality. Therefore the Euclidian distance has reduced validity in this system. To this point, it may be that the effect of collagen alignment encouraging unidirectional/bidirectional movement explains the enhanced Euclidian distance migrated in anisotropic versus isotropic scaffolds seeded with MDA-MB-231 cells (Fig. 4.8, Fig. 4.9a) (Ray et al., 2017b). Hence, the choice of migratory path is reduced and directed away from the nucleation point by directional pores, thus increasing migration distance away from that point in anisotropic scaffolds. Conversely, the reduced Euclidian distance migrated in isotropic scaffolds may reflect an increased likelihood of multidirectional movement from the nucleation point (Fig. 4.8, Fig. 4.9). Although this explanation reduces the validity of the Euclidian distance to accurately measure the exact path a cell has travelled, it does have relevance to the metastatic ability of a cancer cell. For example, if the nucleation point represents the edge of a tumour and the scaffold represents the surrounding stroma, the Euclidian distance represents how far a cancer cell has migrated from the tumour into the surrounding tissue. Hence, the further a cell has deviated from the tumour edge the more likely it is to come in contact with a blood vessel or another organ. A longer Euclidian distance is therefore, potentially, an indication of the higher the probability a cell exit the gland and metastasize.

Heat maps were utilised to represent the migration data and compare scaffold/cell types (Fig. 4.9). This helped not only to visualise the data but could also be used for high throughput analysis in future studies. By automating the analysis protocol using computer programming tools such as MATLAB (The MathWorks Inc., 2010), the current more complex ImageJ and Excel analysis could be circumvented. Furthermore, automation and high throughput analysis would create a more attractive prospect for commercialisation of these models.

### 4.3.6 Proliferation of migratory human breast cancer cell lines in collagen scaffolds

Proliferation analyses were used to investigate whether variations in proliferative capacity existed between cell lines, if these differences were associated with their migratory potential and whether proliferation was influenced by collagen anisotropy. Using both EdU and Ki67 staining, analyses were

conducted in both scaffold types and in 2D controls (Fig. 4.11). Differences between EdU and Ki67 ratios were occasionally observed within the same sample type (Fig. 4.11), for example, although the median for the Ki67 ratio was within the interquartile range of EdU ratio for most scaffold types, it was not for MDA-MB-468 anisotropic samples. Additionally, the range and interquartile range was considerably tighter when measuring Ki67 as compared to EdU in all samples. One factor which may attribute to these differences is the number of experimental repeats. However, it would be anticipated that the fewer repeats in Ki67 samples would have created a larger interquartile range, which was not the case. Alternatively, whilst EdU and Ki67 are both markers of proliferation, they indicate different parts of the cell cycle (Gerdes et al., 1983). The Ki67 protein is expressed throughout all stages of the cell cycle and is only absent in non-cycling cells, whereas EdU is only incorporated into newly synthesised DNA (Bologna-Molina et al., 2013; Salic and Mitchison, 2008). Therefore, $EdU^+$ cells represent newly divided cells and are not necessarily still cycling or $Ki67^+$.

Acellular surfaces can be populated by neighbouring cells through migration, proliferation or a combination of the two (De Donatis et al., 2008; Rodriguez et al., 2005; Zahm et al., 1997). MDA-MB-231 cells showed the furthest median Euclidian distance from the nucleation point (Fig. 4.8, Fig. 4.9) but the lowest levels of proliferation (Fig. 4.11), as compared to MDA-MB-468 and MCF7 cells. These data confirmed that the distance travelled by cells within collagen scaffolds does not correlate with the proliferation rate. Accordingly, the increased distance of MDA-MB-231 cells into scaffolds was dependent on their migratory potential rather than their proliferation rate.

A high metastatic potential but low proliferation rate, as observed in MDA-MB-231 cells (Fig. 4.8, Fig. 4.9, Fig. 4.11), is a phenomenon that has been observed in other cancer cell populations and has been attributed to a number of factors (Ampuja et al., 2013; Evdokimova et al., 2009; Flores et al., 2016; Hur et al., 2016; Tsai et al., 2012; Vega et al., 2004). For example, it has been shown that upregulation of the gene *HOXC9*, that is associated with poor patient prognosis, increases migration and reduces the proliferative capacity of breast cancer cells (Hur et al., 2016). Additionally, growth factors such as bone morphogenic protein-4 (BMP4) have been shown to enhance migration whilst reducing proliferation (Ampuja et al., 2013). Of note, EMT, a process which can induce a migratory phenotype in untransformed cell types, has been shown in some studies to reduce proliferation (Evdokimova et al., 2009; Flores et al., 2016; Tsai et al., 2012; Vega et al., 2004). Interestingly, the highest migratory potential and lowest proliferation rates were observed in the MDA-MB-231 cells; a claudin-low TNBC cell line with a mesenchymal phenotype (Fig. 4.8, Fig. 4.9, Fig. 4.11) (Neve et al., 2006). It is possible that the proliferation rate of MDA-MB-231 cells may have been affected by the original EMT event during its transformation *in vivo* and thus caused a high migratory/low

proliferation phenotype, however this is speculation. MDA-MB-468 cells showed increased migration in anisotropic collagen scaffolds upon EGF-mediated EMT induction (Fig. 4.14). Future study investigating the proliferative capacity of MDA-MB-468 EMT cells may elucidate whether this cell line exhibited an EMT-related reduced proliferation rate, as reported for other cell lines (Evdokimova et al., 2009; Flores et al., 2016; Tsai et al., 2012; Vega et al., 2004).

The proliferation rate of cells measured by Ki67 expression was higher during 2D culture on glass cover slips than 3D collagen scaffold cultures for each cell type (Fig. 4.11). However, a number of caveats were apparent during this comparison. Cells in 2D culture were stained using an immunocytochemistry (ICC) protocol which meant direct fixation, blocking and exposure to the Ki67 antibody. For 3D scaffolds, samples were stained using an IHC paraffin embedding protocol and therefore required a number of extra steps for IHC analysis, such as dewaxing, rehydration and antigen retrieval, before exposure to the Ki67 antibody. Although these protocols were staggered so that antibody exposure times were equivalent, distinct unavoidable differences in their processing and sensitivity may have affected the experimental outcome. Furthermore, cells were cultured and exposed to two different materials: glass and collagen I. These two materials hold dramatically different mechanical properties which has been shown to effect proliferation rate (Lawyer et al., 2012). Additionally, due to the surface chemistries of the two materials, integrin binding differs between the substrates which can also affect proliferation (Bachhuka et al., 2017; García et al., 1999). Future studies could reduce these effects of substrate variation by collagen coating and chemical cross-linking glass coverslips before cell seeding.

Another explanation for the differences in proliferation on 2D and 3D scaffolds could be variations in waste, nutrient and $O_2$ diffusion. Cells cultured in 2D are in direct contact with culture medium and are able to secrete waste products into a relatively diffuse environment. Within 3D cultures, cells are situated within a matrix to which diffusion can be compromised. This issue is exacerbated in static culture systems and could be partially alleviated with a bioreactor setup that provides a constant flow of media and can increase cellular proliferation (Varley et al., 2017; Zhang et al., 2009). Bioreactors are, however, complex and expensive and the benefits need be carefully assessed if the scaffold system were to be scaled up for commercial purposes.

### 4.3.7 ECM substrate

It has been reported that each cell line used in these migration assays, expresses different levels of integrin receptors (Gui et al., 1995; Taherian et al., 2011). Considering integrins are vital to the attachment and interaction of cells with the various ECM proteins *in vivo*, it is likely that the cell lines used will attach and interact with the collagen scaffold at different capacities. Furthermore, cells

that interact more strongly with other ECM components, such as hyaluronic acid, may exhibit a more accurate migratory phenotype *in vitro* with the inclusion of these ECM proteins into the scaffold. Nonetheless, collagen I is the most abundant ECM protein in the interstitial matrix of the mammary gland and is often pervasive at the breast tumour–stroma edge (Bonnans et al., 2014; Boyd et al., 2011; Erler et al., 2006; Provenzano et al., 2006). The model therefore includes the major ECM protein surrounding breast tumours but could be improved through the addition of other ECM proteins.

### 4.3.8 Comparison to the Boyden chamber assay

In the literature, studies commonly utilise Boyden chambers/transwell inserts to investigate the migration of cells in 3D (Boyden, 1962; Chioni and Grose, 2012; Hsieh and Huang, 2016; McSherry et al., 2011; Nagelkerke et al., 2013). In Boyden assays cells are seeded in a well separated from another well by a porous membrane that permits the passage of cells. Migratory potential can be assessed with relative simplicity; the read-out being a count of migratory cells found on the opposite side of the membrane. It therefore requires little technical ability as compared to other 3D culture analysis and, due to its common use in migration studies, protocols describing its execution are well documented (Albini and Benelli, 2007; Chen, 2005; Goncharova et al., 2007). However, although cells can move laterally on Boyden chamber membranes via the X- and Y-axes, as well as through it on the Z axis, the cell count read-out only measures cell migration on the Z-axis. Furthermore, unlike the scaffold migration assay, it only represents the frequency of cells that have traversed the thickness of the membrane and gives no indication of the individual distance each cell has travelled.

The breast cancer cell migration assays described in Chapter 4 are more complex than traditional Boyden chamber assays, both in terms of technical skill and analysis/interpretation of results. For example, the cell migration assays required extra steps, such as placing the scaffold into a Boyden chamber, precise seeding of cells into the scaffold funnel, removing and bisecting the scaffold and imaging the cells. Combined with the additional analyses associated with cell migration assays, it could be argued that the Boyden chamber assay be the preferred model due to its simplicity. However, the employment of a natural polymer such as collagen, found in abundance in stroma surrounding breast tumours, displays a level of superiority in recapitulating the *in vivo* scenario when using the cell migration assays. Analyses are more complex and time-consuming compared to the simple read-out of the Boyden assay, and data output is more intricate. However, this provides the user with a greater level of detail by providing the migratory potential of each individual cell. Accordingly, observation of the spread of cells to varying distances within scaffolds and future

studies investigating the genetic differences between invasive and non-invasive clones could elucidate a deeper understanding of cancer cell migration and its mechanisms.

### 4.3.9 Conclusion

In terms of fully recapitulating the tumour microenvironment *in vitro*, a number of improvements could be applied to the cell migration assay described here. These improvements include, but are not restricted to, the addition of growth factors and/or hormones present *in vivo*, the addition of other stromal cell types such as adipocytes and immune cells, and the addition of ECM basement membrane proteins. Importantly, however, this would add layers of complexity and expense to the system and could reduce the likelihood of either mass production or its use in research laboratories as common practice.

Collectively, this assay demonstrated the cell-type dependent effects of anisotropy on human breast cancer cell migration. The vast current and future potential of the assay to analyse migration in a number of contexts and to a high level of detail, validates its utility as a sophisticated tool to analyse the movement of cancer cells. With the inclusion of either a range of cell lines or possibly cell inoculates from a tumour biopsy, automation of analysis and modifications to the scaffold composition, the model holds promise in becoming a commonly used assay in the field of cancer research and drug discovery.

# 5 Tumour cell invasiveness and response to chemotherapeutics in adipocyte invested 3D engineered anisotropic collagen scaffolds

# 5.1 Introduction

Breast cancer mortality is a consequence of tumour metastasis to a variety of sites including lung, brain and bone. Distinguishing tumours that will metastasise from those that will not is challenging and often results in un-necessary or inappropriate treatment of women with primary breast cancer. As a step towards personalised medicine, it is essential to be able to predict the capacity of a tumour to metastasise and to respond to particular therapeutic regimes. A further confounding factor is the heterogeneous nature of many breast tumours where a subclone of tumour cells may behave differently to the bulk tumour. This is unlike the more homogeneous cell populations observed in established cell lines. Thus, this chapter sought to develop an *in vitro* culture model that accurately recapitulates the breast stroma in 3D and allows individual cells from a tumour biopsy fragment to invade this stromal milieu. In addition, it aimed to develop techniques that permit assessment/visualization of this 'metastatic' potential and the response of invading cells to a panel of therapeutic drugs.

A crucial component of the breast tumour stroma is the fat pad, which provides an adipocyte-rich environment that breast tumour cells must traverse or negotiate. Adipocytes within the fat pad are responsive to various hormones and secrete a variety of components, including adipokines, that can influence cancer cell migration (Balaban et al., 2017; Picon-Ruiz et al., 2016; Rowan et al., 2014). Thus, it was sought to incorporate this stromal component into a 3D model.

In the previous chapter, 3D anisotropic engineered collagen scaffolds were developed and demonstrated their value as a tool to measure the ability of individual cells from established breast cancer cell lines to invade the scaffold. However, breast tumours are heterogeneous in nature, and metastases arise from a minor yet critical subclone of tumour cells that evolve within a specific tumour microenvironment. This chapter reports significant enhancements to the previous migration assay and modifies the synthetic fat pad protocol from chapter 3 by introducing pre-adipocytes into anisotropic collagen scaffolds and differentiating into lipid-filled adipocytes (Davidenko et al. 2010). Further improvements involved implanting primary mammary tumour fragments and measuring both the ability of tumour cells to invade the scaffold and their mode of migration. These results show that this enhanced 3D model permits the distinct migratory behaviours of cells from different types of tumours to be observed and quantitatively analysed. Furthermore, this approach provides a rapid screen of the response of invading cells to therapeutic drugs. Thus, this model can provide an *in vitro* platform for drug screening that will be useful in identifying efficacy and toxicity and may be utilised for personalised breast cancer medicine.

# 5.2 Results

## 5.2.1 Synthesising the Engineered Tumour-Stroma Interaction Model (ET-SIM)

To recapitulate the tumour associated collagen signature-3 (TACS-3) that is frequently observed surrounding aggressive mammary tumours, 3D anisotropic collagen I scaffolds were synthesised using the freeze drying protocol described in chapter 4 (Campbell et al., 2017; Conklin et al., 2011; Provenzano et al., 2006). As adipocytes have been implicated in breast cancer progression through paracrine and endocrine signalling and can effect breast cancer cell line invasion and migration *in vitro*, it was then intended to also incorporate this stromal component into the model (Balaban et al., 2017; Dirat et al., 2011; Duong et al., 2015; Falk Libby et al., 2015; Iyengar et al., 2005; Kim et al., 2009a; Lee et al., 2015; Picon-Ruiz et al., 2016; Wang et al., 2015, 2017). For this purpose a synthetic fat pad within the anisotropic scaffolds was synthesised by seeding 3T3-L1 preadipocytes throughout, culturing for 7 days to fill the scaffold and then switching to differentiation media to induce their conversion into mature adipocytes (Davidenko et al. 2010). Although this protocol had been demonstrated in isotropic collagen scaffolds, it had not been attempted in an anisotropic setting. Since cell differentiation can be effected by 3D culture and the morphology of the ECM substrate to which cells adhere, analysis of successful differentiation was required (Bachhuka et al., 2017; Grover et al., 2012; Kasten et al., 2008; Kim et al., 2014). The work flow to generate this model that is named “Engineered Tumour-Stroma Interaction Model” (ET-SIM) is illustrated in Fig. 5.1a. 3D Immunolocalisation techniques were then utilised to analyse 3T3-L1 differentiation in anisotropic collagen scaffolds.

To ensure that 3T3-L1 preadipocytes could successfully differentiate within anisotropic collagen scaffolds, cells were visualised using 3D immunolocalisation and multi-photon microscopy (Fig. 5.1). Using a two-photon technique known as second harmonic generation (SHG), the collagen I interior of the scaffold could be imaged directly. This technique does not require any prior immunostaining or fluorescent tagging of collagen structures to enable collagen I visualisation. Instead, it relies on the non-centrosymmetric structure of collagen to allow excitation by two photons of the same wavelength and emission of one photon at half the wavelength of the excitation photons (Heinz et al., 1982; Theodossiou et al., 2006). As a result, unlabelled and uncompromised collagen I was visualised, providing further evidence of the anisotropic collagen structure of the scaffolds (Fig. 5.1). Intracellular and extracellular structures can often be altered or destroyed during certain histological processes such as paraffin embedding (D’Andrea, 2004; Pudney and Anderson, 1995). Therefore,

application of a technique such as SHG that can image unaltered tissue structures in 3D is highly advantageous.

Whole scaffold immunostaining in conjunction with two-photon fluorescence microscopy (2pf) and SHG was used to visualise mature adipocytes (Fig. 5.1b, green nuclei, red lipid vesicles) and detect the collagen I scaffold (Fig. 5.1b, grey), respectively. As the SHG (Fig. 5.1b,c, grey) emission wavelengths has spectral overlap with the emission of typical DNA markers that emit within blue wavelengths of light, such as DAPI and Hoechst, the green fluorescent DNA dye SYTO 16 (Fig. 5.1b,c, green) was used as an alternative cell nuclei marker. This provided simple distinction between collagen and cell nuclei by colour rather than relying on morphology. Combined 3D z-stacks as maximum intensity projections show adipocytes located at varying depths in between anisotropic collagen I pores (Fig. 5.1b, left). Individual z-sections show mature adipocytes exhibiting intracellular immunostaining for the lipid vesicle marker perilipin, within anisotropic collagen pores (Fig. 5.1b, i-iii). Within these z-sections, perilipin expression can be observed on lipid vesicle membranes and not within the vesicle itself (Fig. 5.1b, i-iii). These data demonstrate the ability of 3T3-L1 cells to penetrate, proliferate and differentiate to fill anisotropic collagen scaffolds with fat to generate the ET-SIM culture system.

One caveat of the anisotropic collagen I scaffolds synthesised for the cell migration assay described in Chapter 4 is that the scaffolds used only contained one ECM protein; collagen I. Although this protein is the major constituent of the stromal ECM, other proteins are also present, such as collagen IV and laminin which are normally associated with the basement membrane, (Mariman and Wang, 2010; Mori et al., 2014; Vaicik et al., 2014). Furthermore, these proteins have been shown to influence cancer cell phenotype and migratory potential (Favreau et al., 2014; Ishikawa et al., 2014; Öhlund et al., 2013; Sato et al., 2015). The inclusion of other ECM proteins into anisotropic collagen scaffolds would therefore increase its capacity to model the tumour microenvironment, including the surrounding stroma. Previously, it has been reported that 3T3-L1 cells express the basement membrane proteins collagen IV and laminin upon adipogenesis (Aratani and Kitagawa, 1988; Ojima et al., 2016). As shown in Fig. 5.1c, both proteins were deposited in a pericellular fashion during adipogenesis within anisotropic scaffolds. Therefore, ET-SIM comprised not only directional collagen I and adipocytes but also basement membrane proteins. As a result, ET-SIM successfully recapitulated the anisotropic TACS-3 collagenous stromal structure surrounding breast tumours whilst also incorporating stromal mature adipocytes and other constituent ECM proteins, all key components of the mammary tumour stroma (Conklin et al., 2011; Huang et al., 2017; Kusuma et al., 2011; Provenzano et al., 2006).

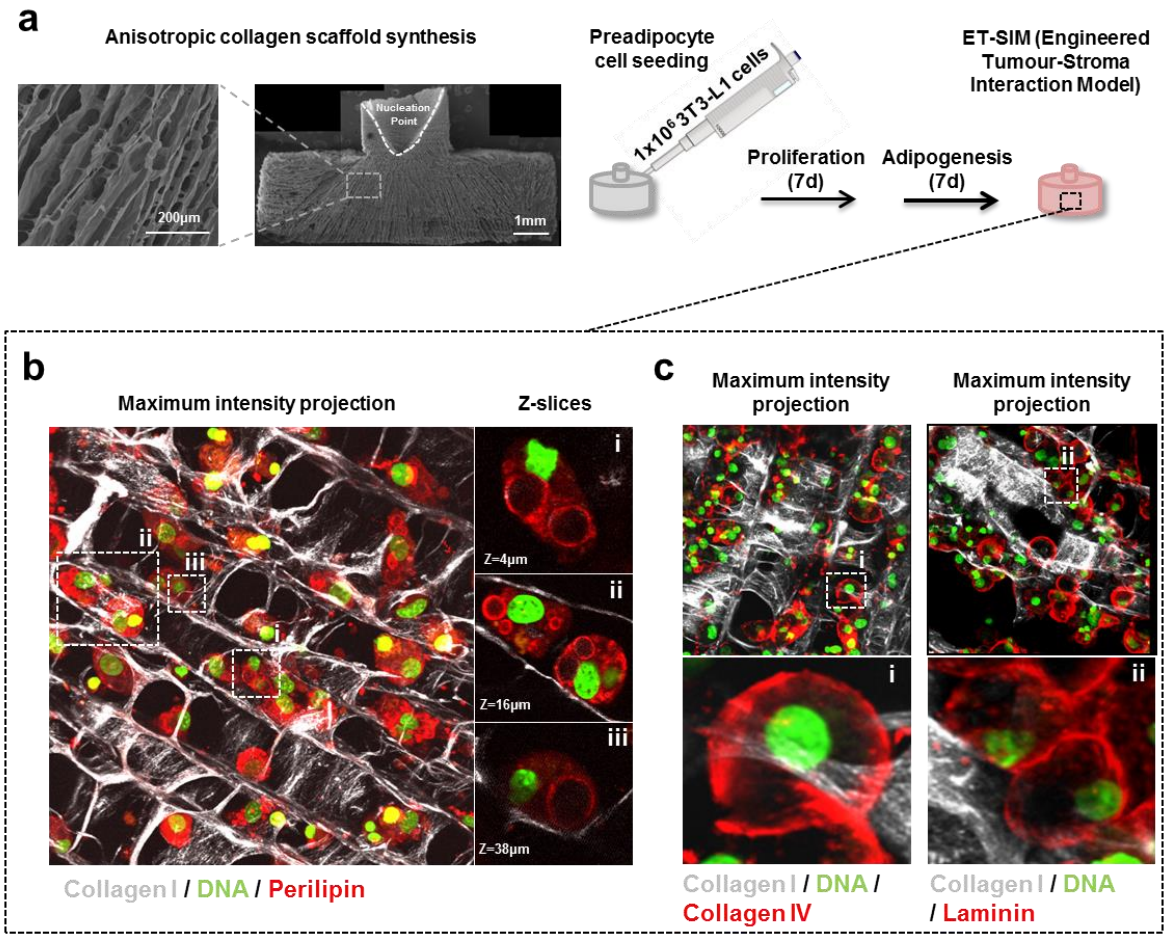


***Figure 5-1: Engineered Tumour-Stroma Interaction Model (ET-SIM)***

(a) Scanning electron micrograph (SEM) of anisotropic collagen scaffold (scaffold nucleation point marked with a white dotted line) with directional collagen pores and schematic of ET-SIM (Engineered Tumour-Stroma Interaction Model) culture. SEM image taken by Dr. Anke Husmann (b) Whole mount immunostained ET-SIM culture imaged using second harmonic generation (SHG, collagen I, grey) and two photon fluorescence (2pf) microscopy z-stacks. Nuclei are stained with green fluorescent dye SYTO16 (green). Lipids are stained with anti-perilipin (red). Z-stacks are displayed as a maximum intensity projections (left) and individual zoomed in z-slices (i-iii, right). (c) Whole mount immunostained ET-SIM culture imaged using SHG and 2pf microscopy z-stacks and displayed as maximum intensity projections. Nuclei are stained with green fluorescent dye SYTO16 (green). Basement membrane proteins are stained with anti-collagen IV (red, left) and anti-laminin (red, right). Digitally magnified maximum intensity projections shown in (i) and (ii).

### 5.2.2 ET-SIM and tumour fragment culture

Having shown in Chapter 4 that anisotropic collagen scaffolds are an effective tool for analysing the migratory behaviour of cultured breast cancer cell lines, this chapter aimed to extend this to investigate the capacity of cells from primary tumours to migrate into a surrounding stroma. This is a more relevant comparison to breast tumour growth and metastasis *in vivo* as the invasive capacity of cells is analysed from the context of intact tumour architecture. Furthermore, this preserves the immediate surrounding tumour microenvironment comprising of cancer-associated fibroblasts, immune cells, cytokines and extracellular matrix. Since there are multiple sub-types of breast cancer and individual breast cancers are highly heterogeneous, a comparison was sought between the invasive behaviour of tumour cells derived from mouse mammary tumour models initiated by different oncogenes.

To investigate the migration of tumour cells through these 3T3-L1-containing anisotropic scaffolds, a protocol was devised to culture primary tumour fragments. Two tumour models were selected for their culture in ET-SIM; the MMTV-*Wnt1* model and MMTV-Her2/*neu* tumour-derived TUBO cells injected into mammary fat pads (Tsukamoto et al. 1988; Rovero et al. 2000). Once established, primary tumours were harvested and frozen for subsequent experiments to provide a biobank of near identical tumour biopsies. After thawing, tumours were revived and dissected in a tissue culture hood using a scalpel blade and a pair of forceps in a petri dish in sterile air. Due to time constraints, as the living tissue was now not contained in culture media and due to the rudimentary process of dissection, fragment sizes were approximated by eye to the same dimensions. As a result, a degree of variation existed between the size and morphology of each tumour fragment. Tumours were dissected to fit within the seeding funnel of ET-SIM cultures as shown schematically in Fig. 5.2. Each tumour yielded approximately 30 tumour fragments of a suitable size for scaffold seeding and therefore provided approximately 30 experiments per tumour. MMTV-*Wnt1* tumours were harvested and gifted by Dr. Peter Kreuzaler (Department of Biochemistry, University of Cambridge). TUBO cells were injected and tumours harvested by Dr. Sara Pensa and Dr. Jessica Hitchcock from the Watson laboratory.

Previous studies have reproduced collagen anisotropy *in vitro* using collagen gels that were aligned along one axis direction (Thomopoulos et al. 2005; Provenzano et al. 2008; Ray et al. 2017; Riching et al. 2014; Stylianopoulos et al. 2010; Dickinson et al. 1994). For anisotropic collagen scaffolds, collagen pores were aligned perpendicular to the surface of the nucleation point in all directions. Therefore, as tumour fragments were seeded in the funnel / on the nucleation point, the scaffold mimicked an anisotropic ECM at the periphery of the tumour in all directions mimicking the TACS-3

phenotype (Provenzano et al., 2006). Accordingly, the radial distribution of collagen anisotropy therefore enhanced the model's performance in reproducing the TACS-3 phenotype when seeded with tumour fragments.

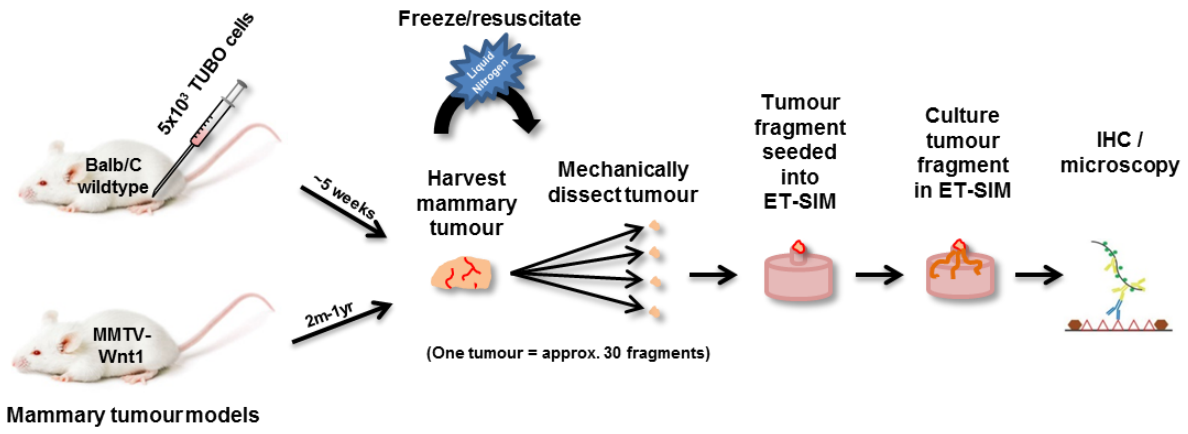


***Figure 5-2: Schematic of tumour fragment and ET-SIM co-culture***

Diagram depicting the workflow of tumour fragment culture in the ET-SIM culture system. Tumours were generated by either fat pad injection of the Her2-overexpressing TUBO mammary cancer cell line into syngeneic mice or spontaneously in MMTV-*Wnt1* transgenic mice. These were harvested and frozen in liquid nitrogen followed by mechanical dissection and seeding into ET-SIM cultures. Tumour fragments were then cultured, fixed and immunostained for confocal microscopy analysis.

### 5.2.3 ET-SIM can distinguish tumour cell migration phenotypes

The first tumour model analysed was the well-established MMTV-*Wnt1* transgenic mouse model (Tsukamoto et al., 1988). Within this model, overexpression of the *Wnt1* proto-oncogene is driven by the MMTV promoter, resulting in mammary adenocarcinoma development in FVB mice. Notably, it has been used to study mammary tumorigenesis for decades in a range of different studies (Bocchinfuso et al., 1999; Cho et al., 2008; Monteiro et al., 2014; Teissedre et al., 2009; Tsukamoto et al., 1988). However, it has been subject to controversy with some debating that the *Wnt1* overexpression subtype does not exist in human tumours.

Wnt / β-catenin pathway activation leads to the nuclear and cytoplasmic localisation of β-catenin, a protein normally located within the cell membrane of luminal cells. It has been shown that this enriched nuclear and/or cytoplasmic localisation of β-catenin is observed in basal-like human breast cancers (Khramtsov et al., 2010). Furthermore, cytoplasmic β-catenin has been shown to be associated with poor patient prognosis (Lopez-Knowles et al., 2010). This indicates that the Wnt1 pathway is activated in human breast tumour subtypes and therefore the MMTV-*Wnt1* mouse model bears relevance to the study of the human disease. Moreover, gene expression profiling has revealed that MMTV-*Wnt1* tumours cluster with human basal-like tumours, further supporting their relevance to this disease (Pfefferle et al., 2013). Importantly, Provenzano et al. first described the TACS-3 phenotype associated with poor patient prognosis in the MMTV-*Wnt1* model. Accordingly, this model was optimal for use within the ET-SIM system that aimed to recapitulate the TACS-3 phenotype *in vitro* (Conklin et al., 2011; Provenzano et al., 2006).

To investigate MMTV-*Wnt1* tumour survival, fragments were cultured in ET-SIM for 72 hours, fixed, paraffin embedded, sectioned and stained with the apoptosis marker cleaved caspase-3 (CC3). IHC revealed low levels of CC3 at both the edge of the tumour free from contact with the scaffold as well as the edge in contact with the scaffold. This indicated that the majority of tumour cells survived in ET-SIM cultures and did not undergo apoptosis (Fig. 5.3iv and Fig. 5.4iv). Therefore, ET-SIM was shown to support the culture of MMTV-*Wnt1* tumour fragments.

A typical characteristic of MMTV-*Wnt1* tumours is a reverse epithelial bilayer phenotype (Monteiro et al., 2014; Teissedre et al., 2009). This is described by a reversed location and polarisation of the normal epithelium, whereby basal cells are found lining the lumen of epithelial structures and luminal cells surround them. The scaffold-free edge of the tumour retained this architecture showing a reverse bilayer phenotype with basal cells, defined by their expression of cytokeratin-14 (K14), α-smooth muscle actin (αSMA) and nuclear p63, located lining the lumen (Fig. 5.3) (Monteiro et al., 2014; Teissedre et al., 2009). At the same edge, luminal cells expressing β-catenin and E-cadherin

showed a hyperplastic, disorganised cobblestone phenotype (Fig. 5.3). In contrast, where the tumour contacted the scaffold, both basal ($K14^+$, $\alpha SMA^+$, $p63^+$) and luminal (E-$cadherin^+$, $\beta$-$catenin^+$) cells were seen invading collectively into the surrounding stroma (Fig. 5.4). These tumour cells migrated parallel to the pores of collagen in the scaffold, demonstrating the directional migratory effect of anisotropic ECM architecture on tumour cell movement (Fig. 5.4). The resultant tendril-like epithelial formation conformed closely to the anisotropic porous architecture of the scaffold, indicating that these scaffolds present 3D surfaces for a structured spatial analysis of tumour infiltration (Fig. 5.4).

The second tumour model utilised was the TUBO tumour model (Rovero et al. 2000). The TUBO cancer cell line was derived from a mammary carcinoma that developed in a BALB/c-Her2/*neu* transgenic mouse. It therefore originated from a Her2 overexpressing tumour within a BALB/c mouse strain and upon its injection into a syngeneic mouse mammary gland from a BALB/c background, mammary tumours are established. This particular model was chosen as overexpression of HER2 occurs in approximately 25% of human breast cancers and is related to a poorer prognosis than the more common oestrogen receptor positive subtypes (Chavarri-Guerra et al., 2017). Therefore, recapitulating its progression and migration *in vitro* is of profound relevance and importance. An advantage to utilising TUBO tumours is that as they arise approximately 5 weeks after cell inoculation (Rovero et al. 2000). This allows faster experimental turnaround compared with the MMTV-*Wnt1* model which requires 2 months to 1 year for spontaneous tumour formation (Monteiro et al., 2014; Teissedre et al., 2009; Tsukamoto et al., 1988). Furthermore, TUBO tumours are established in syngeneic mice and therefore illicit an immune response but are not immune-rejected by the host. As the immune system is heavily implicated in breast tumorigenesis, the model therefore holds advantages over immunodeficient mouse models, by more accurately modelling the immunology component of the disease (Chen et al., 2017; Fujimoto et al., 2009; Georgoudaki et al., 2016; Sousa et al., 2015; Wculek and Malanchi, 2015)

Following 72 hours of TUBO tumour fragment culture in ET-SIM, samples were fixed, embedded in paraffin and sectioned longitudinally (Fig. 5.5, top, schematic). IHC analysis showed a proportion of cells within the tumour fragment and migratory clusters that were negative for CC3 and therefore had not undergone apoptosis (Fig. 5.5). This demonstrated that TUBO primary tumour fragments and migratory TUBO tumour cells were alive and could be supported in ET-SIM cultures.

In stark contrast to the collective outpouring of cells from MMTV-*Wnt1* tumour fragments, the majority of migratory TUBO tumour cells migrated as small clusters (<10 cell) (Fig. 5.5,i-iii) or rarer large clusters (>50 cells) separate from the seeded tumour fragment (Fig. 5.5,iv). Stochastic

expression of the epithelial-to-mesenchymal (EMT) marker vimentin was observed around one edge of cell nuclei in both the seeded tumour fragment and in cells that had migrated into the scaffold (Fig. 5.6).

Thus, through the use of two different tumour models it has been demonstrated that ET-SIM can support the culture of primary mammary tumour fragments. Furthermore, their distinct migratory phenotypes were readily assessed in ET-SIM cultures.

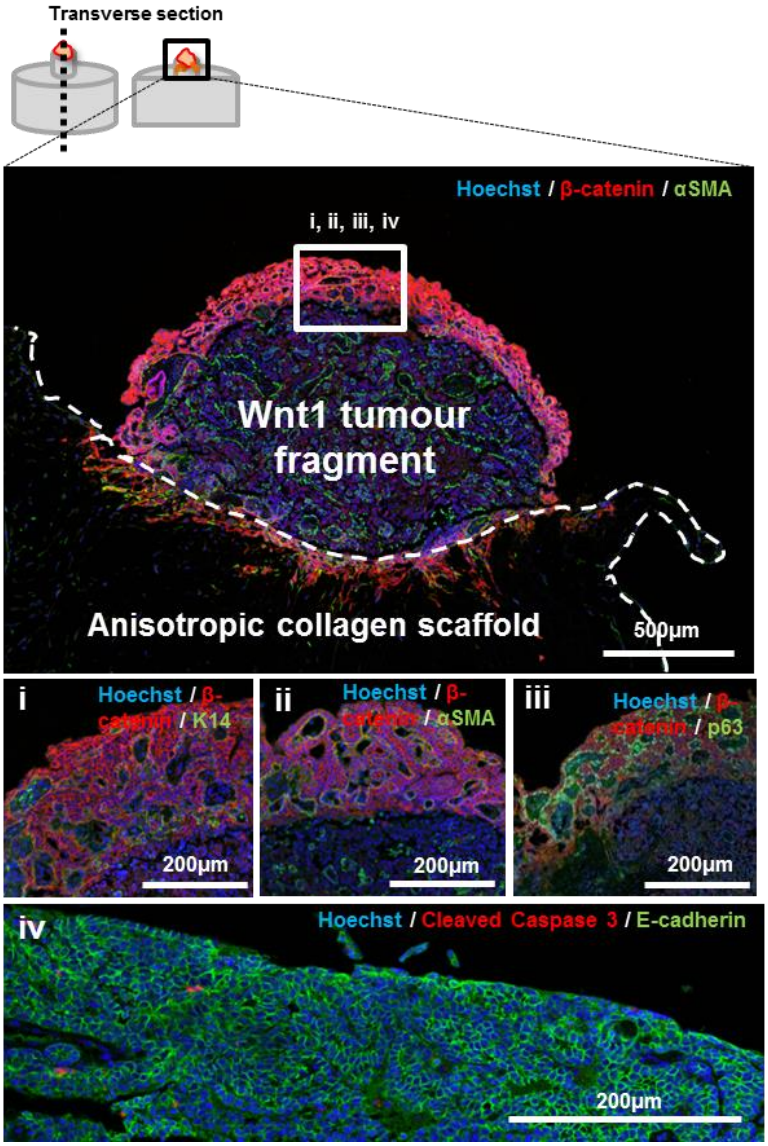


***Figure 5-3: MMTV-Wnt1 driven tumour fragment and ET-SIM co-culture – tumour edge free from scaffold contact***

Immunohistochemical (IHC) analysis of MMTV-*Wnt1* tumour fragment (top), seeded into the nucleation point (top, white dotted line) of an anisotropic scaffold filled with adipocytes (ET-SIM), cultured for 72 hours, embedded in paraffin and transversely sectioned. Tumour fragment and upper section of the scaffold were imaged as depicted in the diagram above (top left). Zoomed in images of the edge of the tumour fragment free from contact with the scaffold (top, white box) are shown in (i-iv). DNA was marked using Hoechst (blue). Luminal tumour cells are marked with anti-β-catenin (red, i-iii) and E-cadherin (green, iv). Basal tumour cells are marked with anti-cytokeratin-14$^{+}$ (K14, green, i), anti-α-smooth muscle actin$^{+}$ (αSMA, green, ii) and anti-p63 (nuclear, green, iii). Apoptotic cells are marked with anti-cleaved caspase-3 (CC3, red, iv)

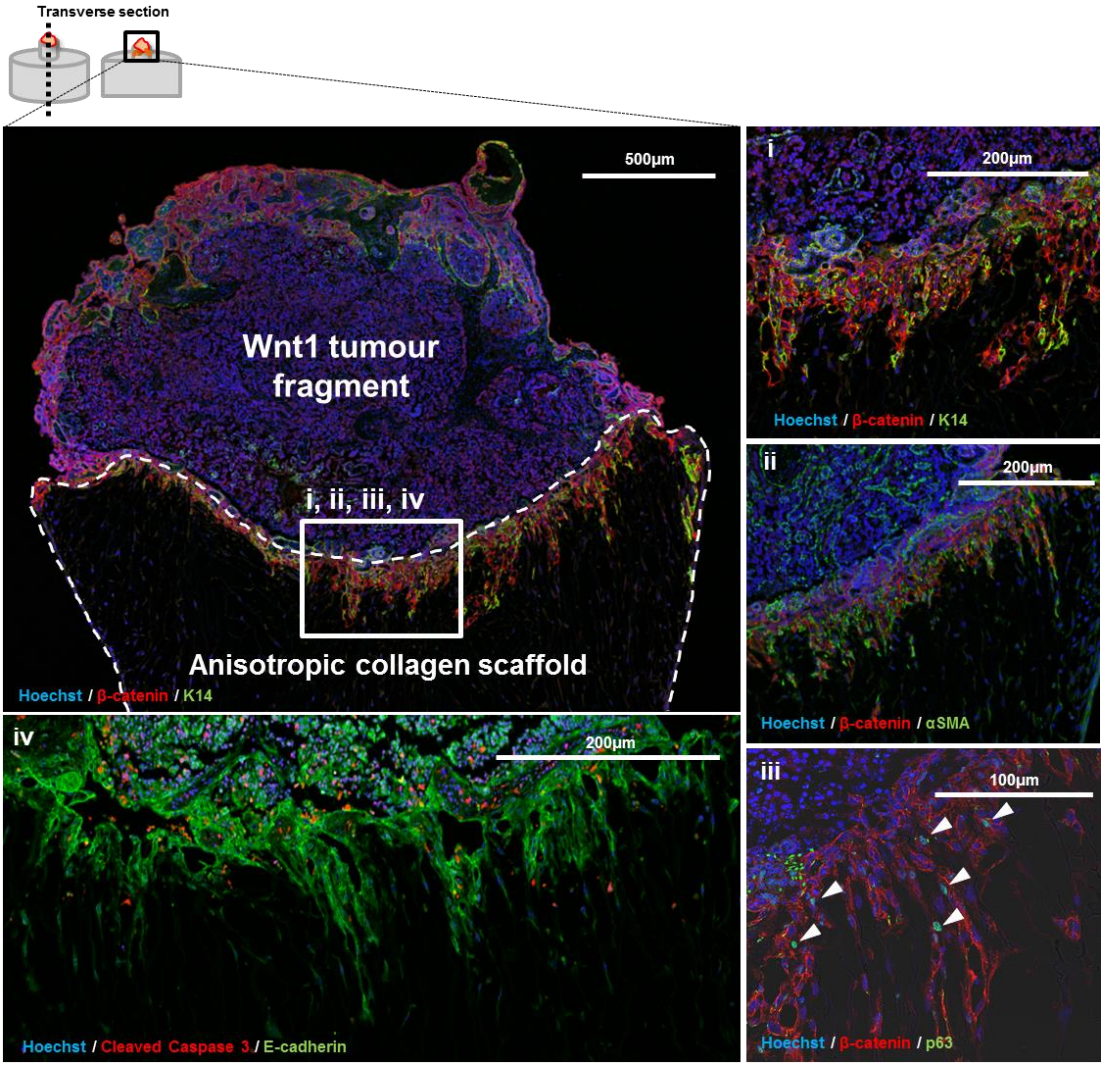


***Figure 5-4: MMTV-Wnt1 driven tumour fragment and ET-SIM co-culture – tumour edge in contact with the scaffold***

Immunohistochemical (IHC) analysis of MMTV-Wnt1 tumour fragment (top), seeded into the nucleation point (top, white dotted line) of an anisotropic scaffold filled with adipocytes (ET-SIM), cultured for 72 hours, embedded in paraffin and transversely sectioned. Tumour fragment and upper section of the scaffold were imaged as depicted in the diagram above (top left). Zoomed in images of the edge of the tumour fragment in contact with the scaffold (top left, white box) are shown in **(i-iv)**. DNA was marked using Hoechst (blue). Luminal tumour cells are marked with anti-β-catenin (red, **i-iii**) and E-cadherin (green, **iv**). Basal tumour cells are marked with anti-cytokeratin-14$^{+}$ (K14, green, **i**), anti-α-smooth muscle actin$^{+}$ (αSMA, green, **ii**) and anti-p63 (nuclear, green, **iii**). Arrowheads in (**iv**) show p63$^{+}$ nuclei. Apoptotic cells are marked with anti-cleaved caspase-3 (CC3, red, **iv)**

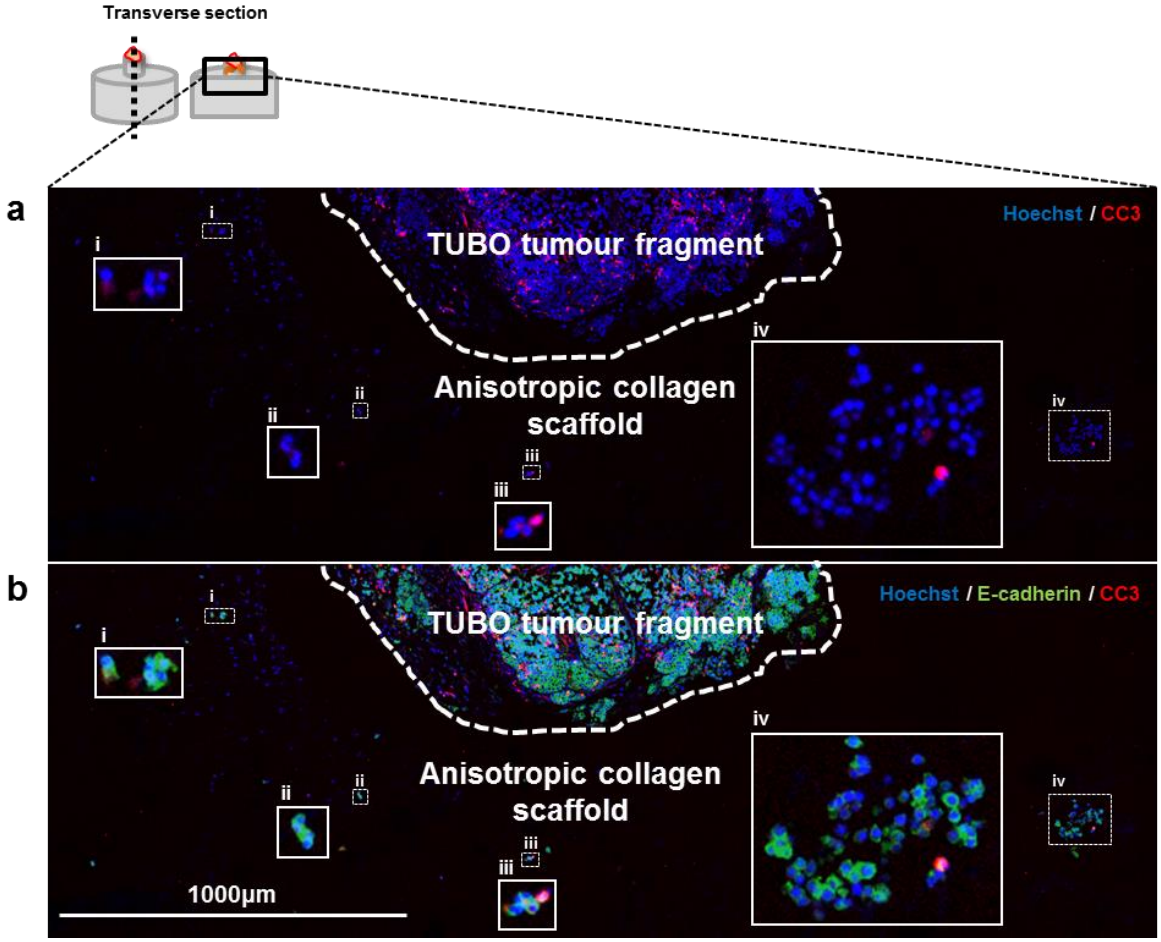


***Figure 5-5: TUBO tumour fragment and ET-SIM co-culture and tumour cell analysis***

Immunohistochemical (IHC) analysis of TUBO (Her2-*neu* overexpressing) tumour fragments (top), seeded into the nucleation point (white dotted line) of an anisotropic collagen scaffold filled with adipocytes (ET-SIM), cultured for 72 hours, embedded in paraffin and transversely sectioned. Tumour fragment and upper section of the scaffold were imaged as depicted in the diagram above (top left). DNA was marked using Hoechst (blue). TUBO tumour cells are marked with anti-E-cadherin (green). Apoptotic cells are marked with anti-cleaved caspase-3 (CC3, red). (a) Hoechst and CC3 merge. (b) Hoechst, E-cadherin and CC3 merge. Image shown as tile scan of the tumour fragment and the top of the scaffold. (i-iv) Magnified images of migratory TUBO cells.

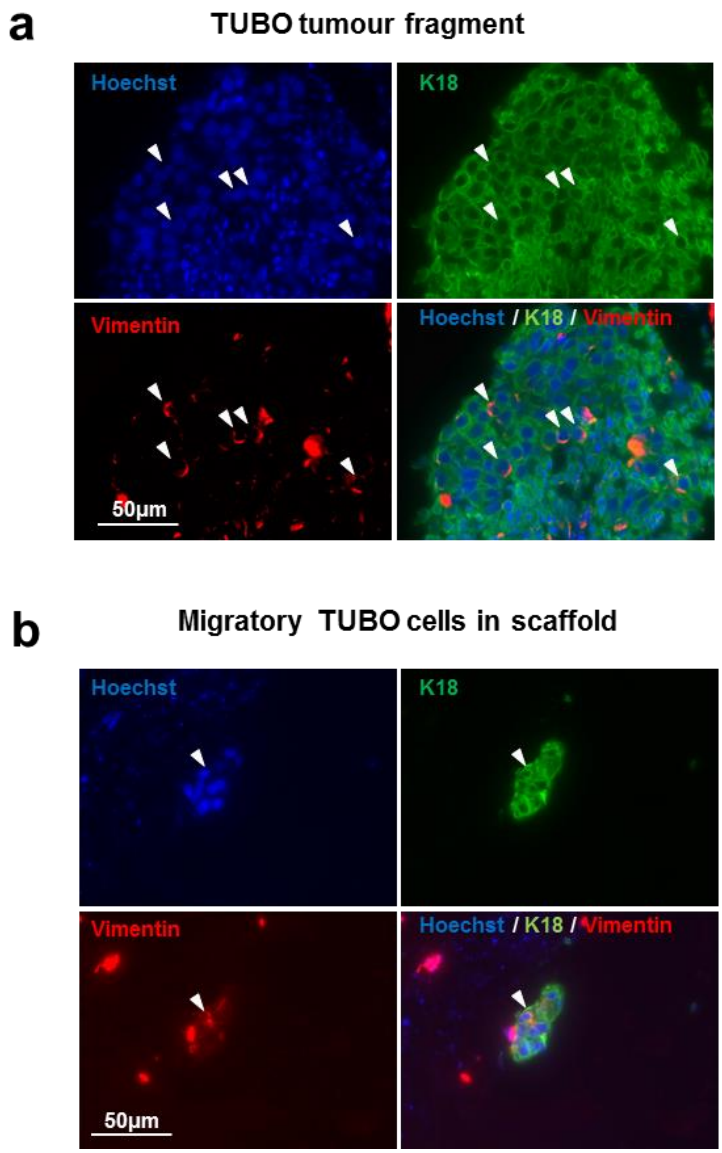


***Figure 5-6: TUBO tumour fragment and ET-SIM co-culture vimentin expression***

Immunohistochemical (IHC) analysis of TUBO (Her2-*neu* overexpressing) tumour fragment, seeded into the nucleation point of an anisotropic collagen scaffold filled with adipocytes (ET-SIM), cultured for 72 hours, embedded in paraffin and transversely sectioned. (a) IHC analysis of TUBO cells within the bulk of the seeded tumour fragment free from contact with the scaffold. TUBO cells were probed with luminal epithelial cell marker anti-cytokeratin-18 (K18, green) and epithelial-to-mesenchymal transition (EMT) marker anti-vimentin (red). Stochastic expression of vimentin is localised around one edge of TUBO cell nuclei (arrowheads). (b) IHC analysis of migratory TUBO tumour cells within an anisotropic collagen scaffold filled with adipocytes (ET-SIM) with similar stochastic vimentin expression in $K18^{+}$ TUBO cells (arrowhead).

### 5.2.4 ET-SIM as a cancer therapeutic testing platform

Following on from the validation of ET-SIM as a method to distinguish different modes of tumour cell migration, subsequent experiments proceeded to test ET-SIM as a cancer therapeutic testing platform. For this assessment, three inhibitors of different pathways implicated in a variety of migratory mechanisms and processes were selected.

Rho-associated protein kinase (ROCK) is a kinase that promotes a wide range of cellular processes including proliferation, apoptosis, migration, adhesion, oncogenic transformation and the cytoskeleton (Bhadriraju et al., 2007; Koyanagi et al., 2008; Mali et al., 2011; Da Silva et al., 2003; Yu et al., 2012). Furthermore, inhibition of the ROCK signalling pathway has also been shown to promote cell survival and colony forming efficiency when used in human breast, mouse mammary and MMTV-*Wnt1* cancer organoid cultures (Isobe et al., 2014; Jamieson et al., 2017; Jardé et al., 2016; Linnemann et al., 2015). The Rho-associated protein kinase (ROCK) inhibitor, Y-27632 (denoted ROCKi hereafter), was therefore chosen as a candidate inhibitor for testing in ET-SIM due to its wide spanning effects.

As matrix metalloproteinases (MMPs) are implicated in tumorigenesis, a number of MMP inhibitors have been developed (Devy et al., 2009; Mao et al., 2010; Mehner et al., 2015; Poola et al., 2005; Rider et al., 2013; Somiari et al., 2006; Sparano et al., 2004; Suojanen et al., 2009). The pan-MMP inhibitor GM6001 has been used in a number of studies to investigate the role of MMPs in migration and was therefore chosen as the second candidate inhibitor (Haeger et al., 2014; Ilunga et al., 2004; Peyri et al., 2009; Raviraj et al., 2012).

The ErbB receptors, epidermal growth factor receptor (EGFR), HER2 and ErbB-4 all play roles in breast tumour progression (Ali et al., 2017; Kim et al., 2016; Singh et al., 2014). As HER2 is expressed in 30% of breast cancer and due to the influence of other ErbB receptors in breast cancer, inhibitors targeting these receptors have been developed (Slamon et al., 1987). Canertinib is one such inhibitor that was developed to target EGFR, HER2 and ErbB-4 and has been shown to inhibit proliferation and induce apoptosis in breast cancer cells (Galmarini, 2004; Li et al., 2008; Tan et al., 2016). Consequently, Canertinib was chosen as the final candidate inhibitor.

MMTV-*Wnt1* tumour fragments were cultured with and without the three candidate inhibitors for 72 hours or 10 days in either empty scaffolds or ET-SIM to elucidate both therapeutic efficacy and adipocyte influence on migration. Use of empty scaffolds provided a negative control to the mature adipocytes present in ET-SIM cultures. This allowed the interpretation of adipocyte effects on tumour cell migration and on inhibitor efficacy compared to vehicle controls. Furthermore, it

permitted the investigation of the adipogenic influence for each individual therapeutic testing regime. As all three inhibitors were dissolved in dimethyl sulfoxide (DMSO), this reagent was selected as the vehicle control. DMSO has been shown to have anti-tumour effects and its use ensured that any deleterious activities of the reagent were controlled for (Wang et al., 2012). Migration distance was quantified through analysis of IHC sections of fixed samples, distinguishing tumour cells from stroma based upon their αSMA and β-catenin expression. Every migratory cell distance from 4 separate scaffold experiments was then pooled and plotted graphically for the 72 hour (Fig. 5.7, Fig. 5.8) and 10 day time points (Fig. 5.13, Fig. 5.14). Each drug treatment in empty scaffolds was then statistically compared with DMSO vehicle controls (Fig. 5.7a, 5.13a), followed by the same comparison in ET-SIM cultures (Fig. 5.7b, 5.13b).

To compare the effects of ET-SIM cultures and therefore adipocytes on each drug treatment, migration distance in empty scaffolds was compared with ET-SIM cultures for every individual treatment regime (Fig. 5.8, Fig. 5.14). The total frequency of migratory cells was also measured and plotted graphically (Fig. 5.9, Fig. 5.10, Fig. 5.15, Fig. 5.16). Again, this was compared to DMSO controls (Fig. 5.9, 5.15) or in empty scaffolds versus ET-SIM for each individual drug treatment regime (Fig. 5.10, Fig. 5.16).

At 72 hours, migration distance analysis revealed Canertinib to have an anti-migratory effect on MMTV-*Wnt1* tumour fragments seeded in empty scaffolds when compared to vehicle (DMSO) controls (Fig. 5.7a). IHC analysis of CC3 expression at this time point revealed that this effect could have resulted from high levels of cell death, before cells were able to migrate into the scaffold (Fig. 5.11). In contrast, ROCKi exerted a pro-migratory effect on cancer cells in empty scaffolds, enhancing migration distance compared to vehicle controls (Fig. 5.7a).

Adipocyte signalling has been shown to influence breast tumour progression (Balaban et al., 2017; Dirat et al., 2011; Duong et al., 2015; Picon-Ruiz et al., 2016; Wang et al., 2015). To elucidate whether adipocytes were affecting migration in our system, the individual inhibitors were compared with tumour fragments in empty scaffolds versus ET-SIM scaffolds at 72 hours. ROCKi exerted a pro-migratory effect when compared to vehicle controls regardless of adipocyte status (Fig. 5.7a,b). However, adipocytes enhanced this pro-migratory effect when comparing ROCKi in empty scaffolds to ROCKi in ET-SIM cultures (Fig. 5.8b). Interestingly, although adipocytes enhanced migration in ROCKi samples compared to ROCKi empty scaffold samples, they also reduced the total frequency of cells that had migrated into the scaffold (Fig. 5.10b).

The anti-migratory effects of Canertinib observed in empty scaffolds versus vehicle controls (Fig. 5.7a) were not observed in ET-SIM cultures (Fig. 5.7b). Nevertheless, cells migrated further in Canertinib ET-SIM samples compared to Canertinib empty scaffold samples (Fig. 5.8d). The total frequency of migratory cells was significantly reduced in Canertinib samples compared to vehicle controls regardless of adipocyte status (Fig. 5.9a,b). This reduction in the frequency of migratory cells may have been due to the increased CC3 expression and therefore cell death also observed in these Canertinib-treated samples (Fig. 5.11).

In contrast, GM6001 exerted no significant effect on migration in empty scaffolds compared to vehicle controls (Fig. 5.7a) but reduced migration a small but significant amount in ET-SIM cultures compared to vehicle controls (Fig. 5.7b) at 72 hours. The total frequency of migratory cells was not affected in either case (Fig. 5.9a,b). Additionally, an anti-migratory effect of adipocytes was seen when comparing GM6001 ET-SIM to GM6001 empty scaffolds (Fig. 5.8c).

Interestingly, DMSO vehicle controls also revealed a subtle but significant adipocyte-mediated anti-migratory effect on distance and a reduction in the overall frequency of cells migrated, at 72 hours (Fig. 5.8a, Fig. 5.10a). This contrasts with studies showing adipocytes to increase breast cancer cell migration *in vitro* (Balaban et al., 2017; Picon-Ruiz et al., 2016; Wang et al., 2015).

These data suggest that the influence of adipocytes is complex particularly with regard to their effect on the distance migrated and the overall frequency of migratory cells at 72 hours (Fig. 5.7-5.11). While a lower frequency of tumour cells migrated in all treatment conditions in ET-SIM cultures compared to empty scaffolds, this difference varied between inhibitor treatments and did not reach statistical significance in all cases (Fig. 5.10).

Migration distance was increased in ROCKi and Canertinib ET-SIM cultures (Fig. 5.8b,d) but the overall frequency of migratory cells in ROCKi and Canertinib ET-SIM cultures trended to a decrease, at 72 hours (Fig. 5.10b,d). This suggests adipocytes may have facilitated the migration of certain subsets of tumour cells while suppressing the invasiveness of others. Thus ET-SIM cultures have the capacity to reveal the heterogeneity of tumours and allow even small numbers of invasive cells to be detected.

To investigate whether the therapeutic and adipocyte-mediated responses observed at 72 hours were restricted to the initiation of migration only, a longer time course was carried out culturing tumour fragments for up to 10 days. IHC analysis revealed that the extent of tumour cell migration was strikingly increased in ROCKi samples compared to vehicle controls (Fig. 5.12). Tracts of cells can be seen protruding in all directions from the tumour fragment into the scaffolds, with some cells

migrating more than 20 times the distance of vehicle controls. The most distal cells (>500μm) from the tumour fragment showed a thin mesenchymal phenotype and expressed both β-catenin and αSMA (Fig. 5.12b, i,ii). Cells found closer to the tumour fragment tended to be more clustered and also expressed both β-catenin and αSMA (Fig. 5.12b, iii,iv).

After 10 days, migration distance analysis and total frequency of migratory cells analysis revealed that Canertinib completely abolished cell migration in both empty scaffolds and ET-SIM cultures (Fig. 5.13, Fig. 5.14, data not shown - absence of distance or frequency data to plot graphically). This demonstrated the high efficacy of Canertinib at longer time-points independent of adipocyte status.

The MMP inhibitor, GM6001, showed anti-migratory effects in both empty scaffold and ET-SIM cultures after 10 days culture compared to vehicle controls (Fig. 5.13). Thus, MMP induced matrix remodelling was at least partially responsible for MMTV-*Wnt1* tumour cell migration and occurred irrespective of adipocyte status. This mode of MMP-mediated cell migration has also been observed in other studies (Fisher et al., 2009; Somiari et al., 2006). Moreover, ET-SIM culture increased migration in GM6001 samples compared to empty scaffolds (Fig. 5.14c).

ROCKi effects on migration distance were clearly more pronounced in longer term treatments, with a subset of cells reaching >3000μm in empty scaffolds and >4000μm in ET-SIM cultures after 10 days culture (Fig. 5.13). This was highly significant ($p<0.0001$) when compared to vehicle controls independent of adipocyte status (Fig. 5.13). Furthermore, this ROCKi pro-migratory effect was further enhanced in ET-SIM cultures compared to empty scaffolds (Fig. 5.14b). The total frequency of migratory cells in ROCKi samples at 10 days was then analysed (Fig. 5.15, Fig. 5.16b). Although not significant, these data suggest that ROCKi treatment increases the total number of migratory cancer cells and is independent of adipocyte status when compared to vehicle controls (Fig. 5.15). This is indicative of a pro-survival/proliferative effect of ROCKi on migratory cells in Wnt1 tumours.

All drug treatments at 10 days showed a significant increase in migration distance in ET-SIM cultures compared to empty scaffolds (Fig. 5.14). This showed that adipocytes promoted later stages of cell migration in all therapeutic regimes tested at 10 days, therefore underscoring the need for oncologists and drug discovery laboratories to be conscious of adipocyte influences when selecting medicines.

In concordance with 72 hour data, although not significant, ET-SIM cultures showed a decreasing trend in the total frequency of migratory cancer cells compared to empty scaffolds for all therapeutic treatments (Fig. 5.16). Interestingly, there was therefore an inverse trend of increased migration distance (Fig. 5.14) to a decreased frequency of migratory cancer cells (Fig. 5.16) when

comparing ET-SIM to empty scaffold cultures, at 10 days. This indicates that adipocyte pro-migratory effects are likely not on the entire population of tumour cells but rather a particular subset. Moreover, it also suggests adipocytes are suppressive of certain cellular subsets in the system, preventing them from gaining a migratory phenotype. Hence, these data demonstrated the influence of intra-tumour heterogeneity and its detection within the ET-SIM culture system.

In conclusion, adipocytes had an unpredictable and significant effect on the outcome of drug treatment and highlight the importance of using an adipocyte invested 3D environment within a drug testing platform. 72 hour and 10 day samples demonstrated the time-dependent effects of adipocytes and their influence on the efficacy of therapeutic regimes. Importantly, the response of invasive cells to therapeutic drugs was readily assessed and the most appropriate drug treatment to suppress metastatic tumour cell subpopulations was determined.

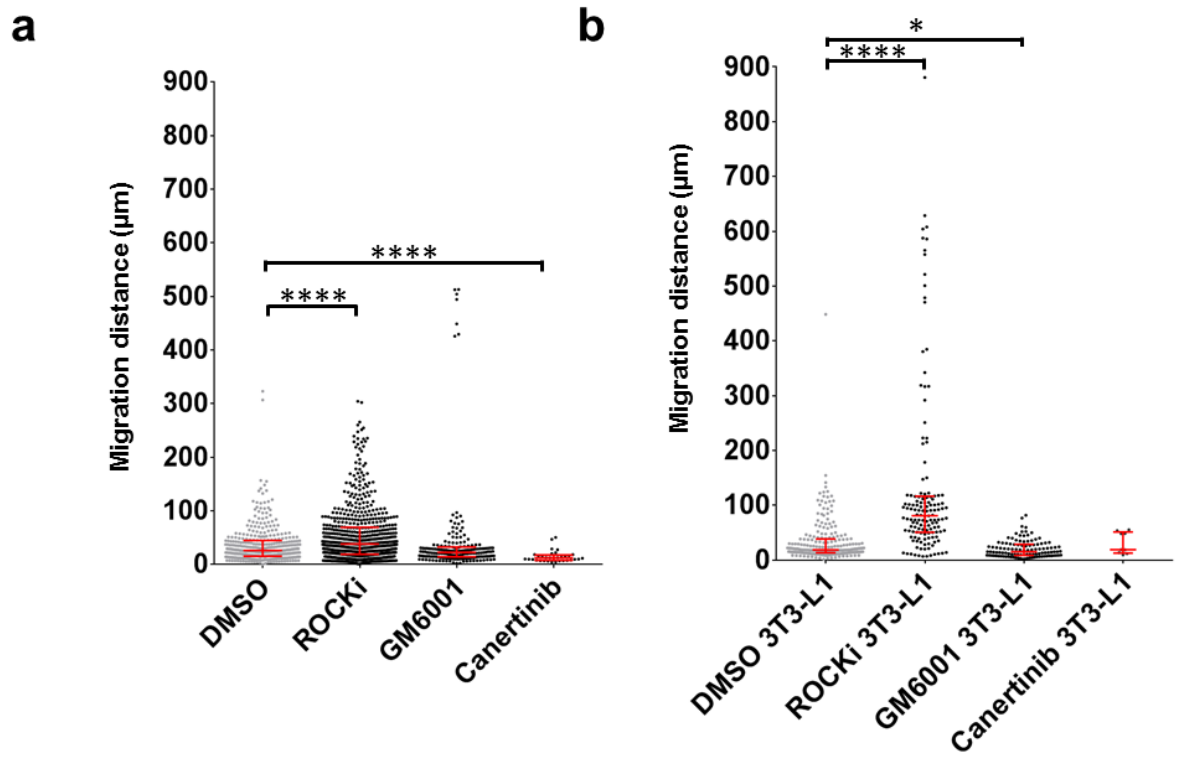


***Figure 5-7: MMTV-Wnt1 tumour fragment culture and therapeutic testing with migration distance analysis (72 hours) – comparison to DMSO vehicle controls***

MMTV-*Wnt1* tumour cell migration distance from anisotropic collagen scaffold nucleation points was measured and plotted graphically after 72 hours culture with ROCKi, GM6001 and Canertinib inhibitors. DMSO was used a vehicle control to which all treatments were compared statistically. Each migratory cell is marked as an individual point. (a) MMTV-*Wnt1* tumour fragments were seeded and cultured in empty scaffolds with inhibitors. (b) Tumour fragments were seeded in ET-SIM cultures with inhibitors. Samples were compared statistically with the non-parametric unpaired/matching Kruskal-Wallis ANOVA and a Geisser-greenhouse correction combined with a Dunn's multiple comparison test. *$p<0.05$, ****$p<0.0001$.

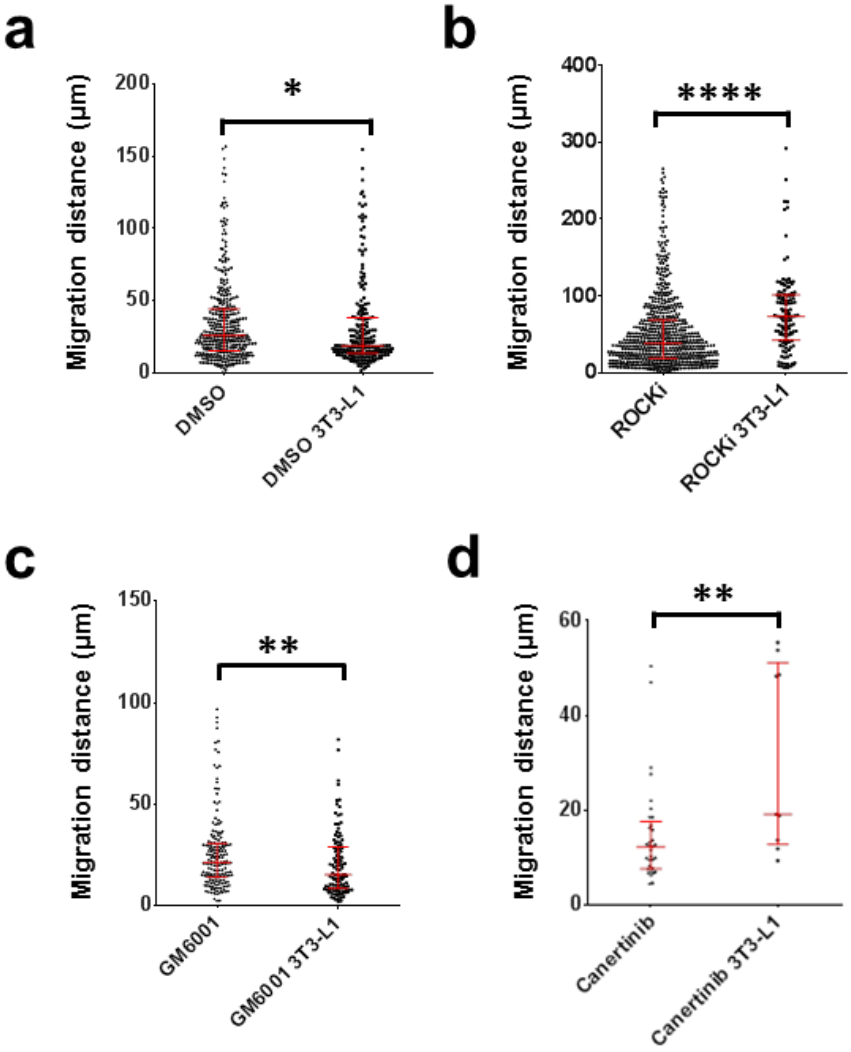


***Figure 5-8: MMTV-Wnt1 tumour fragment culture and therapeutic testing with migration distance analysis (72h) – comparison of empty scaffold versus ET-SIM cultures***

MMTV-*Wnt1* tumour cell migratory distance from anisotropic collagen scaffold nucleation points was measured and plotted graphically after 72 hours culture with ROCKi, GM6001 and Canertinib inhibitors. Each treatment was compared individually with/without ET-SIM cultures. (a) DMSO vehicle (b) ROCKi (c) GM6001 (d) Canertinib. Samples were compared statistically with the non-parametric unpaired Mann-Whitney test (n=4). *p<0.05, **p<0.01, ****p<0.0001.

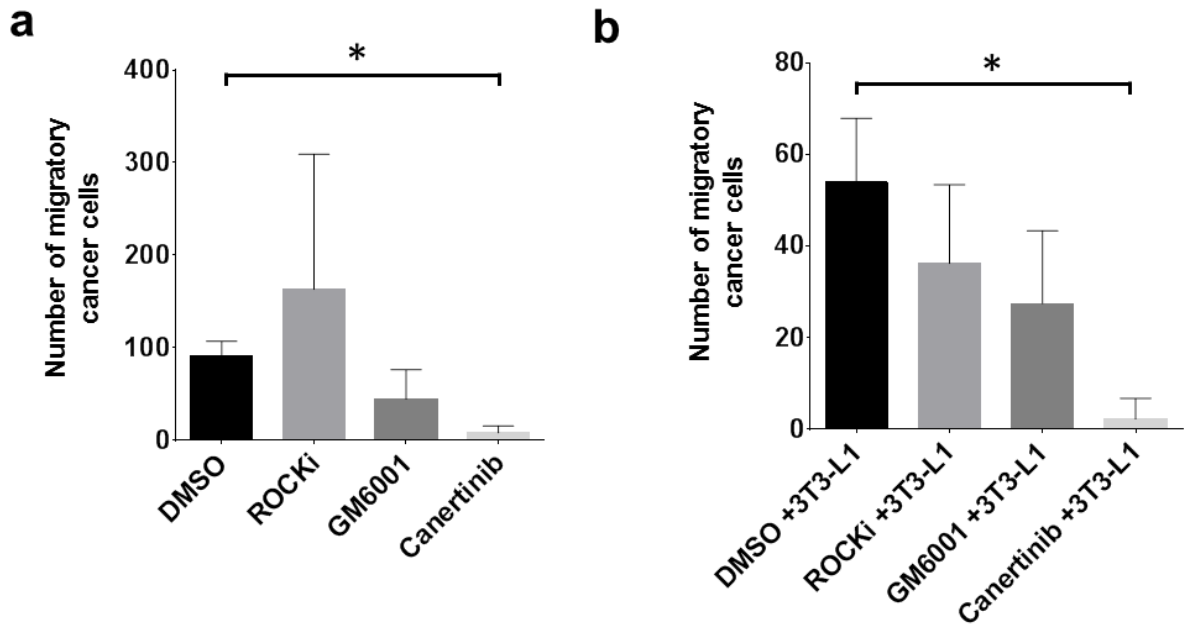


***Figure 5-9: MMTV-Wnt1 tumour fragment culture and therapeutic testing with total migratory cell frequency analysis (72 hours) – comparison to DMSO vehicle controls***

The total frequency of migratory MMTV-*Wnt1* tumour cells in anisotropic collagen scaffolds was measured and plotted graphically after 72 hours culture with ROCKi, GM6001 and Canertinib inhibitors. DMSO was used a vehicle control to which all treatments were compared statistically. (a) Tumour fragments were seeded in empty scaffolds and treated with inhibitors. (b) Tumour fragments were seeded in ET-SIM co-cultures and treated with inhibitors. Samples were compared statistically with the non-parametric unpaired/matching Kruskal-Wallis ANOVA and a Geisser-greenhouse correction combined with a Dunn's multiple comparison test (n=4). *$p<0.05$.

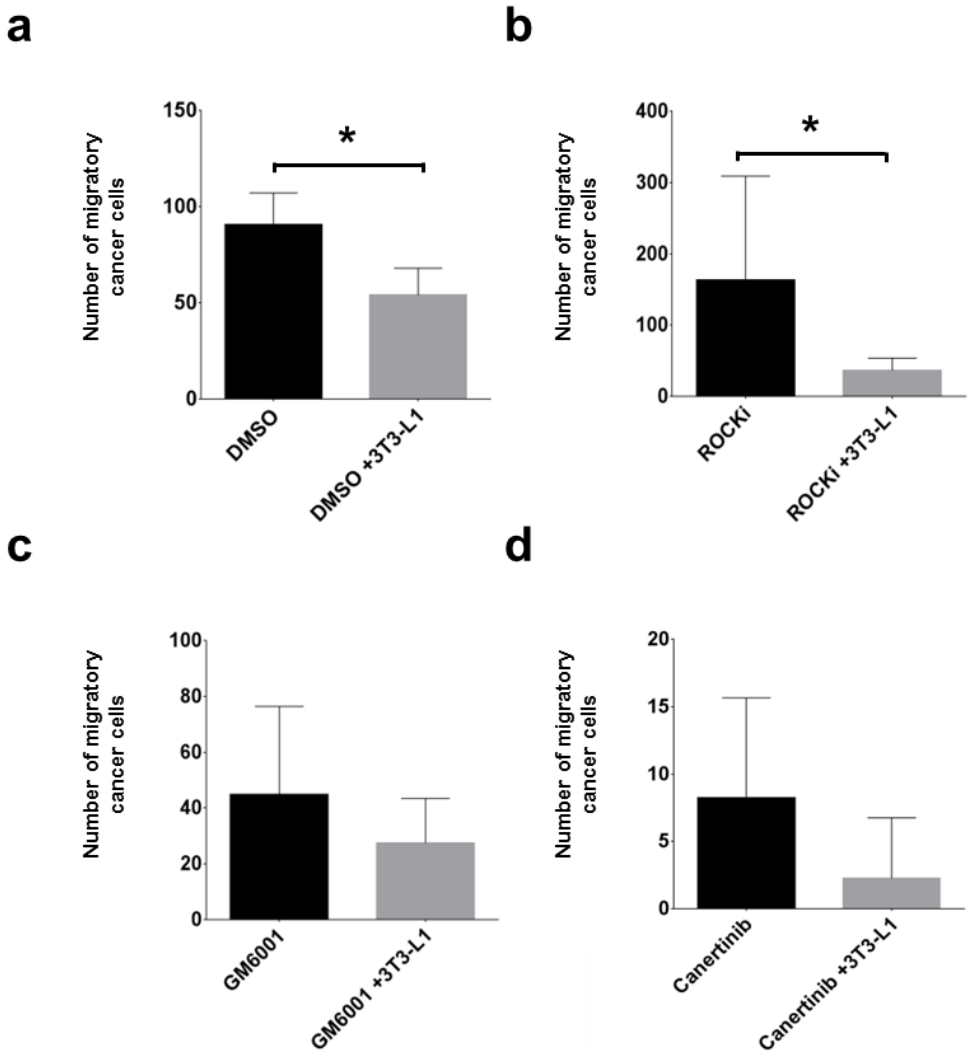


***Figure 5-10: MMTV-Wnt1 tumour fragment culture and therapeutic testing with total migratory cell frequency analysis (72h) – comparison of empty scaffold versus ET-SIM cultures***

The total number of migratory MMTV-*Wnt1* tumour cells in anisotropic collagen scaffolds was measured and plotted graphically after 72 hours culture with ROCKi, GM6001 and Canertinib inhibitors. Each treatment was compared individually in empty scaffolds versus ET-SIM cultures. (a) DMSO vehicle (b) ROCKi (c) GM6001 (d) Canertinib. Samples were compared statistically with the non-parametric unpaired Mann-Whitney test (n=4). *$p<0.05$.

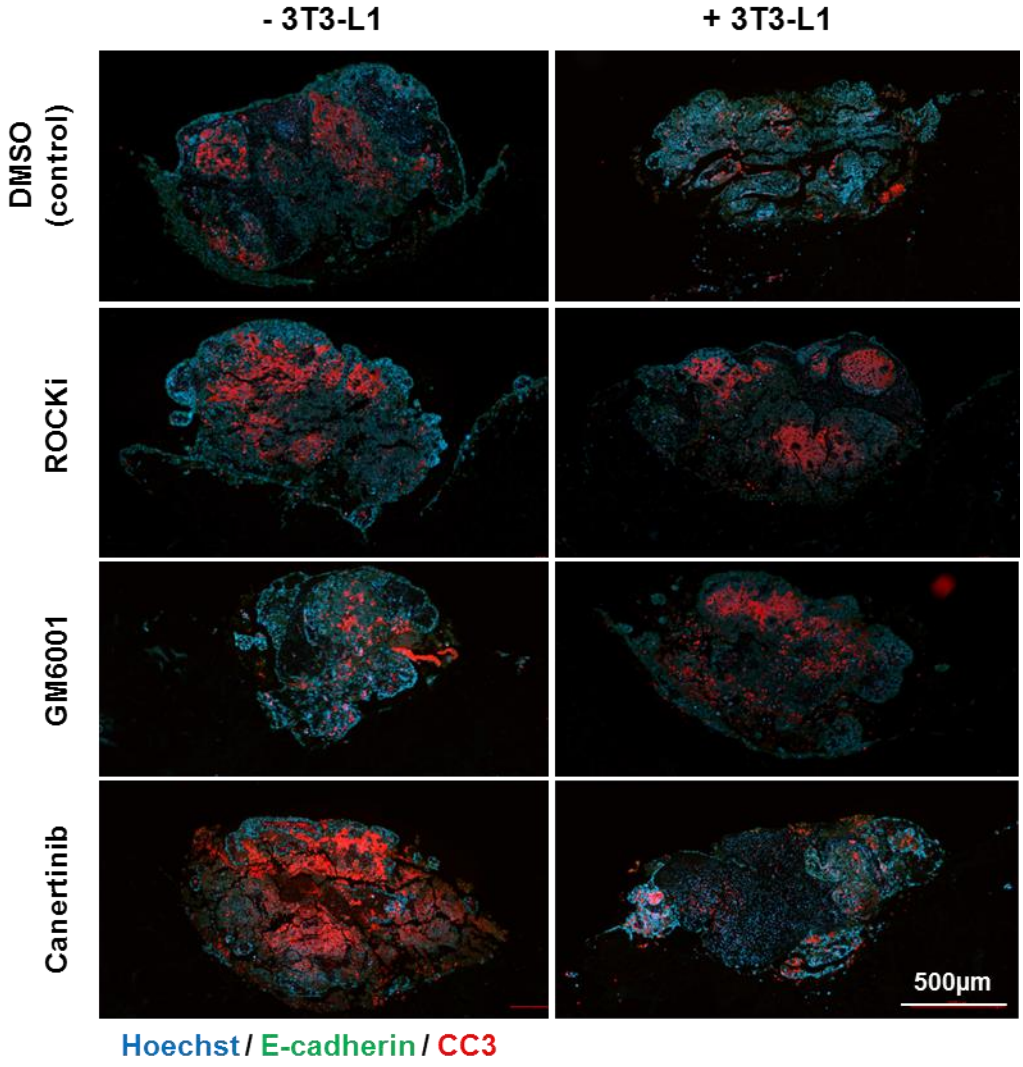


***Figure 5-11: Apoptosis in MMTV-Wnt1 tumour fragment culture during therapeutic testing (72 hours)***

Immunohistochemical analysis of MMTV-*Wnt1* tumour fragments in scaffolds, cultured for 72 hours with/without 3T3-L1 adipocytes (ET-SIM), treated with DMSO (control), ROCKi (Y-27632), GM6001 or Canertinib, and immunostained with apoptosis marker anti-cleaved caspase 3 (CC3, red) and tumour cell marker E-cadherin (green). Cell nuclei are stained with Hoechst (blue). 12 random subjects were shown IHC of the different therapeutic testing strategies (n=3) in a blinded test. 100% selected Canertinib treatment without 3T3-L1 as showing the highest CC3 levels.

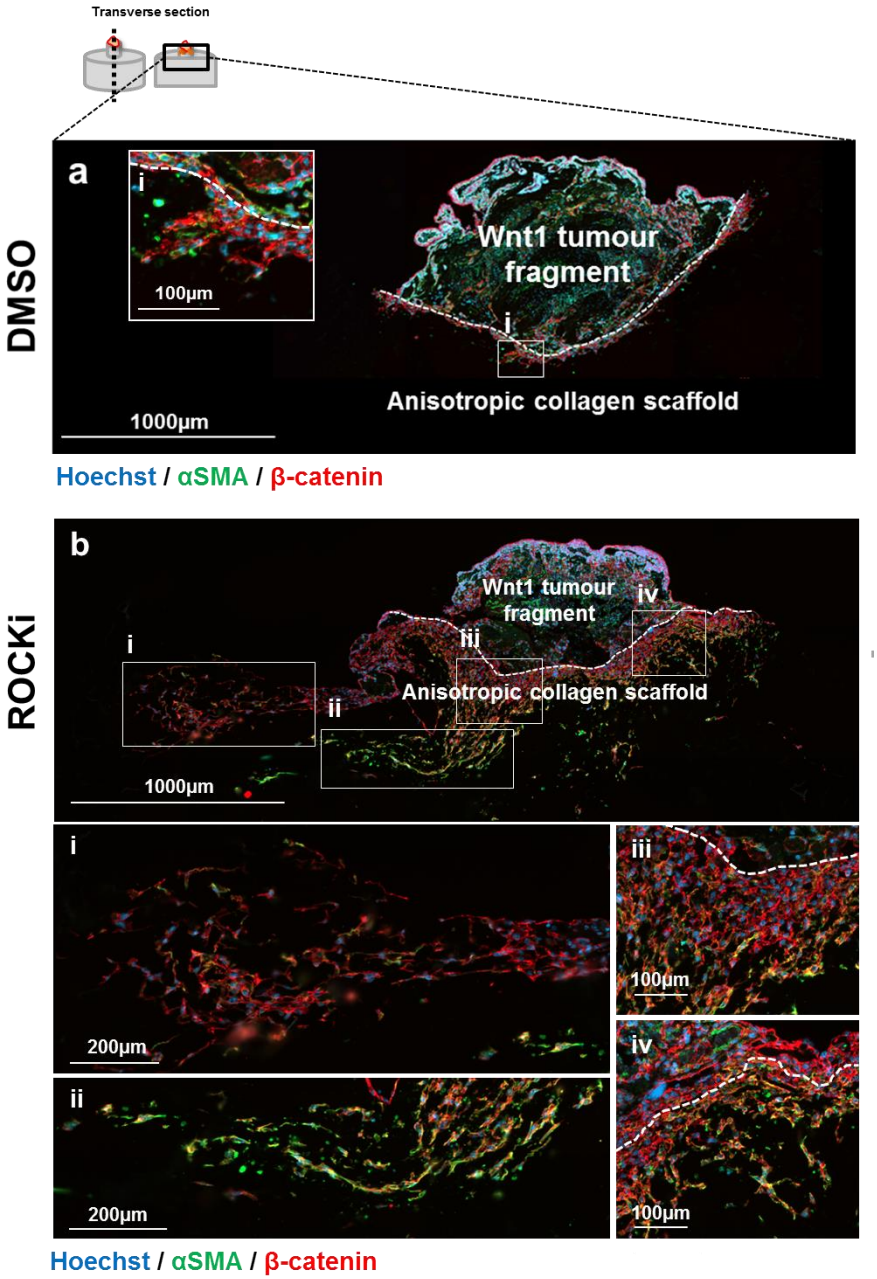


***Figure 5-12: MMTV-Wnt1 tumours have increased migration in anisotropic collagen scaffolds when treated with ROCKi (10 days)***

(a) Immunohistochemical analysis of MMTV-*Wnt1* tumour fragment seeded into anisotropic collagen scaffold nucleation points (white dotted line), cultured for 10 days, embedded in paraffin and transversely sectioned. Migratory cancer cells were marked with αSMA (green) and β-catenin (red). DNA was marked with Hoechst. (i) shows migratory cells near the nucleation point. (b) As in (a) but cultured for 10 days in ROCKi (Y-27632). (i) and (ii) show migratory cells at distances at >500µm. (iii) and (iv) show migratory cells at <500µm near the nucleation point.

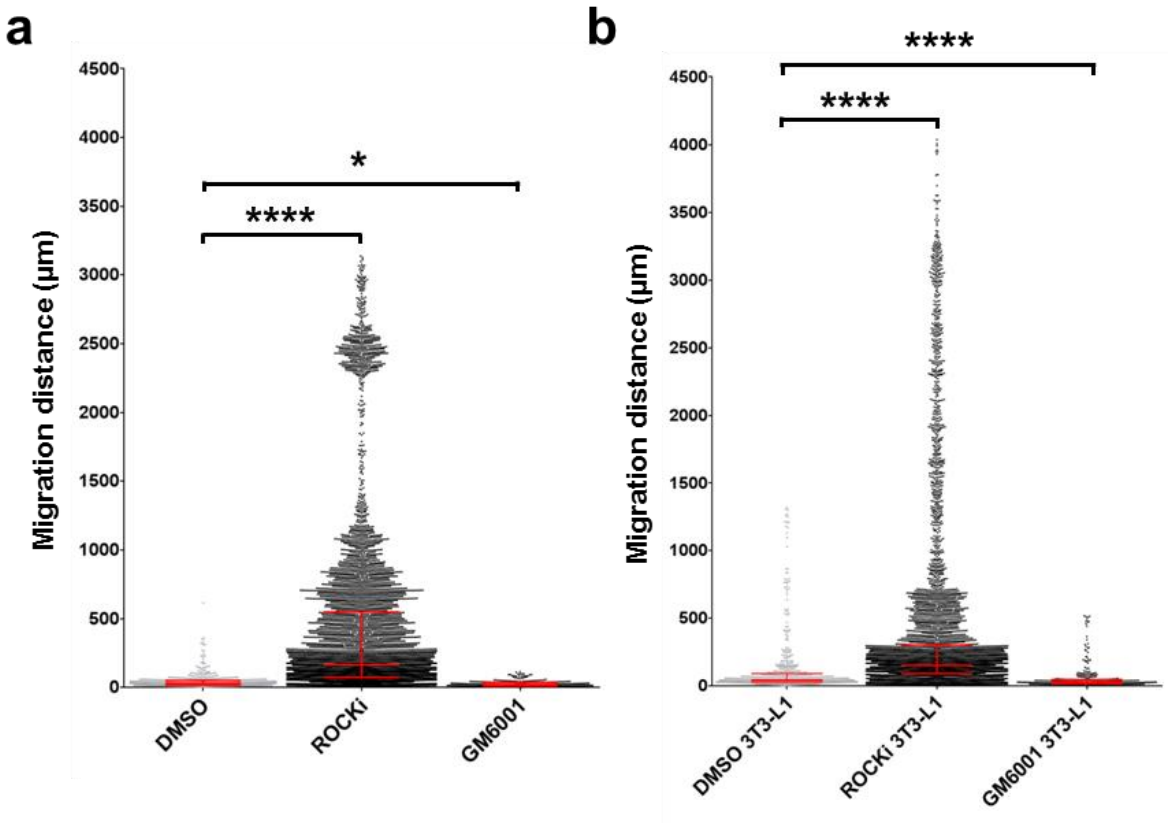


***Figure 5-13: MMTV-Wnt1 tumour fragment culture and therapeutic testing with migration distance analysis (10days) – comparison to DMSO vehicle controls***

MMTV-*Wnt1* tumour cell migratory distance from anisotropic collagen scaffold nucleation points was measured and plotted graphically after 10 days culture with ROCKi, GM6001 and Canertinib inhibitors. DMSO was used a vehicle control to which all treatments were compared statistically. (a) Tumour fragments were seeded in empty scaffolds with inhibitor treatment. (b) Tumour fragments were seeded in ET-SIM co-cultures with inhibitor treatment. Canertinib treatment yielded no detectable migratory cells and hence data was not shown. Samples were compared statistically with the non-parametric unpaired/matching Kruskal-Wallis ANOVA and a Geisser-greenhouse correction combined with a Dunn's multiple comparison test (n=4). *p<0.05, ****p<0.0001.

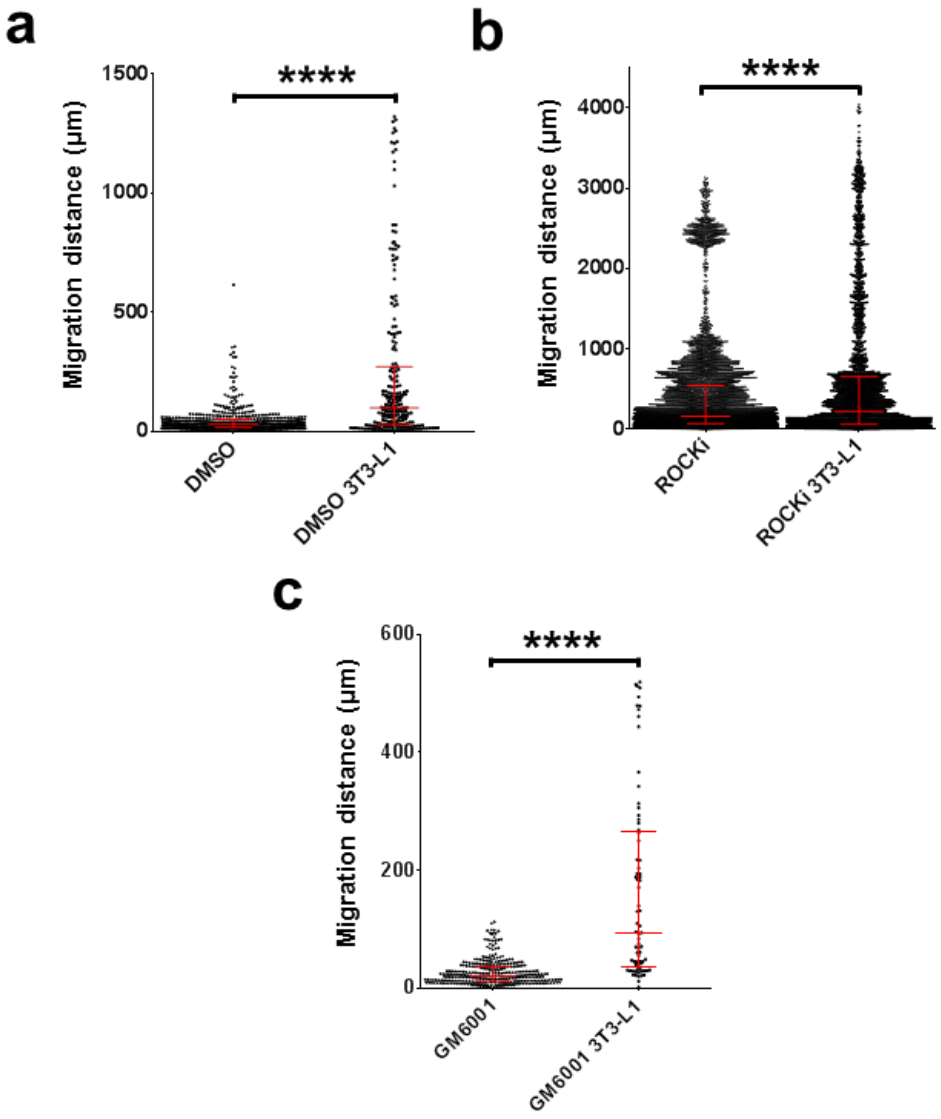


***Figure 5-14: MMTV-Wnt1 tumour fragment culture and therapeutic testing with migration distance analysis (10days) – comparison of empty scaffold versus ET-SIM cultures***

MMTV-*Wnt1* tumour cell migratory distance from anisotropic collagen scaffold nucleation points was measured and plotted graphically after 72hrs culture with ROCKi, GM6001 and Canertinib inhibitors. Each treatment was compared individually with/without ET-SIM cultures. (**a**) DMSO vehicle (**b**) ROCKi (**c**) GM6001. Canertinib treatment yielded no detectable migratory cells and hence data was not shown. Samples were compared statistically with the non-parametric unpaired Mann-Whitney test (n=4). ****p<0.0001.

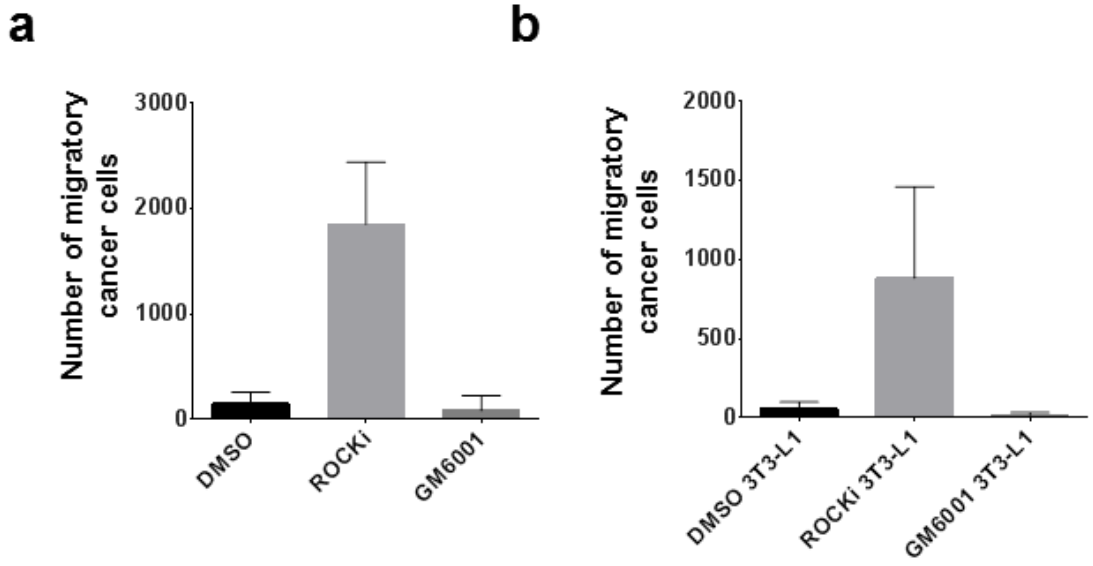


***Figure 5-15: MMTV-Wnt1 tumour fragment culture and therapeutic testing with total migratory cell frequency analysis (10days) – comparison to DMSO vehicle controls***

The total number of migratory MMTV-*Wnt1* tumour cells in anisotropic collagen scaffolds was measured and plotted graphically after 10 days culture with ROCKi, GM6001 and Canertinib inhibitors. DMSO was used a vehicle control to which all treatments were compared statistically. (a) Tumour fragments were seeded in empty scaffolds with inhibitor treatments. (b) Tumour fragments were seeded in ET-SIM co-cultures with inhibitor treatments. Canertinib treatment yielded no detectable migratory cells and hence data was not shown. Samples were compared statistically with the non-parametric unpaired/matching Kruskal-Wallis ANOVA and a Geisser-greenhouse correction combined with a Dunn's multiple comparison test. No significant differences were found (n=4).

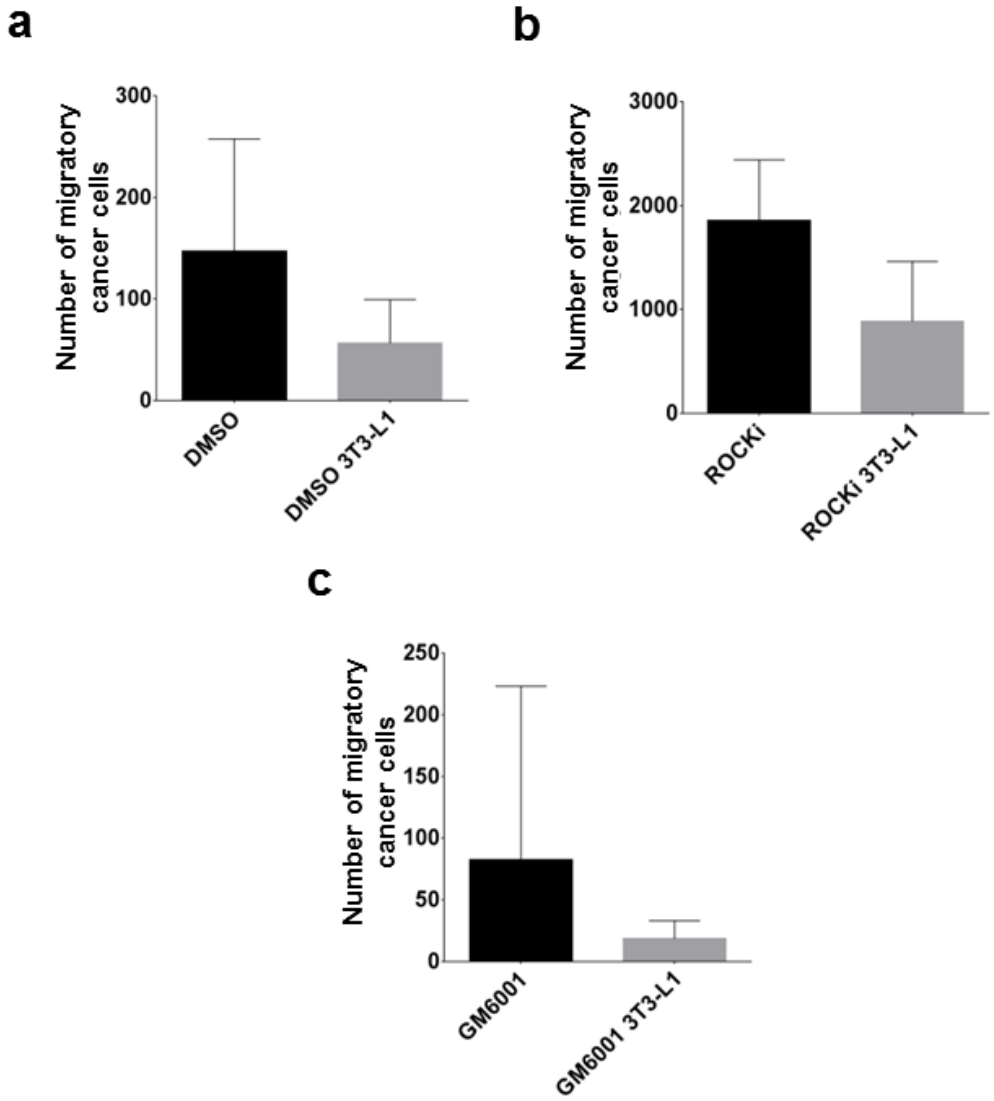


***Figure 5-16: MMTV-Wnt1 tumour fragment culture and therapeutic testing with total migratory cell frequency analysis (10 days) – comparison of empty scaffold versus ET-SIM cultures***

The total frequency of migratory MMTV-*Wnt1* tumour cells in anisotropic collagen scaffolds was measured and plotted graphically after 10 days culture with ROCKi, GM6001 and Canertinib inhibitors. Each treatment was compared individually with/without ET-SIM cultures. (a) DMSO vehicle (b) ROCKi (c) GM6001. Canertinib treatment yielded no detectable migratory cells and hence data was not shown. Samples were compared statistically with the non-parametric unpaired Mann-Whitney test (n=4).

### 5.2.6 Optical clearing allows visualisation of tumour / ET-SIM cultures to analyse therapeutic effect

The CUBIC optical clearing method increases tissue sample transparency by the removal of light scattering lipids and matching the refractive indices of a tissue, through immersion in hydrophilic agents (Susaki et al., 2014, 2015). Using this process the tissue is optically cleared whilst minimising the quenching of any fluorophores in the sample (Lloyd-Lewis et al., 2016; Susaki et al., 2015). CUBIC therefore permits the 3D immunolocalisation of protein and allows deeper laser penetration and z-sectioning by confocal microscopy of whole mounts. Previously it has been reported that TUBO tumours can be optically cleared and imaged using this approach (Lloyd-Lewis et al., 2016). In this section it was therefore sought to utilise this method to optically clear scaffolds, tumours and their combination to enhance the analysis of TUBO tumour cell migration and their responses to therapeutics.

Initial clearing experiments were carried out to confirm the presence of the TACS-3 phenotype in the mouse models used throughout this chapter; MMTV-*Wnt1* and TUBO tumour models. As TACS-3 was first described by Provenzano et al. in MMTV-*Wnt1* tumours, it was anticipated that the phenotype would be likely observed in those samples (Provenzano et al., 2006). However, for the TUBO tumour model it was unknown whether a TACS-3 phenotype would be observed. Following CUBIC clearing stereoscopic images showed an increased transparency in both tumour types (Fig. 5.17a). Clearing was then used in conjunction with whole mount immunostaining and 2pf to confirm whether cancerous epithelial cells could be identified and located within cleared samples (Fig. 5.17b, red). TUBO cells were successfully identified with anti-HER2 immunostaining (Fig. 5.17b, i, red) and MMTV-*Wnt1* cancerous cells were identified with β-catenin immunostaining (Fig. 5.17b, ii, iii, red). SHG was then utilised to directly image collagen (Fig. 5.17b, blue) and permitted the 3D visualisation of the anisotropic TACS-3 phenotype in both tumour types (Fig. 5.17b, white dotted arrows).

Subsequent experiments focused on the clearing, immunostaining and imaging of TUBO tumour fragments in empty scaffold and ET-SIM after 10 days culture (Fig. 5.18-5.22). Clearing increased transparency in scaffold and scaffold / tumour cultures (Fig. 5.18). Combining CUBIC with whole mount immunostaining for E-cadherin, TUBO empty scaffold and ET-SIM cultures that were treated with the candidate inhibitors ROCKi, GM6001 and Canertinib, were imaged using fluorescent stereoscopy (Fig. 5.19a). Macroscopically visible colonies of migratory TUBO cells were observed at varying distances from the seeded tumour fragments (Fig. 5.19a, white arrowheads).

The number of samples with >1 macroscopically visible colony of migratory cells was then quantified (Fig. 5.19b). Using this metric, all DMSO vehicle controls and ROCKi treated samples showed

migration, independent of their adipocyte status (Fig. 5.19b). In contrast, GM6001 suppressed macroscopically visible migration in 50% of samples when seeded in empty scaffolds, indicating an anti-migratory effect of MMP inhibition (Fig. 5.19). This effect was reversed when the tumours were embedded in ET-SIM cultures, demonstrating that adipocytes exert a pro-migratory effect during GM6001 treatment (Fig. 5.19). Similar to effects on MMTV-*Wnt1* tumours, Canertinib showed a pronounced anti-migratory affect in TUBO tumours with no macroscopically visible migratory colonies in 100% of samples, independent of adipocyte status (Fig. 5.19).

To investigate whether migration was observed microscopically, CUBIC clearing and immunostaining were used in combination with confocal microscopy (Fig. 5.20-5.22). TUBO cells were marked with E-cadherin and HER2 antibodies and imaged using deep 1mm z-stacks. Following Canertinib treatment, no migratory cells were observed in either empty scaffold (Fig. 5.20a) or ET-SIM cultures (Fig. 5.20b). Non-migratory cells within Canertinib-treated empty scaffolds samples did not express an anticipated membranous localisation of E-cadherin or HER2 which may indicate high levels of cell death (Fig. 5.20a). Similarly, non-migratory cells within Canertinib-treated ET-SIM exhibited unanticipated localisation of E-cadherin and HER2, except in rare small groups of cells (Fig. 5.20b, i, ii).

Confocal microscope tile scan z-stacks revealed that TUBO cells in ROCKi treated tumours migrated x-, y- and z-distances ≥ 1000µm (Fig. 5.21, Fig. 5.22) from the seeded tumour fragment (dotted line, Fig. 5.21, Fig. 5.22). Furthermore, heterogeneous membranous expression of Her2 and E-cadherin in both empty scaffold and ET-SIM cultures was observed (Fig. 5.21, Fig. 5.22). These techniques underscore the superiority of the ET-SIM system in combination with tissue clearing and 3D imaging, to analyse tumour migration and drug efficacy.

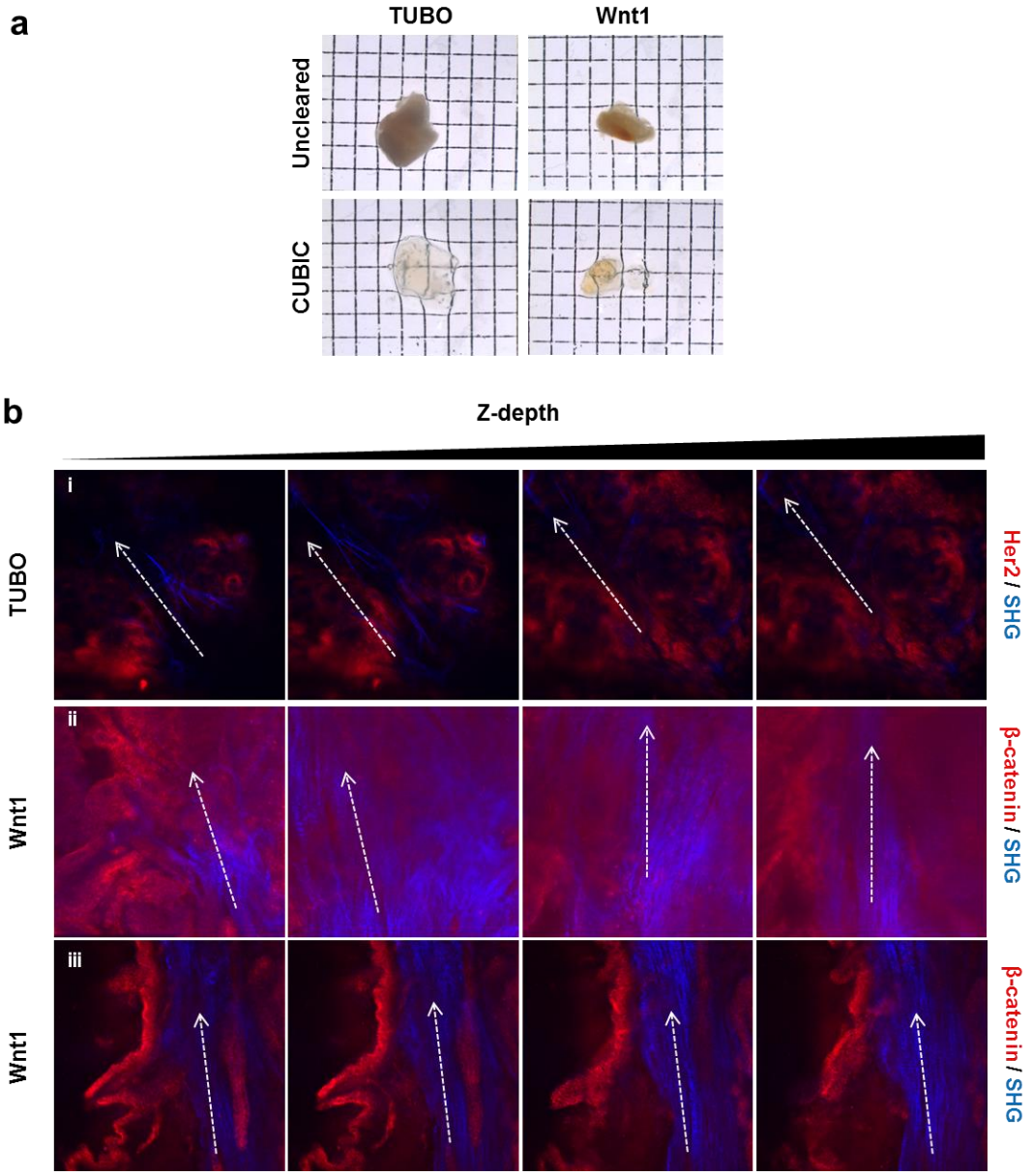


***Figure 5-17: CUBIC clearing and collagen anisotropy of TUBO and MMTV-Wnt1 tumours***

Tumours were generated by either injection of TUBO (Her2-*neu* overexpressing) cells into a syngeneic mouse or spontaneously in MMTV-*Wnt1* transgenic mice. Tumours were then harvested, optically cleared and whole mount immunostained. (a) Transmission stereoscopic images of uncleared and CUBIC optically cleared TUBO and MMTV-*Wnt1* tumours from a top down view (b) Whole mount CUBIC cleared tumours immunostained for Her2 (i, red, TUBO) and β-catenin (ii-iii, red, MMTV-*Wnt1*). Immunostaining was imaged using 2-photon fluorescence microscopy (2pf). Collagen (blue) was imaged directly using second harmonic generation (SHG). Directional collagen fibres surrounding tumour cells are marked with white arrows. Z stacks are displayed as individual z-slices showing increasing depth from left to right (0-100µm).

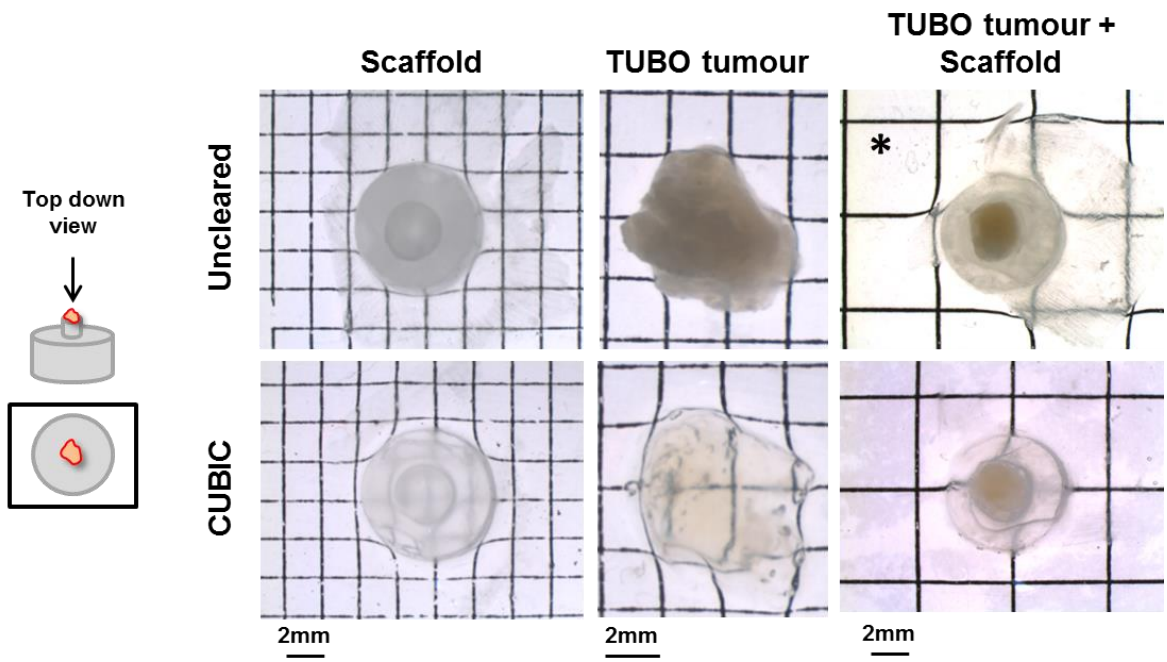


***Figure 5-18: Optical clearing of anisotropic collagen scaffolds, TUBO tumours and TUBO tumour fragment cultures***

Tumours were generated by injection of TUBO (Her2-*neu* overexpressing) cells into a syngeneic mouse. Tumours were then harvested and either optically cleared using CUBIC or seeded in anisotropic collagen I scaffolds then optically cleared using CUBIC. Transmission stereoscopic images were then taken of uncleared and optically cleared (CUBIC): anisotropic collagen scaffold, TUBO tumour and their combination, all from a top down view. *Uncleared TUBO/scaffold combination image was unintentionally taken with increased light levels.

**a**

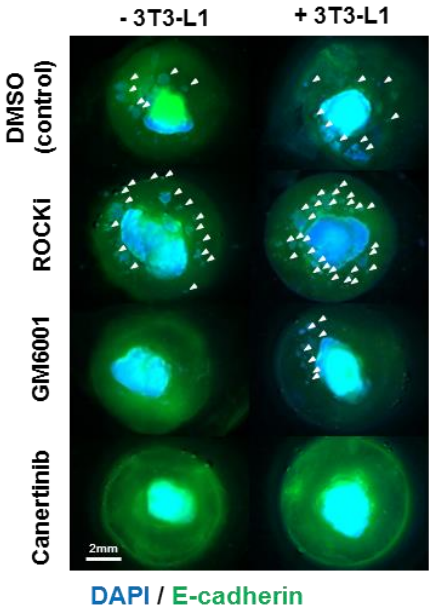


**b**

| Therapeutic / Adipocyte status | Number of scaffolds with visible colonies | % |
|---|---|---|
| DMSO | 5/5 | 100% |
| DMSO 3T3-L1 | 6/6 | 100% |
| ROCKi | 6/6 | 100% |
| ROCKi 3T3-L1 | 6/6 | 100% |
| GM6001 | 3/6 | 50% |
| GM6001 3T3-L1 | 6/6 | 100% |
| Canertinib | 0/6 | 0% |
| Canertinib 3T3-L1 | 0/6 | 0% |

***Figure 5-19: Macroscopically visible migration of TUBO tumour cells in empty scaffolds and ET-SIM cultures in the presence of candidate inhibitors***

(a) Fluorescent stereoscopic images of TUBO tumour fragments seeded in scaffolds, cultured for 10 days with/without adipocytes (3T3-L1), treated with DMSO (control), ROCKi (Y-27632), GM6001 or Canertinib, CUBIC cleared and immunostained for E-cadherin (green) and Her2 (not shown). Cell nuclei are stained with DAPI (blue). Clusters of cancer cells that have migrated away from the central tumour fragment are marked with arrowheads. (b) Quantification of the number of tumour/scaffolds that contain >1 visible (via fluorescent stereoscopy) migratory cell clusters. One DMSO empty scaffold sample was compromised during the clearing and immunostaining stages and was not analysed and therefore only 5 repeats were analysed. For all other samples n=6.

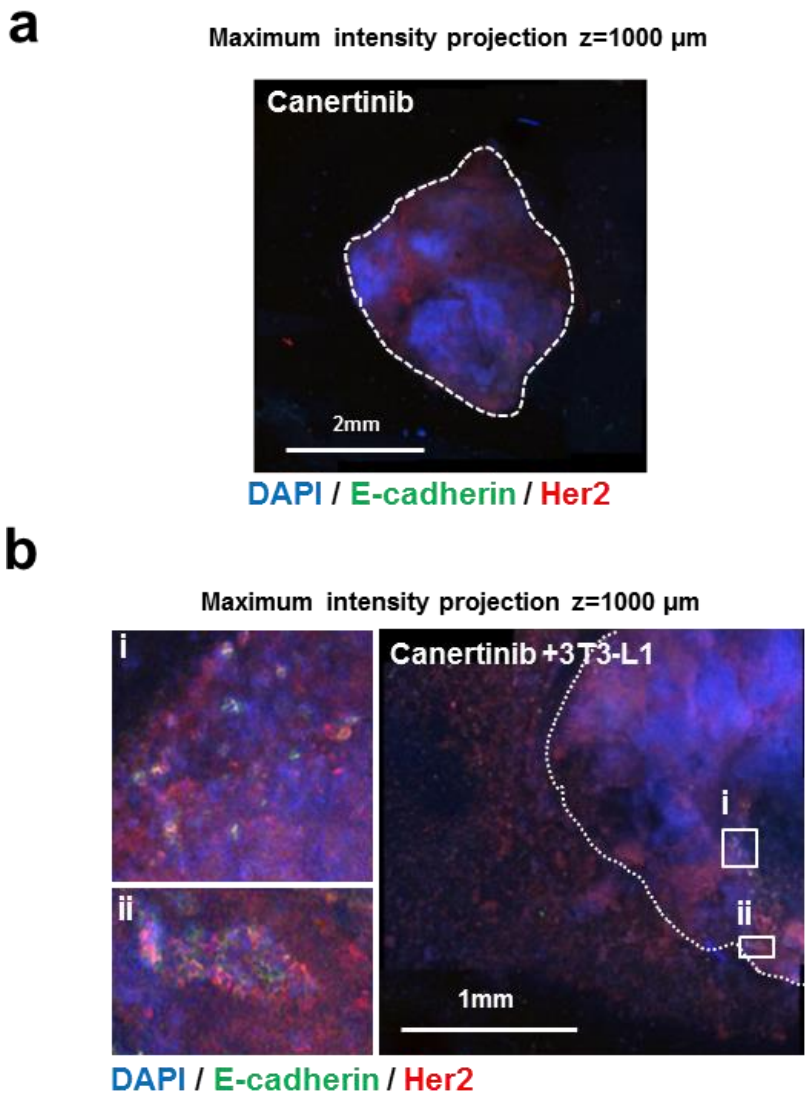


***Figure 5-20: Canertinib abrogates microscopically visible migration of TUBO tumour cells in empty scaffolds and ET-SIM cultures***

Primary TUBO tumour fragment seeded into an (a) empty anisotropic collagen scaffold or (b) anisotropic collagen scaffold invested with differentiated 3T3-L1 cells (ET-SIM). TUBO-scaffold and TUBO-ET-SIM were then cultured for 10 days whilst being treated with Canertinib, CUBIC cleared and immunostained for E-cadherin (green) and Her2 (red). Cell nuclei are stained with DAPI (blue). The seeded tumour fragment is outlined (white dotted line). (a) No migratory cells were observed and no cells with the correct membranous localisation of E-cadherin or Her2 were observed. (b) No migratory cells were observed. (b, i, ii) Few cells with the correct membranous localisation of E-cadherin or Her2 were observed and were only found in the original tumour fragment. Images were taken using confocal microscopy tile scan z-stacks (z=1000µm).

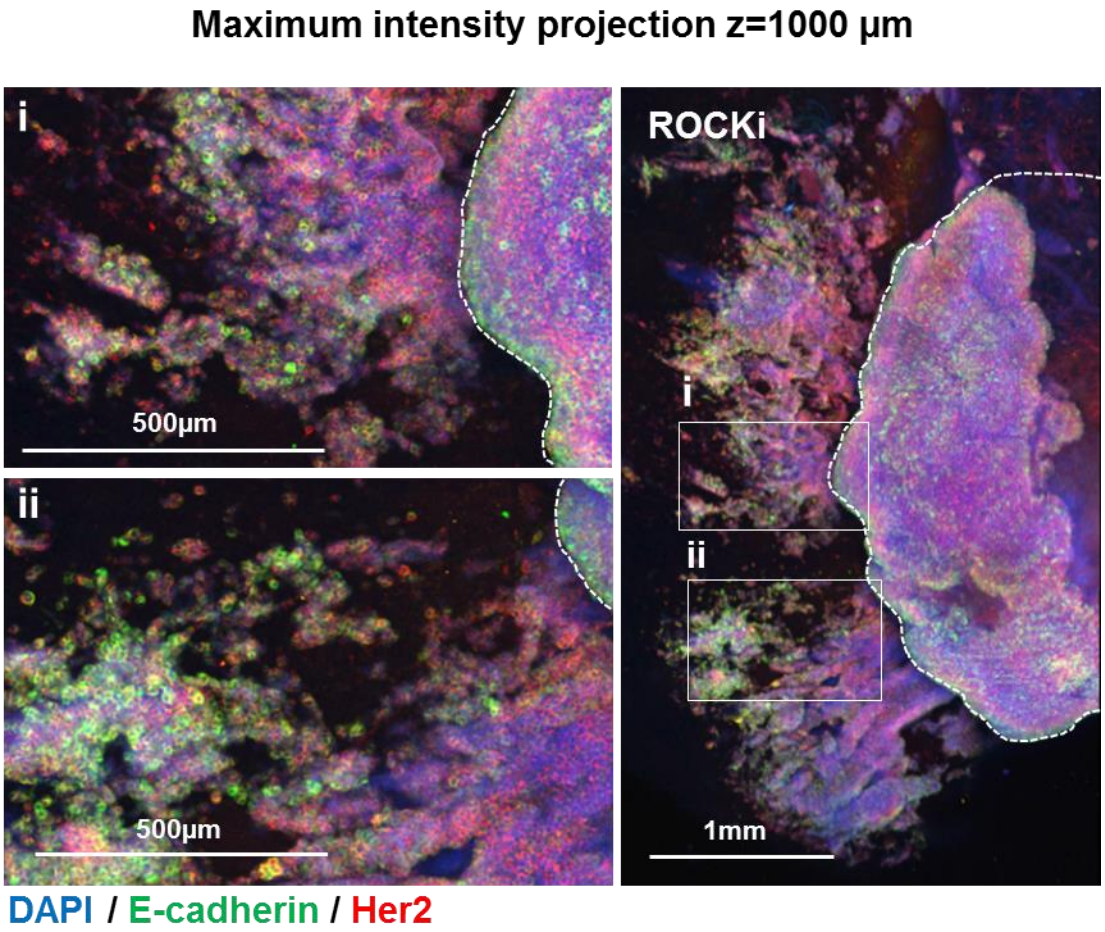


***Figure 5-21: ROCKi allows migration distances of over 1000µm for TUBO tumour fragments in empty scaffold cultures***

Primary TUBO tumour fragment seeded into an anisotropic collagen scaffold, cultured for 10 days without adipocytes (-3T3-L1), treated with ROCKi, CUBIC optically cleared and immunostained for E-cadherin (green) and Her2 (red). Cell nuclei are stained with DAPI (blue). The seeded tumour fragment is outlined (white dotted line). (i) and (ii) show zoomed in images of migratory clusters of Her2 and E-cadherin positive cells. Images were taken using confocal microscopy tile scan z-stacks (z=1000µm).

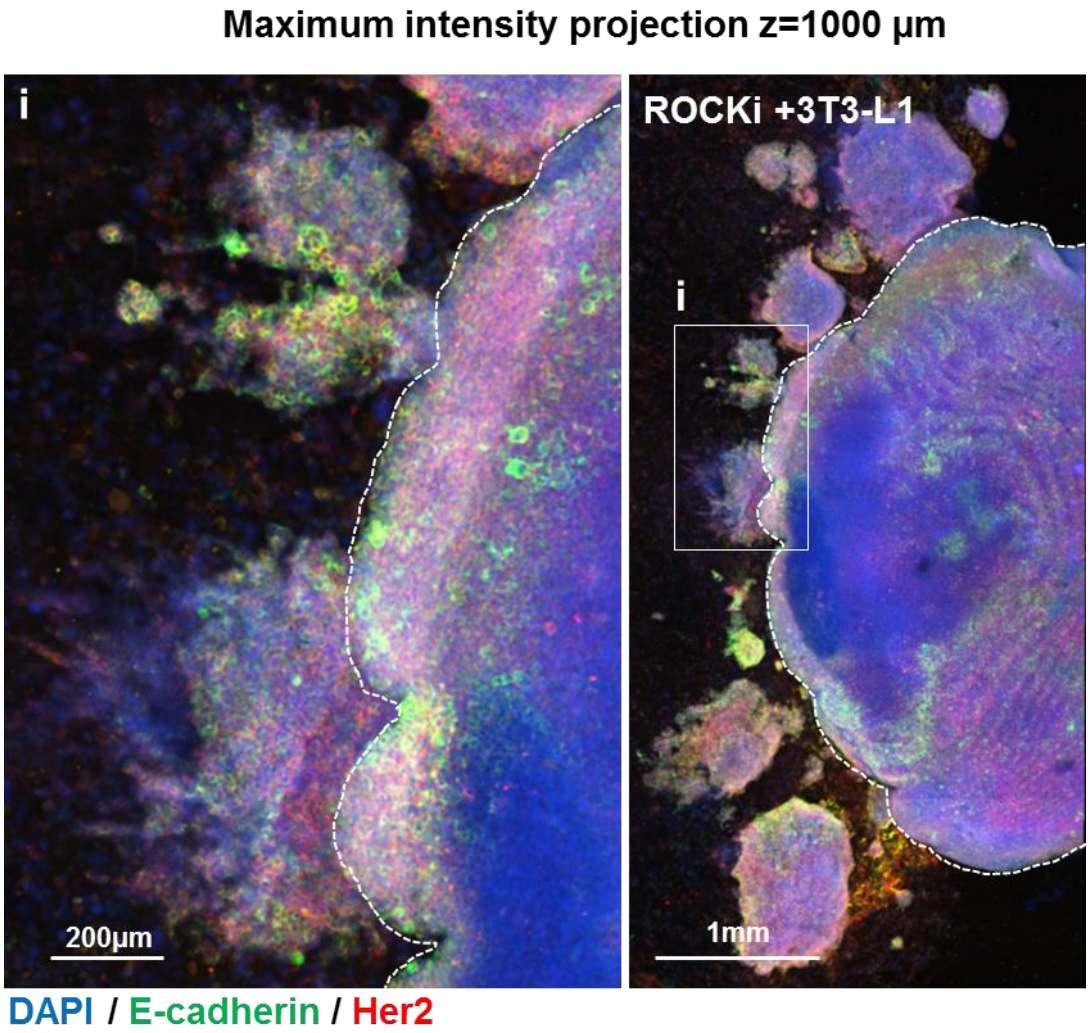


***Figure 5-22: ROCKi allows migration distances of over 1000µm for TUBO tumour fragments in ET-SIM cultures***

Primary TUBO tumour fragment seeded into an anisotropic collagen scaffold, cultured for 10 days in ET-SIM (+3T3-L1), treated with ROCKi, CUBIC cleared and immunostained for E-cadherin (green) and Her2 (red). Cell nuclei are stained with DAPI (blue). The seeded tumour fragment is outlined (white dotted line). (i) shows zoomed in images of migratory clusters of Her2 and E-cadherin positive cells. Images were taken using confocal microscopy tile scan z-stacks (z=1000µm).

# 5.3 Discussion

## 5.3.1 The Engineered Tumour-Stroma Interaction Model (ET-SIM)

A previous report has shown breast tumours can be grouped according to three different tumour-associated collagen signatures (TACS) (Provenzano et al. 2006). In this previous study, invasive MMTV-*Wnt1* tumours remodel surrounding stromal ECM into a TACS-3 phenotype where collagen fibres run perpendicular to the tumour boundary creating localised anisotropy that provides a highway for metastatic cells. Importantly, a similar TACS-3 phenotype has been reported in human breast tumours that are associated with poor patient prognosis (Conklin et al., 2011). As shown in Chapter 4, anisotropic collagen I scaffolds were synthesised to recapitulate the TACS-3 phenotype *in vitro*. The Engineered Tumour-Stroma Interaction Model (ET-SIM) improved upon this system through the addition of adipocytes to the anisotropic scaffolds.

SHG and 2pf were used to confirm whether preadipocytes could differentiate in the collagen anisotropic scaffolds of the ET-SIM model. Combination of SHG with immunostaining and two-photon fluorescence (2pf) microscopy permitted the visualisation of mature adipocytes as well as their 3D localisation within the anisotropic collagen pores in which they reside (Fig. 5.1). As the anisotropic scaffolds varied in pore size and shape with distance from the nucleation point, future experiments could utilise SHG and 2pf microscopy to study the collagen structure surrounding individual migratory tumour cells. Interactions with the scaffold ECM could then be probed through 3D immunostaining of proteins such as integrins. Furthermore, SHG does not damage living cells and could be combined with live cell imaging to investigate the mechanism by which a cell migrates along anisotropic collagen pores. In addition, live imaging could permit investigation into ECM remodelling by migratory cells and/or adipocytes in real-time, however, imaging depths present a current restraint of the system without the use of fixation and optical clearing agents.

During adipogenesis it has been shown that 3T3-L1 cells produce basement membrane proteins (Aratani and Kitagawa, 1988; Ojima et al., 2016). Likewise, 3T3-L1 cells in anisotropic scaffolds also produced both collagen IV and laminin upon adipogenesis (Fig. 5.1). The ET-SIM model therefore included other naturally occurring ECM proteins other than collagen I formed by *de novo* synthesis, that migratory breast cancer cells would likely come into contact with *in vivo* and could influence their migratory phenotype.

## 5.3.2 Tumour heterogeneity

One concern of using fresh tumour fragments for the ET-SIM studies, was that these fragments varied in size and morphology, as described in section 5.2.2. Nevertheless, it could be argued that *in*

*vivo* tumours are also subject to high variability in size and morphology. *In vivo* tumours are frequently measured by callipers or bioluminescence using a luciferase reporter and hence *in vivo* measurements are also an approximation of actual tumour size (Zagozdzon et al., 2012). One advantage however of *in vitro* systems is that they are more malleable; there is a greater degree of control over the system. To improve tumour fragment variability, tools to provide tumour fragments of similar sizes could be designed, such as a core needle biopsy gun machined to the dimensions of the scaffold funnel. This would reduce the human error made by estimating tumour fragment size, increasing accuracy and reproducibility within the ET-SIM system to increase assay robustness and therefore increase the likelihood of the model's use in the wider scientific community.

An inherent variable within the ET-SIM tumour culture system is inter-tumour heterogeneity and intra-tumour heterogeneity (ITH) (Gerlinger et al., 2012; Hernandez et al., 2012; Patani et al., 2011; Shipitsin et al., 2007). Inter-tumour heterogeneity is defined as differences in cell phenotype between different tumours, whereas ITH describes differences in cell phenotype within the same tumour which can arise due to processes such as clonal evolution or the cancer stem cell hierarchy (Drobysheva et al., 2015; Lim et al., 2010; Ng et al., 2015; Nowell, 1976; Quintana et al., 2010; Wang et al., 2014b). For example, the MMTV-*Wnt1* tumour model used in ET-SIM has been described in the literature to exhibit a number of different phenotypes between different tumours *in vivo* thus showing inter-tumour heterogeneity (Li et al., 2000; Monteiro et al., 2014; Teissedre et al., 2009; Zhang et al., 2005). Here, in MMTV-*Wnt1* tumour fragments in ET-SIM cultures, ITH was apparent by the mixed basal and luminal phenotypes and varied structures observed within the same tumour mass (Fig. 5.3). Despite TUBO tumours being established through injection of a relatively homogenous mammary tumour cell line, they also displayed ITH, as seen by the varied vimentin expression between cells (Fig. 5.6).

Inter-tumour heterogeneity and ITH are both characteristics that have been described in patient samples (Shipitsin et al., 2007). Moreover, they are frequently attributed to poor drug efficacy and disease relapse (Moore et al., 2012; Nim et al., 2017; Sharma et al., 2010; Zhao et al., 2014). Modelling these factors is therefore paramount to the investigation of tumour cell migration and the response to various drugs *in vitro*. Both tumour models in this study display ITH, therefore increasing the system's ability to recapitulate the *in vivo* tumour microenvironment. Although ITH introduces variation in the data, this variation is inherent within the human population and therefore modelling ITH may increase translatability into the clinic.

After seeding and culturing MMTV-*Wnt1* and TUBO tumour fragments in ET-SIM, two different migratory phenotypes were observed (Fig. 5.4, Fig. 5.5). Cells from MMTV-*Wnt1* tumours collectively

migrated into ET-SIM cultures with elongated tendril-like protrusions of cells aligned with collagen pores emanating from the tumour mass into the scaffolds (Fig. 5.4). Conversely, TUBO tumour cells migrated as singular or small clusters of cells with a round morphology, separated from the tumour mass (Fig. 5.5). These differences demonstrate that the model can distinguish these two tumour types based on their migratory phenotype. These phenotypes may be a result of different modes of migration adopted by each tumour cell type. Based on morphology alone, MMTV-*Wnt1* cells exhibited similarity with a mesenchymal phenotype and potentially may have undergone an EMT to permit a mesenchymal mode of migration (Johansson et al., 2015) (Fig. 5.4). For TUBO tumour cells, cell shape resembled an amoeboid mode of migration due to the singular rounded morphology observed (Gao et al., 2017) (Fig. 5.5). Amoeboid movement in cancer cells is characterised by low adhesion and a higher velocity than mesenchymal movement (Paňková et al., 2010). This may explain the larger migration distances achieved by TUBO cells during migration over such a short time period (Fig. 5.5).

### 5.3.3 Rho-associated protein kinase (ROCK) inhibition effects on MMTV-*Wnt1* tumour cultures

A striking increase in MMTV-*Wnt1* tumour cell migration distance was observed with the ROCK inhibitor Y-27632 (ROCKi) treatment. This effect was seen at 72 hours and 10 days both in ET-SIM and empty scaffold cultures (Fig. 5.7, Fig. 5.12, Fig. 5.13). Previous literature is divided on the effects of ROCKi on cancer cell migration with some studies showing that ROCK inhibition supresses or inhibits migration, while others show that ROCK inhibition increases invasive potential (Bhandary et al., 2015; Provenzano et al., 2008a; Riching et al., 2014; Vishnubhotla et al., 2012; Yang and Kim, 2014). These studies vary in the systems used, suggesting that ROCKi exerts cell type specific and context dependent effects.

Previously it has been shown that collagen gels are aligned *in vitro* by cells within seeded tumour explants to produce regions of collagen anisotropy at the tumour edge (Provenzano et al., 2008b). Similar to what was observed with MDA-MB-231 cells in Chapter 4 for anisotropic versus isotropic scaffolds; this study showed these anisotropic regions of collagen enhanced the migration of tumour explant cells over regions of isotropy. Subsequently, they treated explants with H1152; an alternative ROCK inhibitor to Y-27632 (ROCKi) used in ET-SIM studies in Chapter 5, and found ROCK inhibition decreased matrix reorganisation at the tumour-collagen gel interface and consequently reduced migration. Their findings suggest that ROCK signalling is required for the initial reorganisation of isotropic ECM into a TACS-3 phenotype at the tumour edge and subsequent tumour cell migration. However, as the anisotropic collagen scaffolds used in Chapter 5 were already

pre-aligned, ROCK signalling was not required for the remodelling of collagen into an anisotropic phenotype and this comparison is therefore not directly applicable. Furthermore, ROCK inhibition in ET-SIM cultures produced the opposite effect to the aforementioned study, by increasing migration rather than supressing it (Fig. 5.7, Fig. 5.12, Fig. 5.13).

Additionally, in the aforementioned study on tumour-collagen anisotropy, the effects of ROCK inhibition in magnetically pre-aligned collagen gels were examined (Provenzano et al., 2008b). This approach is comparable to experiments involving ROCK inhibition in ET-SIM cultures due to the pre-aligned collagen structures present in both systems. In this example, ROCK inhibition did not affect migration, reinforcing that ROCK signalling is only required for initial matrix alignment to increase migration. However, this does not explain the increased migration during ROCK inhibition observed in ET-SIM cultures (Fig. 5.7, Fig. 5.12, Fig. 5.13). Importantly, there were distinct differences in the studies, which may contribute to the varied effects observed with ROCK inhibition. These include the use of gels rather than scaffolds, the specific ROCK inhibitors used and the mouse models from which tumours were derived.

ROCKi treated MMTV-*Wnt1* tumours exhibited an elongated morphology in cells that had migrated furthest in anisotropic collagen scaffolds (Fig. 5.12b,i,ii). Interestingly, it has been shown that elongated cells do not require ROCK signalling in order to migrate (Sahai and Marshall, 2003). Therefore ROCK inhibition may have favoured the migration of elongated cells from MMTV-*Wnt1* tumours into the scaffold. ROCK inhibition can also enhance the migration of cells with large mature focal adhesions attaching them to the surrounding ECM (Goetsch et al., 2014). This is achieved by reducing the size and increasing the number of focal adhesions. In this case, cell morphology is converted from a more rounded morphology to a compact body with elongated protrusions. This conversion of morphological phenotype was also observed in ROCKi treated MMTV-*Wnt1* tumour cells, specifically in the more migratory population (Fig. 5.12b,i,ii). Therefore, a reduction in the number of focal adhesions may serve as an alternative explanation to the increased migratory phenotype observed in ROCKi treated MMTV-*Wnt1* tumour cultures.

Additionally, ROCKi has been shown to promote cell survival and colony forming efficiency when used in organoid cultures of human breast, mouse mammary gland and MMTV-*Wnt1* tumours (Isobe et al., 2014; Jamieson et al., 2017; Jardé et al., 2016; Linnemann et al., 2015). Enhanced cell survival could explain the increased frequency of migratory cells observed in ROCKi treated samples, by providing migratory cells with a survival advantage over vehicle controls (Fig. 5.15). Collectively, these data indicate that due to the variation observed with ROCK inhibition across models, their therapeutic application should be very carefully considered

### 5.3.4 Matrix metalloproteinase inhibition effects on MMTV-*Wnt1* tumour cultures

The broad spectrum matrix metalloproteinase (MMP) inhibitor GM6001 showed varying effects on migration distance at different time points. When applied to MMTV-*Wnt1* tumour fragments in empty scaffolds, no statistically significant difference in migration was observed relative to DMSO controls at 72 hours (Fig. 5.7a). The majority of cells showed a decreased migration distance compared to DMSO, which may be explained by a small separate highly migratory population of 7 cells observed at distances over 400 µm and thus affected the average distance calculated (Fig. 5.7a). This population could reflect a small subset of particularly aggressive tumour cells. At 10 days, the suppressive effects of GM6001 compared to DMSO vehicle controls were apparent in both empty scaffold and ET-SIM cultures (Fig. 5.13). The discrepancy between the two time points may reflect a subtle or delayed effect of GM6001 or a lack of sensitivity in the system to pick up effects at the shorter time point.

When comparing GM6001 treatment in empty scaffolds versus in ET-SIM, adipocytes reduced migration at 72 hours (Fig. 5.8c). Interestingly, this effect was reversed at 10 days (Fig. 5.14c). This time-dependent adipocyte-mediated effect highlights the importance of both the inclusion of stromal cells and the extension of the assay to longer time points.

Migration distance was decreased at 10 days with GM6001 treatment compared to DMSO controls (Fig. 5.13), suggesting migration is partially reliant on ECM remodelling via MMP activity in both the ET-SIM and empty scaffold cultures. Importantly, although migration distance was reduced, it was not completely abolished, suggesting that another form of migration that is MMP-independent occurs. Although MMP activity was inhibited, it cannot be assumed that migration in the presence of GM6001 is a completely protease independent mechanism. Other proteases not affected by MMP inhibitors which also remodel ECM, such as serine and cysteine proteases, would still be functional (Krepela et al., 1998; Provenzano et al., 2008a; Waxler and Rabito, 2003). To investigate protease dependent migration more fully, a cocktail of protease inhibitors would be required.

### 5.3.5 ErbB inhibition effects on MMTV-*Wnt1* tumour cultures

Treatment with the pan-ErbB inhibitor Canertinib on MMTV-*Wnt1* tumours in empty scaffolds significantly reduced migration distance after 72 hours culture (Fig. 5.7a). However, there was no difference observed in ET-SIM cultures relative to DMSO vehicle control (Fig. 5.7b). This suggests that at this time point, adipocytes provide a pro-migratory phenotype strong enough to reverse the effects of Canertinib on migration distance. Indeed, consistent with this notion, exposing breast

cancer cells to adipocyte conditioned medium has been shown to reduce the therapeutic efficacy of certain cancer drugs (Duong et al., 2015).

Canertinib-treated empty scaffold samples showed a significant reduction in the frequency of migratory cells compared to DMSO vehicle controls after 72 hours (Fig. 5.9a). Furthermore, elevated apoptosis was observed in these samples, demonstrated by increased expression of cleaved caspase-3 (CC3) (Fig. 5.11). Although there was a reduction in the frequency of migratory cells in Canertinib ET-SIM compared to DMSO ET-SIM (Fig. 5.9b), comparably low expression of CC3 was observed (Fig. 5.11). It is possible that other CC3-independent cell death mechanisms, such as necrosis or necroptosis, may account for the reduced frequency of migratory cells observed (Kim et al., 2017; Yang et al., 2013). Alternatively, cell death may have occurred before 72 hours and so CC3 was either degraded and not detected by IHC or was washed out of the tumours during daily media changes. A virally transfected CC3 fluorescent reporter and live cell imaging could be used to investigate this further and would provide the assay with a live read-out of apoptotic cell death as it occurs.

By 10 days of culture, no migratory cells were present in any Canertinib-treated samples and therefore no migratory distances or frequencies could be recorded. Any migratory cells found at earlier time points were therefore killed by Canertinib treatment and were not detected. A limitation of the current assay is the use of fixed end-point analysis; and thus development of live imaging could vastly increase the analytical power of these studies. If the system were made amenable to fluorescent tagging and live imaging, the progression of fluorescent migratory tumour cells during treatment could be assessed. For example, TUBO cells could be genetically engineered to express tdTomato and imaged using multi-photon techniques in real-time. With future incorporation of these techniques into the assay, drug dosages could be investigated to determine the minimal dose and timing a drug requires to eliminate tumour cell migration. This would be extremely useful in the drug discovery field, whereby determining optimal therapeutic dosages could potentially lessen the unwanted side-effects associated with chemotherapy.

### 5.3.6 Adipocyte effects on MMTV-*Wnt1* tumour cultures

Comparison of DMSO controls in empty scaffolds versus DMSO controls in ET-SIM cultures at 72 hours illustrated a subtle but significant suppressive effect of adipocytes at 72 hours (Fig. 5.8a). Following 10 days culture, this effect had been reversed with adipocytes providing an enhanced migratory effect (Fig. 5.14a). These data may suggest that adipocytes secrete suppressive factors at earlier time points and pro-migratory factors at later time points. Collectively, these observations

highlight the complex bivalent effects of adipocytes and the need to incorporate stromal cells and a range of time-points into drug efficacy studies.

After 10 days culture, adipocytes enhanced the migration distance of MMTV-*Wnt1* tumour cells in all DMSO, ROCKi and GM6001 samples (Fig. 5.14). This pro-migratory effect of adipocytes on breast cancer cells is aligned with the majority of the literature, despite studies using alternative systems to measure migration (Balaban et al., 2017; Falk Libby et al., 2015; Iyengar et al., 2005; Kim et al., 2009a; Lee et al., 2015; Picon-Ruiz et al., 2016; Wang et al., 2015, 2017). A range of factors could be responsible for an adipocyte-mediated pro-migratory phenotype. These include factors secreted by adipocytes such as chemokine (C-C motif) ligand 20 (CCL20), the hormone adiponectin and ECM protein collagen VI (Falk Libby et al., 2015; Iyengar et al., 2005; Kim et al., 2009a). Furthermore, adipocytes can induce a cancer cell EMT resulting in an enhanced migratory phenotype (Lee et al., 2015). Additionally, breast cancer cells have been shown to induce lipolysis in adipocytes to subsequently increase cancer cell metabolism via uptake of adipocyte-derived fatty acids and increase cancer cell migratory potential (Balaban et al., 2017). Collection of ET-SIM culture supernatants in future studies for enzyme-linked immunosorbent assay (ELISA) analyses could enable the system to become amenable to the investigation of adipocyte-tumour signalling analyses. Furthermore, immunostaining for EMT markers, other ECM proteins and lipid droplets would enable future investigation of these factors which may explain the adipocyte-mediated pro-migratory phenotype. 3D immunolocalisation would permit a more detailed analysis of the spatial position of these factors and correlate them to the more or less invasive subsets of tumour cells. For example, 3D imaging could provide information on the size and distribution of lipids in 3T3-L1 cells and whether this is affected by proximity to more/less migratory tumour cells.

Despite adipocytes enhancing the distance that Wnt1 tumour cells migrate after 10 days in culture (Fig. 5.14), adipocytes showed a trend (not significant) to reduce the overall number of migratory cells (Fig. 5.16). This may suggest that they act as a physical selective barrier or filter – impeding some cells while facilitating penetration of more aggressive cancer cells. Alternatively, adipokines released by adipocytes may influence the migration of different subpopulations of tumour cells, demonstrating the relevance of ITH. Accordingly, ET-SIM cultures reveal heterogeneous cellular behaviour. It is therefore ideally suited to identify whether drugs target subpopulations responsible for metastatic spread, rather than generically de-bulking a tumour without effectively eliminating persistent migratory subsets.

### 5.3.7 Optical clearing of TUBO tumour / ET-SIM cultures

In chapter 5, it was demonstrated that anisotropic collagen scaffolds, ET-SIM cultures, tumour fragments and their combination could be optically cleared and immunostained using CUBIC (Fig. 5.18). This enabled fluorescent stereoscopic imaging and analysis of TUBO tumour cell migration in response to the candidate therapeutics (Fig. 5.19). These aforementioned techniques require low skill and little training, as they require moving samples through a number of different reagents and imaging on a stereoscope. It is therefore plausible that with the humanisation of the system using patient samples, the model could be translated into the clinic for routine diagnostics testing. Furthermore, stereoscopic imaging permitted quantitative analysis of the diverse effects of pathway-specific inhibitory drugs and has significant potential as a tool for rapid 'first pass' investigation of drug efficacy. Although stereoscopic image analysis permitted macroscopic visualisation of migratory colonies of cells, it is important to note that microscopic colonies were not detected with this methodology.

CUBIC enabled deep (1000μm) z-sectioning of TUBO / ET-SIM cultures, which, in conjunction with 3D immunostaining and confocal microscopy, facilitated visualisation of microscopic colonies of migratory cells, investigating cell phenotype and location (Fig. 5.19 – 5.22). This approach enabled the identification of ITH through stochastic expression of E-cadherin and HER2 in neighbouring TUBO cells. As observed with the MMTV-*Wnt1* tumours, Canertinib completely abolished TUBO tumour cell migration in both empty scaffolds and ET-SIM cultures (Fig. 5.19, Fig. 5.20). Canertinib is a pan-ErbB inhibitor that blocks HER2 signalling as well as other ErbB signalling pathways (Galmarini, 2004). TUBO cells were derived from a HER2 overexpressing breast carcinoma and therefore express HER2, as observed during microscopic analyses (Fig. 5.19 – 5.22) (Rovero et al., 2000). Potentially, Canertinib-mediated abrogation of HER2 signalling may have caused the anti-migratory effects observed in TUBO tumours.

As TUBO tumour cultures were utilised for CUBIC experiments, these samples were unavailable for paraffin embedding and subsequent migration distance analysis. Without these measurements, the adipocyte-mediated effects on this tumour type in ET-SIM cultures are unknown. Using the same Euclidian distance and frequency analyses applied to MMTV-*Wnt1* tumours in ET-SIM, future experiments could discern any differences between empty scaffold and ET-SIM cultures. Nonetheless, scaffolds treated with GM6001 increased the number of macroscopically visible colonies of migratory cells when cultured in ET-SIM (Fig. 5.19). This provides an indication of adipocyte effects, however, significant confocal analysis is required to confirm whether this difference was also observed on a microscopic scale.

### 5.3.8 Limitations of the ET-SIM system

A limitation of ET-SIM cultures is the possibility that any external factors introduced such as the inhibitory drugs used in this study, may not reach the core of the tumour fragment due to inefficient diffusion. To address this, media and inhibitors were replaced every 24 hours, encouraging diffusion. Further elaboration of the system would involve the use of a bioreactor to maintain a constant media flow, mimicking a patient's blood circulation. Nevertheless, the static system recapitulates a feature of many solid tumours where changes in tumour vasculature limit therapeutic efficacy by impairing drug penetration into the centre of the tumour (Grantab et al., 2006; Varia et al., 1998; Yu et al., 2015). It has been previously shown that collagen fibre anisotropy in proximity to tumours *in vivo* creates diffusion anisotropy, effecting how drugs reach target cells (Stylianopoulos et al., 2010). Therefore the anisotropic scaffolds may influence the diffusion of therapeutics and future comparison with isotropic scaffolds should address this.

### 5.3.9 Conclusion

ET-SIM is a versatile system, amenable to a number of microscopic techniques and the investigation of tumour cell migration in the presence of a range of therapeutic interventions. Its potential use as a drug discovery assay makes it an attractive prospect for the field of cancer research. Successful long term culture of tumour fragments permitted a complex understanding of adipocyte-mediated and therapeutic-mediated effects on migration. Furthermore, inclusion of primary tumour fragments that model inter- and intra- tumour heterogeneity facilitated the investigation of therapeutic efficacy and cell migration in a more relevant context than conventionally used *in vitro* assays.

# 6 Development of an *in vitro* human fat pad for breast cancer cell migration studies

# 6.1 Introduction

Mouse models are used extensively in experimental biology to provide insights into human diseases. Mice and humans experience a similar cancer incidence of 30% by the end of their respective lifetimes (American Cancer Society, 2016; Rabbany et al., 2003). However, several factors limit the utility of murine models. For example, mice live approximately 2-3 years compared to a human lifespan of 70-80 years and 30% of human cancers do not develop within this 3 year time frame. Furthermore, during drug discovery experiments murine animal models inaccurately predict toxicity for humans in over half of cases (Olson et al., 2000). Experiments combining results obtained in mice with those from another non-rodent model still only delivers an approximately 70% correct prediction for human toxicity. These factors have led this project to seek humanisation of the ET-SIM culture system described in chapter 5.

Initial experiments set out to confirm if the previously described TACS-3 phenotype could be observed in a human breast cancer sample (Conklin et al., 2011; Provenzano et al., 2006). Utilising histology, CUBIC clearing, whole mount immunofluorescence and multi-photon microscopy, samples were analysed for the presence of a TACS-3 phenotype. This rigorous analysis is intended to provide a solid rationale for proceeding with humanisation of the scaffold-based system.

As described in chapters 3 and 5, collagen scaffolds were invested with murine 3T3-L1 preadipocytes and differentiated into mature adipocytes, to synthesize a synthetic fat pad or ET-SIM cultures. To humanise the fat pad, the murine 3T3-L1 cells were replaced by primary human mesenchymal stem cells (MSCs) isolated from a reduction mammoplasty that were immortalised by retroviral insertion of either hTERT or the human papillomavirus E6E7 gene. Subsequent experiments tested whether these cells could avoid senescence, differentiate into mature adipocytes in 2D, differentiate into adipocytes in anisotropic collagen scaffolds and support the migration of the MDA-MB-231 human breast cancer cell line. The goal of this work was to progress towards future experiments where combination of a humanised ET-SIM (hET-SIM) with human tumour biopsies could be utilized to provide a therapeutic drug testing tool and a personalised medicine platform, to combat breast cancer.

# 6.2 Results

## 6.2.1 Human primary tumour biopsy displays a tumour associated collagen signature-3 (TACS-3) phenotype

Reproducibility has become a subject of concern in recent years with scientists unable to replicate the results of other published studies (Begley and Ellis, 2012). Previously it was confirmed that the TACS-3 phenotype first described in MMTV-*Wnt1* mouse tumours is also found in human breast tumours and is associated with a poor prognosis (Conklin et al., 2011; Provenzano et al., 2006). As these findings were of profound importance to the latter portion of the project, it was logical to attempt to reproduce these results on a human breast cancer biopsy sample. Additionally, using CUBIC and 3D immunolocalisation, the TACS-3 phenotype was investigated in an increased level of detail.

A human tumour biopsy, kindly provided by Dr. Jennifer Gomm (Queen Mary University of London (QMUL), Bart's Institute), was analysed for evidence of a TACS-3 phenotype. Pathologists at QMUL confirmed that the original tumour was an $ER^{+}/HER2^{-}$ grade 2 invasive ductal carcinoma (IDC). Following surgery, the biopsy was fixed and bisected with one half embedded in paraffin for histological analyses and the other half processed for CUBIC clearing. In order to visualise collagen and assess whether a TACS-3 phenotype was present in fixed histological sections, a Masson's Trichrome stain was employed (Fig.6.1). This stains collagens blue, nuclei dark purple and cytoplasm red. Directional anisotropic collagen fibres (Fig. 6.1, arrows) were aligned perpendicular to the periphery of the tumour (Fig. 6.1, left, tumour bulk) projecting between the adipocytes constituting the surrounding fat pad (Fig. 6.1, right, asterisks, fat pad). Cancerous epithelial cells were identified by their round morphology and a cytoplasm that was easily distinguishable from its nucleus. These epithelial cells were observed in the tumour bulk, on anisotropic collagen fibres at the tumour periphery and in the surrounding stroma (Fig. 6.1). This discrimination of epithelial tumour cells from other stromal cell types and structures within the Masson's Trichrome stained section was further confirmed by Dr. Raza Ali (University of Cambridge, CRUK), a trained medical pathologist.

To investigate the TACS-3 phenotype in 3D, the CUBIC clearing protocol was utilised in conjunction with whole mount immunofluorescence and multi-photon techniques. Stereoscopic visualisation of the tumour following clearing revealed that CUBIC increased transparency considerably (Fig. 6.2). Cells within cleared samples were marked with DAPI and fibres of collagen were imaged using 2pf microscopy and SHG, respectively (Fig. 6.3). As the DAPI and SHG signals overlapped in their excitation and emission spectra their signal was collected simultaneously (Fig. 6.3, grey). Anisotropic collagen fibres running from right to left between cells were observed frequently within the cleared

tumour sample (Fig. 6.3). To confirm that these cells located on anisotropic collagen fibres derived from the $ER^+$ IDC, samples were also stained with the nuclear marker ER and the cytoplasmic epithelial marker K8. Visualising the same z-sections as in Fig. 6.3, tracts of $ER^+$ $K8^+$ cells were often observed aligned between anisotropic collagen fibres (Fig. 6.4).

These data confirm the TACS-3 phenotype reported by Provenzano et al. (Provenzano et al., 2006). Thus, clearing, whole mount immunofluorescence and multi-photon techniques facilitated the detailed visualisation and permitted 3D localisation of tumour cells associated with anisotropic collagen fibres.

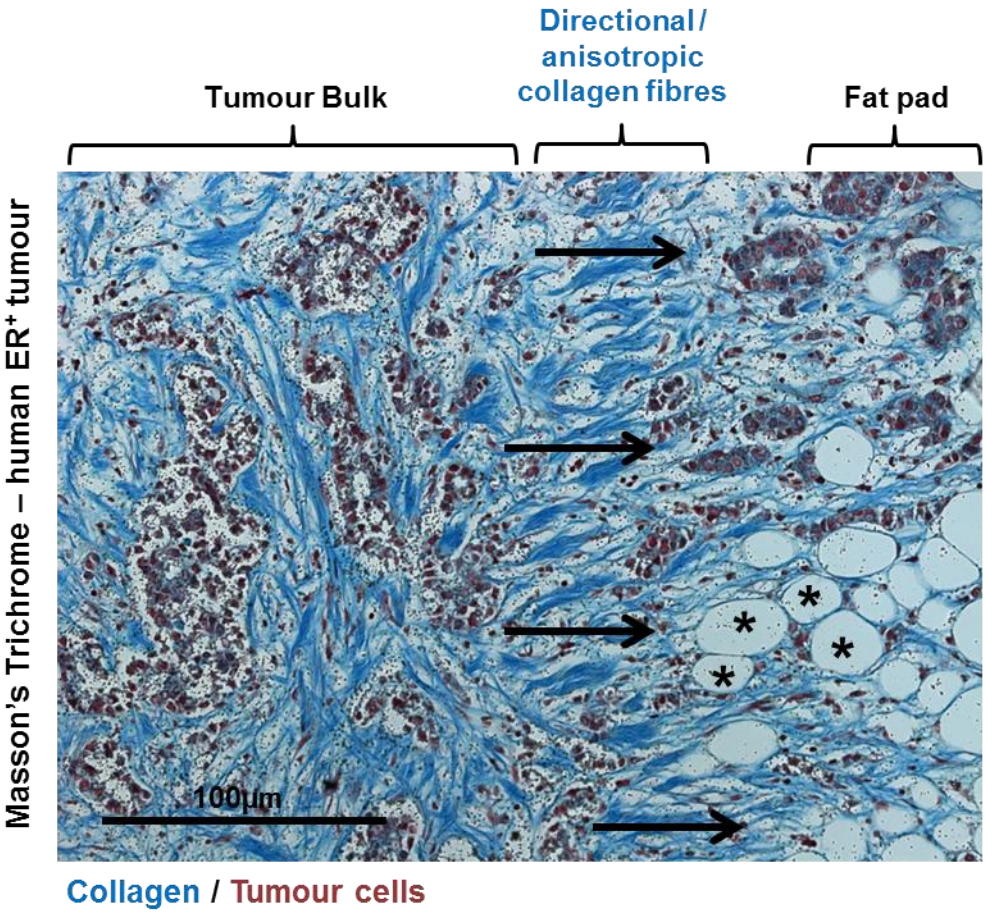


***Figure 6-1: Human ER+ invasive ductal carcinoma (IDC) with anisotropic collagen fibres at the periphery of the tumour - TACS-3 phenotype***

Fresh human oestrogen receptor positive HER2 receptor negative grade 2 invasive ductal carcinoma of the breast ($ER^+/HER2^-$ IDC grade 2) biopsy was fixed, embedded in paraffin, sectioned and stained with Masson's Trichrome (collagens = blue, nuclei = dark purple and cytoplasm = red). Grade, ER status and HER2 status was determined by a trained medical pathologist (QMUL, Bart's Institute) and kindly provided by Dr. Jenny Gomm (QMUL, Bart's Institute). Columns of tumour cells exhibiting round morphology with a distinguishable cytoplasm can be seen invading between adipocytes of the surrounding fat pad (*) via anisotropic collagen fibres (blue structures marked by black arrows). Tumour cells and structures identified by Masson's Trichrome were confirmed by Dr. Raza Ali (University of Cambridge, CRUK), a trained medical pathologist.

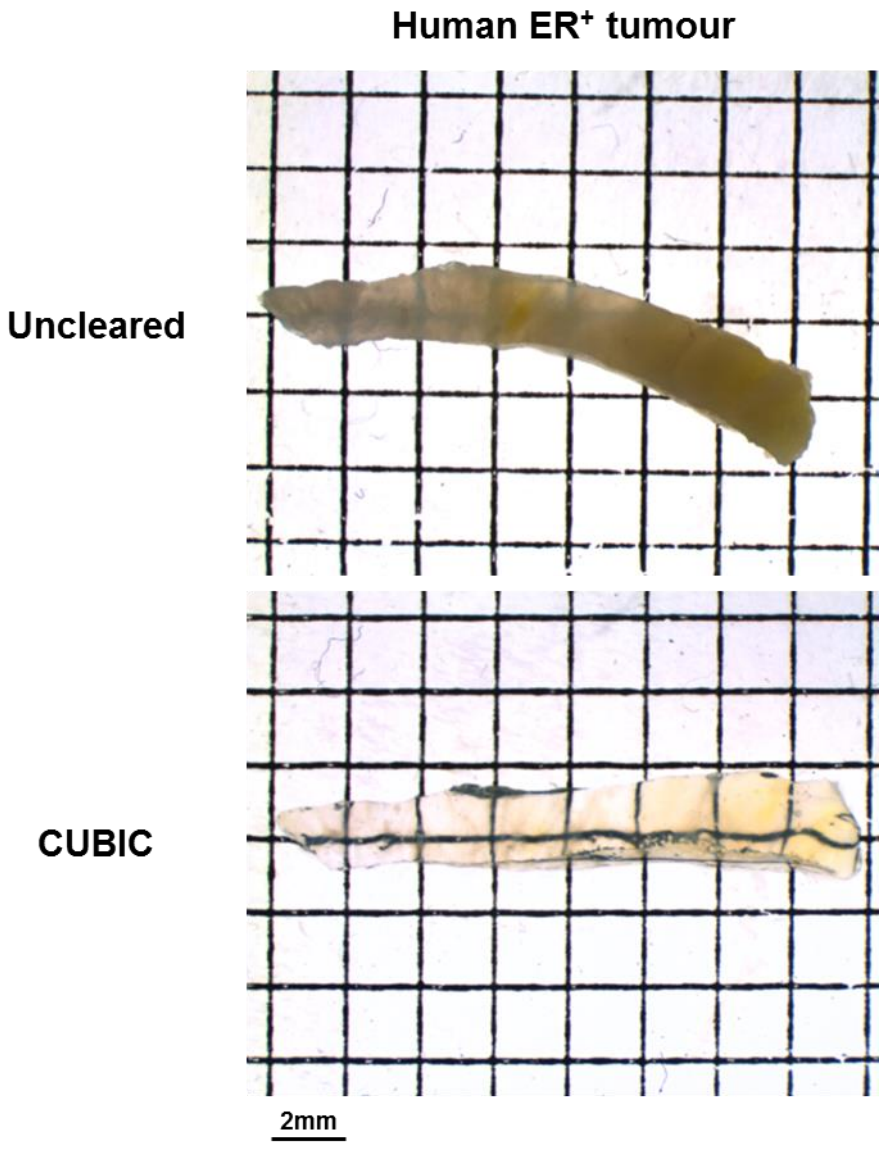


***Figure 6-2: Human ER+/HER2- invasive ductal carcinoma (IDC) optically cleared using CUBIC***

A fragment of a fresh human grade 2 $ER^+/HER2^-$ invasive ductal carcinoma of the breast (IDC) was fixed (top), then optically cleared using CUBIC (bottom) and imaged using a stereoscopic microscope.

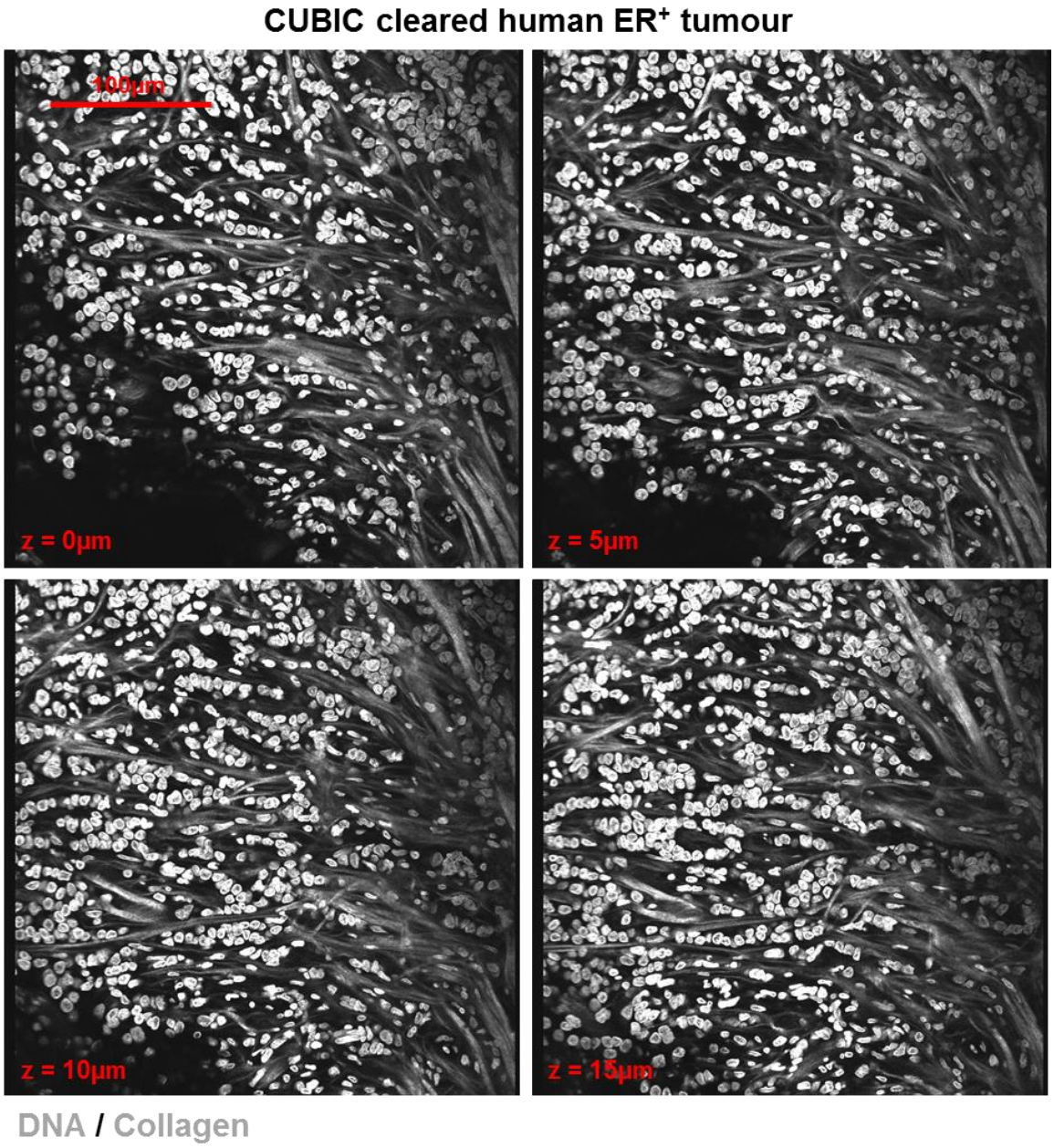


***Figure 6-3: Human ER+ IDC with anisotropic collagen fibres – second harmonic generation (SHG)***

A fragment of a fresh human ER+/HER2- IDC grade 2 biopsy was fixed, optically cleared using CUBIC and whole mount immunostained for keratin-8 (not shown) and ER (not shown). Nuclei were marked with DAPI (round, grey) and imaged using two-photon fluorescence microscopy (2pf). Collagen was imaged directly using second harmonic generation (SHG, long fibrous, grey). Directional anisotropic collagen fibres can be observed running right to left. DAPI and SHG were excited and collected at the same wavelengths. A 15µm z-stack is shown as individual z slices.

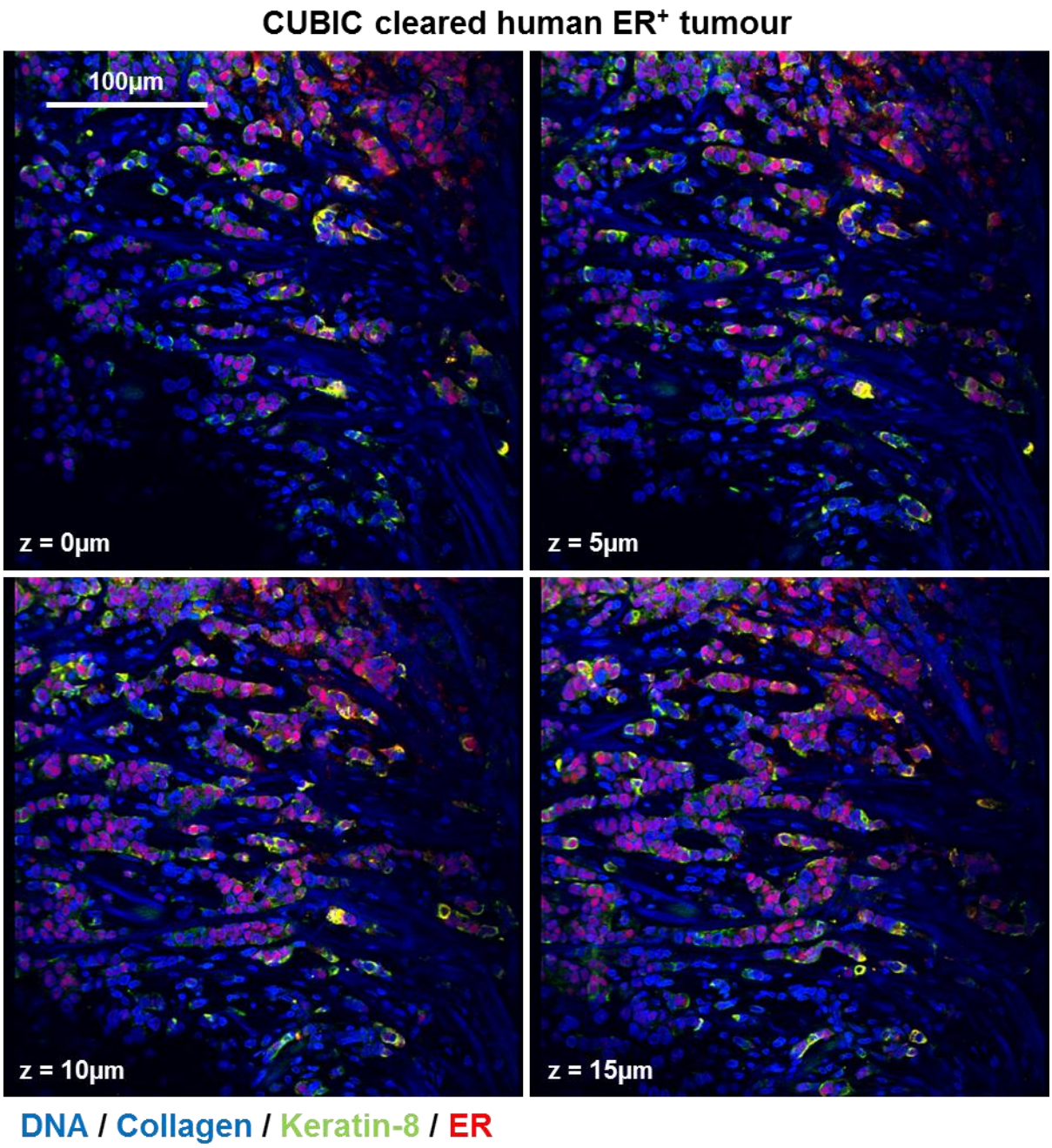


***Figure 6-4: Human ER+ IDC has tumour cells aligned with anisotropic collagen fibres***

A fragment of a fresh human ER+/HER2- IDC grade 2 biopsy was fixed, optically cleared using CUBIC and whole mount immunostained for cytokeratin-8 (K8, cytoplasmic, green) and ER (nuclei, red). All nuclei were marked with DAPI (blue) and imaged using two-photon fluorescence microscopy (2pf). Collagen was imaged directly using SHG (long blue fibres). Keratin-8$^+$ ER$^+$ tumour cells can be observed often in single file procession directionally aligned with anisotropic collagen fibres. DAPI and SHG were excited and collected at the same wavelengths. Z-stack is shown as the same individual z slices as in Fig. 6.3.

### 6.2.2 Mesenchymal stem cells (MSCs) can be immortalised by retroviral insertion of the E6E7 gene but not the hTERT gene

The following experiments aimed to replace the murine 3T3-L1 cell line in ET-SIM cultures with an equivalent human cell line. For this purpose human MSCs were selected due to their adipogenic potential *in vitro* (Pittenger et al., 1999). MSCs were isolated from a reduction mammoplasty using a previously published protocol and kindly provided by Professor Mohamed Bentires-Alj (Universität Basel) (Duss et al., 2014). Previously, it was shown that primary MSCs reach senescence in under 10 passages (Bonab et al., 2006). Due to this limited proliferative capacity and in the interests of designing a reproducible human ET-SIM (hET-SIM) system, successive experiments focussed on immortalising MSCs via retroviral insertion of either the hTERT or E6E7 genes.

During cell replication, telomeres that are located at the ends of chromosomes shorten. Once this reaches a critical length known as the Hayflick limit, DNA damage occurs and is sensed by proteins such as p53 thus causing replicative senescence (Fagagna et al., 2003; Hayflick and Moorhead, 1961; Saretzki et al., 1999). The E6 gene is derived from the human papillomavirus (HPV) and its product affects the cell cycle through the destruction and therefore inactivation of p53 (Foster et al., 1994). Furthermore, the E6 protein also targets other substrates for degradation that repress human telomerase reverse transcriptase (hTERT) synthesis (Gardiol et al., 1999; Klingelhutz et al., 1996). As hTERT maintains telomere length, this increased expression of hTERT prevents the shortening of the telomeres that would normally result in a cell reaching its Hayflick limit.

Also derived from HPV is the E7 gene, which targets the tumour suppressor retinoblastoma protein (pRB) (Chellappan et al., 1992). The E7 protein forms a complex with pRB inactivating its function. As pRB is required for cell cycle arrest to prevent a cell from replicating too early or too quickly, its inactivation can lead to increased proliferation and immortalisation (Goodrich et al., 1991; Yang and Hinds, 2007). Hence, insertion of E6 and E7 genes has been used to generate cell lines that are not subject to replicative senescence and provided the rationale for their retroviral insertion into MSCs (Lee et al., 2001; Omi et al., 2009). The choice of hTERT gene for retroviral insertion was to induce immortalisation by lengthening the telomeres of MSCs and consequently increase chromosomal stability (Hayflick and Moorhead, 1961; Morales et al., 1999; Tsai et al., 2010).

In order to ensure that only successfully transduced cells were cultured following retroviral infection, antibiotic selection was carried out to select this population of cells, as the plasmid that contained the E6E7 gene also coded for neomycin resistance. Geneticin (G418), an analogue of neomycin sulphate, was titrated in a kill curve using uninfected MSCs (Table 6.1). This provided the minimum concentration of 600 μg/ml required to kill 100% of uninfected MSCs over a 5 day period (Table 6.1).

Following retroviral transduction, antibiotic selection at this concentration was used to purify the E6E7-MSC population and kill any uninfected MSCs (Table 6.2). Similarly, the plasmid containing the hTERT gene also coded for puromycin resistance (Table 6.1). Puromycin was therefore titrated in a kill curve using uninfected MSCs, providing the minimum concentration of 1 μg/ml to kill 100% of uninfected MSCs over a 5 day period (Table 6.1). Following retroviral transduction, the hTERT MSC population was then purified via puromycin selection (Table 6.2).

To investigate whether these transduced cells had escaped senescence *in vitro*, a β-galactosidase senescence staining protocol was employed. Using this procedure, senescent cells that were unable to overcome their Hayflick limit, and therefore had not been immortalised, stained green. As this protocol lacks sensitivity, raw images as well as uniformly enhanced images have been provided to enable the visualisation of the distinctions between samples (Fig. 6.5) (Cahu and Sola, 2013). These data show that a high proportion of uninfected MSCs (Fig. 6.5, MSC) and MSCs transduced with a retrovirus containing the hTERT gene (Fig. 6.5, hTERT MSC) had become senescent. In contrast, MSCs transduced with a retrovirus containing the E6E7 gene (Fig. 6.5, E6E7-MSC) were likely immortalised as few senescent cells were observed.

The process of immortalising cells can increase their proliferative capacity (Gong et al., 2011). For further confirmation that the E6E7-MSCs had undergone immortalisation, IHC staining for the proliferation marker Ki67 was carried out with subsequent ImageJ analysis (Fig. 6.6). MSCs were analysed either at pre-confluency or post-confluency plus 11 days of adipogenesis. At pre-confluency significantly more proliferating E6E7-MSCs (≈90%) were observed compared to both uninfected MSC (≈30%) and hTERT MSC (≈40%) (Fig. 6.6). As adipogenesis induces terminal differentiation, low proliferation rates were anticipated in these samples (Estefanía et al., 2012; Jaiswal et al., 2000). Interestingly however, after 11 days of adipogenesis a small proportion (≈7%) of E6E7-MSC continued to express the proliferation marker Ki67 (Fig. 6.6a, white arrows, Fig. 6.6b, grey bar). These are most likely immortalised cells that have not terminally differentiated to adipocytes.

Collectively, these data demonstrate that MSCs can be successfully immortalised through viral insertion of the E6E7 gene. E6E7-MSCs were able to escape senescence and exhibited an enhanced superior proliferative capacity. This provides a potentially very useful candidate human cell line to replace the 3T3-L1 murine cell line in the ET-SIM system.

| Antibiotic | Concentration (μg/ml) | Dead MSC after 5 days (approx.) |
|---|---|---|
| Geneticin (G418) | 0 | 1% |
| | 150 | 75% |
| | 300 | 90% |
| | 400 | 98% |
| | 500 | 99% |
| | 600 | 100% |
| Puromycin | 0 | 1% |
| | 0.05 | 10% |
| | 0.1 | 30% |
| | 0.2 | 50% |
| | 0.5 | 95% |
| | 1 | 100% |

***Table 6-1: Kill curve to determine minimum antibiotic concentration required for the selection of immortalised human mesenchymal stem cells (MSC)***

Human mesenchymal stem cells (MSC) isolated from routine breast reduction mammoplasty surgery were kindly provided by Dr. Mohammed Bentirez-Alj (Friedrich Miescher Institute, Basel, Switzerland). Uninfected mesenchymal stem cells (MSC) were cultured to 75% confluency and treated with increasing concentrations of Geneticin/G418 and Puromycin. After 5 days treatment, cell death was quantified by an estimation of the percentage of non-attached cells observed using light microscopy.

| Plasmid name | Immortalising Gene | Antibiotic resistance | Concentration for selection |
|---|---|---|---|
| pLXSN-neo-E6E7 | E6E7 | Neomycin / G418 /Genetecin | 600 µg/ml |
| pBABE-puro-hTERT | hTERT | Puromycin | 1 µg/ml |

***Table 6-2: Optimal antibiotic concentrations for the selection of immortalised MSC***

The plasmids used for retroviral insertion of the E6E7 and hTERT genes for immortalisation and the corresponding antibiotic concentrations used for selection in human mesenchymal stem cells (MSC) derived from a reduction mammoplasty.

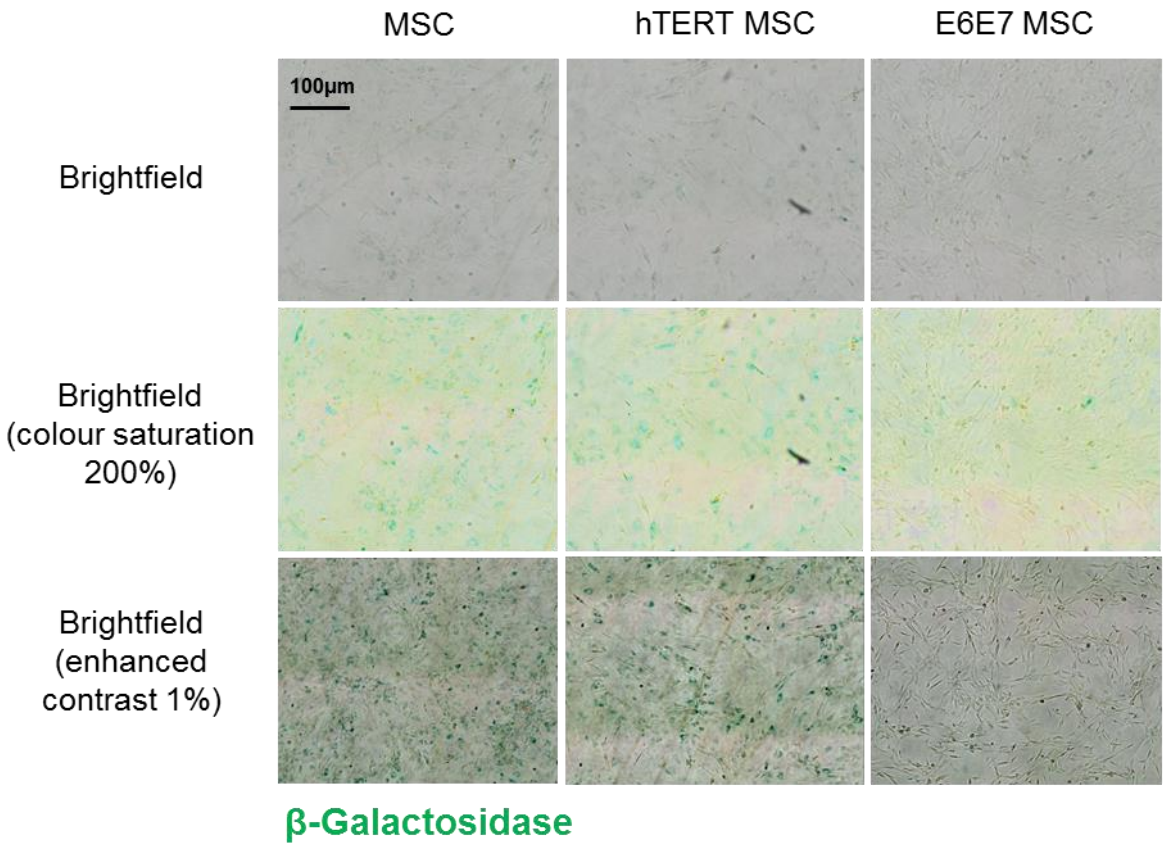


***Figure 6-5: MSCs immortalised via viral insertion of the E6E7 gene (E6E7-MSC) are able to avoid senescence***

Human mesenchymal stem cells (MSC) isolated from routine breast reduction mammoplasty surgery were kindly provided by Dr. Mohammed Bentirez-Alj (Friedrich Miescher Institute, Basel, Switzerland). Human telomerase reverse transcriptase (hTERT) or E6E7 genes were retrovirally inserted into MSC to produce immortalised cell lines. Senescent cells were marked using β-galactosidase staining. Image manipulation (colour saturation and contrast) was applied equally to each image to highlight subtle differences in β-galactosidase staining. Cells analysed were at passage 12.

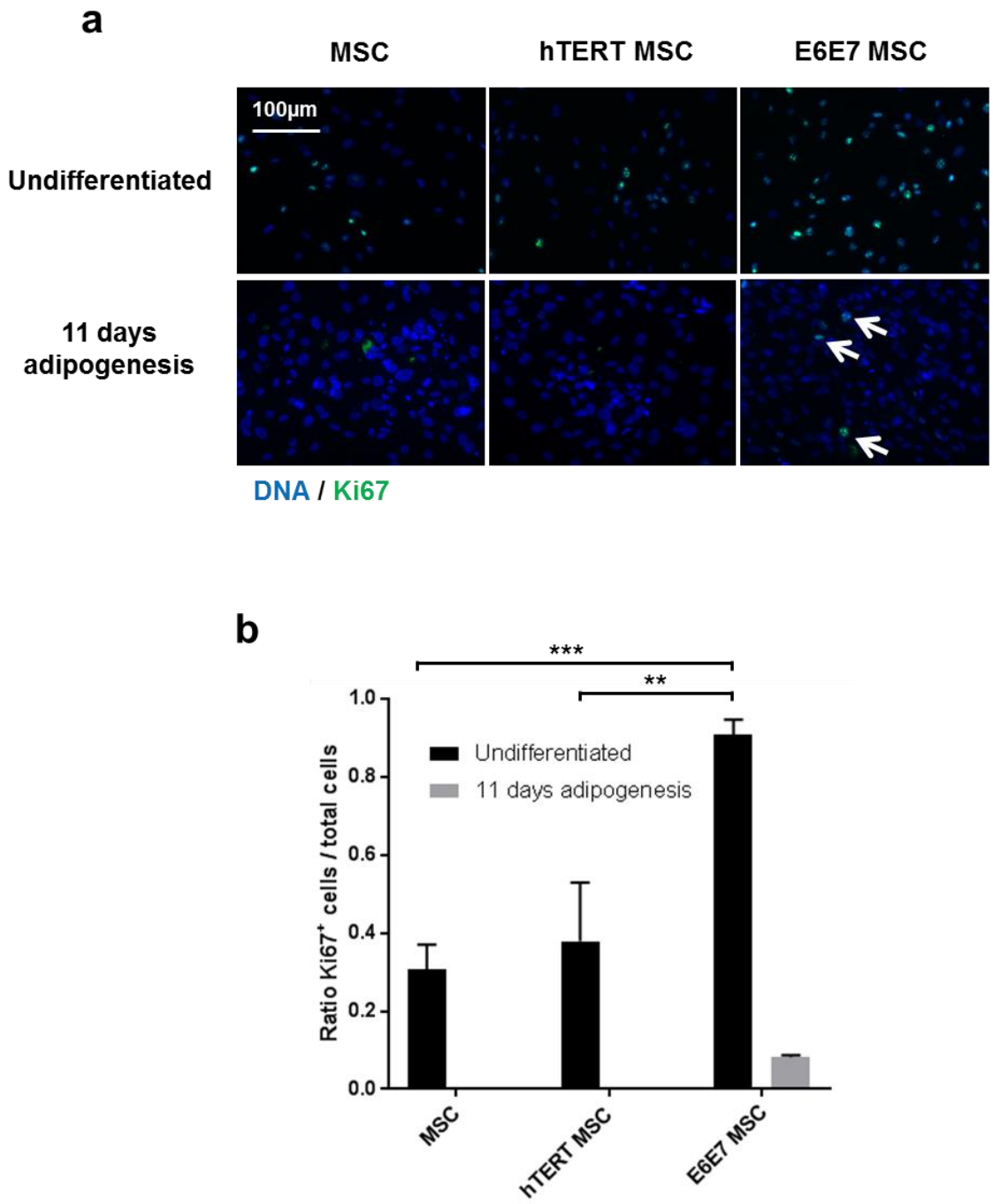


***Figure 6-6: E6E7-MSC proliferate at a higher rate than uninfected MSC***

(a) Immunocytochemistry of uninfected MSC, hTERT-MSC and E6E7-MSC for proliferation marker Ki67 (green). Nuclei were marked with Hoechst dye (blue). Cells were fixed at approximately 70% confluency for undifferentiated samples and 100% confluency after 11 days treatment with an adipogenic cocktail for adipogenesis samples. (b) A ratio of $Ki67^+$ nuclei to all cell nuclei was plotted for each cell type. Statistical significance was determined using an unpaired one-way ANOVA test (n=3, different passages). **p<0.01, ***p<0.001.

### 6.2.3 E6E7-MSCs successfully undergo adipogenesis in 2D

In order to replace 3T3-L1 cells with human cells in the ET-SIM system, it was necessary to ascertain whether immortalised MSCs could successfully undergo differentiation into adipocytes. Adipogenesis was first assessed in 2D on tissue culture plastic (TCP). MSCs were cultured to 100% confluency and differentiated for 11 days using an adipogenic cocktail. Lipids were then detected using the fat soluble dye Oil Red O which produces a red stain (Fig. 6.7a). Undifferentiated MSCs were used as a negative control as these cells do not produce detectable lipid droplets. Differentiated uninfected MSCs, which have previously been shown to differentiate into adipocytes and produce lipid droplets under these conditions, were used as a positive control (Jaiswal et al., 2000; Pittenger et al., 1999). These data showed that uninfected MSC, hTERT MSC and E6E7-MSC, failed to generate lipid droplets in their undifferentiated state (Fig. 6.7a). However, upon adipogenesis, both uninfected MSC and E6E7-MSC generated multiple lipid droplets in the cytoplasm of the majority of cells (Fig. 6.7a). hTERT MSC produced little to no lipid droplets as detected by Oil Red O staining (Fig. 6.7a).

For further confirmation of adipogenesis, cell lysates of the immortalised cell lines were compared by probing for the lipid vesicle membrane marker perilipin using SDS-PAGE and western blotting analysis (Fig. 6.7b). In agreement with Fig. 6.7a, perilipin was undetectable in cell lysates of undifferentiated uninfected MSC, hTERT MSC and E6E7-MSC (Fig. 6.7b) whereas differentiated uninfected MSC and E6E7-MSC both expressed perilipin (Fig. 6.7b). Perilipin was undetectable in hTERT MSC regardless of adipogenic induction, indicating that this cell line is unable to differentiate successfully (Fig. 6.7b). These data show that E6E7-MSC were able to undergo adipogenesis to produce lipid vesicles in a comparable level to that of uninfected MSC and thus immortalisation does not have an adverse effect on their ability to differentiate.

Upon adipogenesis *in vitro*, both 3T3-L1 cells and MSCs synthesise collagen IV and laminin, two major constituent ECM proteins of the basement membrane (Aratani and Kitagawa, 1988; Noro et al., 2013; Ojima et al., 2016; Sillat et al., 2012). As the basement membrane surrounds the epithelium of the mammary gland, expression of its constituent proteins adds further support for this *in vitro* model's ability to recapitulate mammary tissue. Therefore, as an additional metric of differentiation, subsequent experiments included the immunocytochemistry of MSCs in 2D probing for collagen IV and laminin (Fig. 6.8).

Fluorescence microscopy imaging revealed an increased deposition of laminin (Fig. 6.8a) and collagen IV (Fig. 6.8b) in differentiated uninfected MSC, hTERT-MSC and E6E7-MSC compared to undifferentiated cells. To quantify expression levels, fluorescence was measured using Image J and

displayed graphically as arbitrary units (Fig. 6.8c,d). This analysis confirmed that both uninfected MSC and E6E7-MSC expressed significantly higher levels of laminin (Fig. 6.8c) and collagen IV (Fig. 6.8d) upon adipogenic induction compared to undifferentiated samples. In contrast, although hTERT-MSC showed increased expression levels of laminin (Fig. 6.8c) and collagen IV (Fig. 6.8d) during adipogenic induction, this result was less dramatic and did not achieve statistical significance. This is not surprising given the relative inability of hTERT-MSCs to respond to adipogenic media.

Overall, these data showed that E6E7-MSCs were able to synthesise lipids, lipid vesicles, laminin and collagen IV upon adipogenic induction in 2D at comparable levels to that of uninfected MSCs. However, hTERT-MSCs exhibited a limited ability to differentiate and were inferior to uninfected MSCs. Thus, E6E7-MSCs were selected as the candidate cell line to replace 3T3-L1 cells in subsequent experiments.

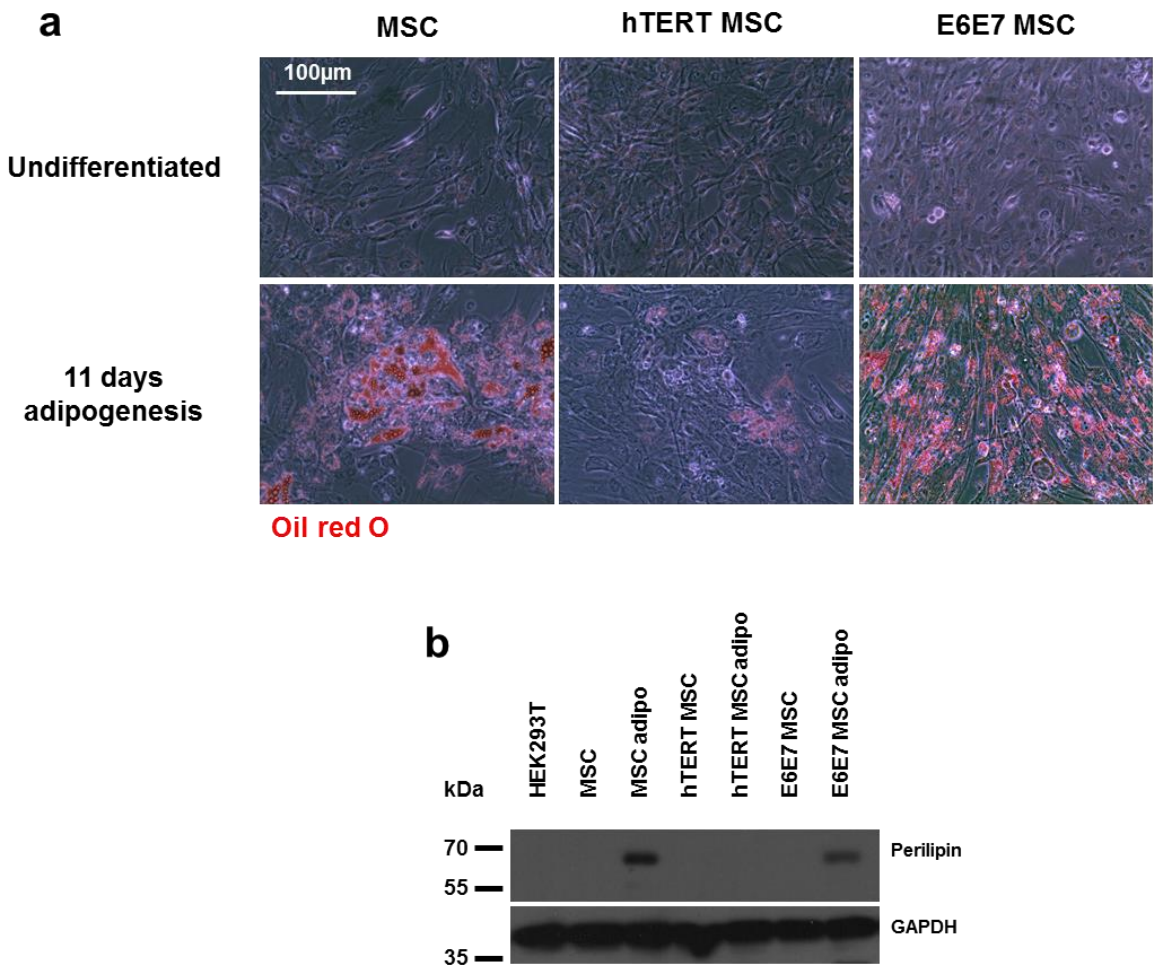


***Figure 6-7: E6E7-MSC successfully undergo adipogenesis in 2D***

(a) Oil red O staining for intracellular lipids (a marker of adipogenic differentiation) in uninfected MSC, hTERT-MSC and E6E7-MSC samples that were either undifferentiated or following 11 days adipogenic induction. (b) Western blotting of extracts of the cells in (a) for the lipid vesicle marker perilipin (62 kDa) (a marker of adipogenic differentiation). GAPDH (37 kDa) was used as a loading control. HEK293T cells were used as a negative control.

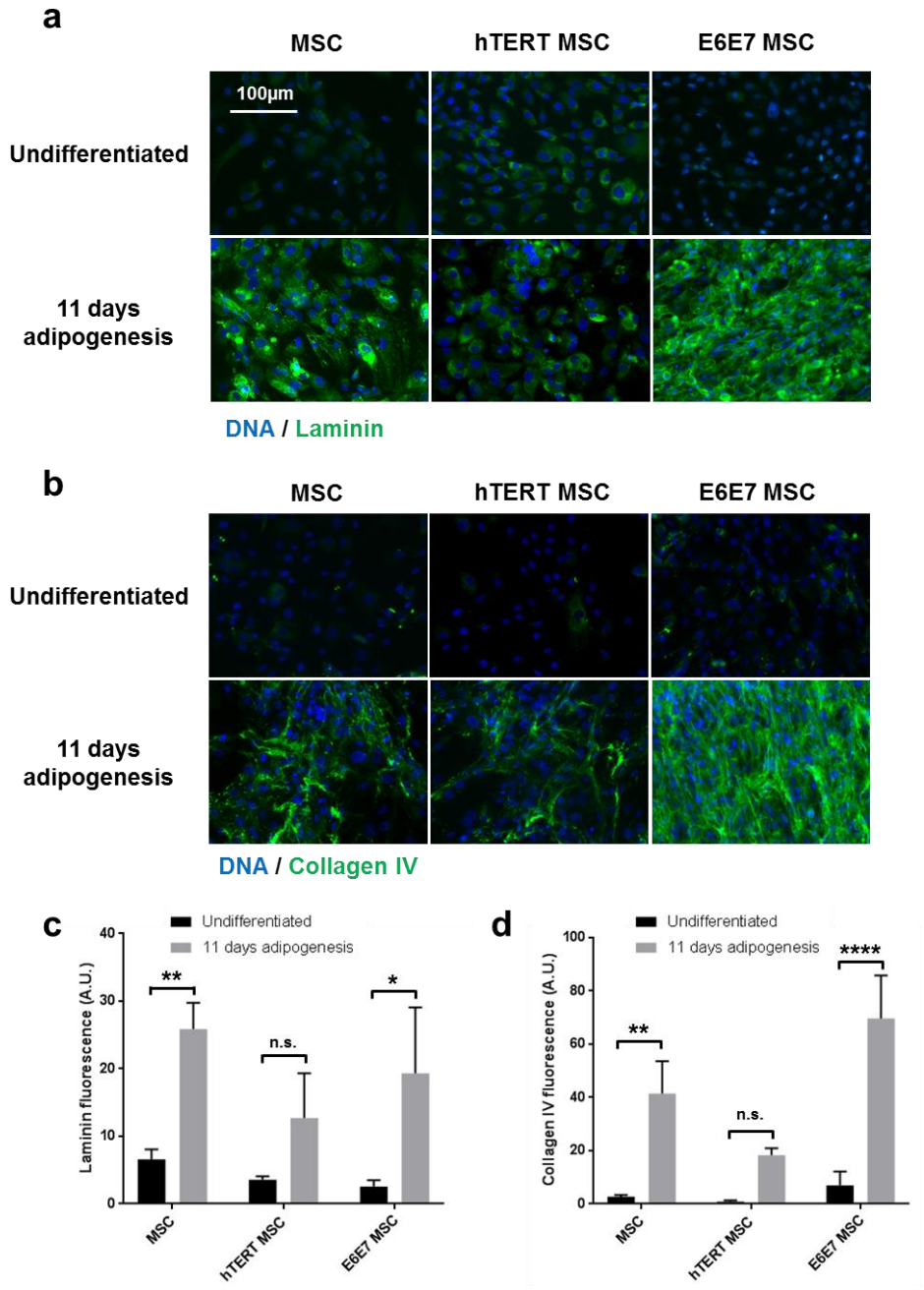


***Figure 6-8: E6E7-MSC successfully synthesize basement membrane proteins following adipogenesis***

Immunocytochemistry of either undifferentiated or differentiated for 11 days culture in adipogenic media of uninfected MSC, hTERT-MSC and E6E7-MSC for basement membrane proteins (a) laminin (green) and (b) collagen IV (green). Nuclei were marked with Hoechst dye (blue). Image J analysis of detectable fluorescence for (c) laminin and (d) collagen IV. A.U. stands for arbitrary units. One way ANOVA statistical test was used to compare samples (n=3, different passages). *p<0.05, **p<0.01, ****p<0.0001.

### 6.2.4 E6E7-MSC successfully undergo adipogenesis within anisotropic collagen scaffolds

Following successful adipogenesis of E6E7-MSC in 2D conditions, subsequent experiments investigated their adipogenic potential in 3D after seeding into anisotropic collagen scaffolds, with the aim of creating a humanised 3D model: hET-SIM. E6E7-MSC were cultured in anisotropic collagen scaffolds for 1 week to allow proliferating cells to fill the scaffold, and then exposed to an adipogenic cocktail for 11 days to induce differentiation to adipocytes. After fixation in PFA, whole mount immunofluorescence, confocal microscopy and 2pf microscopy techniques were employed to analyse adipogenic differentiation.

Whole scaffolds were stained with anti-perilipin to mark lipid vesicles and imaged using confocal microscopy (Fig. 6.9). Tile scans of bisected scaffolds (Fig. 6.9, dotted line) revealed differentiated E6E7-MSC covering large areas of the internal architecture. High magnification images revealed perilipin staining around lipid vesicles in the majority of cells (Fig. 6.9i,ii), indicating that E6E7-MSC had undergone differentiation into mature adipocytes.

Multiphoton techniques were employed to further confirm that perilipin positive vesicles contained lipids (Fig. 6.10). Two-photon fluorescence (2pf) was used to image both DAPI marked DNA (Fig. 6.10, grey) and anti-perilipin antibody staining (Fig. 6.10, green). Second harmonic generation (SHG) was used to image collagen I directly without the requirement for any dye or marker (Fig. 6.10, grey). Similarly, coherent anti-raman spectroscopy (CARS) was used to image lipids directly without markers or dye (Fig. 6.10, red). As DAPI and SHG have overlapping excitation/emission spectra they collected in the same image channel on the microscope and hence were represented with the same colour visually (Fig. 6.10, grey). These images show a proportion of E6E7-MSC attached to anisotropic collagen I pores that contained vesicles with a perilipin positive membrane and an interior CARS signal (Fig. 6.10). Smaller vesicles appeared to give a weaker CARS signal (Fig. 6.10). As the CARS input signal was specifically adjusted to the molecular vibration of lipids, the output signal (red) indicated that lipids were located within perilipin positive vesicles. These data show that E6E7-MSC successfully undergo adipogenic differentiation in anisotropic collagen scaffolds. CARS imaging was carried out with the assistance of Dr. Lorraine Berry (Cambridge Research Institute, University of Cambridge).

As E6E7-MSC express the basement membrane proteins laminin and collagen IV upon adipogenic differentiation in 2D cultures, it was investigated if this also occurred in anisotropic collagen scaffolds by whole mount immunofluorescence. Laminin expression was observed in all cells with some displaying deposition in a surrounding halo (Fig. 6.11). 3D confocal imaging revealed that cells

found at different z-depths were able to synthesise laminin generating a 3D lattice (Fig. 6.11, pseudo-coloured spectrum image). Likewise, 3D confocal imaging further revealed that collagen IV deposition was also observed in all cells (Fig. 6.12, blue and green image) and at different z-depths (Fig. 6.12, pseudo-coloured spectrum image). Interestingly, collagen IV deposition appeared to be directional, aligning in the direction of anisotropic collagen I pores (Fig. 6.12).

Taken together, these data demonstrate that E6E7-MSC can successfully differentiate into mature adipocytes within anisotropic collagen I scaffolds. E6E7-MSC distributed throughout the scaffold synthesized lipid filled vesicles and basement membrane proteins upon adipogenic differentiation. Thus it can be concluded that E6E7-MSC are a suitable candidate to replace 3T3-L1 cells in order to synthesize a human synthetic fat pad in the hET-SIM culture system.

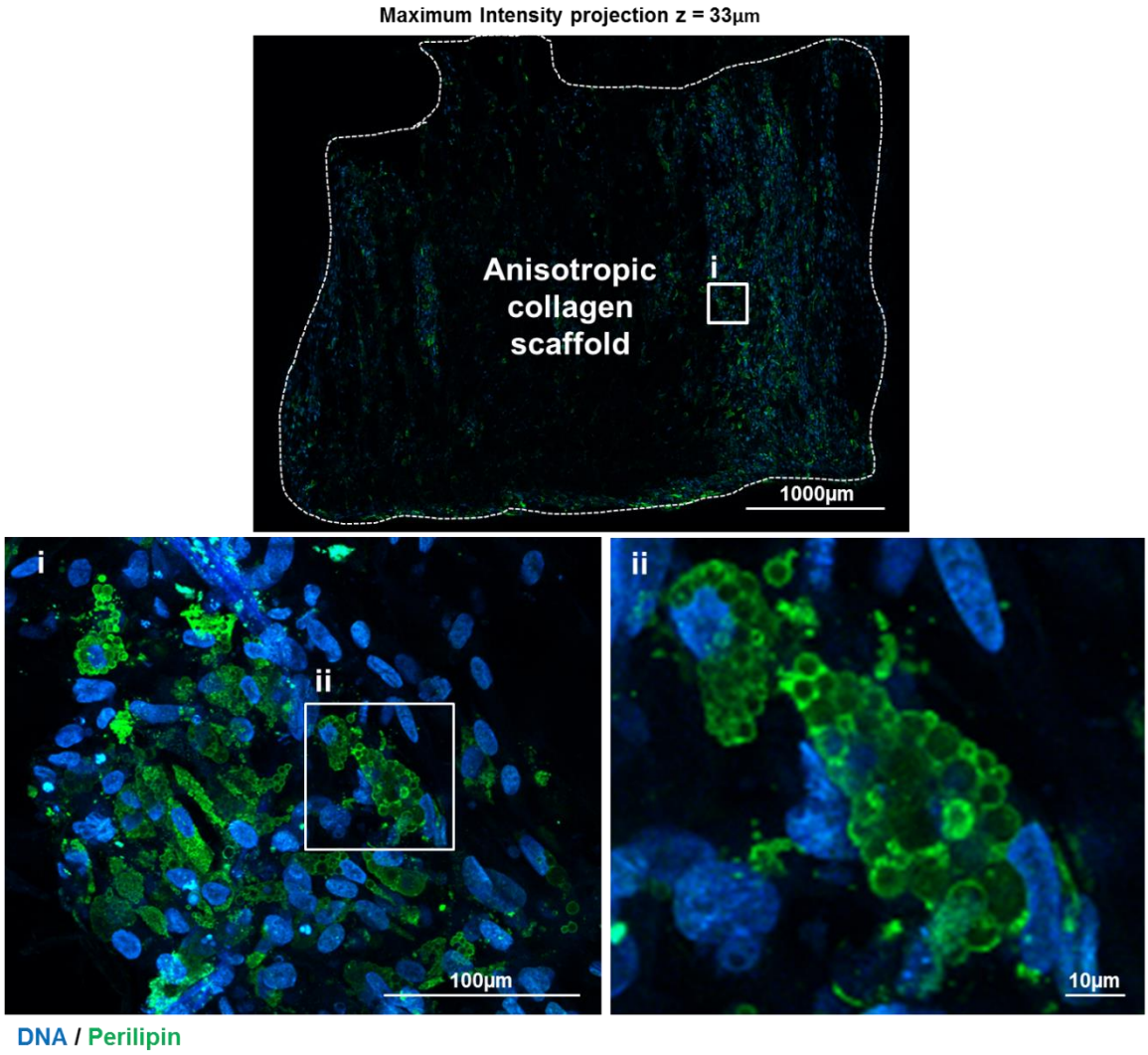


***Figure 6-9: E6E7-MSC successfully undergo adipogenesis in anisotropic collagen scaffolds***

Anisotropic collagen scaffolds seeded with E6E7-MSC were cultured for 7 days and then differentiated with adipogenic media for 11 days. Scaffolds were fixed and stained for the lipid vesicle marker perilipin as a marker of adipogenic differentiation with anti-perilipin antibodies (green). DNA was marked with DAPI (blue). (a) Tile scan z-stack of one face of a bisected scaffold. (i) Zoomed in image of (a). (ii) Digitally magnified image of (i). Images were taken using a confocal microscope.

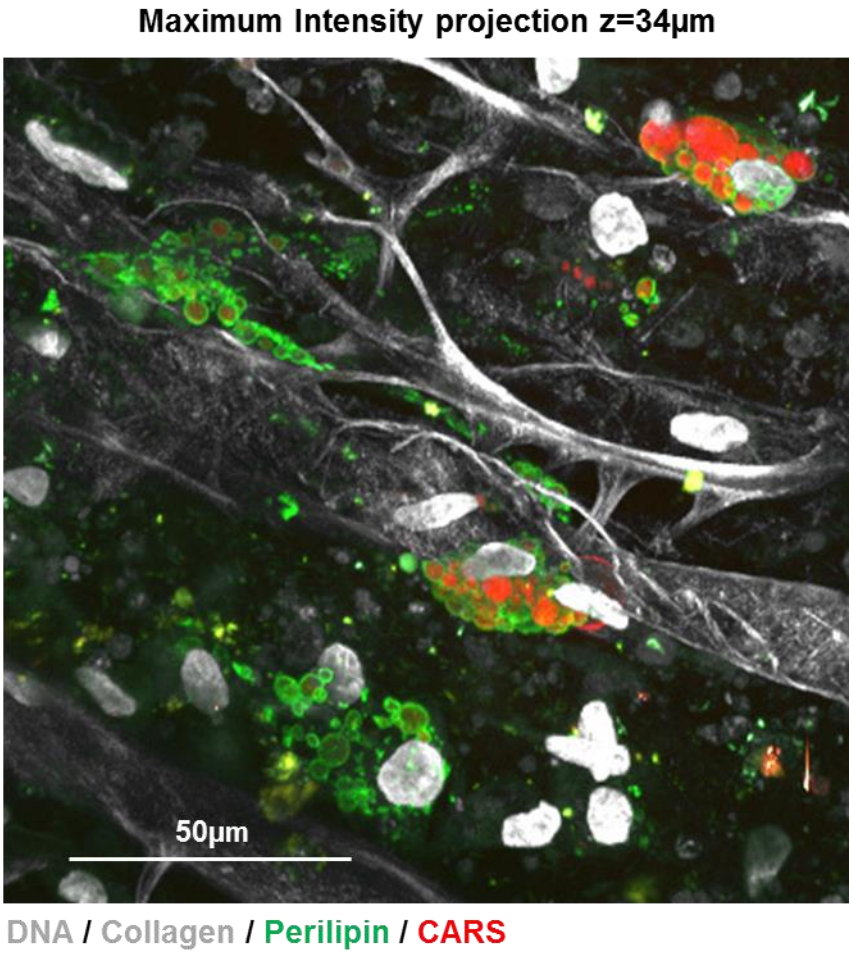


***Figure 6-10: Lipids generated by E6E7-MSC in anisotropic collagen scaffolds imaged using coherent anti-raman spectroscopy (CARS)***

Anisotropic collagen scaffolds seeded with E6E7-MSC were cultured for 7 days then differentiated with adipogenic media for 11 days. Scaffolds were fixed and stained for the lipid vesicle marker perilipin (green). DNA was marked with DAPI (grey, round). Fluorescent markers were imaged using 2pf microscopy. Collagen was imaged directly using SHG microscopy (grey, fibres). Lipids were imaged directly using coherent anti-raman spectroscopy (CARS) microscopy. Image is shown as a maximum intensity projection of a 34 µm z-stack.

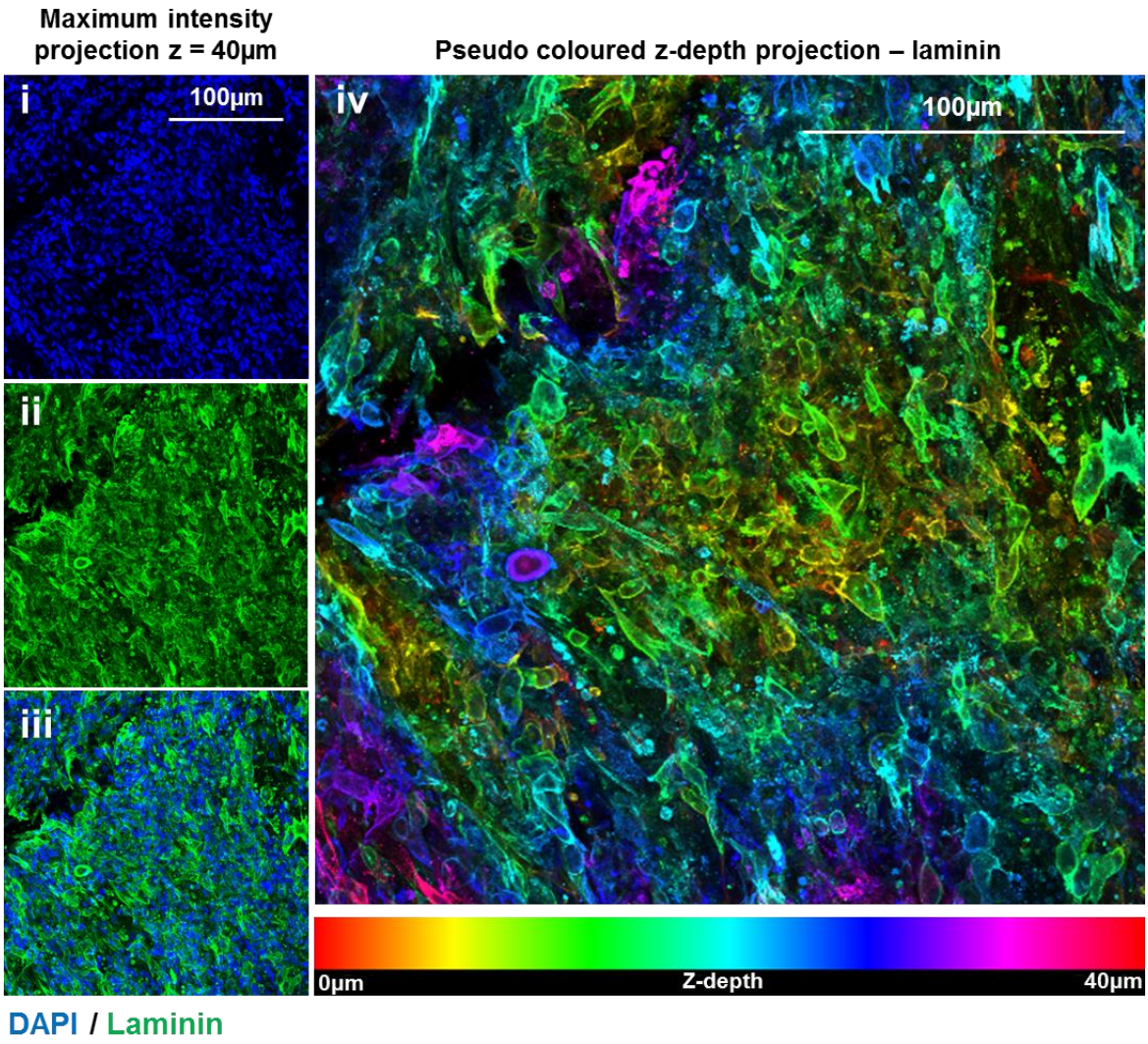


***Figure 6-11: E6E7-MSC successfully synthesize laminin upon adipogenesis in anisotropic collagen scaffolds***

Anisotropic collagen scaffolds seeded with E6E7-MSC were cultured for 7 days then differentiated for 11 days in adipogenic media. Scaffolds were fixed and whole mount immunostained for the basement membrane protein laminin (green). DNA was marked with DAPI (blue). Images were taken using a confocal microscope. Images are shown as maximum intensity projections of the individual channels (i) DAPI, (ii) laminin and (iii) merged or as a (iv) z-depth colour coded image of the laminin channel.

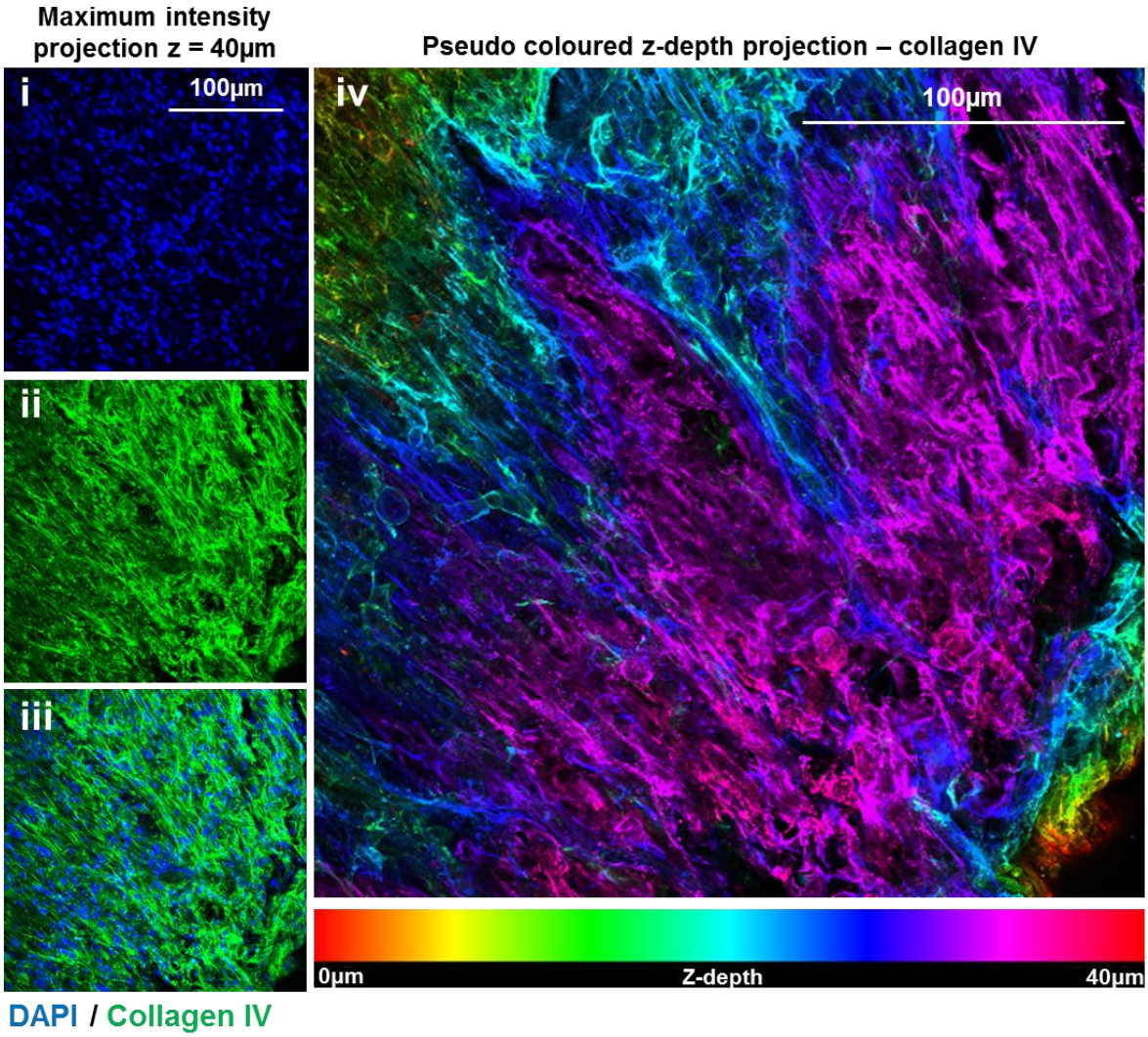


***Figure 6-12: E6E7-MSC successfully synthesize collagen IV upon adipogenesis in anisotropic collagen scaffolds***

Anisotropic collagen scaffolds seeded with E6E7-MSC were cultured for 7 days then differentiated for 11 days in adipogenic media. Scaffolds were fixed and stained for the basement membrane protein collagen IV (green). DNA was marked with DAPI (blue). Images were taken using a confocal microscope. Images are shown as maximum intensity projections of the individual channels (i) DAPI, (ii) laminin and (iii) merged or as a (iv) z-depth colour coded image of the collagen IV channel.

### 6.2.5 E6E7-MSCs support the migration of MDA-MB-231 cells

Having established a humanised 'fat pad', subsequent experiments aimed to evaluate whether hET-SIM could support the migration of human breast cancer cells. For this purpose, the human breast cancer cell line MDA-MB-231 was selected because of its highly migratory phenotype.

MDA-MB-231 cells were labelled with tdTomato using lentiviral tagging methods to distinguish them from E6E7-MSC in the hET-SIM system. The tdTomato fluorophore was selected because it has very high fluorescence intensity compared to other fluorophores when imaged with 2pf (Drobizhev et al., 2011). FACS analysis confirmed tdTomato expression in transduced MDA-MB-231 cells compared to negative controls (Fig. 6.13a). Cells with the highest levels of tdTomato expression (top 34.4%) were then collected via FACS (Fig. 6.13a) and placed in culture (Fig. 6.13b). Fluorescence microscopy demonstrated that transduced cells expressed sufficient levels of tdTomato to allow their visualisation and discrimination from uninfected cells, during microscopy (Fig. 6.13b).

In chapter 4, migration of MDA-MB-231 cells to all depths of anisotropic scaffolds was observed after 10 days culture in the presence of a serum gradient (chapter 4, Fig. 4.3, Fig. 4.4a). In the following experiments, anisotropic scaffolds invested with differentiated E6E7-MSC (hET-SIM) alongside empty scaffold controls were placed into Boyden chambers with no serum gradient. The absence of a serum gradient was intended to prevent migration to the extremities of the scaffolds and reduce the likelihood of cells exiting the scaffold from the opposite edge to which they were seeded. This would permit differences between hET-SIM and empty scaffolds to be more readily identified and reduce the possibility of missing data points. hET-SIM and empty scaffolds were seeded with tdTomato$^+$ MDA-MB-231 cells and cultured for 7 days. Samples were then fixed, bisected and imaged using multiphoton microscopy techniques (Fig. 6.14).

Collagen I structures within anisotropic collagen scaffolds were imaged directly using SHG (Fig. 6.14, blue). As 2pf signals from DAPI and SHG overlapped excitation/emission spectra in previous experiments, the green fluorescent DNA dye SYTO16 (Fig. 6.14, green) was utilised to more accurately distinguish cell nuclei from collagen. E6E7-MSC were identified by their single positive green nuclei from tdTomato$^+$ MDA-MB-231 cells with double positive green/red nuclei and a red cytoplasm (Fig. 6.14b). After 7 days of culture, the majority of tdTomato$^+$ MDA-MB-231 cells in empty scaffolds were located within close proximity of the funnel in which they were seeded (Fig. 6.14a). E6E7-MSC in hET-SIM were successfully seeded throughout the scaffold and were observed at all depths (Fig. 6.14b). tdTomato$^+$ MDA-MB-231 in empty scaffolds were restricted to an area near the seeding funnel and on the outer surface of the scaffold (Fig. 6.14a). A few migratory tdTomato$^+$ MDA-MB-231 cells in empty scaffolds were observed at considerable depths within the centre of the

scaffold (Fig. 6.14a, white box). In contrast, tdTomato$^{+}$ MDA-MB-231 in hET-SIM were observed at all depths of the scaffold and were not confined to the funnel region (Fig. 6.14b, white box). This showed that hET-SIM enhanced the migratory phenotype of MDA-MB-231 cells when compared to empty scaffolds.

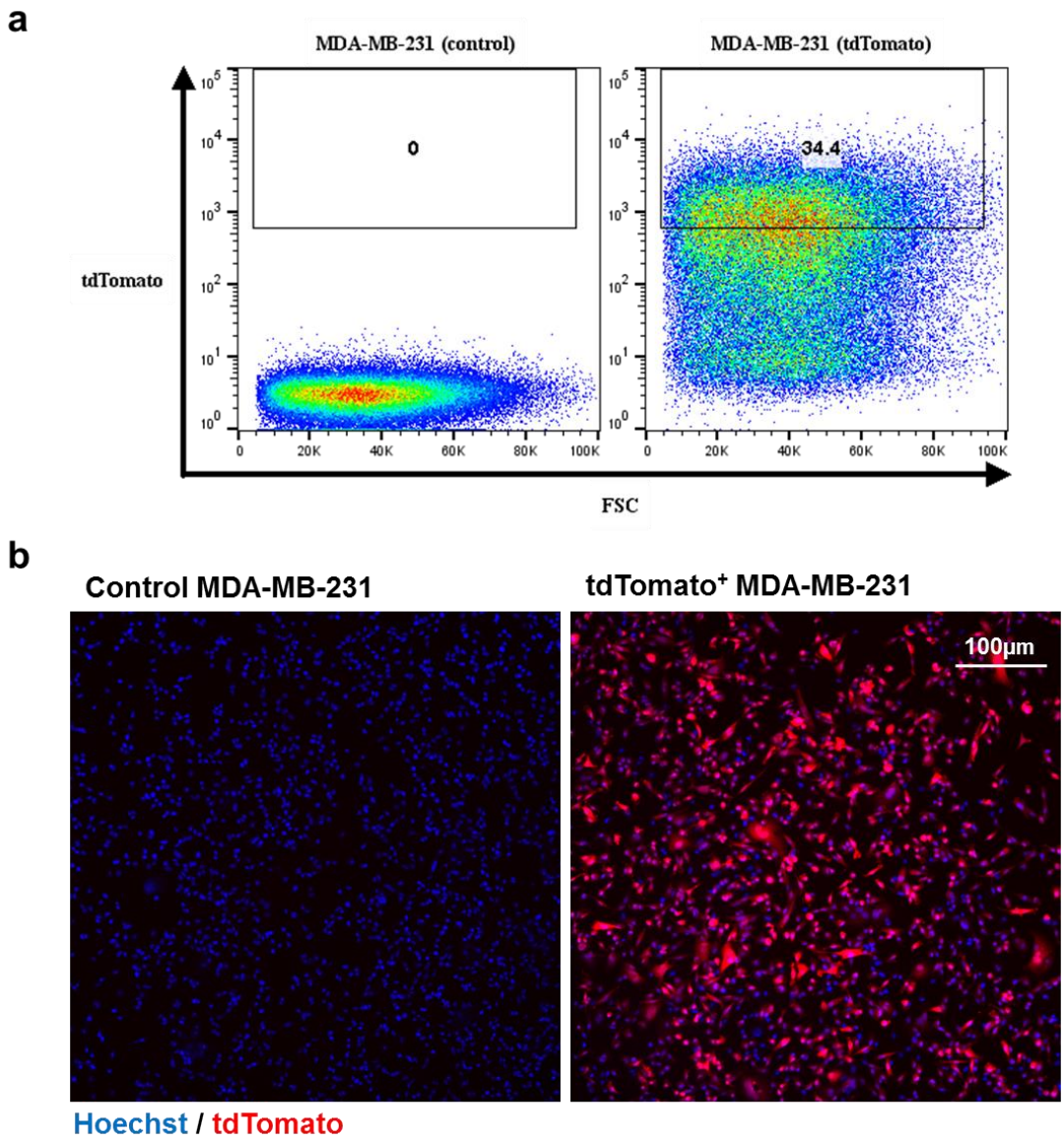


***Figure 6-13: Lentiviral transduction of MDA-MB-231 cells with tdTomato expression construct and FACS enrichment of tdTomato-expressing cells***

MDA-MB-231 breast cancer cells were lentivirally transduced to express the tdTomato fluorescent protein. This virus was genome edited by Dr. Michael D'Angelo (Watson lab, Cambridge). (a) Transduced MDA-MB-231 cells were FACS sorted based on their tdTomato fluorescence. Uninfected MDA-MB-231 cells were used as a negative control. (b) Immunofluorescence of tdTomato MDA-MB-231 cells based on tdTomato fluorescence (red). Uninfected MDA-MB-231 cells were used as a negative control. DNA was marked using Hoechst dye (blue).

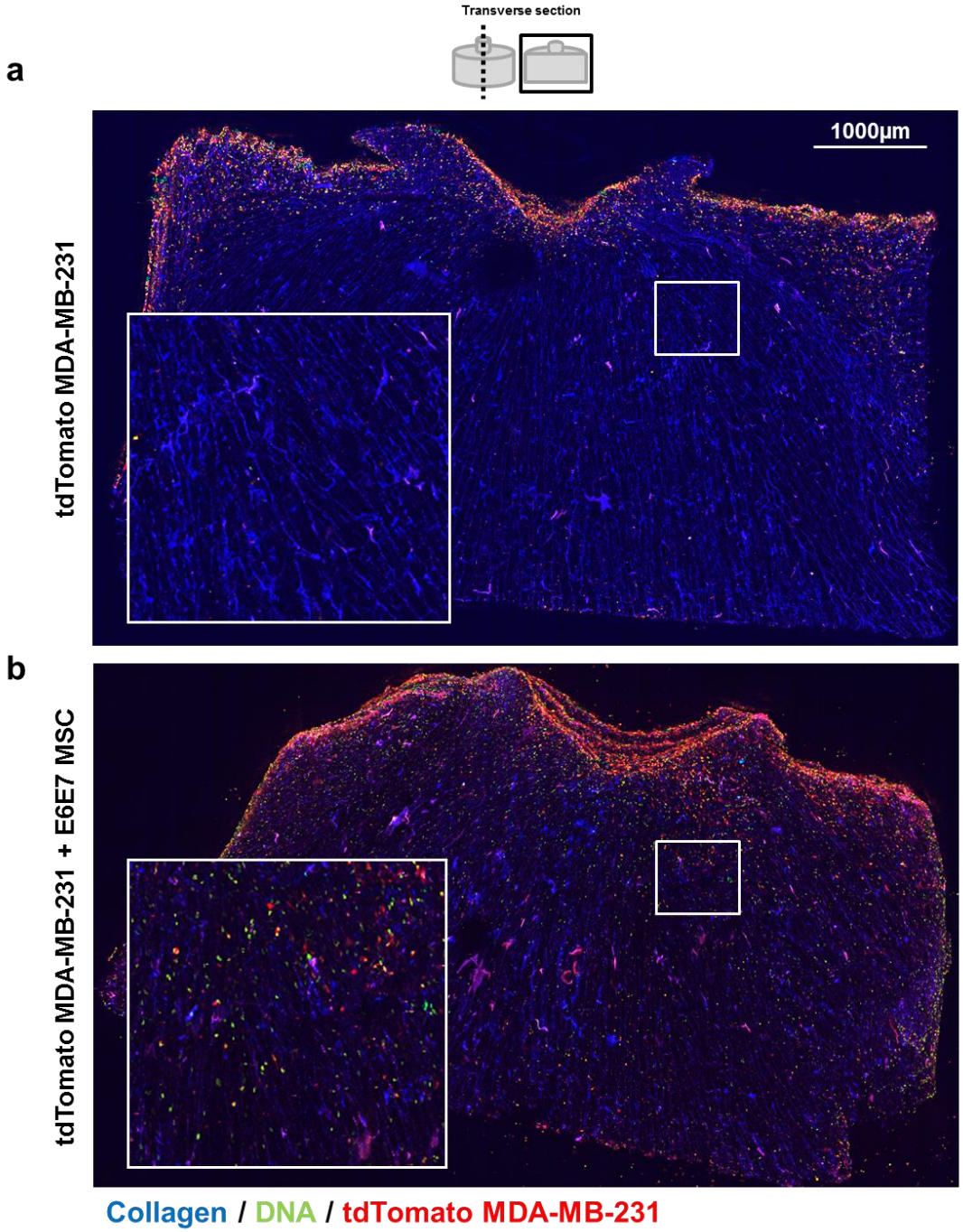


***Figure 6-14: MDA-MB-231 cells co-cultured with E6E7-MSC in anisotropic collagen scaffolds***

Scaffolds were seeded (a) without or (b) with E6E7-MSC throughout the scaffold, cultured for 7 days then differentiated for 11 days. Both scaffold types were then seeded with tdTomato MDA-MB-231 cells (red) into the scaffold funnel and cultured for 7 days. Scaffolds were then fixed and bisected and DNA was marked using SYTO16 (green). Collagen was imaged directly using SHG (blue). SYTO16 and tdTomato were imaged using 2pf.

## 6.3 Discussion

### 6.3.1 The Tumour Associated Collagen-3 (TACS-3) phenotype in a human tumour biopsy

To determine whether TACS-3 was present in a human breast tumour biopsy, a histological stain called Masson's Trichrome was used to visualise collagen structures (Fig. 6.1). Collagen fibres aligned perpendicular to the tumour edge and protruding into the surrounding stroma were first identified and later confirmed by a trained medical pathologist for validation. This meant that identifying the phenotype was a relatively simple task as it was recognised by both untrained and trained pathologists. Accordingly, it could be plausible to hypothesise that, due to the association of TACS-3 with poor prognosis and the relative ease in identifying the phenotype histologically, the identification of TACS should become part of routine diagnostics in breast cancer clinics.

CUBIC, in conjunction with immunostaining and multiphoton imaging, were used to identify and visualise TACS-3 in greater detail. By avoiding paraffin embedding of tissue samples and through direct imaging of collagen with SHG, the structural integrity of the tissue was uncompromised. Human epithelial cells within the tumour bulk were identified by immunostaining (Fig. 6.4), supporting the potential future study of human tumour cell migration following the seeding of human biopsies into anisotropic collagen scaffold cultures.

### 6.3.2 The human Engineered Tumour-Stroma Interaction Model (hET-SIM)

Chapter 6 described the isolation of human mesenchymal stem cells (MSC) from the adipose tissue of a reduction mammoplasty and their immortalisation via retroviral transduction of both the E6 and E7 genes, simultaneously (Section 6.2.2). E6E7-MSC exhibited an ability to escape senescence and an increased proliferative capacity (Fig. 6.5, Fig. 6.6). Retroviral transduction of the hTERT gene into MSCs however, did not result in their immortalisation as cells were unable to escape senescence and did not exhibit an increased proliferative capacity (Fig. 6.5, Fig. 6.6). One explanation for the success of the E6E7 over hTERT immortalisation, is that the combination of both E6 and E7 gene products targeted multiple effectors of the cell cycle, increasing the likelihood of immortalisation. This method of transducing multiple genes either simultaneously or sequentially to increase immortalisation efficiency has been shown in other cell lines (Kyo et al., 2003; Lundberg et al., 2002; Zhu et al., 1999). In contrast, hTERT targeted only the maintenance of the telomeres and therefore did not meet the threshold required to immortalise the MSCs in this particular case. An alternative further explanation may be that DNA damage had already occurred in the majority of cells and

therefore p53 activity in these cells caused a senescent phenotype that increased hTERT expression alone could not overcome.

The rationale for inclusion of the hTERT retroviral plasmid in immortalisation experiments was two-fold. Firstly, to increase the number of separate immortalising agents and subsequently increase the likelihood of generating an immortalised cell line. Secondly, viral insertion of genes involved in the cell cycle into cultured cells can result in oncogenic transformation of the target cell line (Black and Rowe, 1963; Bocchetta et al., 2000; Elenbaas et al., 2001). hTERT transduction however, has been shown to be less likely to induce oncogenic transformation and more likely to produce 'normal' immortalised cell lines with less phenotypic changes (Jiang et al., 1999; Morales et al., 1999; Toouli et al., 2002).

When trying to recapitulate a stromal component of the human breast *in vitro*, as in hET-SIM, it is important to select a cell line that closely mimics the phenotype of native stromal cells. Hence, using a non-tumorigenic immortalised cell line is preferred over an oncogenic line. A limitation of E6E7 immortalisation is the risk of oncogenic transformation. For example, if the differentiated E6E7-MSC cell line more closely resembled a tumour of the adipose tissue such as a liposarcoma, it no longer exhibits the phenotype of normal adipose tissue. Following adipogenesis, approximately 7% of E6E7-MSC did not undergo terminal differentiation and continued to proliferate (Fig. 6.6). Although the majority of cells did undergo the correct replicative senescence, this sub-population displayed an unexpected phenotype. Therefore, future analysis of the tumorigenic potential of E6E7-MSC *in vitro* and *in vivo* in an appropriate mouse model may be required to confirm the cell line has not undergone oncogenic transformation during immortalisation.

During differentiation experiments E6E7-MSC exhibited an adipogenic potential comparable to uninfected MSC, whereas hTERT exhibited impaired adipogenesis (Fig. 6.7). This was not anticipated as it has been shown previously that adipose-derived MSC can be immortalised with hTERT without adverse effects to their adipogenic potential (Wolbank et al., 2009). An explanation for this phenotype may have been that hTERT MSC incurred a mutation during/before the immortalisation process and/or during sub culturing, impairing their adipogenic capacity.

E6E7-MSC synthesised the basement membrane proteins laminin and collagen IV upon adipogenic differentiation, a process also observed in uninfected MSC and the murine preadipocyte 3T3-L1 cell line (Aratani and Kitagawa, 1988; Noro et al., 2013; Ojima et al., 2016; Sillat et al., 2012). The inclusion of these proteins into the model poses a number of advantages, similar to the advantages in the ET-SIM model, as outlined in Section 5.3.1.

Following their adipogenic induction in 2D, E6E7-MSC were differentiated in anisotropic collagen scaffolds to synthesise human ET-SIM (hET-SIM) (Fig. 6.9-6.12). Although 2D adipogenesis was successful, it could not be presumed that scaffold culture would produce similar results. This is because MSC differentiation potential is affected by factors such as 3D culture, ECM substrate and surface topography (Jung et al., 2016; Santiago et al., 2009; Zhang and Kilian, 2013). Synthesis of lipids, laminin and collagen IV are all indicative of complete adipogenesis of E6E7-MSC and was a milestone in the development of hET-SIM (Fig. 6.9-6.12).

To investigate human breast cancer migration in hET-SIM, the highly aggressive MDA-MB-231 cell line was fluorescently tagged, seeded into scaffold funnels and cultured (Fig. 6.13, Fig. 6.14). Multiphoton microscopy was used to distinguish MDA-MB-231 cells from E6E7 MSC and visualise the internal collagen structure of the scaffolds. MDA-MB-231 cells migrated further in hET-SIM than in empty scaffolds (Fig. 6.14). Quantification of migration distances using methods described in Chapter 4, accompanied with therapeutic testing as described in Chapter 5, would elevate the significance of hET-SIM as an assay and exhibit its versatility.

### 6.3.3 Limitations of hET-SIM

The human breast and mouse mammary gland differ in their respective anatomies. The breast comprises epithelial tissue separated from adipose tissue by a distinct portion of interstitial collagenous stroma (Haagensen, 1971). In contrast, the mouse mammary gland comprises ducts and alveoli individually surrounded by a relatively small portion of interstitial collagenous stroma all located within an adipocyte-rich fat pad and therefore is closely associated with adipocytes (Campbell et al., 2014a). A limitation of hET-SIM is that it consisted of adipocytes seeded throughout the ECM, similar to the mouse fat pad and was not distinct from ET-SIM in its stromal organisation. To improve hET-SIM, a method of seeding E6E7-MSC on one edge of the scaffold could be developed to synthesise a distinct region of collagen ECM separating adipose tissue from any cultured epithelial tissue. Nonetheless, in the case of a human breast tumour, it is entirely possible that the tumour would have expanded into the region of adipose tissue. Hence, the merit of altering the seeding methodology for the investigation of human breast cancer migration would have to be assessed and could be decided on a case-by-case basis in future studies.

### 6.3.4 Conclusion

It is envisaged that future humanisation of hET-SIM would involve combining human tumour culture strategies, similar to murine tumour cultures described in ET-SIM. Biopsies could be initially screened for their tumour associated collagen signature (TACS) to determine whether they should be seeded into an isotropic or anisotropic version of hET-SIM. Screening of a panel of therapeutics

could then inform oncologists of the most effective treatment, thus providing personalised medicine to the patient.

# 7 Discussion

## 7.1 Overall context of the thesis

Traditional cell culture protocols originally employed techniques for the propagation of cells as a 2D monolayer on tissue culture plastic (TCP). This provided scientists with a setting to study cell biology *in vitro* and has permitted many seminal works to be performed (Carrel and Burrows, 1911; Russell et al., 1977; Scherer et al., 1953). These *in vitro* systems are more malleable than their *in vivo* counterparts; enabling more direct control over environmental factors by tuning culture conditions appropriate for the context of the study. Importantly, however, 2D cell culture is often limited by a significant caveat; cells are no longer within their native setting and their *in vitro* phenotype may not reflect the *in vivo* reality. To increase the relevance of cell culture and thus improve its translation to human biology, studies developed 3D culture techniques (Kleinman et al., 1982; Williams et al., 1978). By propagating cells in a 3D matrix comprising ECM proteins, these studies sought to provide a more physiologically relevant model. Likewise, this thesis used collagen scaffolds throughout, with the intention of mimicking the mammary gland ECM and stroma using an *in vitro* model.

## 7.2 Stem cell culture assay

With an ever evolving 3D tissue culture field, new protocols to improve mammary organoid culture conditions are continuously being developed (Carter et al., 2017; Jamieson et al., 2017; Jardé et al., 2016; Nguyen-Ngoc et al., 2015). Chapter 3 aimed to contribute to this area of research by culturing FACS sorted mammary stem cells in adipocyte-invested collagen scaffolds. Although mimicking the mammary stem cell niche was not achieved during organoid cultures, limitations of cross-linked collagen scaffolds as a model system and possible areas for improvement were identified.

## 7.3 Collagen scaffolds

It is estimated that over 1.5 million people are diagnosed with breast cancer per year worldwide with over half a million deaths as a result (Ghoncheh et al., 2016). Identifying the mechanisms that permit the spread of breast cancer cells to essential organs that is ultimately responsible for the lethality of the disease, is therefore of profound importance. It has been shown that breast cancer cells move across surfaces and within the ECM by the process of migration which is can be enhanced when travelling on directional or anisotropic fibres (Ray et al., 2017a). In breast cancer, the tumour-associated collagen signature-3 (TACS-3) phenotype, described as anisotropic collagen fibres orientated perpendicular to edge of breast tumours, enhances the migration of tumour cells and is

associated with a poor patient prognosis (Conklin et al., 2011; Provenzano et al., 2006). Models have been developed to investigate this phenomenon *in vitro*, by aligning collagen gels in one axis direction (Provenzano et al., 2008a; Ray et al., 2017a, 2017b; Riching et al., 2014). These collagen gels are subject to unpredictable swelling and cellular remodelling. In Chapter 4, cross-linked anisotropic collagen scaffolds were developed with a funnel for the seeding of cells in a controlled manner. Rather than aligning in one axis direction, the scaffolds exhibited a radial distribution of anisotropic collagen and therefore mimicked the TACS-3 phenotype from the seeding funnel in all directions, unlike current models. Furthermore, collagen scaffolds are not subject to swelling or dramatic cellular remodelling and thus display advantages over current models when considering assay reproducibility. It is envisaged that this method of scaffold synthesis, with its versatility in regards to mould shape and design, will become a common laboratory investigative tool for the study of breast cancer.

## 7.4 Human breast cancer cell line migration assay

During migration assay experiments, isotropic and anisotropic collagen scaffolds facilitated the ability to discern the inherent migratory potentials of three different breast cancer cell lines. Interestingly, it was demonstrated that anisotropy provided enhanced migration of MDA-MB-231 human breast cancer cells, highlighting the affect that stromal ECM architecture can have on the spread of cancer. Furthermore, anisotropy did not affect the migration of the MDA-MB-468 or MCF7 cell lines suggesting that anisotropic stromal ECM only enhances migration of certain subtypes of breast tumour cells. By extending studies to a larger panel of breast cancer cell lines, and possibly other cancer cells that may encounter anisotropic collagen surfaces, future studies propose to extend the assay to a wider range of cancer subtypes.

The triple negative breast cancer (TNBC) cell line, MDA-MB-468, showed minimal migration in both isotropic and anisotropic scaffolds. As this may have been a result of their mode of migration and migratory potential, subsequent experiments sought to further transform MDA-MB-468 cells by inducing an epithelial-to-mesenchymal transition (EMT) and investigating its effects on migration. This has been previously studied using Boyden chamber assays but not within the context of 3D ECM (Davis et al., 2013). Data from migration assays demonstrated that EMT enhanced migration of MDA-MB-468 cells in the model, further validating its ability to distinguish migratory phenotypes in a physiologically relevant 3D setting.

In summary, a 3D *in vitro* assay of cancer cell migration has been developed that may be amenable to high-throughput analyses with increased reproducibility. This could advance current *in vitro* methods for assessing cancer cell invasiveness and migratory status. Anisotropic collagen scaffolds were readily able to support the full depth migration of the invasive breast cancer cell line MDA-MB-231 over a 10 day time period. Additionally, the model successfully differentiated MDA-MB-468 cells on the basis of an induced invasive phenotype by exposure to EGF. This demonstrated the utility for anisotropic structures to distinguish these phenotypes *in vitro* by tracking their effects on migration. Furthermore, it is proposed that this model could be developed further in the future for testing of cancer therapeutics, drug efficacy and toxicity in this more relevant *in vitro* setting.

## 7.5 Engineered Tumour-Stroma Interaction Model (ET-SIM) tumour culture and therapeutic testing assay

Breast cancer is a highly heterogeneous disease and it is becoming increasingly apparent from genome wide sequencing of breast tumours that these differ dramatically in terms of driver and passenger mutations (Nik-Zainal et al., 2016). Furthermore, the expansion of individual clones of tumour cells results in tumours that are sustained by a number of different stem-like cells (Lee et al., 2017; Lim et al., 2010; Ponti et al., 2005; Wang et al., 2016). This complex tumour landscape presents major challenges for the breast oncologist and there is an urgent need for current pathological techniques to be complemented by new approaches that provide whole tumour analysis. Furthermore, effective treatments for lethal subtypes, such as triple negative breast cancers (TNBC), have yet to be developed and despite the efficacy of anti-oestrogen therapies, a considerable proportion of $ER^+$ tumours become resistant to therapy resulting in recurrence of disease. Thus, there is a pressing need for new therapeutic drugs and a screening system that mimics the *in vivo* tumour environment. With these aims in mind, Chapter 5 developed an *in vitro* system that can be utilised to assess the invasive/metastatic capacity of breast cancer biopsy material and the response of invasive cells to drug treatment. This system, that has been named ET-SIM, could be scaled up to provide a medium throughput drug screening approach.

Current cell culture models are limited in their ability to recapitulate the cellular and ECM complexity of the tumour microenvironment. Thus, there is much interest in building 3D culture systems that incorporate stromal components that accurately reflect the *in vivo* environment. In Chapter 5 an organotypic *in vitro* assay has been pioneered that recapitulates essential aspects of the *in vivo* mammary tumour microenvironment. The ET-SIM system improves upon the human breast cancer

cell migration assay in Chapter 4 by combining anisotropic 3D spatial ECM architecture with an adipocyte rich environment. Furthermore, it was shown that ET-SIM supports culture of tumour fragments, permits visualization and quantitative analysis of distinct modes of tumour cell migration, reveals tumour heterogeneity, and can be used to test tumour cell responsiveness to drug treatments. It is suggested that these features demonstrate potential utility as a drug discovery platform.

In summary, a new enhanced organotypic mammary tumour culture system has been established. It has been demonstrated that this system provides both qualitative and quantitative insight into mammary tumour cell migration, the complex bivalent effects of adipocytes on this process and the effects of anti-metastatic drugs. It is envisaged that humanisation of this model will pave the way for improved personalised medicine strategies for patients with breast cancer. Patient derived tumour biopsy fragments containing both stromal and tumours cells, derived from different geographical regions and cultured in our ET-SIM system, would provide oncologists with another tool to use in concert with standard strategies to provide personalised medicine for breast cancers. Furthermore, future modifications of the ET-SIM system could include additional or alternative stromal cells to mimic the stromal environment of other organs. Inclusion of other ECM proteins during scaffold synthesis would also permit the tailoring of ET-SIM to recapitulate the ECM of other stromal environments. Development of ET-SIM could therefore potentially allow the investigation of a range of cancer types and their surrounding microenvironment.

## 7.6 The TACS-3 phenotype in a human breast cancer biopsy

The work described in Chapter 6 demonstrates that human breast tumour biopsies can be optically cleared, whole mount immunostained and imaged using multi-photon microscopy. Using these methodologies, the TACS-3 phenotype described by Provenzano et al. was confirmed and observed microscopically in much greater detail in a human $ER^+$ IDC biopsy (Provenzano et al. 2006). These data further support the relevance and importance of modelling and investigating the TACS-3 phenotype using *in vitro* systems.

## 7.7 Human Engineered Tumour-Stroma Interaction Model (hET-SIM) assay

Human and mouse biology vary on a number of levels. As a result, drug discovery experiments often have low translation efficiencies when testing between the two organisms. To increase the relevance of the ET-SIM model and thus increase potential future translation into the clinic, a human mesenchymal cell line was generated for the replacement of the 3T3-L1 cells as the stromal cell component in the model. This was used in order to synthesise an *in vitro* human fat pad that was named hET-SIM. Human MSC were immortalised by retroviral insertion of the E6E7 gene, permitting cells to escape senescence and exhibit an increased proliferative capacity. Moreover, E6E7-MSCs were capable of undergoing adipogenic differentiation and produced basement membrane proteins at a comparable level to that of normal MSC. This was demonstrated both in 2D and within 3D anisotropic collagen scaffolds (the hET-SIM model).

The utility of the hET-SIM model was demonstrated using a migration assay with breast cancer cells. Fluorescently tagged MDA-MB-231 cells were tracked in the hET-SIM model and could be distinguished from adipocytes. These data demonstrated that human breast cancer cells can be successfully co-cultured with E6E7-MSC derived mature adipocytes and resulted in enhanced migration in the hET-SIM system. These results are in accord with the literature, where migration of MDA-MB-231 cells has been shown to be enhanced by their co-culture with adipocytes (Lee et al. 2015; Kim et al. 2009; Balaban et al. 2017; Libby et al. 2015). Of note, these studies often utilised human MDA-MB-231 cells with murine 3T3-L1 cell line in Boyden chamber assays (Balaban et al., 2017; Lee et al., 2015). This mismatch of cell species potentially presents concerns to the validity of the studies in question. hET-SIM overcomes this issue by incorporating cancer and stromal cells that are both of a human origin. Furthermore, hET-SIM enables the study of human adipocyte influence on breast cancer in a more physiologically relevant environment of anisotropic collagen ECM compared with commonly utilised Boyden chamber assays.

In summary, the hET-SIM model, comprised of an anisotropic ECM invested with human adipocytes and therefore successfully recapitulated aspects of the TACS-3 phenotype surrounding aggressive human breast tumours *in vivo* (Conklin et al., 2011). Whilst 3D *in vitro* culture techniques are continuously becoming more popular due to an increased understanding of the impact of 3D versus 2D culture, it is hoped that hET-SIM will contribute to the field of breast cancer research. With future incorporation of patient-derived breast tumour biopsies, the hET-SIM system holds potential as a drug discovery platform and a therapeutic assay for personalised medicine strategies.

## 7.8 Implications for the National Centre for the Refinement, Reduction and Replacement of animals in research (NC3Rs)

This thesis aimed to develop a number of assays that would reduce or replace the use of animals in mammary gland development and cancer research, and hence impact upon the NC3Rs.

### 7.8.1 Collagen scaffolds and human breast cancer cell line migration assays

All scaffolds used throughout this thesis were synthesised with collagen I sourced from bovine Achilles tendon. This protein is isolated from cadavers that are primarily used for other purposes, such as meat consumption, and thus no additional animals are specifically required or culled for its production. During human breast cancer cell line migration assays in collagen scaffolds, no murine material was required. Although this method is not sufficient to completely replace any animal experimentation in the study of cancer cell migration, it intends to supplement *in vitro* techniques to reduce the burden on *in vivo* experimentation.

### 7.8.2 Stem cell experiments

Stem cell experiments intended to decrease the frequency of mice required for fat pad transplantation assays by replacing recipient mice with collagen scaffolds invested with adipocytes. K14-cre$^{ERT2}$/Rosa26-tdTomato mice provided insufficient cell yields during FACS and did not form organoids within the model during culture. In this case, neither a reduction nor replacement of animals was achieved and thus future work with this line was ruled out. Cells isolated from Axin2-cre$^{ERT2}$/Rosa26-tdTomato mice were successfully expanded, enabling multiple experiments to be performed from the cells isolated from one mouse. However, with rare organoid formation and non-physiological organization of these cells, this system did not fulfill its requirements as a valid assay and unfortunately did not provide an NC3Rs impact.

### 7.8.3 ET-SIM experiments

For murine tumour ET-SIM experiments, one tumour was dissected into multiple fragments to permit numerous experiments and the testing of a selection of candidate inhibitors. Future validation of this model with *in vivo* models would ensure its reliability and accuracy. It is then intended that the impact of this work and its implementation in the drug discovery sector, would reduce the number of animals required in this field.

### 7.8.4 hET-SIM experiments

Both immortalised MSC and MBA-MB-231 breast cancer cells utilised in hET-SIM were derived from a human origin. Future development of the system envisages inclusion of breast cancer patient biopsies and the screening of a panel of cancer therapeutics, to provide personalised treatments. This model intends to completely replace animal research in this area by delivering a fully humanised assay for the oncologists' armamentarium.

### 7.8.5 Conclusion

In conclusion, three novel assays were developed for the investigation of breast cancer migration. Utilising 3D culture techniques, the native stroma of the human breast and murine mammary gland were recapitulated *in vitro*. Subsequent analysis of cell line and tumour cell migration was achieved in a variety of settings and the influence of collagen anisotropy assessed. Furthermore, a range of imaging techniques were implemented to investigate migration at different magnitudes and resolutions. Additionally, tumour cell migration was challenged with a selection of inhibitors, validating the model's competence for therapeutic assays. These versatile assays investigating migratory potentials and therapeutic efficacy hold potential for future use in the fields of cancer research, the biotech industry and the clinic.

# Bibliography

Akhtar, N., and Streuli, C.H. (2012). An integrin–ILK–microtubule network orients cell polarity and lumen formation in glandular epithelium. Nat. Cell Biol. *15*, 17–27.

Al-Hajj, M., Wicha, M.S., Benito-Hernandez, A., Morrison, S.J., and Clarke, M.F. (2003). Prospective identification of tumorigenic breast cancer cells. Proc. Natl. Acad. Sci. U. S. A. *100*, 3983–3988.

Albini, A., and Benelli, R. (2007). The chemoinvasion assay: a method to assess tumor and endothelial cell invasion and its modulation. Nat. Protoc. *2*, 504–511.

Alcaraz, J., Mori, H., Ghajar, C.M., Brownfield, D., Galgoczy, R., and Bissell, M.J. (2011). Collective epithelial cell invasion overcomes mechanical barriers of collagenous extracellular matrix by a narrow tube-like geometry and MMP14-dependent local softening. Integr. Biol. *3*, 1153.

Alexander, S., Koehl, G.E., Hirschberg, M., Geissler, E.K., and Friedl, P. (2008). Dynamic imaging of cancer growth and invasion: a modified skin-fold chamber model. Histochem. Cell Biol. *130*, 1147–1154.

Ali, R., Wendt, M.K., Koh, J., Wu, H.-G., Wie, L., and Jørgensen, L. (2017). The paradoxical functions of EGFR during breast cancer progression. Signal Transduct. Target. Ther. *2*, 16042.

American Cancer Society (2016). Cancer Facts & Figures 2016.

Ampuja, M., Jokimäki, R., Juuti-Uusitalo, K., Rodriguez-Martinez, A., Alarmo, E.-L., and Kallioniemi, A. (2013). BMP4 inhibits the proliferation of breast cancer cells and induces an MMP-dependent migratory phenotype in MDA-MB-231 cells in 3D environment. BMC Cancer *13*, 429.

Aratani, Y., and Kitagawa, Y. (1988). Enhanced synthesis and secretion of type IV collagen and entactin during adipose conversion of 3T3-L1 cells and production of unorthodox laminin complex. J. Biol. Chem. *263*, 16163–16169.

Arpino, G., Bardou, V.J., Clark, G.M., and Elledge, R.M. (2004). Infiltrating lobular carcinoma of the breast: tumor characteristics and clinical outcome. Breast Cancer Res. *6*, R149-56.

Arps, D.P., Healy, P., Zhao, L., Kleer, C.G., and Pang, J.C. (2013). Invasive ductal carcinoma with lobular features: a comparison study to invasive ductal and invasive lobular carcinomas of the breast. Breast Cancer Res. Treat. *138*, 719–726.

Awad, H.A., Butler, D.L., Boivin, G.P., Smith, F.N.L., Malaviya, P., Huibregtse, B., and Caplan, A.I. (1999). Autologous Mesenchymal Stem Cell-Mediated Repair of Tendon. Tissue Eng. *5*, 267–277.

Bachhuka, A., Hayball, J.D., Smith, L.E., and Vasilev, K. (2017). The Interplay between Surface Nanotopography and Chemistry Modulates Collagen I and III Deposition by Human Dermal Fibroblasts. ACS Appl. Mater. Interfaces *9*, 5874–5884.

Baharvand, H., Hashemi, S.M., Kazemi Ashtiani, S., and Farrokhi, A. (2006). Differentiation of human embryonic stem cells into hepatocytes in 2D and 3D culture systems in vitro. Int. J. Dev. Biol. *50*, 645–652.

Balaban, S., Shearer, R.F., Lee, L.S., van Geldermalsen, M., Schreuder, M., Shtein, H.C., Cairns, R., Thomas, K.C., Fazakerley, D.J., Grewal, T., et al. (2017). Adipocyte lipolysis links obesity to breast cancer growth: adipocyte-derived fatty acids drive breast cancer cell proliferation and migration.

Cancer Metab. *5*, 1.

Balekouzou, A., Yin, P., Pamatika, C.M., Bishwajit, G., Nambei, S.W., Djeintote, M., Ouansaba, B.E., Shu, C., Yin, M., Fu, Z., et al. (2016). Epidemiology of breast cancer: retrospective study in the Central African Republic. BMC Public Health *16*, 1230.

Bani-Sacchi, T., Bianchi, S., Bani, G., and Bigazzi, M. (1987). Ultrastructural studies on white adipocyte differentiation in the mouse mammary gland following estrogen and relaxin. Acta Anat. (Basel). *129*, 1–9.

Batlle, E., Henderson, J.T., Beghtel, H., van den Born, M.M.W., Sancho, E., Huls, G., Meeldijk, J., Robertson, J., van de Wetering, M., Pawson, T., et al. (2002). Beta-catenin and TCF mediate cell positioning in the intestinal epithelium by controlling the expression of EphB/ephrinB. Cell *111*, 251–263.

Begley, C.G., and Ellis, L.M. (2012). Drug development: Raise standards for preclinical cancer research. Nature *483*, 531–533.

Begley, R.F., Harvey, A.B., and Byer, R.L. (1974). Coherent anti-Stokes Raman spectroscopy. Appl. Phys. Lett. *25*, 387–390.

Beltrami, A.P., Barlucchi, L., Torella, D., Baker, M., Limana, F., Chimenti, S., Kasahara, H., Rota, M., Musso, E., Urbanek, K., et al. (2003). Adult cardiac stem cells are multipotent and support myocardial regeneration. Cell *114*, 763–776.

Benya, P.D., and Shaffer, J.D. (1982). Dedifferentiated chondrocytes reexpress the differentiated collagen phenotype when cultured in agarose gels. Cell *30*, 215–224.

Bhadriraju, K., Yang, M., Alom Ruiz, S., Pirone, D., Tan, J., and Chen, C.S. (2007). Activation of ROCK by RhoA is regulated by cell adhesion, shape, and cytoskeletal tension. Exp. Cell Res. *313*, 3616–3623.

Bhandary, L., Whipple, R.A., Vitolo, M.I., Charpentier, M.S., Boggs, A.E., Chakrabarti, K.R., Thompson, K.N., Martin, S.S., Bhandary, L., Whipple, R.A., et al. (2015). ROCK inhibition promotes microtentacles that enhance reattachment of breast cancer cells. Oncotarget *6*, 6251–6266.

Bian, L., Angione, S.L., Ng, K.W., Lima, E.G., Williams, D.Y., Mao, D.Q., Ateshian, G.A., and Hung, C.T. (2009). Influence of decreasing nutrient path length on the development of engineered cartilage. Osteoarthr. Cartil. *17*, 677–685.

Bidan, C.M., Kommareddy, K.P., Rumpler, M., Kollmannsberger, P., Fratzl, P., and Dunlop, J.W.C. (2013). Geometry as a Factor for Tissue Growth: Towards Shape Optimization of Tissue Engineering Scaffolds. Adv. Healthc. Mater. *2*, 186–194.

Bissell, M.J., Farson, D., and Tung, A.S. (1977). Cell shape and hexose transport in normal and virus-transformed cells in culture. J Supramol Struct *6*, 1–12.

Bissell, M.J., Radisky, D.C., Rizki, A., Weaver, V.M., and Petersen, O.W. (2002). The organizing principle: microenvironmental influences in the normal and malignant breast. Differentiation. *70*, 537–546.

Black, P.H., and Rowe, W.P. (1963). An analysis of SV40-induced transformation of hamster kidney tissue in vitro. I. General characteristics. Proc. Natl. Acad. Sci. U. S. A. *50*, 606–613.

Bocchetta, M., Di Resta, I., Powers, A., Fresco, R., Tosolini, A., Testa, J.R., Pass, H.I., Rizzo, P., and

Carbone, M. (2000). Human mesothelial cells are unusually susceptible to simian virus 40-mediated transformation and asbestos cocarcinogenicity. Proc. Natl. Acad. Sci. *97*, 10214–10219.

Bocchinfuso, W.P., Hively, W.P., Couse, J.F., Varmus, H.E., and Korach, K.S. (1999). A mouse mammary tumor virus-Wnt-1 transgene induces mammary gland hyperplasia and tumorigenesis in mice lacking estrogen receptor-alpha. Cancer Res. *59*, 1869–1876.

Boj, S.F., Hwang, C.-I., Baker, L.A., Chio, I.I.C., Engle, D.D., Corbo, V., Jager, M., Ponz-Sarvise, M., Tiriac, H., Spector, M.S., et al. (2015). Organoid models of human and mouse ductal pancreatic cancer. Cell *160*, 324–338.

Bologna-Molina, R., Mosqueda-Taylor, A., Molina-Frechero, N., Mori-Estevez, A.-D., and Sánchez-Acuña, G. (2013). Comparison of the value of PCNA and Ki-67 as markers of cell proliferation in ameloblastic tumors. Med. Oral Patol. Oral Cir. Bucal *18*, e174-9.

Bonab, M.M., Alimoghaddam, K., Talebian, F., Ghaffari, S.H., Ghavamzadeh, A., and Nikbin, B. (2006). Aging of mesenchymal stem cell in vitro. BMC Cell Biol. *7*, 14.

Bondarenko, G., Ugolkov, A., Rohan, S., Kulesza, P., Dubrovskyi, O., Gursel, D., Mathews, J., O'Halloran, T. V., Wei, J.J., and Mazar, A.P. (2015). Patient-Derived Tumor Xenografts Are Susceptible to Formation of Human Lymphocytic Tumors. Neoplasia *17*, 735–741.

Bonnans, C., Chou, J., and Werb, Z. (2014). Remodelling the extracellular matrix in development and disease. Nat. Rev. Mol. Cell Biol. *15*, 786–801.

de Both, N.J., Vermey, M., Dinjens, W.N., and Bosman, F.T. (1999). A comparative evaluation of various invasion assays testing colon carcinoma cell lines. Br. J. Cancer *81*, 934–941.

Bouchard, L., Lamarre, L., Tremblay, P.J., and Jolicoeur, P. (1989). Stochastic appearance of mammary tumors in transgenic mice carrying the MMTV/c-neu oncogene. Cell *57*, 931–936.

Bowman, W. (1840). On the Minute Structure and Movements of Voluntary Muscle. Philos. Trans. R. Soc. London *130*, 457–501.

Bowman, A.N., van Amerongen, R., Palmer, T.D., and Nusse, R. (2013). Lineage tracing with Axin2 reveals distinct developmental and adult populations of Wnt/ -catenin-responsive neural stem cells. Proc. Natl. Acad. Sci. *110*, 7324–7329.

Boyd, N.F., Martin, L.J., Yaffe, M.J., and Minkin, S. (2011). Mammographic density and breast cancer risk: current understanding and future prospects. Breast Cancer Res. *13*, 223.

Boyden, S. (1962). The chemotactic effect of mixtures of antibody and antigen on polymorphonuclear leucocytes. J. Exp. Med. *115*, 453–466.

Breast International Group (BIG) 1-98 Collaborative Group, Thürlimann, B., Keshaviah, A., Coates, A.S., Mouridsen, H., Mauriac, L., Forbes, J.F., Paridaens, R., Castiglione-Gertsch, M., Gelber, R.D., et al. (2005). A Comparison of Letrozole and Tamoxifen in Postmenopausal Women with Early Breast Cancer. N. Engl. J. Med. *353*, 2747–2757.

Bremer, C., Tung, C.-H., and Weissleder, R. (2001). In vivo molecular target assessment of matrix metalloproteinase inhibition. Nat. Med. *7*, 743–748.

Brisken, C., Heineman, A., Chavarria, T., Elenbaas, B., Tan, J., Dey, S.K., McMahon, J.A., McMahon, A.P., and Weinberg, R.A. (2000). Essential function of Wnt-4 in mammary gland development downstream of progesterone signaling. Genes Dev. *14*, 650.

Brooks, P.C., Strömblad, S., Sanders, L.C., von Schalscha, T.L., Aimes, R.T., Stetler-Stevenson, W.G., Quigley, J.P., and Cheresh, D.A. (1996). Localization of matrix metalloproteinase MMP-2 to the surface of invasive cells by interaction with integrin alpha v beta 3. Cell *85*, 683–693.

Brownfield, D.G., Venugopalan, G., Lo, A., Mori, H., Tanner, K., Fletcher, D.A., and Bissell, M.J. (2013). Patterned Collagen Fibers Orient Branching Mammary Epithelium through Distinct Signaling Modules. Curr. Biol. *23*, 703–709.

Burden, N., Chapman, K., Sewell, F., and Robinson, V. (2015). Pioneering better science through the 3Rs: an introduction to the national centre for the replacement, refinement, and reduction of animals in research (NC3Rs). J. Am. Assoc. Lab. Anim. Sci. *54*, 198–208.

Cahu, J., and Sola, B. (2013). A sensitive method to quantify senescent cancer cells. J. Vis. Exp.

Campbell, J.J., Davidenko, N., Caffarel, M.M., Cameron, R.E., Watson, C.J., Chin, W.-C., Campbell, J.J., Davidenko, N., Caffarel, M.M., Cameron, R.E., et al. (2011). A multifunctional 3D co-culture system for studies of mammary tissue morphogenesis and stem cell biology. PLoS One *6*, e25661.

Campbell, J.J., Hume, R.D., and Watson, C.J. (2014a). Engineering Mammary Gland in Vitro Models for Cancer Diagnostics and Therapy. Mol Pharm.

Campbell, J.J., Botos, L.-A.A., Sargeant, T.J., Davidenko, N., Cameron, R.E., and Watson, C.J. (2014b). A 3-D in vitro co-culture model of mammary gland involution. Integr Biol *6*, 618–626.

Campbell, J.J., Husmann, A., Hume, R.D., Watson, C.J., and Cameron, R.E. (2017). Development of three-dimensional collagen scaffolds with controlled architecture for cell migration studies using breast cancer cell lines. Biomaterials *114*, 34–43.

Carey, S.P., Rahman, A., Kraning-Rush, C.M., Romero, B., Somasegar, S., Torre, O.M., Williams, R.M., and Reinhart-King, C.A. (2015). Comparative mechanisms of cancer cell migration through 3D matrix and physiological microtracks. Am. J. Physiol. Cell Physiol. *308*, C436-47.

Carrel, A., and Burrows, M.T. (1911). CULTIVATION OF TISSUES IN VITRO AND ITS TECHNIQUE. J. Exp. Med. *13*, 387–396.

Carter, E.P., Gopsill, J.A., Gomm, J.J., Jones, J.L., and Grose, R.P. (2017). A 3D in vitro model of the human breast duct: a method to unravel myoepithelial-luminal interactions in the progression of breast cancer. Breast Cancer Res. *19*, 50.

Casey, J., Yue, X., Nguyen, T.D., Acun, A., Zellmer, V.R., Zhang, S., and Zorlutuna, P. (2017). 3D hydrogel-based microwell arrays as a tumor microenvironment model to study breast cancer growth. Biomed. Mater. *12*, 25009.

Cavo, M., Fato, M., Peñuela, L., Beltrame, F., Raiteri, R., and Scaglione, S. (2016). Microenvironment complexity and matrix stiffness regulate breast cancer cell activity in a 3D in vitro model. Sci. Rep. *6*, 35367.

Cellurale, C., Girnius, N., Jiang, F., Cavanagh-Kyros, J., Lu, S., Garlick, D.S., Mercurio, A.M., and Davis, R.J. (2012). Role of JNK in Mammary Gland Development and Breast Cancer. Cancer Res. *72*, 472–481.

Chakrabarti, R., Wei, Y., Romano, R.A., DeCoste, C., Kang, Y., and Sinha, S. (2012). Elf5 regulates mammary gland stem/progenitor cell fate by influencing notch signaling. Stem Cells *30*, 1496–1508.

Chaudhuri, O., Koshy, S.T., Branco da Cunha, C., Shin, J.-W., Verbeke, C.S., Allison, K.H., and Mooney,

D.J. (2014). Extracellular matrix stiffness and composition jointly regulate the induction of malignant phenotypes in mammary epithelium. Nat. Mater. *13*, 970–978.

Chavarri-Guerra, Y., St. Louis, J., Bukowski, A., Soto-Perez-de-Celis, E., Liedke, P.E.R., Symecko, H., Moy, B., Higgins, M., Finkelstein, D.M., and Goss, P.E. (2017). Real world patterns of care in HER2-overexpressing breast cancer: Results of a survey of TEACH clinical trial investigators in 2011. The Breast *31*, 197–201.

Chellappan, S., Kraus, V.B., Kroger, B., Munger, K., Howley, P.M., Phelps, W.C., and Nevins, J.R. (1992). Adenovirus E1A, simian virus 40 tumor antigen, and human papillomavirus E7 protein share the capacity to disrupt the interaction between transcription factor E2F and the retinoblastoma gene product. Proc. Natl. Acad. Sci. U. S. A. *89*, 4549–4553.

Chen, H.-C. (2005). Boyden chamber assay. Methods Mol. Biol. *294*, 15–22.

Chen, Y., Zhang, S., Wang, Q., and Zhang, X. (2017). Tumor-recruited M2 macrophages promote gastric and breast cancer metastasis via M2 macrophage-secreted CHI3L1 protein. J. Hematol. Oncol. *10*, 36.

Chieh, H.-F., Sun, Y., Liao, J.-D., Su, F.-C., Zhao, C., Amadio, P.C., and An, K.-N. (2010). Effects of cell concentration and collagen concentration on contraction kinetics and mechanical properties in a bone marrow stromal cell-collagen construct. J. Biomed. Mater. Res. A *93*, 1132–1139.

Chioni, A.-M., and Grose, R. (2012). FGFR1 cleavage and nuclear translocation regulates breast cancer cell behavior. J. Cell Biol. *197*, 801–817.

Cho, R.W., Wang, X., Diehn, M., Shedden, K., Chen, G.Y., Sherlock, G., Gurney, A., Lewicki, J., and Clarke, M.F. (2008). Isolation and Molecular Characterization of Cancer Stem Cells in MMTV- *Wnt-1* Murine Breast Tumors. Stem Cells *26*, 364–371.

Choi, Y.S., Zhang, Y., Xu, M., Yang, Y., Ito, M., Peng, T., Cui, Z., Nagy, A., Hadjantonakis, A.-K., Lang, R.A., et al. (2013). Distinct functions for Wnt/β-catenin in hair follicle stem cell proliferation and survival and interfollicular epidermal homeostasis. Cell Stem Cell *13*, 720.

Chu, E.Y., Hens, J., Andl, T., Kairo, A., Yamaguchi, T.P., Brisken, C., Glick, A., Wysolmerski, J.J., and Millar, S.E. (2004). Canonical WNT signaling promotes mammary placode development and is essential for initiation of mammary gland morphogenesis. Development *131*, 4819–4829.

Conklin, M.W., Eickhoff, J.C., Riching, K.M., Pehlke, C.A., Eliceiri, K.W., Provenzano, P.P., Friedl, A., and Keely, P.J. (2011). Aligned Collagen Is a Prognostic Signature for Survival in Human Breast Carcinoma. Am. J. Pathol. *178*, 1221–1232.

Costell, M., Gustafsson, E., Aszódi, A., Mörgelin, M., Bloch, W., Hunziker, E., Addicks, K., Timpl, R., and Fässler, R. (1999). Perlecan maintains the integrity of cartilage and some basement membranes. J. Cell Biol. *147*, 1109–1122.

Cousin, B., Cinti, S., Morroni, M., Raimbault, S., Ricquier, D., Penicaud, L., and Casteilla, L. (1992). Occurrence of brown adipocytes in rat white adipose tissue: molecular and morphological characterization. J. Cell Sci. *103*.

Cunningham-Rundles, S., Filippa, D.A., Braun, D.W., Antonelli, P., and Ashikari, H. (1981). Natural cytotoxicity of peripheral blood lymphocytes and regional lymph node cells in breast cancer in women. J. Natl. Cancer Inst. *67*, 585–590.

Cypess, A.M., Lehman, S., Williams, G., Tal, I., Rodman, D., Goldfine, A.B., Kuo, F.C., Palmer, E.L.,

Tseng, Y.-H., Doria, A., et al. (2009). Identification and Importance of Brown Adipose Tissue in Adult Humans. N. Engl. J. Med. *360*, 1509–1517.

D'Andrea, M. (2004). Collagenase predigestion on paraffin sections enhances collagen immunohistochemical detection without distorting tissue morphology. Biotech. Histochem. *79*, 55–64.

Daniel, C.W., De Ome, K.B., Young, J.T., Blair, P.B., and Faulkin, L.J. (1968). The in vivo life span of normal and preneoplastic mouse mammary glands: a serial transplantation study. Proc. Natl. Acad. Sci. U. S. A. *61*, 53–60.

Daniel, C.W., Berger, J.J., Strickland, P., and Garcia, R. (1984). Similar growth pattern of mouse mammary epithelium cultivated in collagen matrix in vivo and in vitro. Dev. Biol. *104*, 57–64.

Davidenko, N., Campbell, J.J., Thian, E.S., Watson, C.J., and Cameron, R.E. (2010). Collagen-hyaluronic acid scaffolds for adipose tissue engineering. Acta Biomater. *6*, 3957–3968.

Davidenko, N., Gibb, T., Schuster, C., Best, S.M.M., Campbell, J.J.J., Watson, C.J.J., and Cameron, R.E.E. (2012). Biomimetic collagen scaffolds with anisotropic pore architecture. Acta Biomater *8*, 667–676.

Davies, C., Godwin, J., Gray, R., Clarke, M., Cutter, D., Darby, S., McGale, P., Pan, H.C., Taylor, C., Wang, Y.C., et al. (2011). Relevance of breast cancer hormone receptors and other factors to the efficacy of adjuvant tamoxifen: patient-level meta-analysis of randomised trials. Lancet *378*, 771–784.

Davis, F.M., Azimi, I., Faville, R.A., Peters, A.A., Jalink, K., Putney, J.W., Goodhill, G.J., Thompson, E.W., Roberts-Thomson, S.J., Monteith, G.R., et al. (2013). Induction of epithelial–mesenchymal transition (EMT) in breast cancer cells is calcium signal dependent. Oncogene *33*, 2307–2316.

Davis, F.M., Lloyd-Lewis, B., Harris, O.B., Kozar, S., Winton, D.J., Muresan, L., and Watson, C.J. (2016). Single-cell lineage tracing in the mammary gland reveals stochastic clonal dispersion of stem/progenitor cell progeny. Nat. Commun. *7*, 13053.

Debnath, J., Muthuswamy, S.K., and Brugge, J.S. (2003). Morphogenesis and oncogenesis of MCF-10A mammary epithelial acini grown in three-dimensional basement membrane cultures. Methods *30*, 256–268.

Denk, W., Strickler, J.H., and Webb, W.W. (1990). Two-photon laser scanning fluorescence microscopy. Science *248*, 73–76.

Deome, K.B., Faulkin, L.J., Bern, H.A., Blair, P.B., Faulkin Jr., L.J., Bern, H.A., and Blair, P.B. (1959). Development of mammary tumors from hyperplastic alveolar nodules transplanted into gland-free mammary fat pads of female C3H mice. Cancer Res *19*, 515–520.

Desiderio, V., De Francesco, F., Schiraldi, C., De Rosa, A., La Gatta, A., Paino, F., d'Aquino, R., Ferraro, G.A., Tirino, V., and Papaccio, G. (2013). Human Ng2 $^{+}$ adipose stem cells loaded in vivo on a new crosslinked hyaluronic acid-lys scaffold fabricate a skeletal muscle tissue. J. Cell. Physiol. *228*, 1762–1773.

Desmoulière, A., Redard, M., Darby, I., and Gabbiani, G. (1995). Apoptosis mediates the decrease in cellularity during the transition between granulation tissue and scar. Am. J. Pathol. *146*, 56–66.

Devy, L., Huang, L., Naa, L., Yanamandra, N., Pieters, H., Frans, N., Chang, E., Tao, Q., Vanhove, M., Lejeune, A., et al. (2009). Selective inhibition of matrix metalloproteinase-14 blocks tumor growth,

invasion, and angiogenesis. Cancer Res. *69*, 1517–1526.

Dickinson, R.B., Guido, S., and Tranquillo, R.T. (1994). Biased cell migration of fibroblasts exhibiting contact guidance in oriented collagen gels. Ann. Biomed. Eng. *22*, 342–356.

Dirat, B., Bochet, L., Dabek, M., Daviaud, D., Dauvillier, S., Majed, B., Wang, Y.Y., Meulle, A., Salles, B., Le Gonidec, S., et al. (2011). Cancer-Associated Adipocytes Exhibit an Activated Phenotype and Contribute to Breast Cancer Invasion. Cancer Res. *71*, 2455–2465.

De Donatis, A., Comito, G., Buricchi, F., Vinci, M.C., Parenti, A., Caselli, A., Camici, G., Manao, G., Ramponi, G., and Cirri, P. (2008). Proliferation *Versus* Migration in Platelet-derived Growth Factor Signaling. J. Biol. Chem. *283*, 19948–19956.

Drobizhev, M., Makarov, N.S., Tillo, S.E., Hughes, T.E., and Rebane, A. (2011). Two-photon absorption properties of fluorescent proteins. Nat. Methods *8*, 393–399.

Drobysheva, D., Smith, B.A., McDowell, M., Guillen, K.P., Ekiz, H.A., and Welm, B.E. (2015). Transformation of enriched mammary cell populations with polyomavirus middle T antigen influences tumor subtype and metastatic potential. Breast Cancer Res. *17*, 132.

Drost, J., van Jaarsveld, R.H., Ponsioen, B., Zimberlin, C., van Boxtel, R., Buijs, A., Sachs, N., Overmeer, R.M., Offerhaus, G.J., Begthel, H., et al. (2015). Sequential cancer mutations in cultured human intestinal stem cells. Nature *521*, 43–47.

Drost, J., Karthaus, W.R., Gao, D., Driehuis, E., Sawyers, C.L., Chen, Y., and Clevers, H. (2016). Organoid culture systems for prostate epithelial and cancer tissue. Nat. Protoc. *11*, 347–358.

Druso, J.E., Endo, M., Lin, M.J., Peng, X., Antonyak, M.A., Meller, S., and Cerione, R.A. (2016). An Essential Role for Cdc42 in the Functioning of the Adult Mammary Gland. J. Biol. Chem. *291*, 8886–8895.

Du, J., Chen, X., Liang, X., Zhang, G., Xu, J., He, L., Zhan, Q., Feng, X.-Q., Chien, S., and Yang, C. (2011). Integrin activation and internalization on soft ECM as a mechanism of induction of stem cell differentiation by ECM elasticity. Proc. Natl. Acad. Sci. U. S. A. *108*, 9466–9471.

Dulbecco, R., Henahan, M., and Armstrong, B. (1982). Cell types and morphogenesis in the mammary gland. Proc. Natl. Acad. Sci. U. S. A. *79*, 7346–7350.

Duong, M.N., Cleret, A., Matera, E.-L., Chettab, K., Mathé, D., Valsesia-Wittmann, S., Clémenceau, B., and Dumontet, C. (2015). Adipose cells promote resistance of breast cancer cells to trastuzumab-mediated antibody-dependent cellular cytotoxicity. Breast Cancer Res. *17*, 57.

Duss, S., Brinkhaus, H., Britschgi, A., Cabuy, E., Frey, D.M., Schaefer, D.J., and Bentires-Alj, M. (2014). Mesenchymal precursor cells maintain the differentiation and proliferation potentials of breast epithelial cells. Breast Cancer Res. *16*, R60.

Elenbaas, B., Spirio, L., Koerner, F., Fleming, M.D., Zimonjic, D.B., Donaher, J.L., Popescu, N.C., Hahn, W.C., and Weinberg, R.A. (2001). Human breast cancer cells generated by oncogenic transformation of primary mammary epithelial cells. Genes Dev. *15*, 50–65.

Elias, J.J., Pitelka, D.R., and Armstrong, R.C. (1973). Changes in fat cell morphology during lactation in the mouse. Anat. Rec. *177*, 533–547.

Elshof, L.E., Schaapveld, M., Schmidt, M.K., Rutgers, E.J., van Leeuwen, F.E., and Wesseling, J. (2016). Subsequent risk of ipsilateral and contralateral invasive breast cancer after treatment for ductal

carcinoma in situ: incidence and the effect of radiotherapy in a population-based cohort of 10,090 women. Breast Cancer Res. Treat. *159*, 553–563.

Erler, J.T., Bennewith, K.L., Nicolau, M., Dornhöfer, N., Kong, C., Le, Q.-T., Chi, J.-T.A., Jeffrey, S.S., and Giaccia, A.J. (2006). Lysyl oxidase is essential for hypoxia-induced metastasis. Nature *440*, 1222–1226.

Ervasti, J.M., and Campbell, K.P. (1991). Membrane organization of the dystrophin-glycoprotein complex. Cell *66*, 1121–1131.

Espina, V., Wulfkuhle, J.D., Calvert, V.S., VanMeter, A., Zhou, W., Coukos, G., Geho, D.H., Petricoin, E.F., and Liotta, L.A. (2006). Laser-capture microdissection. Nat. Protoc. *1*, 586–603.

Estefanía, M.M., Ganier, O., Hernández, P., Schvartzman, J.B., Mechali, M., and Krimer, D.B. (2012). DNA replication fading as proliferating cells advance in their commitment to terminal differentiation. Sci. Rep. *2*, 279.

Evdokimova, V., Tognon, C., Ng, T., Ruzanov, P., Melnyk, N., Fink, D., Sorokin, A., Ovchinnikov, L.P., Davicioni, E., Triche, T.J., et al. (2009). Translational Activation of Snail1 and Other Developmentally Regulated Transcription Factors by YB-1 Promotes an Epithelial-Mesenchymal Transition. Cancer Cell *15*, 402–415.

Faber, D.R., Kalkhoven, E., Westerink, J., Bouwman, J.J., Monajemi, H.M., and Visseren, F.L.J. (2012). Conditioned media from (pre)adipocytes stimulate fibrinogen and PAI-1 production by HepG2 hepatoma cells. Nutr. Diabetes *2*, e52.

Fagagna, F. d'Adda di, Reaper, P.M., Clay-Farrace, L., Fiegler, H., Carr, P., von Zglinicki, T., Saretzki, G., Carter, N.P., and Jackson, S.P. (2003). A DNA damage checkpoint response in telomere-initiated senescence. Nature *426*, 194–198.

Falk Libby, E., Liu, J., Li, Y., Lewis, M., Demark‐Wahnefried, W., and Hurst, D. (2015). Globular adiponectin enhances invasion in human breast cancer cells. Oncol. Lett. *11*, 633–641.

Faraldo, M.M., Deugnier, M.A., Thiery, J.P., and Glukhova, M.A. (2000). Development of mammary gland requires normal beta 1-integrin function. Adv. Exp. Med. Biol. *480*, 169–174.

Favreau, A.J., Vary, C.P.H., Brooks, P.C., and Sathyanarayana, P. (2014). Cryptic collagen IV promotes cell migration and adhesion in myeloid leukemia. Cancer Med. *3*, 265–272.

Fernandez, P., and Bausch, A.R. (2009). The compaction of gels by cells: a case of collective mechanical activity. Integr. Biol. *1*, 252.

Filmus, J., Pollak, M.N., Cailleau, R., and Buick, R.N. (1985). MDA-468, a human breast cancer cell line with a high number of epidermal growth factor (EGF) receptors, has an amplified EGF receptor gene and is growth inhibited by EGF. Biochem. Biophys. Res. Commun. *128*, 898–905.

Fisher, B., Costantino, J.P., Wickerham, D.L., Cecchini, R.S., Cronin, W.M., Robidoux, A., Bevers, T.B., Kavanah, M.T., Atkins, J.N., Margolese, R.G., et al. (2005). Tamoxifen for the Prevention of Breast Cancer: Current Status of the National Surgical Adjuvant Breast and Bowel Project P-1 Study. JNCI J. Natl. Cancer Inst. *97*, 1652–1662.

Fisher, K.E., Sacharidou, A., Stratman, A.N., Mayo, A.M., Fisher, S.B., Mahan, R.D., Davis, M.J., and Davis, G.E. (2009). MT1-MMP- and Cdc42-dependent signaling co-regulate cell invasion and tunnel formation in 3D collagen matrices. Doi.org 4558–4569.

Flores, I.L., Kawahara, R., Miguel, M.C.C., Granato, D.C., Domingues, R.R., Macedo, C.C.S., Carnielli, C.M., Yokoo, S., Rodrigues, P.C., Monteiro, B.V.B., et al. (2016). EEF1D modulates proliferation and epithelial-mesenchymal transition in oral squamous cell carcinoma. Clin. Sci. *130*, 785–799.

Folkman, J.J., and Moscona, A. (1978). Role of cell shape in growth control. Nature *273*, 345–349.

Forster, N., Saladi, S.V.V., van Bragt, M., Sfondouris, M.E.E., Jones, F.E.E., Li, Z., Ellisen, L.W.W., van Bragt, M., Sfondouris, M.E.E., Jones, F.E.E., et al. (2014). Basal Cell Signaling by p63 Controls Luminal Progenitor Function and Lactation via NRG1. Dev. Cell *28*, 147–160.

Foster, S.A., Demers, G.W., Etscheid, B.G., and Galloway, D.A. (1994). The ability of human papillomavirus E6 proteins to target p53 for degradation in vivo correlates with their ability to abrogate actinomycin D-induced growth arrest. J. Virol. *68*, 5698–5705.

Francis, O., Williams, K.J., SYKESt, B.C., Smith, R., and O Francis, M.J. (1981). The relative amounts of the collagen chains «1(1), «2 and «1(111) in the skin of 31 patients with osteogenesis imperfecta. Clin. Sci. *60*, 617–623.

Frohlich, E.M., Zhang, X., Charest, J.L., Goodenough, D. a., Mooseker, M.S., Suh, K.Y., Guertin, D.A., Chang, J.H., Lindquist, R.A., Moffat, J., et al. (2012). The use of controlled surface topography and flow-induced shear stress to influence renal epithelial cell function. Integr. Biol. *4*, 75–83.

Fujimoto, H., Sangai, T., Ishii, G., Ikehara, A., Nagashima, T., Miyazaki, M., and Ochiai, A. (2009). Stromal MCP-1 in mammary tumors induces tumor-associated macrophage infiltration and contributes to tumor progression. Int. J. Cancer *125*, 1276–1284.

Fukuda, K., Kamoshida, Y., Kurokawa, T., Yoshida, M., Fujita-Yamaguchi, Y., and Nakata, M. (2014). Migration of breast cancer cells into reconstituted type I collagen gels assessed via a combination of frozen sectioning and azan staining. Biosci. Trends *8*, 212–216.

Gadea, G., Sanz-Moreno, V., Self, A., Godi, A., and Marshall, C.J. (2008). DOCK10-Mediated Cdc42 Activation Is Necessary for Amoeboid Invasion of Melanoma Cells. Curr. Biol. *18*, 1456–1465.

Gaggioli, C., Hooper, S., Hidalgo-Carcedo, C., Grosse, R., Marshall, J.F., Harrington, K., and Sahai, E. (2007). Fibroblast-led collective invasion of carcinoma cells with differing roles for RhoGTPases in leading and following cells. Nat. Cell Biol. *9*, 1392–1400.

Galmarini, C.M. (2004). Canertinib pfizer. IDrugs *7*, 58–63.

Gangadhara, S., and Bertelli, G. (2009). Long-term efficacy and safety of anastrozole for adjuvant treatment of early breast cancer in postmenopausal women. Ther. Clin. Risk Manag. *5*, 291–300.

Gao, Y., Wang, Z., Hao, Q., Li, W., Xu, Y., Zhang, J., Zhang, W., Wang, S., Liu, S., Li, M., et al. (2017). Loss of ERα induces amoeboid-like migration of breast cancer cells by downregulating vinculin. Nat. Commun. Publ. Online 7 March 2017; | doi10.1038/ncomms14483 *147*, 423–431.

García, A.J., Vega, M.D., and Boettiger, D. (1999). Modulation of cell proliferation and differentiation through substrate-dependent changes in fibronectin conformation. Mol. Biol. Cell *10*, 785–798.

Gardiol, D., Kühne, C., Glaunsinger, B., Lee, S.S., Javier, R., and Banks, L. (1999). Oncogenic human papillomavirus E6 proteins target the discs large tumour suppressor for proteasome-mediated degradation. Oncogene *18*, 5487–5496.

Ge, L., Shenoy, S.K., Lefkowitz, R.J., and DeFea, K. (2004). Constitutive protease-activated receptor-2-mediated migration of MDA MB-231 breast cancer cells requires both beta-arrestin-1 and -2. J. Biol.

Chem. *279*, 55419–55424.

Georgoudaki, A.-M., Prokopec, K.E., Boura, V.F., Hellqvist, E., Sohn, S., Östling, J., Dahan, R., Harris, R.A., Rantalainen, M., Klevebring, D., et al. (2016). Reprogramming Tumor-Associated Macrophages by Antibody Targeting Inhibits Cancer Progression and Metastasis. Cell Rep. *15*, 2000–2011.

Gerdes, J., Schwab, U., Lemke, H., and Stein, H. (1983). Production of a mouse monoclonal antibody reactive with a human nuclear antigen associated with cell proliferation. Int. J. Cancer *31*, 13–20.

Gerlinger, M., Rowan, A.J., Horswell, S., Larkin, J., Endesfelder, D., Gronroos, E., Martinez, P., Matthews, N., Stewart, A., Tarpey, P., et al. (2012). Intratumor Heterogeneity and Branched Evolution Revealed by Multiregion Sequencing. N. Engl. J. Med. *366*, 883–892.

Ghoncheh, M., Pournamdar, Z., and Salehiniya, H. (2016). Incidence and Mortality and Epidemiology of Breast Cancer in the World. Asian Pac. J. Cancer Prev. *17*, 43–46.

Giauque, W.F., and Meads, P.F. (1941). The Heat Capacities and Entropies of Aluminum and Copper from 15 to 300°K. J. Am. Chem. Soc. *63*, 1897–1901.

Gillio-Meina, C., Swan, C.L., Crellin, N.K., Stocco, D.M., and Chedrese, P.J. (2000). Generation of stable cell lines by spontaneous immortalization of primary cultures of porcine granulosa cells. Mol. Reprod. Dev. *57*, 366–374.

Glukhova, M., Koteliansky, V., Sastre, X., and Thiery, J.P. (1995). Adhesion systems in normal breast and in invasive breast carcinoma. Am. J. Pathol. *146*, 706–716.

Goetsch, K.P., Snyman, C., Myburgh, K.H., and Niesler, C.U. (2014). ROCK-2 Is Associated With Focal Adhesion Maturation During Myoblast Migration. J. Cell. Biochem. *115*, 1299–1307.

Gogia, A., Raina, V., Deo, S.V.S., Shukla, N.K., and Mohanti, B.K. (2014). Triple-negative breast cancer: An institutional analysis. Indian J. Cancer *51*, 163–166.

Goncharova, E.A., Goncharov, D.A., and Krymskaya, V.P. (2007). Assays for in vitro monitoring of human airway smooth muscle (ASM) and human pulmonary arterial vascular smooth muscle (VSM) cell migration. Nat. Protoc. *1*, 2933–2939.

Gong, M., Bi, Y., Jiang, W., Zhang, Y., Chen, L., Hou, N., Liu, Y., Wei, X., Chen, J., and Li, T. (2011). Immortalized mesenchymal stem cells: an alternative to primary mesenchymal stem cells in neuronal differentiation and neuroregeneration associated studies. J. Biomed. Sci. *18*, 87.

Goodrich, D.W., Wang, N.P., Qian, Y.W., Lee, E.Y., and Lee, W.H. (1991). The retinoblastoma gene product regulates progression through the G1 phase of the cell cycle. Cell *67*, 293–302.

Gordon, K.E., Binas, B., Chapman, R.S., Kurian, K.M., Clarkson, R.W., Clark, A.J., Lane, E.B., and Watson, C.J. (2000). A novel cell culture model for studying differentiation and apoptosis in the mouse mammary gland. Breast Cancer Res *2*, 222–235.

Gordon, L.A., Mulligan, K.T., Maxwell-Jones, H., Adams, M., Walker, R.A., and Jones, J.L. (2003). Breast cell invasive potential relates to the myoepithelial phenotype. Int. J. Cancer *106*, 8–16.

Goss, P.E., Ingle, J.N., Alés-Martínez, J.E., Cheung, A.M., Chlebowski, R.T., Wactawski-Wende, J., McTiernan, A., Robbins, J., Johnson, K.C., Martin, L.W., et al. (2011). Exemestane for Breast-Cancer Prevention in Postmenopausal Women. N. Engl. J. Med. *364*, 2381–2391.

Gouon-Evans, V., and Pollard, J.W. (2002). Unexpected Deposition of Brown Fat in Mammary Gland During Postnatal Development. Mol. Endocrinol. *16*, 2618–2627.

Grantab, R., Sivananthan, S., and Tannock, I.F. (2006). The Penetration of Anticancer Drugs through Tumor Tissue as a Function of Cellular Adhesion and Packing Density of Tumor Cells. Cancer Res. *66*, 1033–1039.

Grinnell, F., Ho, C.-H., Tamariz, E., Lee, D.J., and Skuta, G. (2003). Dendritic fibroblasts in three-dimensional collagen matrices. Mol. Biol. Cell *14*, 384–395.

Grodin, J.M., Siiteri, P.K., and Macdonald, P.C. (1973). Source of Estrogen Production in Postmenopausal Women1. J. Clin. Endocrinol. Metab. *36*, 207–214.

Grover, C.N., Gwynne, J.H., Pugh, N., Hamaia, S., Farndale, R.W., Best, S.M., and Cameron, R.E. (2012). Crosslinking and composition influence the surface properties, mechanical stiffness and cell reactivity of collagen-based films. Acta Biomater. *8*, 3080–3090.

Gudjonsson, T., Rønnov-Jessen, L., Villadsen, R., Rank, F., Bissell, M.J., and Petersen, O.W. (2002). Normal and tumor-derived myoepithelial cells differ in their ability to interact with luminal breast epithelial cells for polarity and basement membrane deposition. J. Cell Sci. *115*, 39–50.

Gui, G.P., Puddefoot, J.R., Vinson, G.P., Wells, C.A., and Carpenter, R. (1995). In vitro regulation of human breast cancer cell adhesion and invasion via integrin receptors to the extracellular matrix. Br. J. Surg. *82*, 1192–1196.

Guy, C.T., Webster, M.A., Schaller, M., Parsons, T.J., Cardiff, R.D., and Muller, W.J. (1992). Expression of the neu protooncogene in the mammary epithelium of transgenic mice induces metastatic disease. Proc. Natl. Acad. Sci. U. S. A. *89*, 10578–10582.

Guy, C.T., Cardiff, R.D., and Muller, W.J. (1996). Activated neu induces rapid tumor progression. J. Biol. Chem. *271*, 7673–7678.

Haagensen, C.D. (1971). The physiology of the breast as it concerns the clinician. Am. J. Obstet. Gynecol. *109*, 206–209.

Hadjipanayi, E., Mudera, V., and Brown, R.A. (2009). Close dependence of fibroblast proliferation on collagen scaffold matrix stiffness. J. Tissue Eng. Regen. Med. *3*, 77–84.

Haeger, A., Krause, M., Wolf, K., and Friedl, P. (2014). Cell jamming: Collective invasion of mesenchymal tumor cells imposed by tissue confinement. Biochim. Biophys. Acta - Gen. Subj. *1840*, 2386–2395.

Hannink, G., Geutjes, P.J., Daamen, W.F., and Buma, P. (2013). Evaluation of collagen/heparin coated TCP/HA granules for long-term delivery of BMP-2. J. Mater. Sci. Mater. Med. *24*, 325–332.

Harrell, J.C., Prat, A., Parker, J.S., Fan, C., He, X., Carey, L., Anders, C., Ewend, M., and Perou, C.M. (2012). Genomic analysis identifies unique signatures predictive of brain, lung, and liver relapse. Breast Cancer Res. Treat. *132*, 523–535.

Harris, C.A., Ward, R.L., Dobbins, T.A., Drew, A.K., Pearson, S., Costa, L., Andrade, S., and Batel-Marques, F. (2011). The efficacy of HER2-targeted agents in metastatic breast cancer: a meta-analysis. Ann. Oncol. *22*, 1308–1317.

Hashim, P., Ridzwan, M.S.M., and Bakar, J. (2014). Isolation and Characterization of Collagen from Chicken Feet. Int. J. Biol. Biomol. Agric. Food Biotechnol. Eng. *8*, 147–151.

Hawley-Nelson, P., Vousden, K.H., Hubbert, N.L., Lowy, D.R., and Schiller, J.T. (1989). HPV16 E6 and E7 proteins cooperate to immortalize human foreskin keratinocytes. EMBO J. *8*, 3905–3910.

Hayflick, L., and Moorhead, P.S. (1961). The serial cultivation of human diploid cell strains. Exp. Cell Res. *25*, 585–621.

Hefti, M.M., Hu, R., Knoblauch, N.W., Collins, L.C., Haibe-Kains, B., Tamimi, R.M., and Beck, A.H. (2013). Estrogen receptor negative/progesterone receptor positive breast cancer is not a reproducible subtype. Breast Cancer Res. *15*.

Heinz, T.F., Chen, C.K., Ricard, D., and Shen, Y.R. (1982). Spectroscopy of molecular monolayers by resonant second-harmonic generation. Phys. Rev. Lett. *48*, 478–481.

Hens, J.R., Dann, P., Zhang, J.-P.P., Harris, S., Robinson, G.W., and Wysolmerski, J. (2007). BMP4 and PTHrP interact to stimulate ductal outgrowth during embryonic mammary development and to inhibit hair follicle induction. Development *134*, 1221–1230.

Hernandez, L., Wilkerson, P.M., Lambros, M.B., Campion-Flora, A., Rodrigues, D.N., Gauthier, A., Cabral, C., Pawar, V., Mackay, A., A'Hern, R., et al. (2012). Genomic and mutational profiling of ductal carcinomas in situ and matched adjacent invasive breast cancers reveals intra-tumour genetic heterogeneity and clonal selection. J. Pathol. *227*, 42–52.

Hongisto, H., Vuoristo, S., Mikhailova, A., Suuronen, R., Virtanen, I., Otonkoski, T., and Skottman, H. (2012). Laminin-511 expression is associated with the functionality of feeder cells in human embryonic stem cell culture. Stem Cell Res. *8*, 97–108.

Hou, S., Isaji, T., Hang, Q., Im, S., Fukuda, T., and Gu, J. (2016). Distinct effects of β1 integrin on cell proliferation and cellular signaling in MDA-MB-231 breast cancer cells. Sci. Rep. *6*, 18430.

Hsieh, C.-C., and Huang, Y.-S. (2016). Aspirin Breaks the Crosstalk between 3T3-L1 Adipocytes and 4T1 Breast Cancer Cells by Regulating Cytokine Production. PLoS One *11*, e0147161.

Hsu, C.Y.M., and Uludag, H. (2012). A simple and rapid nonviral approach to efficiently transfect primary tissue?derived cells using polyethylenimine. Nat. Protoc. *7*, 935–945.

Hu, G., Li, L., and Xu, W. (2017). Extracellular matrix in mammary gland development and breast cancer progression. Front. Lab. Med.

Huang, C.-K., Chang, P.-H., Kuo, W.-H., Chen, C.-L., Jeng, Y.-M., Chang, K.-J., Shew, J.-Y., Hu, C.-M., and Lee, W.-H. (2017). Adipocytes promote malignant growth of breast tumours with monocarboxylate transporter 2 expression via β-hydroxybutyrate. Nat. Commun. *8*, 14706.

Hughes, C.S., Postovit, L.M., and Lajoie, G.A. (2010). Matrigel: a complex protein mixture required for optimal growth of cell culture. Proteomics *10*, 1886–1890.

Hugo, E.R., Borcherding, D.C., Gersin, K.S., Loftus, J., and Ben-Jonathan, N. (2008). Prolactin Release by Adipose Explants, Primary Adipocytes, and LS14 Adipocytes. J. Clin. Endocrinol. Metab. *93*, 4006–4012.

Hur, H., Lee, J.-Y., Yang, S., Kim, J.M., Park, A.E., and Kim, M.H. (2016). HOXC9 Induces Phenotypic Switching between Proliferation and Invasion in Breast Cancer Cells. J. Cancer *7*, 768–773.

Husmann, A., Pawelec, K., Burdett, C., Best, S., and Cameron, R. (2015). Numerical simulations to determine the influence of mould design on ice-templated scaffold structures. J. Biomed. Eng. Informatics *1*, 47.

Ilunga, K., Nishiura, R., Inada, H., El-Karef, A., Imanaka-Yoshida, K., Sakakura, T., and Yoshida, T. (2004). Co-stimulation of human breast cancer cells with transforming growth factor-beta and

tenascin-C enhances matrix metalloproteinase-9 expression and cancer cell invasion. Int. J. Exp. Pathol. *85*, 373–379.

Ingman, W. V., Wyckoff, J., Gouon-Evans, V., Condeelis, J., and Pollard, J.W. (2006). Macrophages promote collagen fibrillogenesis around terminal end buds of the developing mammary gland. Dev. Dyn. *235*, 3222–3229.

Inic, Z., Zegarac, M., Inic, M., Markovic, I., Kozomara, Z., Djurisic, I., Inic, I., Pupic, G., and Jancic, S. (2014). Difference between Luminal A and Luminal B Subtypes According to Ki-67, Tumor Size, and Progesterone Receptor Negativity Providing Prognostic Information. Clin. Med. Insights. Oncol. *8*, 107–111.

Ishikawa, T., Wondimu, Z., Oikawa, Y., Gentilcore, G., Kiessling, R., Egyhazi Brage, S., Hansson, J., and Patarroyo, M. (2014). Laminins 411 and 421 differentially promote tumor cell migration via α6β1 integrin and MCAM (CD146). Matrix Biol. *38*, 69–83.

Isobe, T., Hisamori, S., Hogan, D.J., Zabala, M., Hendrickson, D.G., Dalerba, P., Cai, S., Scheeren, F., Kuo, A.H., Sikandar, S.S., et al. (2014). miR-142 regulates the tumorigenicity of human breast cancer stem cells through the canonical WNT signaling pathway. Elife *3*, 2346–2351.

Iyengar, P., Espina, V., Williams, T.W., Lin, Y., Berry, D., Jelicks, L.A., Lee, H., Temple, K., Graves, R., Pollard, J., et al. (2005). Adipocyte-derived collagen VI affects early mammary tumor progression in vivo, demonstrating a critical interaction in the tumor/stroma microenvironment. J. Clin. Invest. *115*, 1163–1176.

Jaiswal, R.K., Jaiswal, N., Bruder, S.P., Mbalaviele, G., Marshak, D.R., and Pittenger, M.F. (2000). Adult human mesenchymal stem cell differentiation to the osteogenic or adipogenic lineage is regulated by mitogen-activated protein kinase. J. Biol. Chem. *275*, 9645–9652.

Jalkanen, M., Rapraeger, A., and Bernfield, M. (1988). Mouse mammary epithelial cells produce basement membrane and cell surface heparan sulfate proteoglycans containing distinct core proteins. J. Cell Biol. *106*, 953–962.

Jamieson, P.R., Dekkers, J.F., Rios, A.C., Fu, N.Y., Lindeman, G.J., and Visvader, J.E. (2017). Derivation of a robust mouse mammary organoid system for studying tissue dynamics. Development *144*, 1065–1071.

Jardé, T., Lloyd-Lewis, B., Thomas, M., Kendrick, H., Melchor, L., Bougaret, L., Watson, P.D., Ewan, K., Smalley, M.J., and Dale, T.C. (2016). Wnt and Neuregulin1/ErbB signalling extends 3D culture of hormone responsive mammary organoids. Nat. Commun. *7*, 13207.

Jiang, R., Zeng, X., Sun, S., Ma, Z., and Wang, X. (2016). Assessing Detection, Discrimination, and Risk of Breast Cancer According to Anisotropy Parameters of Diffusion Tensor Imaging. Med. Sci. Monit. *22*, 1318–1328.

Jiang, X.-R., Jimenez, G., Chang, E., Frolkis, M., Kusler, B., Sage, M., Beeche, M., Bodnar, A.G., Wahl, G.M., Tlsty, T.D., et al. (1999). Telomerase expression in human somatic cells does not induce changes associated with a transformed phenotype. Nat. Genet. *21*, 111–114.

Jo, M., Lester, R.D., Montel, V., Eastman, B., Takimoto, S., and Gonias, S.L. (2009). Reversibility of Epithelial-Mesenchymal Transition (EMT) Induced in Breast Cancer Cells by Activation of Urokinase Receptor-dependent Cell Signaling. J. Biol. Chem. *284*, 22825–22833.

Johansson, J., Tabor, V., Wikell, A., Jalkanen, S., and Fuxe, J. (2015). TGF-β1-Induced Epithelial-Mesenchymal Transition Promotes Monocyte/Macrophage Properties in Breast Cancer Cells. Front.

Oncol. *5*, 3.

Jokinen, J., Dadu, E., Nykvist, P., Käpylä, J., White, D.J., Ivaska, J., Vehviläinen, P., Reunanen, H., Larjava, H., Häkkinen, L., et al. (2004). Integrin-mediated cell adhesion to type I collagen fibrils. J. Biol. Chem. *279*, 31956–31963.

Jung, J.P., Bache-Wiig, M.K., Provenzano, P.P., and Ogle, B.M. (2016). Heterogeneous Differentiation of Human Mesenchymal Stem Cells in 3D Extracellular Matrix Composites. Biores. Open Access *5*, 37–48.

Jungst, C., Winterhalder, M.J., and Zumbusch, A. (2011). Fast and long term lipid droplet tracking with CARS microscopy. J. Biophotonics *4*, 435–441.

Kaanta, A.S., Virtanen, C., Selfors, L.M., Brugge, J.S., and Neel, B.G. (2013). Evidence for a multipotent mammary progenitor with pregnancy-specific activity. Breast Cancer Res. *15*, R65.

Kakkad, S., Zhang, J., Akhbardeh, A., Jacob, D., Krishnamachary, B., Solaiyappan, M., Jacobs, M.A., Raman, V., Leibfritz, D., Glunde, K., et al. (2016). Collagen fibers mediate MRI-detected water diffusion and anisotropy in breast cancers. Neoplasia *18*, 585–593.

Kasten, P., Beyen, I., Niemeyer, P., Luginbühl, R., Bohner, M., and Richter, W. (2008). Porosity and pore size of β-tricalcium phosphate scaffold can influence protein production and osteogenic differentiation of human mesenchymal stem cells: An in vitro and in vivo study. Acta Biomater. *4*, 1904–1915.

Kaushik, S., Pickup, M.W., and Weaver, V.M. (2016). From transformation to metastasis: deconstructing the extracellular matrix in breast cancer. Cancer Metastasis Rev. *35*, 655–667.

Keller, H., and Eggli, P. (1998). Protrusive activity, cytoplasmic compartmentalization, and restriction rings in locomoting blebbing Walker carcinosarcoma cells are related to detachment of cortical actin from the plasma membrane. Cell Motil. Cytoskeleton *41*, 181–193.

Keller, P.J., Lin, A.F., Arendt, L.M., Klebba, I., Jones, A.D., Rudnick, J.A., DiMeo, T.A., Gilmore, H., Jefferson, D.M., Graham, R.A., et al. (2010). Mapping the cellular and molecular heterogeneity of normal and malignant breast tissues and cultured cell lines. Breast Cancer Res. *12*, R87.

Kenny, P.A., Lee, G.Y., Myers, C.A., Neve, R.M., Semeiks, J.R., Spellman, P.T., Lorenz, K., Lee, E.H., Barcellos-Hoff, M.H., Petersen, O.W., et al. (2007). The morphologies of breast cancer cell lines in three-dimensional assays correlate with their profiles of gene expression. Mol. Oncol. *1*, 84–96.

Van Keymeulen, A., Rocha, A.S., Ousset, M., Beck, B., Bouvencourt, G., Rock, J., Sharma, N., Dekoninck, S., and Blanpain, C. (2011). Distinct stem cells contribute to mammary gland development and maintenance. Nature *479*, 189–193.

Khramtsov, A.I., Khramtsova, G.F., Tretiakova, M., Huo, D., Olopade, O.I., and Goss, K.H. (2010). Wnt/β-Catenin Pathway Activation Is Enriched in Basal-Like Breast Cancers and Predicts Poor Outcome. Am. J. Pathol. *176*, 2911–2920.

Kikuchi, K., Li, X., Zheng, Y., and Takano, Y. (2011). Invasion of breast cancer cells into collagen matrix requires TGF-α and Cdc42 signaling. FEBS Lett. *585*, 286–290.

Kim, H.-J., Hwang, K.-E., Park, D.-S., Oh, S.-H., Jun, H.Y., Yoon, K.-H., Jeong, E.-T., Kim, H.-R., and Kim, Y.-S. (2017). Shikonin-induced necroptosis is enhanced by the inhibition of autophagy in non-small cell lung cancer cells. J. Transl. Med. *15*, 123.

Kim, J.-Y., Jung, H.H., Do, I.-G., Bae, S., Lee, S.K., Kim, S.W., Lee, J.E., Nam, S.J., Ahn, J.S., Park, Y.H., et al. (2016). Prognostic value of ERBB4 expression in patients with triple negative breast cancer. BMC Cancer *16*, 138.

Kim, K.-Y., Baek, A., Park, Y.S., Park, M.Y., Kim, J.H., Lim, J.-S., Lee, M.-S., Yoon, S.R., Lee, H.G., Yoon, Y., et al. (2009a). Adipocyte culture medium stimulates invasiveness of MDA-MB-231 cell via CCL20 production. Oncol. Rep. *22*, 1497–1504.

Kim, M.-H., Sawada, Y., Taya, M., and Kino-Oka, M. (2014). Influence of surface topography on the human epithelial cell response to micropatterned substrates with convex and concave architectures. J. Biol. Eng. *8*, 13.

Kim, Y., Clark, R.J., Pelegri, F., and Alexander, C.M. (2009b). Wnt4 is not sufficient to induce lobuloalveolar mammary development. BMC Dev. Biol. *9*, 55.

Kleinman, H.K., and Martin, G.R. (2005). Matrigel: Basement membrane matrix with biological activity. Semin. Cancer Biol. *15*, 378–386.

Kleinman, H.K., McGarvey, M.L., Liotta, L.A., Robey, P.G., Tryggvason, K., and Martin, G.R. (1982). Isolation and characterization of type IV procollagen, laminin, and heparan sulfate proteoglycan from the EHS sarcoma. Biochemistry *21*, 6188–6193.

Klingelhutz, A.J., Foster, S.A., and McDougall, J.K. (1996). Telomerase activation by the E6 gene product of human papillomavirus type 16. Nature *380*, 79–82.

Koebel, C.M., Vermi, W., Swann, J.B., Zerafa, N., Rodig, S.J., Old, L.J., Smyth, M.J., and Schreiber, R.D. (2007). Adaptive immunity maintains occult cancer in an equilibrium state. Nature *450*, 903–907.

Kordon, E.C., and Smith, G.H. (1998). An entire functional mammary gland may comprise the progeny from a single cell. Development *125*, 1921–1930.

Koyanagi, M., Takahashi, J., Arakawa, Y., Doi, D., Fukuda, H., Hayashi, H., Narumiya, S., and Hashimoto, N. (2008). Inhibition of the Rho/ROCK pathway reduces apoptosis during transplantation of embryonic stem cell-derived neural precursors. J. Neurosci. Res. *86*, 270–280.

Krause, S., Maffini, M. V., Soto, A.M., and Sonnenschein, C. (2008). A Novel 3D *In Vitro* Culture Model to Study Stromal–Epithelial Interactions in the Mammary Gland. Tissue Eng. Part C Methods *14*, 261–271.

Krepela, E., Procházka, J., Kárová, B., Cermák, J., and Roubková, H. (1998). Cysteine proteases and cysteine protease inhibitors in non-small cell lung cancer. Neoplasma *45*, 318–331.

Kreuzaler, P.A., Staniszewska, A.D., Li, W., Omidvar, N., Kedjouar, B., Turkson, J., Poli, V., Flavell, R.A., Clarkson, R.W., and Watson, C.J. (2011). Stat3 controls lysosomal-mediated cell death in vivo. Nat Cell Biol *13*, 303–309.

Kusuma, N., Anderson, R.L., and Pouliot, N. (2011). Laminin α5-derived peptides modulate the properties of metastatic breast tumour cells. Clin. Exp. Metastasis *28*, 909–921.

Kwon, J., Eom, K.-Y., Koo, T.R., Kim, B.H., Kang, E., Kim, S.-W., Kim, Y.J., Park, S.Y., and Kim, I.A. (2017). A Prognostic Model for Patients with Triple-Negative Breast Cancer: Importance of the Modified Nottingham Prognostic Index and Age. J. Breast Cancer *20*, 65–73.

Kyo, S., Nakamura, M., Kiyono, T., Maida, Y., Kanaya, T., Tanaka, M., Yatabe, N., and Inoue, M. (2003). Successful immortalization of endometrial glandular cells with normal structural and

functional characteristics. Am. J. Pathol. *163*, 2259–2269.

Lafkas, D., Rodilla, V., Huyghe, M., Mourao, L., Kiaris, H., and Fre, S. (2013). Notch3 marks clonogenic mammary luminal progenitor cells in vivo. J Cell Biol *203*, 47–56.

Lam, M.T., and Longaker, M.T. (2012). Comparison of several attachment methods for human iPS, embryonic and adipose-derived stem cells for tissue engineering. J. Tissue Eng. Regen. Med. *6 Suppl 3*, s80-6.

Landskroner-Eiger, S., Park, J., Israel, D., Pollard, J.W., and Scherer, P.E. (2010). Morphogenesis of the developing mammary gland: stage-dependent impact of adipocytes. Dev. Biol. *344*, 968–978.

Lane, T.F., and Leder, P. (1997). Wnt-10b directs hypermorphic development and transformation in mammary glands of male and female mice. Oncogene *15*, 2133–2144.

Lawyer, T., McIntosh, K., Clavijo, C., Potekhina, L., and Mann, B.K. (2012). Formulation Changes Affect Material Properties and Cell Behavior in HA-Based Hydrogels. Int. J. Cell Biol. *2012*, 737421.

Lebeau, J., and Goubin, G. (1987). Amplification of the epidermal growth factor receptor gene in the BT20 breast carcinoma cell line. Int. J. Cancer *40*, 189–191.

Lee, M., and Vasioukhin, V. (2008). Cell polarity and cancer - cell and tissue polarity as a non-canonical tumor suppressor. J. Cell Sci. *121*, 1141–1150.

Lee, G.Y., Kenny, P.A., Lee, E.H., and Bissell, M.J. (2007). Three-dimensional culture models of normal and malignant breast epithelial cells. Nat. Methods *4*, 359–365.

Lee, M.-S., Kim, S., Kim, B.G., Won, C., Nam, S.H., Kang, S., Kim, H.-J., Kang, M., Ryu, J., Song, H.E., et al. (2014a). Snail1 induced in breast cancer cells in 3D collagen I gel environment suppresses cortactin and impairs effective invadopodia formation. Biochim. Biophys. Acta - Mol. Cell Res. *1843*, 2037–2054.

Lee, S.Y., Jeong, E.K., Ju, M.K., Jeon, H.M., Kim, M.Y., Kim, C.H., Park, H.G., Han, S.I., and Kang, H.S. (2017). Induction of metastasis, cancer stem cell phenotype, and oncogenic metabolism in cancer cells by ionizing radiation. Mol. Cancer *16*, 10.

Lee, Y., Jung, W.H., and Koo, J.S. (2015). Adipocytes can induce epithelial-mesenchymal transition in breast cancer cells. Breast Cancer Res. Treat. *153*, 323–335.

Lee, Y.-H., Mottillo, E.P., and Granneman, J.G. (2014b). Adipose tissue plasticity from WAT to BAT and in between. Biochim. Biophys. Acta - Mol. Basis Dis. *1842*, 358–369.

Lee, Y.-L., Lee, K.-F., Xu, J.-S., Wang, Y.-L., Tsao, S.-W., and Yeung, W.S.B. (2001). Establishment and characterization of an immortalized human oviductal cell line. Mol. Reprod. Dev. *59*, 400–409.

Levental, K.R., Yu, H., Kass, L., Lakins, J.N., Egeblad, M., Erler, J.T., Fong, S.F.T.T., Csiszar, K., Giaccia, A., Weninger, W., et al. (2009). Matrix Crosslinking Forces Tumor Progression by Enhancing Integrin Signaling. Cell *139*, 891–906.

Levy, S., Herberman, R., Lippman, M., and d'Angelo, T. (1987). Correlation of stress factors with sustained depression of natural killer cell activity and predicted prognosis in patients with breast cancer. J. Clin. Oncol. *5*, 348–353.

Li, D., Ambrogio, L., Shimamura, T., Kubo, S., Takahashi, M., Chirieac, L.R., Padera, R.F., Shapiro, G.I., Baum, A., Himmelsbach, F., et al. (2008). BIBW2992, an irreversible EGFR/HER2 inhibitor highly effective in preclinical lung cancer models. Oncogene *27*, 4702–4711.

Li, D., Zheng, W., and Qu, J.Y. (2011). Integrated multiplex CARS and two-photon fluorescence microscopy for imaging biological systems. A. Periasamy, K. König, and P.T.C. So, eds. p. 790315.

Li, J., Hua, X., Jones, A.C., Williams, S., Jin, Z., Fisher, J., and Wilcox, R.K. (2016). The influence of the representation of collagen fibre organisation on the cartilage contact mechanics of the hip joint. J. Biomech. *49*, 1679–1685.

Li, Q., Xia, J., Yao, Y., Gong, D., Shi, H., and Zhou, Q. (2013). Sulforaphane inhibits mammary adipogenesis by targeting adipose mesenchymal stem cells. Breast Cancer Res. Treat. *141*, 317–324.

Li, S., Van Den Diepstraten, C., D'Souza, S.J., Chan, B.M.C., and Pickering, J.G. (2003). Vascular smooth muscle cells orchestrate the assembly of type I collagen via alpha2beta1 integrin, RhoA, and fibronectin polymerization. Am. J. Pathol. *163*, 1045–1056.

Li, W., Ferguson, B.J., Khaled, W.T., Tevendale, M., Stingl, J., Poli, V., Rich, T., Salomoni, P., and Watson, C.J. (2009). PML depletion disrupts normal mammary gland development and skews the composition of the mammary luminal cell progenitor pool. Proc. Natl. Acad. Sci. U. S. A. *106*, 4725–4730.

Li, Y., Hively, W.P., and Varmus, H.E. (2000). Use of MMTV-Wnt-1 transgenic mice for studying the genetic basis of breast cancer. Oncogene *19*, 1002–1009.

Liang, C.-C., Park, A.Y., and Guan, J.-L. (2007). In vitro scratch assay: a convenient and inexpensive method for analysis of cell migration in vitro. Nat. Protoc. *2*, 329–333.

Liebscher, S., Koi, L., Löck, S., Muders, M.H., and Krause, M. (2017). The HIV protease and PI3K/Akt inhibitor nelfinavir does not improve the curative effect of fractionated irradiation in PC-3 prostate cancer in vitro and in vivo. Clin. Transl. Radiat. Oncol. *2*, 7–12.

Lim, E., Wu, D., Pal, B., Bouras, T., Asselin-Labat, M.-L., Vaillant, F., Yagita, H., Lindeman, G.J., Smyth, G.K., and Visvader, J.E. (2010). Transcriptome analyses of mouse and human mammary cell subpopulations reveal multiple conserved genes and pathways. Breast Cancer Res. *12*, R21.

Ling, C., Svensson, L., Odén, B., Weijdegård, B., Edén, B., Edén, S., and Billig, H. (2003). Identification of Functional Prolactin (PRL) Receptor Gene Expression: PRL Inhibits Lipoprotein Lipase Activity in Human White Adipose Tissue. J. Clin. Endocrinol. Metab. *88*, 1804–1808.

Linnemann, J.R., Miura, H., Meixner, L.K., Irmler, M., Kloos, U.J., Hirschi, B., Bartsch, H.S., Sass, S., Beckers, J., Theis, F.J., et al. (2015). Quantification of regenerative potential in primary human mammary epithelial cells. Development *142*, 3239–3251.

Liu, F., Pawliwec, A., Feng, Z., Yasruel, Z., Lebrun, J.-J., and Ali, S. (2015). Prolactin/Jak2 directs apical/basal polarization and luminal linage maturation of mammary epithelial cells through regulation of the Erk1/2 pathway. Stem Cell Res. *15*, 376–383.

Liu, X., Ory, V., Chapman, S., Yuan, H., Albanese, C., Kallakury, B., Timofeeva, O.A., Nealon, C., Dakic, A., Simic, V., et al. (2012). ROCK Inhibitor and Feeder Cells Induce the Conditional Reprogramming of Epithelial Cells. Am. J. Pathol. *180*, 599–607.

Lloyd-Lewis, B., Davis, F.M., Harris, O.B., Hitchcock, J.R., Lourenco, F.C., Pasche, M., and Watson, C.J. (2016). Imaging the mammary gland and mammary tumours in 3D: optical tissue clearing and immunofluorescence methods. Breast Cancer Res. *18*, 127.

Lo, H.-W., Hsu, S.-C., Xia, W., Cao, X., Shih, J.-Y., Wei, Y., Abbruzzese, J.L., Hortobagyi, G.N., and Hung, M.-C. (2007). Epidermal Growth Factor Receptor Cooperates with Signal Transducer and Activator of

Transcription 3 to Induce Epithelial-Mesenchymal Transition in Cancer Cells via Up-regulation of TWIST Gene Expression. Cancer Res. *67*, 9066–9076.

Lopez-Knowles, E., Zardawi, S.J., McNeil, C.M., Millar, E.K.A., Crea, P., Musgrove, E.A., Sutherland, R.L., and O'Toole, S.A. (2010). Cytoplasmic Localization of  -Catenin is a Marker of Poor Outcome in Breast Cancer Patients. Cancer Epidemiol. Biomarkers Prev. *19*, 301–309.

Lumachi, F., Santeufemia, D.A., and Basso, S.M. (2015). Current medical treatment of estrogen receptor-positive breast cancer. World J. Biol. Chem. *6*, 231.

Lundberg, A.S., Randell, S.H., Stewart, S.A., Elenbaas, B., Hartwell, K.A., Brooks, M.W., Fleming, M.D., Olsen, J.C., Miller, S.W., Weinberg, R.A., et al. (2002). Immortalization and transformation of primary human airway epithelial cells by gene transfer. Oncogene *21*, 4577–4586.

Lundgren, K., Nordenskjöld, B., and Landberg, G. (2009). Hypoxia, Snail and incomplete epithelial-mesenchymal transition in breast cancer. Br. J. Cancer *101*, 1769–1781.

Malhotra, G.K., Zhao, X., Edwards, E., Kopp, J.L., Naramura, M., Sander, M., Band, H., and Band, V. (2014). The role of Sox9 in mouse mammary gland development and maintenance of mammary stem and luminal progenitor cells. BMC Dev. Biol. *14*, 47.

Mali, R., Ramdas, B., Ma, P., Shi, J., Munugalavadla, V., Sims, E., Wei, L., Vemula, S., Nabinger, S., Goodwin, C., et al. (2011). Rho Kinase Regulates the Survival and Transformation of Cells Bearing Oncogenic Forms of KIT, FLT3, and BCR-ABL. Cancer Cell *20*, 357–369.

Mao, L., Yuan, L., Slakey, L.M., Jones, F.E., Burow, M.E., Hill, S.M., Anderson, M., Collins, A., Dai, J., Yuan, L., et al. (2010). Inhibition of breast cancer cell invasion by melatonin is mediated through regulation of the p38 mitogen-activated protein kinase signaling pathway. Breast Cancer Res. 2010 126 *168*, 155–163.

Mariman, E.C.M., and Wang, P. (2010). Adipocyte extracellular matrix composition, dynamics and role in obesity. Cell. Mol. Life Sci. *67*, 1277–1292.

Marzan, C. V., Kupumbati, T.S., Bertran, S.P., Samuels, T., Leibovitch, B., Mira-y-Lopez, R., Ossowski, L., and Farias, E.F. (2011). Adipocyte derived paracrine mediators of mammary ductal morphogenesis controlled by retinoic acid receptors. Dev. Biol. *349*, 125–136.

Matsumoto, M., Nishinakagawa, H., Kurohmaru, M., and Hayashi, Y. (1995). Effects of estrogen and progesterone on the parenchyma and blood vessels of the mammary gland in ovariectomized adult mice. J. Vet. Med. Sci. *57*, 39–44.

McSherry, E.A., Brennan, K., Hudson, L., Hill, A.D., and Hopkins, A.M. (2011). Breast cancer cell migration is regulated through junctional adhesion molecule-A-mediated activation of Rap1 GTPase. Breast Cancer Res. *13*, R31.

McWhorter, F.Y., Wang, T., Nguyen, P., Chung, T., and Liu, W.F. (2013). Modulation of macrophage phenotype by cell shape. Proc. Natl. Acad. Sci. U. S. A. *110*, 17253–17258.

Mehner, C., Miller, E., Nassar, A., Bamlet, W.R., Radisky, E.S., and Radisky, D.C. (2015). Tumor cell expression of MMP3 as a prognostic factor for poor survival in pancreatic, pulmonary, and mammary carcinoma. Genes Cancer *6*, 480–489.

Mercier, I., Casimiro, M.C., Wang, C., Rosenberg, A.L., Quong, J., Minkeu, A., Allen, K.G., Danilo, C., Sotgia, F., Bonuccelli, G., et al. (2008). Human breast cancer-associated fibroblasts (CAFs) show caveolin-1 downregulation and RB tumor suppressor functional inactivation: Implications for the

response to hormonal therapy. Cancer Biol. Ther. *7*, 1212–1225.

Meshel, A.S., Wei, Q., Adelstein, R.S., and Sheetz, M.P. (2005). Basic mechanism of three-dimensional collagen fibre transport by fibroblasts. Nat. Cell Biol. *7*, 157–164.

Minsky, M. (1988). Memoir on inventing the confocal scanning microscope. Scanning *10*, 128–138.

Monteiro, J., Gaspar, C., Richer, W., Franken, P.F., Sacchetti, A., Joosten, R., Idali, A., Brandao, J., Decraene, C., and Fodde, R. (2014). Cancer stemness in Wnt-driven mammary tumorigenesis. Carcinogenesis *35*, 2–13.

Montesano, R., Soriano, J. V, Fialka, I., and Orci, L. (1998). Isolation of EpH4 mammary epithelial cell subpopulations which differ in their morphogenetic properties. In Vitro Cell. Dev. Biol. Anim. *34*, 468–477.

Moore, N., Houghton, J., and Lyle, S. (2012). Slow-Cycling Therapy-Resistant Cancer Cells. Stem Cells Dev. *21*, 1822–1830.

Morales, C.P., Holt, S.E., Ouellette, M., Kaur, K.J., Yan, Y., Wilson, K.S., White, M.A., Wright, W.E., and Shay, J.W. (1999). Absence of cancer-associated changes in human fibroblasts immortalized with telomerase. Nat. Genet. *21*, 115–118.

Morales, F.C., Hayashi, Y., van Pelt, C.S., and Georgescu, M.-M. (2012). NHERF1/EBP50 controls lactation by establishing basal membrane polarity complexes with prolactin receptor. Cell Death Dis. *3*, e391.

Morgan, D.G., and Forsyth, P.A. (1999). Spatial and temporal expression of insulin-like growth factor-I, insulin-like growth factor-II and the insulin-like growth factor-I receptor in the sheep fetal mammary gland. J. Dairy Res.

Morgan, M.R., Humphries, M.J., and Bass, M.D. (2007). Synergistic control of cell adhesion by integrins and syndecans. Nat. Rev. Mol. Cell Biol. *8*, 957–969.

Mori, H., Lo, A.T., Inman, J.L., Alcaraz, J., Ghajar, C.M., Mott, J.D., Nelson, C.M., Chen, C.S., Zhang, H., Bascom, J.L., et al. (2013). Transmembrane/cytoplasmic, rather than catalytic, domains of Mmp14 signal to MAPK activation and mammary branching morphogenesis via binding to integrin β1. Development *140*, 343–352.

Mori, S., Kiuchi, S., Ouchi, A., Hase, T., and Murase, T. (2014). Characteristic expression of extracellular matrix in subcutaneous adipose tissue development and adipogenesis; comparison with visceral adipose tissue. Int. J. Biol. Sci. *10*, 825–833.

Muller, W.J., Sinn, E., Pattengale, P.K., Wallace, R., and Leder, P. (1988). Single-step induction of mammary adenocarcinoma in transgenic mice bearing the activated c-neu oncogene. Cell *54*, 105–115.

Murshed, M., Smyth, N., Miosge, N., Karolat, J., Krieg, T., Paulsson, M., and Nischt, R. (2000). The absence of nidogen 1 does not affect murine basement membrane formation. Mol. Cell. Biol. *20*, 7007–7012.

Nagai, T., Worawattanamateekul, W., Suzuki, N., Nakamura, T., Ito, T., Fujiki, K., Nakao, M., and Yano, T. (2000). Isolation and characterization of collagen from rhizostomous jellyfish (Rhopilema asamushi). Food Chem. *70*, 205–208.

Nagelkerke, A., Bussink, J., Mujcic, H., Wouters, B.G., Lehmann, S., Sweep, F.C.G.J., and Span, P.N.

(2013). Hypoxia stimulates migration of breast cancer cells via the PERK/ATF4/LAMP3-arm of the unfolded protein response. Breast Cancer Res. *15*, R2.

Narijauskaitė, B., Palevičius, A., Gaidys, R., Janušas, G., and Sakalys, R. (2013). Polycarbonate as an elasto-plastic material model for simulation of the microstructure hot imprint process. Sensors (Basel). *13*, 11229–11242.

Nash, C.E., Mavria, G., Baxter, E.W., Holliday, D.L., Tomlinson, D.C., Treanor, D., Novitskaya, V., Berditchevski, F., Hanby, A.M., and Speirs, V. (2015). Development and characterisation of a 3D multi-cellular in vitro model of normal human breast: a tool for cancer initiation studies. Oncotarget *6*, 13731–13741.

Navin, N., Kendall, J., Troge, J., Andrews, P., Rodgers, L., McIndoo, J., Cook, K., Stepansky, A., Levy, D., Esposito, D., et al. (2011). Tumour evolution inferred by single-cell sequencing. Nature *472*, 90–94.

Naylor, M.J., Li, N., Cheung, J., Lowe, E.T., Lambert, E., Marlow, R., Wang, P., Schatzmann, F., Wintermantel, T., Schüetz, G., et al. (2005). Ablation of beta1 integrin in mammary epithelium reveals a key role for integrin in glandular morphogenesis and differentiation. J. Cell Biol. *171*, 717–728.

Neve, R.M., Chin, K., Fridlyand, J., Yeh, J., Baehner, F.L., Fevr, T., Clark, L., Bayani, N., Coppe, J.-P., Tong, F., et al. (2006). A collection of breast cancer cell lines for the study of functionally distinct cancer subtypes. Cancer Cell *10*, 515–527.

Ng, C.K., Martelotto, L.G., Gauthier, A., Wen, H.-C., Piscuoglio, S., Lim, R.S., Cowell, C.F., Wilkerson, P.M., Wai, P., Rodrigues, D.N., et al. (2015). Intra-tumor genetic heterogeneity and alternative driver genetic alterations in breast cancers with heterogeneous HER2 gene amplification. Genome Biol. *16*, 107.

Nguyen-Ngoc, K.-V., and Ewald, A.J. (2013). Mammary ductal elongation and myoepithelial migration are regulated by the composition of the extracellular matrix. J. Microsc. *251*, 212–223.

Nguyen-Ngoc, K.-V., Shamir, E.R., Huebner, R.J., Beck, J.N., Cheung, K.J., and Ewald, A.J. (2015). 3D culture assays of murine mammary branching morphogenesis and epithelial invasion. Methods Mol. Biol. *1189*, 135–162.

Nik-Zainal, S., Davies, H., Staaf, J., Ramakrishna, M., Glodzik, D., Zou, X., Martincorena, I., Alexandrov, L.B., Martin, S., Wedge, D.C., et al. (2016). Landscape of somatic mutations in 560 breast cancer whole-genome sequences. Nature *534*, 47–54.

Nim, H.T., Furtado, M.B., Ramialison, M., and Boyd, S.E. (2017). Combinatorial Ranking of Gene Sets to Predict Disease Relapse: The Retinoic Acid Pathway in Early Prostate Cancer. Front. Oncol. *7*, 30.

Noro, A., Sillat, T., Virtanen, I., Ingerpuu, S., Bäck, N., Konttinen, Y.T., and Korhonen, M. (2013). Laminin production and basement membrane deposition by mesenchymal stem cells upon adipogenic differentiation. J. Histochem. Cytochem. *61*, 719–730.

Nowell, P.C. (1976). The clonal evolution of tumor cell populations. Science *194*, 23–28.

Nurcombe, V., Smart, C.E., Chipperfield, H., Cool, S.M., Boilly, B., and Hondermarck, H. (2000). The proliferative and migratory activities of breast cancer cells can be differentially regulated by heparan sulfates. J. Biol. Chem. *275*, 30009–30018.

O'Brien, J., Lyons, T., Monks, J., Lucia, M.S., Wilson, R.S., Hines, L., Man, Y., Borges, V., and Schedin,

P. (2010). Alternatively Activated Macrophages and Collagen Remodeling Characterize the Postpartum Involuting Mammary Gland across Species. Am. J. Pathol. *176*, 1241–1255.

O'Brien, J., Martinson, H., Durand-Rougely, C., and Schedin, P. (2012). Macrophages are crucial for epithelial cell death and adipocyte repopulation during mammary gland involution. Development *139*, 269–275.

O'Donnell, M.E., McCavert, M., Carson, J., Mullan, F.J., Whiteside, M.W., and Garstin, W.I. (2009). Non-epithelial malignancies and metastatic tumours of the breast. Ulster Med. J. *78*, 105–112.

Öhlund, D., Franklin, O., Lundberg, E., Lundin, C., and Sund, M. (2013). Type IV collagen stimulates pancreatic cancer cell proliferation, migration, and inhibits apoptosis through an autocrine loop. BMC Cancer *13*, 154.

Ojima, K., Oe, M., Nakajima, I., Muroya, S., and Nishimura, T. (2016). Dynamics of protein secretion during adipocyte differentiation. FEBS Open Bio *6*, 816–826.

Oloumi, A., Maidan, M., Lock, F.E., Tearle, H., McKinney, S., Muller, W.J., Aparicio, S.A., and Dedhar, S. (2010). Cooperative signaling between Wnt1 and integrin-linked kinase induces accelerated breast tumor development. Breast Cancer Res. *12*, R38.

Olson, H., Betton, G., Robinson, D., Thomas, K., Monro, A., Kolaja, G., Lilly, P., Sanders, J., Sipes, G., Bracken, W., et al. (2000). Concordance of the Toxicity of Pharmaceuticals in Humans and in Animals. Regul. Toxicol. Pharmacol. *32*, 56–67.

Omi, H., Okamoto, A., Nikaido, T., Urashima, M., Kawaguchi, R., Umehara, N., Sugiura, K., Saito, M., Kiyono, T., and Tanaka, T. (2009). Establishment of an immortalized human extravillous trophoblast cell line by retroviral infection of E6/E7/hTERT and its transcriptional profile during hypoxia and reoxygenation. Int. J. Mol. Med. *23*, 229–236.

Paget, S. (1889). THE DISTRIBUTION OF SECONDARY GROWTHS IN CANCER OF THE BREAST. Lancet *133*, 571–573.

Palecek, S.P., Loftus, J.C., Ginsberg, M.H., Lauffenburger, D.A., and Horwitz, A.F. (1997). Integrin-ligand binding properties govern cell migration speed through cell-substratum adhesiveness. Nature *385*, 537–540.

Paňková, K., Rösel, D., Novotný, M., and Brábek, J. (2010). The molecular mechanisms of transition between mesenchymal and amoeboid invasiveness in tumor cells. Cell. Mol. Life Sci. *67*, 63–71.

Park, C.C., Zhang, H., Pallavicini, M., Gray, J.W., Baehner, F., Park, C.J., and Bissell, M.J. (2006). Beta1 integrin inhibitory antibody induces apoptosis of breast cancer cells, inhibits growth, and distinguishes malignant from normal phenotype in three dimensional cultures and in vivo. Cancer Res. *66*, 1526–1535.

Paszek, M.J., Zahir, N., Johnson, K.R., Lakins, J.N., Rozenberg, G.I., Gefen, A., Reinhart-King, C.A., Margulies, S.S., Dembo, M., Boettiger, D., et al. (2005). Tensional homeostasis and the malignant phenotype. Cancer Cell *8*, 241–254.

Patanaphan, V., Salazar, O.M., and Risco, R. (1988). Breast cancer: metastatic patterns and their prognosis. South. Med. J. *81*, 1109–1112.

Patani, N., Barbashina, V., Lambros, M.B.K., Gauthier, A., Mansour, M., Mackay, A., and Reis-Filho, J.S. (2011). Direct evidence for concurrent morphological and genetic heterogeneity in an invasive ductal carcinoma of triple-negative phenotype. J. Clin. Pathol. *64*, 822–828.

Patsialou, A., Bravo-Cordero, J.J., Wang, Y., Entenberg, D., Liu, H., Clarke, M., and Condeelis, J.S. (2013). Intravital multiphoton imaging reveals multicellular streaming as a crucial component of in vivo cell migration in human breast tumors. IntraVital *2*, e25294.

Pawelec, K.M., Husmann, A., Best, S.M., and Cameron, R.E. (2014). A design protocol for tailoring ice-templated scaffold structure. J. R. Soc. Interface *11*, 20130958.

Perou, C.M., Sørlie, T., Eisen, M.B., van de Rijn, M., Jeffrey, S.S., Rees, C.A., Pollack, J.R., Ross, D.T., Johnsen, H., Akslen, L.A., et al. (2000). Molecular portraits of human breast tumours. Nature *406*, 747–752.

Perry, S.W., Schueckler, J.M., Burke, K., Arcuri, G.L., and Brown, E.B. (2013). Stromal matrix metalloprotease-13 knockout alters Collagen I structure at the tumor-host interface and increases lung metastasis of C57BL/6 syngeneic E0771 mammary tumor cells. BMC Cancer *13*, 411.

Petrie, R.J., Gavara, N., Chadwick, R.S., and Yamada, K.M. (2012). Nonpolarized signaling reveals two distinct modes of 3D cell migration. J. Cell Biol. *197*, 439–455.

Peyri, N., Berard, M., Fauvel-Lafeve, F., Trochon, V., Arbeille, B., Lu, H., Legrand, C., and Crepin, M. (2009). Breast tumor cells transendothelial migration induces endothelial cell anoikis through extracellular matrix degradation. Anticancer Res. *29*, 2347–2355.

Pfefferle, A.D., Herschkowitz, J.I., Usary, J., Harrell, J.C., Spike, B.T., Adams, J.R., Torres-Arzayus, M.I., Brown, M., Egan, S.E., Wahl, G.M., et al. (2013). Transcriptomic classification of genetically engineered mouse models of breast cancer identifies human subtype counterparts. Genome Biol. *14*, R125.

Picon-Ruiz, M., Pan, C., Drews-Elger, K., Jang, K., Besser, A.H., Zhao, D., Morata-Tarifa, C., Kim, M., Ince, T.A., Azzam, D.J., et al. (2016). Interactions between Adipocytes and Breast Cancer Cells Stimulate Cytokine Production and Drive Src/Sox2/miR-302b–Mediated Malignant Progression. Cancer Res. *76*, 491–504.

Piltti, J., Varjosalo, M., Qu, C., Häyrinen, J., and Lammi, M.J. (2015). Rho-kinase inhibitor Y-27632 increases cellular proliferation and migration in human foreskin fibroblast cells. Proteomics *15*, 2953–2965.

Pinnell, S.R., and Martin, G.R. (1968). The cross-linking of collagen and elastin: enzymatic conversion of lysine in peptide linkage to alpha-aminoadipic-delta-semialdehyde (allysine) by an extract from bone. Proc. Natl. Acad. Sci. U. S. A. *61*, 708–716.

Pinner, S., and Sahai, E. (2008). PDK1 regulates cancer cell motility by antagonising inhibition of ROCK1 by RhoE. Nat. Cell Biol. *10*, 127–137.

Pinto, D., Gregorieff, A., Begthel, H., and Clevers, H. (2003). Canonical Wnt signals are essential for homeostasis of the intestinal epithelium. Genes Dev. *17*, 1709.

Pittenger, M.F., Mackay, A.M., Beck, S.C., Jaiswal, R.K., Douglas, R., Mosca, J.D., Moorman, M.A., Simonetti, D.W., Craig, S., and Marshak, D.R. (1999). Multilineage potential of adult human mesenchymal stem cells. Science *284*, 143–147.

Ponti, D., Costa, A., Zaffaroni, N., Pratesi, G., Petrangolini, G., Coradini, D., Pilotti, S., Pierotti, M.A., and Daidone, M.G. (2005). Isolation and In vitro Propagation of Tumorigenic Breast Cancer Cells with Stem/Progenitor Cell Properties. Cancer Res. *65*.

Poola, I., DeWitty, R.L., Marshalleck, J.J., Bhatnagar, R., Abraham, J., and Leffall, L.D. (2005).

Identification of MMP-1 as a putative breast cancer predictive marker by global gene expression analysis. Nat. Med. *11*, 481–483.

Poschl, E., Schlötzer-Schrehardt, U., Brachvogel, B., Saito, K., Ninomiya, Y., and Mayer, U. (2004). Collagen IV is essential for basement membrane stability but dispensable for initiation of its assembly during early development. Development *131*, 1619–1628.

Poujade, M., Grasland-Mongrain, E., Hertzog, a, Jouanneau, J., Chavrier, P., Ladoux, B., Buguin, a, and Silberzan, P. (2007). Collective migration of an epithelial monolayer in response to a model wound. Proc. Natl. Acad. Sci. U. S. A. *104*, 15988–15993.

Prater, M.D., Petit, V., Alasdair Russell, I., Giraddi, R.R., Shehata, M., Menon, S., Schulte, R., Kalajzic, I., Rath, N., Olson, M.F., et al. (2014). Mammary stem cells have myoepithelial cell properties. Nat Cell Biol *16*, 942–950.

Prest, S.J., Rees, R.C., Murdoch, C., Marshall, J.F., Cooper, P.A., Bibby, M., Li, G., and Ali, S.A. (1999). Chemokines induce the cellular migration of MCF-7 human breast carcinoma cells: subpopulations of tumour cells display positive and negative chemotaxis and differential in vivo growth potentials. Clin. Exp. Metastasis *17*, 389–396.

Prince, J.M., Klinowska, T.C.M., Marshman, E., Lowe, E.T., Mayer, U., Miner, J., Aberdam, D., Vestweber, D., Gusterson, B., and Streuli, C.H. (2002). Cell-matrix interactions during development and apoptosis of the mouse mammary gland in vivo. Dev. Dyn. *223*, 497–516.

Provenzano, P.P., Eliceiri, K.W., Campbell, J.M., Inman, D.R., White, J.G., and Keely, P.J. (2006). Collagen reorganization at the tumor-stromal interface facilitates local invasion. BMC Med *4*, 38.

Provenzano, P.P., Inman, D.R., Eliceiri, K.W., Trier, S.M., and Keely, P.J. (2008a). Contact guidance mediated three-dimensional cell migration is regulated by Rho/ROCK-dependent matrix reorganization. Biophys J *95*, 5374–5384.

Provenzano, P.P., Inman, D.R., Eliceiri, K.W., Knittel, J.G., Yan, L., Rueden, C.T., White, J.G., and Keely, P.J. (2008b). Collagen density promotes mammary tumor initiation and progression. BMC Med. *6*, 11.

Puchalapalli, M., Zeng, X., Mu, L., Anderson, A., Hix Glickman, L., Zhang, M., Sayyad, M.R., Mosticone Wangensteen, S., Clevenger, C. V., and Koblinski, J.E. (2016). NSG Mice Provide a Better Spontaneous Model of Breast Cancer Metastasis than Athymic (Nude) Mice. PLoS One *11*, e0163521.

Pudney, J., and Anderson, D. (1995). Effects of fixation and paraffin embedding on the immunohistological detection of cell-associated HIV-1 by different monoclonal antibodies. J. Histochem. Cytochem. *43*, 857–862.

Qu, Y., Han, B., Yu, Y., Yao, W., Bose, S., Karlan, B.Y., Giuliano, A.E., and Cui, X. (2015). Evaluation of MCF10A as a Reliable Model for Normal Human Mammary Epithelial Cells. PLoS One *10*, e0131285.

Quintana, E., Shackleton, M., Foster, H.R., Fullen, D.R., Sabel, M.S., Johnson, T.M., and Morrison, S.J. (2010). Phenotypic Heterogeneity among Tumorigenic Melanoma Cells from Patients that Is Reversible and Not Hierarchically Organized. Cancer Cell *18*, 510–523.

Rabbany, S.Y., Heissig, B., Hattori, K., and Rafii, S. (2003). Molecular pathways regulating mobilization of marrow-derived stem cells for tissue revascularization. Trends Mol. Med. *9*, 109–117.

Radisic, M., Malda, J., Epping, E., Geng, W., Langer, R., and Vunjak-Novakovic, G. (2006). Oxygen gradients correlate with cell density and cell viability in engineered cardiac tissue. Biotechnol.

Bioeng. *93*, 332–343.

Raviraj, V., Fok, S., Zhao, J., Chien, H.-Y., Lyons, J.G., Thompson, E.W., and Soon, L. (2012). Regulation of ROCK1 via Notch1 during breast cancer cell migration into dense matrices. BMC Cell Biol. *13*, 12.

Ray, A., Slama, Z.M., Morford, R.K., Madden, S.A., and Provenzano, P.P. (2017a). Enhanced Directional Migration of Cancer Stem Cells in 3D Aligned Collagen Matrices. Biophys. J. *112*, 1023–1036.

Ray, A., Lee, O., Win, Z., Edwards, R.M., Alford, P.W., Kim, D.-H., and Provenzano, P.P. (2017b). Anisotropic forces from spatially constrained focal adhesions mediate contact guidance directed cell migration. Nat. Commun. *8*, 14923.

Reichardt, H.M., Horsch, K., Gröne, H.J., Kolbus, A., Beug, H., Hynes, N., and Schütz, G. (2001). Mammary gland development and lactation are controlled by different glucocorticoid receptor activities. Eur. J. Endocrinol. *145*, 519–527.

Riching, K.M., Cox, B.L., Salick, M.R., Pehlke, C., Riching, A.S., Ponik, S.M., Bass, B.R., Crone, W.C., Jiang, Y., Weaver, A.M., et al. (2014). 3D collagen alignment limits protrusions to enhance breast cancer cell persistence. Biophys. J. *107*, 2546–2558.

Rider, L., Oladimeji, P., and Diakonova, M. (2013). PAK1 regulates breast cancer cell invasion through secretion of matrix metalloproteinases in response to prolactin and three-dimensional collagen IV. Mol. Endocrinol. *27*, 1048–1064.

Rios, A.C., Fu, N.Y., Lindeman, G.J., and Visvader, J.E. (2014). In situ identification of bipotent stem cells in the mammary gland. Nature *506*, 322–327.

Rodriguez, L.G., Wu, X., and Guan, J.-L. (2005). Wound-healing assay. Methods Mol. Biol. *294*, 23–29.

Romanov, S.R., Kozakiewicz, B.K., Holst, C.R., Stampfer, M.R., Haupt, L.M., and Tlsty, T.D. (2001). Normal human mammary epithelial cells spontaneously escape senescence and acquire genomic changes. Nature *409*, 633–637.

Rosel, D., Brabek, J., Tolde, O., Mierke, C.T., Zitterbart, D.P., Raupach, C., Bicanova, K., Kollmannsberger, P., Pankova, D., Vesely, P., et al. (2008). Up-Regulation of Rho/ROCK Signaling in Sarcoma Cells Drives Invasion and Increased Generation of Protrusive Forces. Mol. Cancer Res. *6*, 1410–1420.

Rosman, D.S., Phukan, S., Huang, C.-C., and Pasche, B. (2008). TGFBR1*6A enhances the migration and invasion of MCF-7 breast cancer cells through RhoA activation. Cancer Res. *68*, 1319–1328.

Rovero, S., Amici, A., Di Carlo, E., Bei, R., Nanni, P., Quaglino, E., Porcedda, P., Boggio, K., Smorlesi, A., Lollini, P.L., et al. (2000). DNA vaccination against rat her-2/Neu p185 more effectively inhibits carcinogenesis than transplantable carcinomas in transgenic BALB/c mice. J. Immunol. *165*, 5133–5142.

Rowan, B.G., Gimble, J.M., Sheng, M., Anbalagan, M., Jones, R.K., Frazier, T.P., Asher, M., Lacayo, E.A., Friedlander, P.L., Kutner, R., et al. (2014). Human Adipose Tissue-Derived Stromal/Stem Cells Promote Migration and Early Metastasis of Triple Negative Breast Cancer Xenografts. PLoS One *9*, e89595.

Rucker, R.B., and Murray, J. (1978). Cross-linking amino acids in collagen and elastin. Am. J. Clin. Nutr. *31*, 1221–1236.

Runnebaum, I.B., Nagarajan, M., Bowman, M., Soto, D., and Sukumar, S. (1991). Mutations in p53 as potential molecular markers for human breast cancer. Proc. Natl. Acad. Sci. U. S. A. *88*, 10657–10661.

Ruprecht, V., Wieser, S., Callan-Jones, A., Smutny, M., Morita, H., Sako, K., Barone, V., Ritsch-Marte, M., Sixt, M., Voituriez, R., et al. (2015). Cortical Contractility Triggers a Stochastic Switch to Fast Amoeboid Cell Motility. Cell *160*, 673–685.

Rusnak, D.W., Lackey, K., Affleck, K., Wood, E.R., Alligood, K.J., Rhodes, N., Keith, B.R., Murray, D.M., Knight, W.B., Mullin, R.J., et al. (2001). The Effects of the Novel, Reversible Epidermal Growth Factor Receptor/ErbB-2 Tyrosine Kinase Inhibitor, GW2016, on the Growth of Human Normal and Tumor-derived Cell Lines in Vitro and in Vivo. Mol. Cancer Ther. *1*.

Russell, W.C., Graham, F.L., Smiley, J., and Nairn, R. (1977). Characteristics of a Human Cell Line Transformed by DNA from Human Adenovirus Type 5. J. Gen. Virol. *36*, 59–72.

Sahai, E., and Marshall, C.J. (2003). Differing modes of tumour cell invasion have distinct requirements for Rho/ROCK signalling and extracellular proteolysis. Nat. Cell Biol. *5*, 711–719.

Saito, K., Ozawa, Y., Hibino, K., and Ohta, Y. (2012). FilGAP, a Rho/Rho-associated protein kinase-regulated GTPase-activating protein for Rac, controls tumor cell migration. Mol. Biol. Cell *23*, 4739–4750.

Sakakura, T., Sakagami, Y., and Nishizuka, Y. (1982). Dual origin of mesenchymal tissues participating in mouse mammary gland embryogenesis. Dev. Biol. *91*, 202–207.

Salic, A., and Mitchison, T.J. (2008). A chemical method for fast and sensitive detection of DNA synthesis in vivo. Proc. Natl. Acad. Sci. *105*, 2415–2420.

Sang, L., Coller, H.A., and Roberts, J.M. (2008). Control of the Reversibility of Cellular Quiescence by the Transcriptional Repressor HES1. Science (80-. ). *321*, 1095–1100.

Santiago, J.A., Pogemiller, R., and Ogle, B.M. (2009). Heterogeneous Differentiation of Human Mesenchymal Stem Cells in Response to Extended Culture in Extracellular Matrices. Tissue Eng. Part A *15*, 3911–3922.

dos Santos, C.O., Rebbeck, C., Rozhkova, E., Valentine, A., Samuels, A., Kadiri, L.R., Osten, P., Harris, E.Y., Uren, P.J., Smith, A.D., et al. (2013). Molecular hierarchy of mammary differentiation yields refined markers of mammary stem cells. Proc. Natl. Acad. Sci. *110*, 7123–7130.

dos Santos, P., Zanetti, J.S., Ribeiro-Silva, A., and Beltrão, E.I. (2012). Beta 1 integrin predicts survival in breast cancer: a clinicopathological and immunohistochemical study. Diagn. Pathol. *7*, 104.

Sanz-Moreno, V., Gadea, G., Ahn, J., Paterson, H., Marra, P., Pinner, S., Sahai, E., and Marshall, C.J. (2008). Rac Activation and Inactivation Control Plasticity of Tumor Cell Movement. Cell *135*, 510–523.

Saretzki, G., Sitte, N., Merkel, U., Wurm, R.E., and von Zglinicki, T. (1999). Telomere shortening triggers a p53-dependent cell cycle arrest via accumulation of G-rich single stranded DNA fragments. Oncogene *18*, 5148–5158.

Sargeant, T.J., Lloyd-Lewis, B., Resemann, H.K., Ramos-Montoya, A., Skepper, J., and Watson, C.J. (2014). Stat3 controls cell death during mammary gland involution by regulating uptake of milk fat globules and lysosomal membrane permeabilization. Nat. Cell Biol. *16*, 1057–1068.

Sastre-Garau, X., Jouve, M., Asselain, B., Vincent-Salomon, A., Beuzeboc, P., Dorval, T., Durand, J.-C., Fourquet, A., and Pouillart, P. (1996). Infiltrating lobular carcinoma of the breast: Clinicopathologic analysis of 975 cases with reference to data on conservative therapy and metastatic patterns. Cancer *77*, 113–120.

Sato, H., Higashi, S., and Miyazaki, K. (2015). Amino-terminal fragments of laminin γ2 chain stimulate migration of metastatic breast cancer cells by interacting with CD44. Clin. Exp. Metastasis *32*, 405–415.

Scheele, C.L.G.J., Hannezo, E., Muraro, M.J., Zomer, A., Langedijk, N.S.M., van Oudenaarden, A., Simons, B.D., and van Rheenen, J. (2017). Identity and dynamics of mammary stem cells during branching morphogenesis. Nature *542*, 313–317.

Scherer, W.F., Syverton, J.T., and Gey, G.O. (1953). Studies on the propagation in vitro of poliomyelitis viruses. IV. Viral multiplication in a stable strain of human malignant epithelial cells (strain HeLa) derived from an epidermoid carcinoma of the cervix. J. Exp. Med. *97*, 695–710.

Schor, S.L., Ellis, I.R., Jones, S.J., Baillie, R., Seneviratne, K., Clausen, J., Motegi, K., Vojtesek, B., Kankova, K., Furrie, E., et al. (2003). Migration-stimulating factor: a genetically truncated onco-fetal fibronectin isoform expressed by carcinoma and tumor-associated stromal cells. Cancer Res. *63*, 8827–8836.

Schwan, J., Kwaczala, A.T., Ryan, T.J., Bartulos, O., Ren, Y., Sewanan, L.R., Morris, A.H., Jacoby, D.L., Qyang, Y., and Campbell, S.G. (2016). Anisotropic engineered heart tissue made from laser-cut decellularized myocardium. Sci. Rep. *6*, 32068.

Seagroves, T.N., Peacock, D.L., Liao, D., Schwab, L.P., Krueger, R., Handorf, C.R., Haase, V.H., and Johnson, R.S. (2010). VHL deletion impairs mammary alveologenesis but is not sufficient for mammary tumorigenesis. Am. J. Pathol. *176*, 2269–2282.

Senaratne, L.S., Park, P.J., and Kim, S.K. (2006). Isolation and characterization of collagen from brown backed toadfish (Lagocephalus gloveri) skin. Bioresour. Technol. *97*, 191–197.

Shackleton, M., Vaillant, F., Simpson, K.J., Stingl, J., Smyth, G.K., Asselin-Labat, M.-L., Wu, L., Lindeman, G.J., and Visvader, J.E. (2006). Generation of a functional mammary gland from a single stem cell. Nature *439*, 84–88.

Sharma, S. V., Lee, D.Y., Li, B., Quinlan, M.P., Takahashi, F., Maheswaran, S., McDermott, U., Azizian, N., Zou, L., Fischbach, M.A., et al. (2010). A Chromatin-Mediated Reversible Drug-Tolerant State in Cancer Cell Subpopulations. Cell *141*, 69–80.

Shehata, M., Teschendorff, A., Sharp, G., Novcic, N., Russell, A., Avril, S., Prater, M., Eirew, P., Caldas, C., Watson, C.J., et al. (2012). Phenotypic and functional characterization of the luminal cell hierarchy of the mammary gland. Breast Cancer Res *14*, R134.

Shehata, M., van Amerongen, R., Zeeman, A.L., Giraddi, R.R., and Stingl, J. (2014). The influence of tamoxifen on normal mouse mammary gland homeostasis. Breast Cancer Res. *16*, 411.

Shih, W., and Yamada, S. (2011). Live-cell imaging of migrating cells expressing fluorescently-tagged proteins in a three-dimensional matrix. J. Vis. Exp.

Shim, J.S., Rao, R., Beebe, K., Neckers, L., Han, I., Nahta, R., and Liu, J.O. (2012). Selective Inhibition of HER2-Positive Breast Cancer Cells by the HIV Protease Inhibitor Nelfinavir. JNCI J. Natl. Cancer Inst. *104*, 1576–1590.

Shipitsin, M., Campbell, L.L., Argani, P., Weremowicz, S., Bloushtain-Qimron, N., Yao, J., Nikolskaya, T., Serebryiskaya, T., Beroukhim, R., Hu, M., et al. (2007). Molecular Definition of Breast Tumor Heterogeneity. Cancer Cell *11*, 259–273.

Sikandar, B., Qureshi, M.A., Mirza, T., Khan, S., and Avesi, L. (2015). Differential immune cell densities in ductal carcinoma In-Situ and invasive breast cancer: Possible role of leukocytes in early stages of carcinogenesis. Pakistan J. Med. Sci. *31*, 274–279.

Sillat, T., Saat, R., Pöllänen, R., Hukkanen, M., Takagi, M., and Konttinen, Y.T. (2012). Basement membrane collagen type IV expression by human mesenchymal stem cells during adipogenic differentiation. J. Cell. Mol. Med. *16*, 1485–1495.

Da Silva, J.S., Medina, M., Zuliani, C., Di Nardo, A., Witke, W., and Dotti, C.G. (2003). RhoA/ROCK regulation of neuritogenesis via profilin IIa–mediated control of actin stability. J. Cell Biol. *162*, 1267–1279.

Singh, J.C., Jhaveri, K., and Esteva, F.J. (2014). HER2-positive advanced breast cancer: optimizing patient outcomes and opportunities for drug development. Br. J. Cancer *111*, 1888–1898.

Singh, M., Close, D.A., Mukundan, S., Johnston, P.A., and Sant, S. (2015). Production of Uniform 3D Microtumors in Hydrogel Microwell Arrays for Measurement of Viability, Morphology, and Signaling Pathway Activation. Assay Drug Dev. Technol. *13*, 570–583.

Skedros, J.G., Dayton, M.R., Sybrowsky, C.L., Bloebaum, R.D., and Bachus, K.N. (2006). The influence of collagen fiber orientation and other histocompositional characteristics on the mechanical properties of equine cortical bone. J. Exp. Biol. *209*, 3025–3042.

Slamon, D.J., Clark, G.M., Wong, S.G., Levin, W.J., Ullrich, A., and McGuire, W.L. (1987). Human breast cancer: correlation of relapse and survival with amplification of the HER-2/neu oncogene. Science *235*, 177–182.

Smith, B.N., Burton, L.J., Henderson, V., Randle, D.D., Morton, D.J., Smith, B.A., Taliaferro-Smith, L., Nagappan, P., Yates, C., Zayzafoon, M., et al. (2014). Snail Promotes Epithelial Mesenchymal Transition in Breast Cancer Cells in Part via Activation of Nuclear ERK2. PLoS One *9*, e104987.

Smyth, N., Vatansever, H.S., Murray, P., Meyer, M., Frie, C., Paulsson, M., and Edgar, D. (1999). Absence of basement membranes after targeting the LAMC1 gene results in embryonic lethality due to failure of endoderm differentiation. J. Cell Biol. *144*, 151–160.

Soares, C.P., Midlej, V., Oliveira, M.E.W. de, Benchimol, M., Costa, M.L., and Mermelstein, C. (2012). 2D and 3D-Organized Cardiac Cells Shows Differences in Cellular Morphology, Adhesion Junctions, Presence of Myofibrils and Protein Expression. PLoS One *7*, e38147.

Sokol, E.S., Miller, D.H., Breggia, A., Spencer, K.C., Arendt, L.M., and Gupta, P.B. (2016). Growth of human breast tissues from patient cells in 3D hydrogel scaffolds. Breast Cancer Res. *18*.

Somaiah, C., Kumar, A., Mawrie, D., Sharma, A., Patil, S.D., Bhattacharyya, J., Swaminathan, R., and Jaganathan, B.G. (2015). Collagen Promotes Higher Adhesion, Survival and Proliferation of Mesenchymal Stem Cells. PLoS One *10*, e0145068.

Somiari, S.B., Somiari, R.I., Heckman, C.M., Olsen, C.H., Jordan, R.M., Russell, S.J., and Shriver, C.D. (2006). Circulating MMP2 and MMP9 in breast cancer -- potential role in classification of patients into low risk, high risk, benign disease and breast cancer categories. Int. J. Cancer *119*, 1403–1411.

Sorlie, T., Perou, C.M., Tibshirani, R., Aas, T., Geisler, S., Johnsen, H., Hastie, T., Eisen, M.B., van de

Rijn, M., Jeffrey, S.S., et al. (2001). Gene expression patterns of breast carcinomas distinguish tumor subclasses with clinical implications. Proc. Natl. Acad. Sci. *98*, 10869–10874.

Soule, H.D., Vazguez, J., Long, A., Albert, S., and Brennan, M. (1973). A human cell line from a pleural effusion derived from a breast carcinoma. J. Natl. Cancer Inst. *51*, 1409–1416.

Sousa, S., Brion, R., Lintunen, M., Kronqvist, P., Sandholm, J., Mönkkönen, J., Kellokumpu-Lehtinen, P.-L., Lauttia, S., Tynninen, O., Joensuu, H., et al. (2015). Human breast cancer cells educate macrophages toward the M2 activation status. Breast Cancer Res. *17*, 101.

Sparano, J.A., Bernardo, P., Stephenson, P., Gradishar, W.J., Ingle, J.N., Zucker, S., and Davidson, N.E. (2004). Randomized Phase III Trial of Marimastat Versus Placebo in Patients With Metastatic Breast Cancer Who Have Responding or Stable Disease After First-Line Chemotherapy: Eastern Cooperative Oncology Group Trial E2196. J. Clin. Oncol. *22*, 4683–4690.

Staatz, W.D., Walsh, J.J., Pexton, T., and Santoro, S.A. (1990). The alpha 2 beta 1 integrin cell surface collagen receptor binds to the alpha 1 (I)-CB3 peptide of collagen. J. Biol. Chem. *265*, 4778–4781.

Stewart, T., Tsai, S.C., Grayson, H., Henderson, R., and Opelz, G. (1995). Incidence of de-novo breast cancer in women chronically immunosuppressed after organ transplantation. Lancet (London, England) *346*, 796–798.

Stingl, J., Eirew, P., Ricketson, I., Shackleton, M., Vaillant, F., Choi, D., Li, H.I., and Eaves, C.J. (2006). Purification and unique properties of mammary epithelial stem cells. Nature *439*, 993–997.

Streuli, C.H., Bailey, N., and Bissell, M.J. (1991). <Control of mammary epithelial differentiation basement membrane induces tissue-specific gene expression in the absence of cell-cell interaction and morphological polarity.pdf>. J. Cell Biol. *115*, 1383–1395.

Stylianopoulos, T., Diop-Frimpong, B., Munn, L.L., and Jain, R.K. (2010). Diffusion anisotropy in collagen gels and tumors: the effect of fiber network orientation. Biophys. J. *99*, 3119–3128.

Subik, K., Lee, J.-F., Baxter, L., Strzepek, T., Costello, D., Crowley, P., Xing, L., Hung, M.-C., Bonfiglio, T., Hicks, D.G., et al. (2010). The Expression Patterns of ER, PR, HER2, CK5/6, EGFR, Ki-67 and AR by Immunohistochemical Analysis in Breast Cancer Cell Lines. Breast Cancer (Auckl). *4*, 35–41.

Sun, N., Xu, H.N., Luo, Q., and Li, L.Z. (2016). Potential Indexing of the Invasiveness of Breast Cancer Cells by Mitochondrial Redox Ratios. Adv. Exp. Med. Biol. *923*, 121–127.

Suojanen, J., Salo, T., Koivunen, E., Sorsa, T., and Pirilä, E. (2009). A novel and selective membrane type-1 matrix metalloproteinase (MT1-MMP) inhibitor reduces cancer cell motility and tumor growth. Cancer Biol. Ther. *8*, 2362–2370.

Susaki, E.A., Tainaka, K., Perrin, D., Kishino, F., Tawara, T., Watanabe, T.M., Yokoyama, C., Onoe, H., Eguchi, M., Yamaguchi, S., et al. (2014). Whole-brain imaging with single-cell resolution using chemical cocktails and computational analysis. Cell *157*, 726–739.

Susaki, E.A., Tainaka, K., Perrin, D., Yukinaga, H., Kuno, A., and Ueda, H.R. (2015). Advanced CUBIC protocols for whole-brain and whole-body clearing and imaging. Nat. Protoc. *10*, 1709–1727.

Taherian, A., Li, X., Liu, Y., and Haas, T.A. (2011). Differences in integrin expression and signaling within human breast cancer cells. BMC Cancer *11*, 293.

Takahashi, K., and Yamanaka, S. (2006). Induction of Pluripotent Stem Cells from Mouse Embryonic and Adult Fibroblast Cultures by Defined Factors. Cell *126*, 663–676.

Takeda, Y.S., and Xu, Q. (2015). Neuronal Differentiation of Human Mesenchymal Stem Cells Using Exosomes Derived from Differentiating Neuronal Cells. PLoS One *10*, e0135111.

Taketo, M., Schroeder, A.C., Mobraaten, L.E., Gunning, K.B., Hanten, G., Fox, R.R., Roderick, T.H., Stewart, C.L., Lilly, F., and Hansen, C.T. (1991). FVB/N: an inbred mouse strain preferable for transgenic analyses. Proc. Natl. Acad. Sci. U. S. A. *88*, 2065–2069.

Tan, M., Gschwantler-Kaulich, D., Grunt, T.W., Muhr, D., Wagner, R., Kölbl, H., and Singer, C.F. (2016). HER Specific TKIs Exert Their Antineoplastic Effects on Breast Cancer Cell Lines through the Involvement of STAT5 and JNK. PLoS One *11*, e0146311.

Teissedre, B., Pinderhughes, A., Incassati, A., Hatsell, S.J., Hiremath, M., and Cowin, P. (2009). MMTV-Wnt1 and -ΔN89β-catenin induce canonical signaling in distinct progenitors and differentially activate hedgehog signaling within mammary tumors. PLoS One *4*.

The MathWorks Inc. (2010). MATLAB and statistics toolbox, Release 2010b [computer software].

Theodossiou, T.A., Thrasivoulou, C., Ekwobi, C., and Becker, D.L. (2006). Second Harmonic Generation Confocal Microscopy of Collagen Type I from Rat Tendon Cryosections. Biophys. J. *91*, 4665.

Thomopoulos, S., Fomovsky, G.M., and Holmes, J.W. (2005). The development of structural and mechanical anisotropy in fibroblast populated collagen gels. J. Biomech. Eng. *127*, 742–750.

Thomopoulos, S., Fomovsky, G.M., Chandran, P.L., and Holmes, J.W. (2007). Collagen fiber alignment does not explain mechanical anisotropy in fibroblast populated collagen gels. J. Biomech. Eng. *129*, 642–650.

Thompson, C., Rahim, S., Arnold, J., and Hielscher, A. (2017). Loss of caveolin-1 alters extracellular matrix protein expression and ductal architecture in murine mammary glands. PLoS One *12*, e0172067.

Timoshenko, A. V, Xu, G., Chakrabarti, S., Lala, P.K., and Chakraborty, C. (2003). Role of prostaglandin E2 receptors in migration of murine and human breast cancer cells. Exp. Cell Res. *289*, 265–274.

Todaro, G.J., Lazar, G.K., and Green, H. (1965). The initiation of cell division in a contact-inhibited mammalian cell line. J. Cell. Comp. Physiol. *66*, 325–333.

Tomimatsu, T., Yamaguchi, M., Murakami, T., Ogura, K., Sakata, M., Mitsuda, N., Kanzaki, T., Kurachi, H., Irahara, M., Miyake, A., et al. (1997). Increase of Mouse Leptin Production by Adipose Tissue after Midpregnancy: Gestational Profile of Serum Leptin Concentration. Biochem. Biophys. Res. Commun. *240*, 213–215.

Toouli, C.D., Huschtscha, L.I., Neumann, A.A., Noble, J.R., Colgin, L.M., Hukku, B., and Reddel, R.R. (2002). Comparison of human mammary epithelial cells immortalized by simian virus 40 T-Antigen or by the telomerase catalytic subunit. Oncogene *21*, 128–139.

Trivanović, D., Kocić, J., Mojsilović, S., Krstić, A., Ilić, V., Djordjević, I.O., Santibanez, J.F., Jovcić, G., Terzić, M., and Bugarski, D. (2013). Mesenchymal stem cells isolated from peripheral blood and umbilical cord Wharton's jelly. Srp. Arh. Celok. Lek. *141*, 178–186.

Truong, D., Puleo, J., Llave, A., Mouneimne, G., Kamm, R.D., and Nikkhah, M. (2016). Breast Cancer Cell Invasion into a Three Dimensional Tumor-Stroma Microenvironment. Sci. Rep. *6*, 34094.

Tsai, C.-C., Chen, C.-L., Liu, H.-C., Lee, Y.-T., Wang, H.-W., Hou, L.-T., and Hung, S.-C. (2010).

Overexpression of hTERT increases stem-like properties and decreases spontaneous differentiation in human mesenchymal stem cell lines. J. Biomed. Sci. *17*, 64.

Tsai, J.H., Donaher, J.L., Murphy, D.A., Chau, S., and Yang, J. (2012). Spatiotemporal regulation of epithelial-mesenchymal transition is essential for squamous cell carcinoma metastasis. Cancer Cell *22*, 725–736.

Tsukamoto, A.S., Grosschedl, R., Guzman, R.C., Parslow, T., and Varmus, H.E. (1988). Expression of the int-1 gene in transgenic mice is associated with mammary gland hyperplasia and adenocarcinomas in male and female mice. Cell *55*, 619–625.

Tsutsui, T., Kumakura, S.-I., Yamamoto, A., Kanai, H., Tamura, Y., Kato, T., Anpo, M., Tahara, H., and Barrett, J.C. (2002). Association of p16(INK4a) and pRb inactivation with immortalization of human cells. Carcinogenesis *23*, 2111–2117.

Vaicik, M.K., Thyboll Kortesmaa, J., Movérare-Skrtic, S., Kortesmaa, J., Soininen, R., Bergström, G., Ohlsson, C., Chong, L.Y., Rozell, B., Emont, M., et al. (2014). Laminin α4 Deficient Mice Exhibit Decreased Capacity for Adipose Tissue Expansion and Weight Gain. PLoS One *9*, e109854.

van Amerongen, R., Bowman, A.N., and Nusse, R. (2012). Developmental Stage and Time Dictate the Fate of Wnt/β-Catenin-Responsive Stem Cells in the Mammary Gland. Cell Stem Cell *11*, 387–400.

Varia, M.A., Calkins-Adams, D.P., Rinker, L.H., Kennedy, A.S., Novotny, D.B., Fowler, W.C., and Raleigh, J.A. (1998). Pimonidazole: A Novel Hypoxia Marker for Complementary Study of Tumor Hypoxia and Cell Proliferation in Cervical Carcinoma. Gynecol. Oncol. *71*, 270–277.

Varley, M.C., Markaki, A.E., and Brooks, R.A. (2017). Effect of Rotation on Scaffold Motion and Cell Growth in Rotating Bioreactors. Tissue Eng. Part A *23*, 522–534.

Vega, S., Morales, A. V, Ocaña, O.H., Valdés, F., Fabregat, I., and Nieto, M.A. (2004). Snail blocks the cell cycle and confers resistance to cell death. Genes Dev. *18*, 1131–1143.

Velling, T., Risteli, J., Wennerberg, K., Mosher, D.F., and Johansson, S. (2002). Polymerization of type I and III collagens is dependent on fibronectin and enhanced by integrins alpha 11beta 1 and alpha 2beta 1. J. Biol. Chem. *277*, 37377–37381.

Veltmaat, J.M., Van Veelen, W., Thiery, J.P., and Bellusci, S. (2004). Identification of the mammary line in mouse byWnt10b expression. Dev. Dyn. *229*, 349–356.

Vincent, V.A.M., DeVoss, J.J., Ryan, H.S., and Murphy, G.M. (2002). Analysis of neuronal gene expression with laser capture microdissection. J. Neurosci. Res. *69*, 578–586.

Virnig, B.A., Tuttle, T.M., Shamliyan, T., and Kane, R.L. (2010). Ductal Carcinoma In Situ of the Breast: A Systematic Review of Incidence, Treatment, and Outcomes. JNCI J. Natl. Cancer Inst. *102*, 170–178.

Vishnubhotla, R., Bharadwaj, S., Sun, S., Metlushko, V., and Glover, S.C. (2012). Treatment with Y-27632, a ROCK Inhibitor, Increases the Proinvasive Nature of SW620 Cells on 3D Collagen Type 1 Matrix. Int. J. Cell Biol. *2012*, 1–7.

de Visser, K.E., Ciampricotti, M., Michalak, E.M., Tan, D.W.-M., Speksnijder, E.N., Hau, C.-S., Clevers, H., Barker, N., and Jonkers, J. (2012). Developmental stage-specific contribution of LGR5 $^{+}$ cells to basal and luminal epithelial lineages in the postnatal mammary gland. J. Pathol. *228*, 300–309.

Vitali, a., Murano, I., Zingaretti, M.C., Frontini, A., Ricquier, D., and Cinti, S. (2012). The adipose organ of obesity-prone C57BL/6J mice is composed of mixed white and brown adipocytes. J. Lipid

Res. *53*, 619–629.

Walsh, L.A., and Damjanovski, S. (2011). IGF-1 increases invasive potential of MCF 7 breast cancer cells and induces activation of latent TGF-β1 resulting in epithelial to mesenchymal transition. Cell Commun. Signal. *9*, 10.

Wang, R.N., and Rosenberg, L. (1999). Maintenance of beta-cell function and survival following islet isolation requires re-establishment of the islet-matrix relationship. J. Endocrinol. *163*, 181–190.

Wang, C., Gao, C., Meng, K., Qiao, H., Wang, Y., and Lennartz, B. (2015). Human Adipocytes Stimulate Invasion of Breast Cancer MCF-7 Cells by Secreting IGFBP-2. PLoS One *10*, e0119348.

Wang, C.-C., Lin, S.-Y., Lai, Y.-H., Liu, Y.-J., Hsu, Y.-L., and Chen, J.J.W. (2012). Dimethyl sulfoxide promotes the multiple functions of the tumor suppressor HLJ1 through activator protein-1 activation in NSCLC cells. PLoS One *7*, e33772.

Wang, D., Cai, C., Dong, X., Yu, Q.C., Zhang, X.-O., Yang, L., and Zeng, Y.A. (2014a). Identification of multipotent mammary stem cells by protein C receptor expression. Nature *517*, 81–84.

Wang, D.-Y., Fulthorpe, R., Liss, S.N., and Edwards, E.A. (2004). Identification of Estrogen-Responsive Genes by Complementary Deoxyribonucleic Acid Microarray and Characterization of a Novel Early Estrogen-Induced Gene: *EEIG1*. Mol. Endocrinol. *18*, 402–411.

Wang, H.B., Dembo, M., and Wang, Y.L. (2000). Substrate flexibility regulates growth and apoptosis of normal but not transformed cells. Am. J. Physiol. Cell Physiol. *279*, C1345-50.

Wang, P., Ballestrem, C., and Streuli, C.H. (2011). The C terminus of talin links integrins to cell cycle progression. J. Cell Biol. *195*, 499–513.

Wang, Y., Waters, J., Leung, M.L., Unruh, A., Roh, W., Shi, X., Chen, K., Scheet, P., Vattathil, S., Liang, H., et al. (2014b). Clonal evolution in breast cancer revealed by single nucleus genome sequencing. Nature *512*, 155–160.

Wang, Y., Liu, J., Ying, X., Lin, P.C., and Zhou, B.P. (2016). Twist-mediated Epithelial-mesenchymal Transition Promotes Breast Tumor Cell Invasion via Inhibition of Hippo Pathway. Sci. Rep. *6*, 24606.

Wang, Y.Y., Attané, C., Milhas, D., Dirat, B., Dauvillier, S., Guerard, A., Gilhodes, J., Lazar, I., Alet, N., Laurent, V., et al. (2017). Mammary adipocytes stimulate breast cancer invasion through metabolic remodeling of tumor cells. JCI Insight *2*, e87489.

Watanabe, K., Fallahi, M., and Dai, X. (2014). Chromatin effector Pygo2 regulates mammary tumor initiation and heterogeneity in MMTV-Wnt1 mice. Oncogene *33*, 632–642.

Waters, E.A., Cronin, K.A., Graubard, B.I., Han, P.K., and Freedman, A.N. (2010). Prevalence of tamoxifen use for breast cancer chemoprevention among U.S. women. Cancer Epidemiol. Biomarkers Prev. *19*, 443–446.

Waxler, B., and Rabito, S.F. (2003). Aprotinin: a serine protease inhibitor with therapeutic actions: its interaction with ACE inhibitors. Curr. Pharm. Des. *9*, 777–787.

Wculek, S.K., and Malanchi, I. (2015). Neutrophils support lung colonization of metastasis-initiating breast cancer cells. Nature *528*, 413–417.

Weaver, V.M., Petersen, O.W., Wang, F., Larabell, C.A., Briand, P., Damsky, C., and Bissell, M.J. (1997). Reversion of the malignant phenotype of human breast cells in three-dimensional culture and in vivo by integrin blocking antibodies. J. Cell Biol. *137*, 231–245.

Weigelin, B., Bakker, G.-J., and Friedl, P. (2012). Intravital third harmonic generation microscopy of collective melanoma cell invasion. IntraVital *1*, 32–43.

Wenstrup, R.J., Florer, J.B., Brunskill, E.W., Bell, S.M., Chervoneva, I., and Birk, D.E. (2004). Type V collagen controls the initiation of collagen fibril assembly. J. Biol. Chem. *279*, 53331–53337.

Williams, B.R., Gelman, R.A., Poppke, D.C., and Piez, K.A. (1978). Collagen fibril formation. Optimal in vitro conditions and preliminary kinetic results. J. Biol. Chem. *253*, 6578–6585.

Wiseman, B.S., Sternlicht, M.D., Lund, L.R., Alexander, C.M., Mott, J., Bissell, M.J., Soloway, P., Itohara, S., and Werb, Z. (2003). Site-specific inductive and inhibitory activities of MMP-2 and MMP-3 orchestrate mammary gland branching morphogenesis. J. Cell Biol. *162*.

Witty, J.P., Wright, J.H., and Matrisian, L.M. (1995). Matrix metalloproteinases are expressed during ductal and alveolar mammary morphogenesis, and misregulation of stromelysin-1 in transgenic mice induces unscheduled alveolar development. Mol. Biol. Cell *6*, 1287–1303.

Wolbank, S., Stadler, G., Peterbauer, A., Gillich, A., Karbiener, M., Streubel, B., Wieser, M., Katinger, H., van Griensven, M., Redl, H., et al. (2009). Telomerase immortalized human amnion- and adipose-derived mesenchymal stem cells: maintenance of differentiation and immunomodulatory characteristics. Tissue Eng. Part A *15*, 1843–1854.

Wolf, K., Mazo, I., Leung, H., Engelke, K., von Andrian, U.H., Deryugina, E.I., Strongin, A.Y., Bröcker, E.-B., and Friedl, P. (2003). Compensation mechanism in tumor cell migration. J. Cell Biol. *160*.

Wolf, K., Te Lindert, M., Krause, M., Alexander, S., Te Riet, J., Willis, A.L., Hoffman, R.M., Figdor, C.G., Weiss, S.J., and Friedl, P. (2013). Physical limits of cell migration: control by ECM space and nuclear deformation and tuning by proteolysis and traction force. J. Cell Biol. *201*, 1069–1084.

Wright, M.C., Reed-Geaghan, E.G., Bolock, A.M., Fujiyama, T., Hoshino, M., and Maricich, S.M. (2015). Unipotent, Atoh1+ progenitors maintain the Merkel cell population in embryonic and adult mice. J. Cell Biol. *208*, 367–379.

Wuidart, A., Ousset, M., Rulands, S., Simons, B.D., Van Keymeulen, A., and Blanpain, C. (2016). Quantitative lineage tracing strategies to resolve multipotency in tissue-specific stem cells. Genes Dev. *30*, 1261–1277.

Wyckoff, J.B., Pinner, S.E., Gschmeissner, S., Condeelis, J.S., Sahai, E., Condeelis, J., Kito, H., Tochigi, N., Shinbo, M., Nemori, R., et al. (2006). ROCK- and myosin-dependent matrix deformation enables protease-independent tumor-cell invasion in vivo. Curr. Biol. *16*, 1515–1523.

Xu, R., Nelson, C.M., Muschler, J.L., Veiseh, M., Vonderhaar, B.K., and Bissell, M.J. (2009). Sustained activation of STAT5 is essential for chromatin remodeling and maintenance of mammary-specific function. *184*, 57–66.

Xu, X., Hou, Y., Yin, X., Bao, L., Tang, A., Song, L., Li, F., Tsang, S., Wu, K., Wu, H., et al. (2012). Single-Cell Exome Sequencing Reveals Single-Nucleotide Mutation Characteristics of a Kidney Tumor. Cell *148*, 886–895.

Yan, K.S., Janda, C.Y., Chang, J., Zheng, G.X.Y., Larkin, K.A., Luca, V.C., Chia, L.A., Mah, A.T., Han, A., Terry, J.M., et al. (2017). Non-equivalence of Wnt and R-spondin ligands during Lgr5+ intestinal stem-cell self-renewal. Nature *545*, 238–242.

Yang, H.-S., and Hinds, P.W. (2007). pRb-mediated control of epithelial cell proliferation and Indian hedgehog expression in mouse intestinal development. BMC Dev. Biol. *7*, 6.

Yang, S., and Kim, H.-M. (2014). ROCK Inhibition Activates MCF-7 Cells. PLoS One *9*, e88489.

Yang, N., Mosher, R., Seo, S., Beebe, D., and Friedl, A. (2011). Syndecan-1 in breast cancer stroma fibroblasts regulates extracellular matrix fiber organization and carcinoma cell motility. Am. J. Pathol. *178*, 325–335.

Yang, Y., Hou, L., Li, Y., Ni, J., and Liu, L. (2013). Neuronal necrosis and spreading death in a Drosophila genetic model. Cell Death Dis. *4*, e723.

Yao, E.S., Zhang, H., Chen, Y.-Y., Lee, B., Chew, K., Moore, D., and Park, C. (2007). Increased 1 Integrin Is Associated with Decreased Survival in Invasive Breast Cancer. Cancer Res. *67*, 659–664.

Yu, M., Lee, C., Wang, M., and Tannock, I.F. (2015). Influence of the proton pump inhibitor lansoprazole on distribution and activity of doxorubicin in solid tumors. Cancer Sci. *106*, 1438–1447.

Yu, Z., Liu, M., Fu, P., Xie, M., Wang, W., and Luo, X. (2012). ROCK inhibition with Y27632 promotes the proliferation and cell cycle progression of cultured astrocyte from spinal cord. Neurochem. Int. *61*, 1114–1120.

Yurchenco, P.D., Tsilibary, E.C., Charonis, A.S., and Furthmayr, H. (1986). Models for the self-assembly of basement membrane. J. Histochem. Cytochem. *34*, 93–102.

Zagozdzon, A.M., O'Leary, P., Callanan, J.J., Crown, J., Gallagher, W.M., and Zagozdzon, R. (2012). Generation of a new bioluminescent model for visualisation of mammary tumour development in transgenic mice. BMC Cancer *12*, 209.

Zahm, J.-M., Kaplan, H., Hérard, A.-L., Doriot, F., Pierrot, D., Somelette, P., and Puchelle, E. (1997). Cell migration and proliferation during the in vitro wound repair of the respiratory epithelium. Cell Motil. Cytoskeleton *37*, 33–43.

Zebisch, K., Voigt, V., Wabitsch, M., and Brandsch, M. (2012). Protocol for effective differentiation of 3T3-L1 cells to adipocytes.

Zhang, D., and Kilian, K.A. (2013). The effect of mesenchymal stem cell shape on the maintenance of multipotency. Biomaterials *34*, 3962–3969.

Zhang, X., Podsypanina, K., Huang, S., Mohsin, S.K., Chamness, G.C., Hatsell, S., Cowin, P., Schiff, R., and Li, Y. (2005). Estrogen receptor positivity in mammary tumors of Wnt-1 transgenic mice is influenced by collaborating oncogenic mutations. Oncogene *24*, 4220–4231.

Zhang, X., Claerhout, S., Prat, A., Dobrolecki, L.E., Petrovic, I., Lai, Q., Landis, M.D., Wiechmann, L., Schiff, R., Giuliano, M., et al. (2013). A Renewable Tissue Resource of Phenotypically Stable, Biologically and Ethnically Diverse, Patient-Derived Human Breast Cancer Xenograft Models. Cancer Res. *73*, 4885–4897.

Zhang, X., Martinez, D., Koledova, Z., Qiao, G., Streuli, C.H., and Lu, P. (2014). FGF ligands of the postnatal mammary stroma regulate distinct aspects of epithelial morphogenesis. Development *141*, 3352–3362.

Zhang, Y., Goss, A.M., Cohen, E.D., Kadzik, R., Lepore, J.J., Muthukumaraswamy, K., Yang, J., DeMayo, F.J., Whitsett, J.A., Parmacek, M.S., et al. (2008). A Gata6-Wnt pathway required for epithelial stem cell development and airway regeneration. Nat. Genet. *40*, 862–870.

Zhang, Z.-Y., Teoh, S.H., Chong, W.-S., Foo, T.-T., Chng, Y.-C., Choolani, M., and Chan, J. (2009). A biaxial rotating bioreactor for the culture of fetal mesenchymal stem cells for bone tissue

engineering. Biomaterials *30*, 2694–2704.

Zhao, B., Hemann, M.T., and Lauffenburger, D.A. (2014). Intratumor heterogeneity alters most effective drugs in designed combinations. Proc. Natl. Acad. Sci. *111*, 10773–10778.

Zhu, J., and Kaufman, L.J. (2014). Collagen I self-assembly: revealing the developing structures that generate turbidity. Biophys. J. *106*, 1822–1831.

Zhu, J., Wang, H., Bishop, J.M., and Blackburn, E.H. (1999). Telomerase extends the lifespan of virus-transformed human cells without net telomere lengthening. Proc. Natl. Acad. Sci. U. S. A. *96*, 3723–3728.

Zhu, J.Y., Abate, M., Rice, P.W., and Cole, C.N. (1991). The ability of simian virus 40 large T antigen to immortalize primary mouse embryo fibroblasts cosegregates with its ability to bind to p53. J Virol *65*, 6872–6880.

Zietarska, M., Maugard, C.M., Filali-Mouhim, A., Alam-Fahmy, M., Tonin, P.N., Provencher, D.M., and Mes-Masson, A.-M. (2007). Molecular description of a 3D in vitro model for the study of epithelial ovarian cancer (EOC). Mol. Carcinog. *46*, 872–885.

Zinger, M., McFarland, M., and Ben-Jonathan, N. (2003). Prolactin Expression and Secretion by Human Breast Glandular and Adipose Tissue Explants. J. Clin. Endocrinol. Metab. *88*, 689–696.

Zumbusch, A., Holtom, G.R., and Xie, X.S. (1999). Three-Dimensional Vibrational Imaging by Coherent Anti-Stokes Raman Scattering. Phys. Rev. Lett. *82*, 4142–4145.

# Appendix A: Histology – additional controls

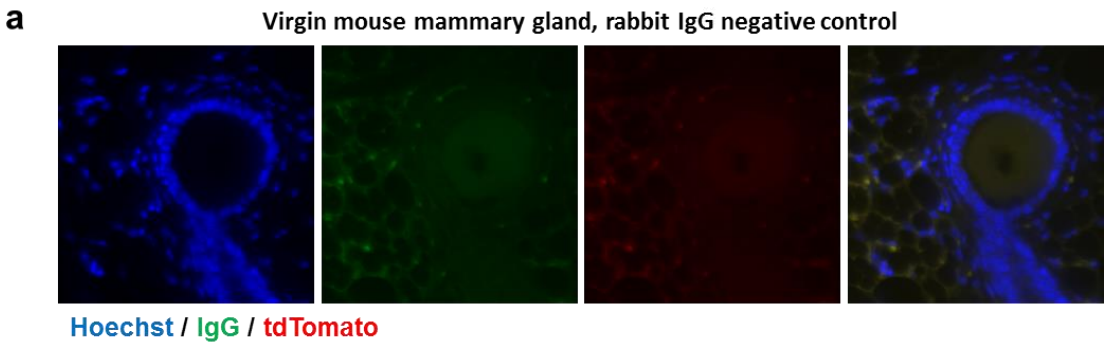


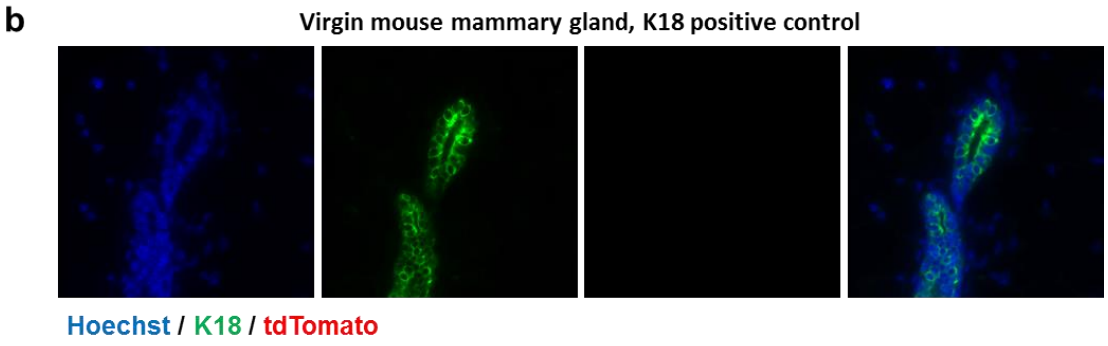


***Appendix 1: Rabbit immunoglobulin G (IgG) negative control and Cytokeratin-18 (K18) positive control***

A virgin mouse mammary gland was paraffin embedded, sectioned and stained with (a) non-specific rabbit IgG (green) or (b) anti-K18 (green) antibody. Both samples were then stained with AlexaFluor488 secondary antibody. (a) Used as a negative control to any anti-rabbit primary antibodies, IgG shows a small amount of unspecific binding in adipocytes of the gland. (b) Used as a positive control, K18 shows expected specificity to luminal cells of the mammary gland. Both (a) and (b) were also utilised as negative controls for the tdTomato fluorescent protein (red). DNA was marked with Hoechst dye (blue).

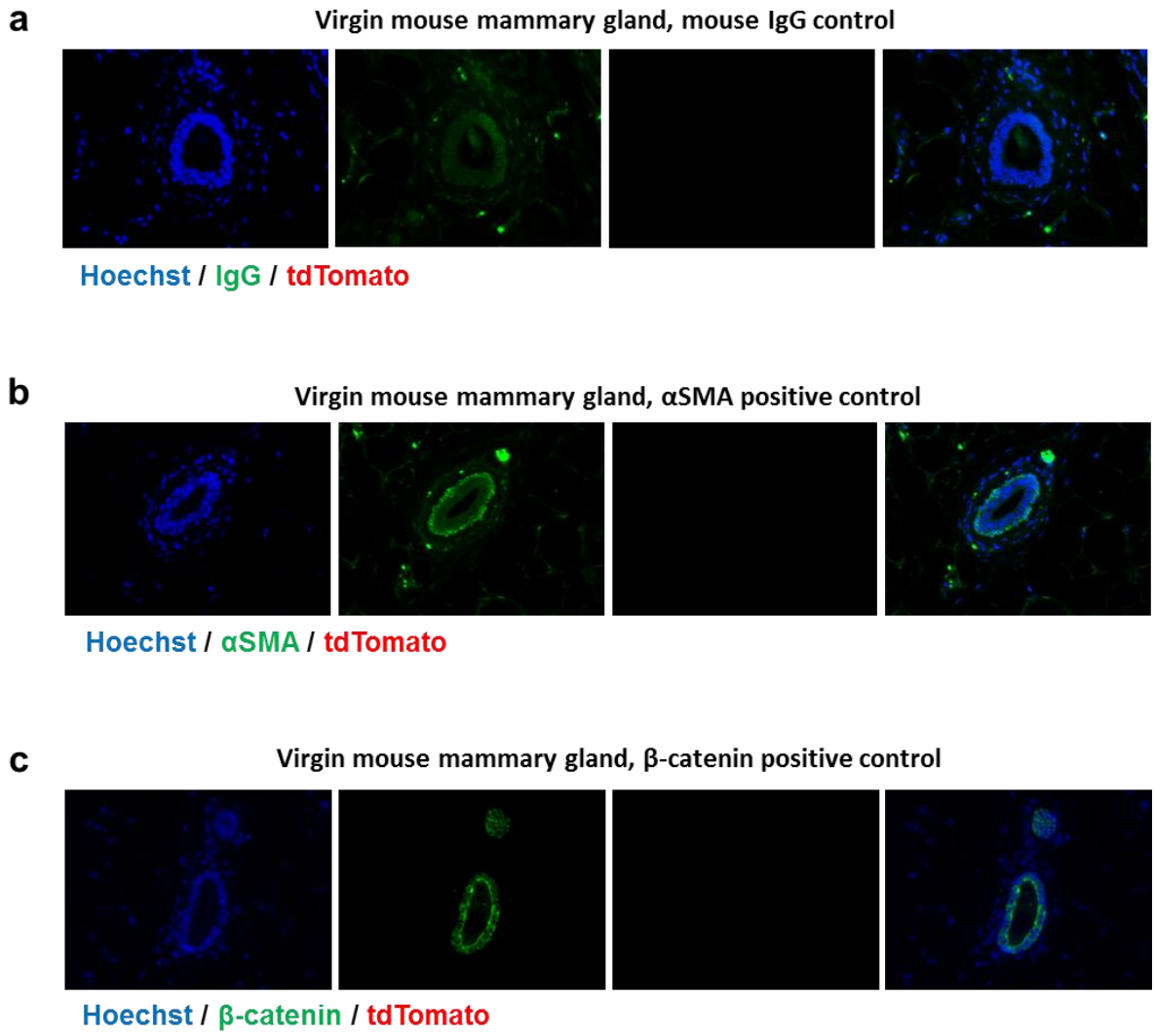


***Appendix 2: Mouse immunoglobulin G (IgG) negative control, α-smooth muscle actin (αSMA) positive control and β-catenin positive control***

A virgin mouse mammary gland was paraffin embedded, sectioned and stained with (a) non-specific mouse IgG (green), (b) anti- αSMA (green) antibody or (c) anti-β-catenin (green) antibody. All were then stained with AlexaFluor488 secondary antibody. (a) Used as a negative control to any anti-mouse antibodies, IgG shows small areas of unspecific binding with intense patches of green. (b) Used as a positive control, αSMA shows expected specificity to basal cells of the mammary gland but with similar small patches of unspecific binding observed in IgG negative control. (c) Used as a positive control, β-catenin shows expected specificity to luminal cells of the mammary gland. (a), (b) and (c) were also utilised as negative controls for the tdTomato fluorescent protein. DNA was marked with Hoechst dye (blue).

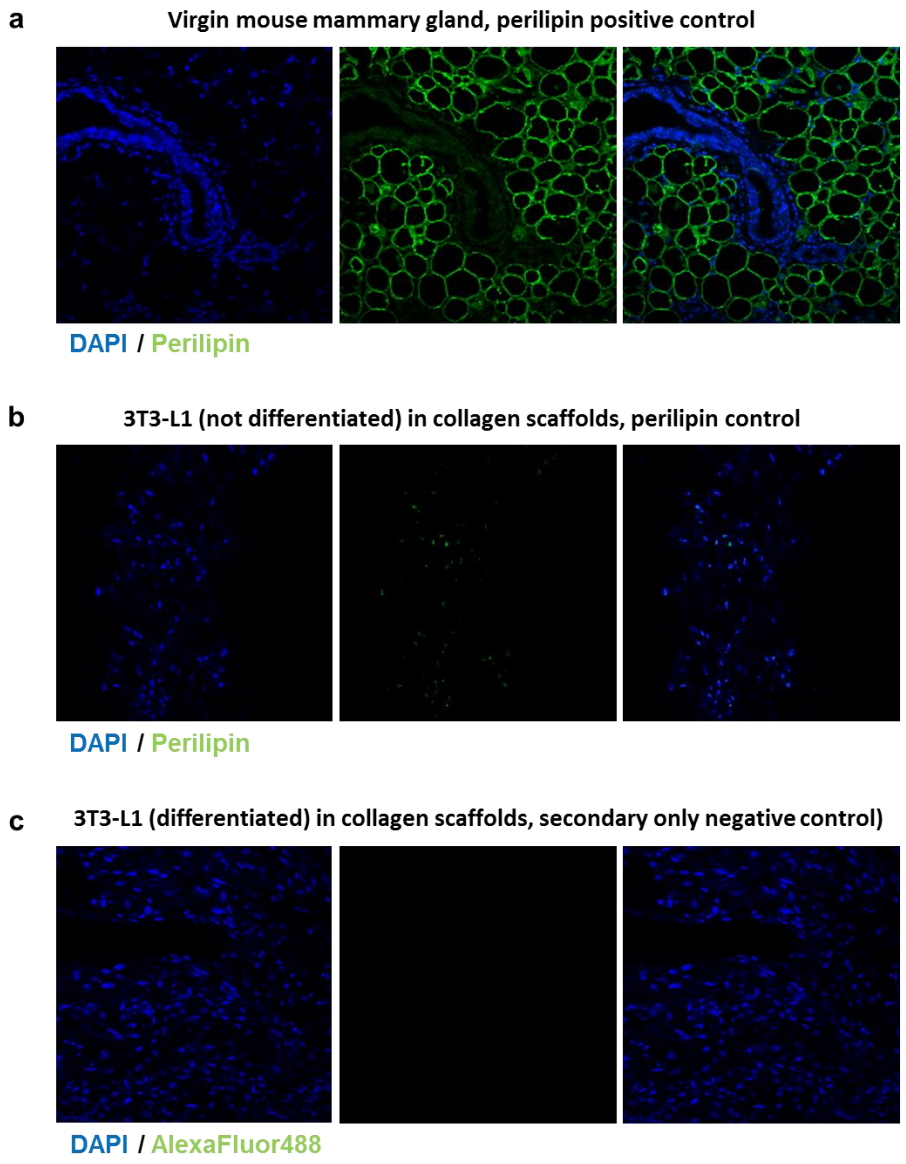


***Appendix 3: Perilipin positive control, undifferentiated 3T3-L1 perilipin control and AlexaFluor488 secondary only negative control***

(a) A virgin mouse mammary gland was paraffin embedded, sectioned and stained for anti-perilipin antibody as a positive control. As expected perilipin marked adipocyte lipid vesicles within the mammary fat pad. (b) 3T3-L1 cells were seeded into collagen scaffolds and fixed before any adipogenic media was added. Scaffolds were then whole scaffold stained using an anti-perilipin as a primary antibody. Small amounts of unspecific binding can be observed in cell nuclei. (c) 3T3-L1 cell seeded into collagen scaffolds and fixed before any adipogenic media was added. Scaffolds were then whole scaffold stained without the use of a primary antibody and was used as a secondary only control. No unspecific binding was observed. (a-c) were all stained with the secondary antibody AlexaFluor488. DNA was marked with DAPI dye (blue).

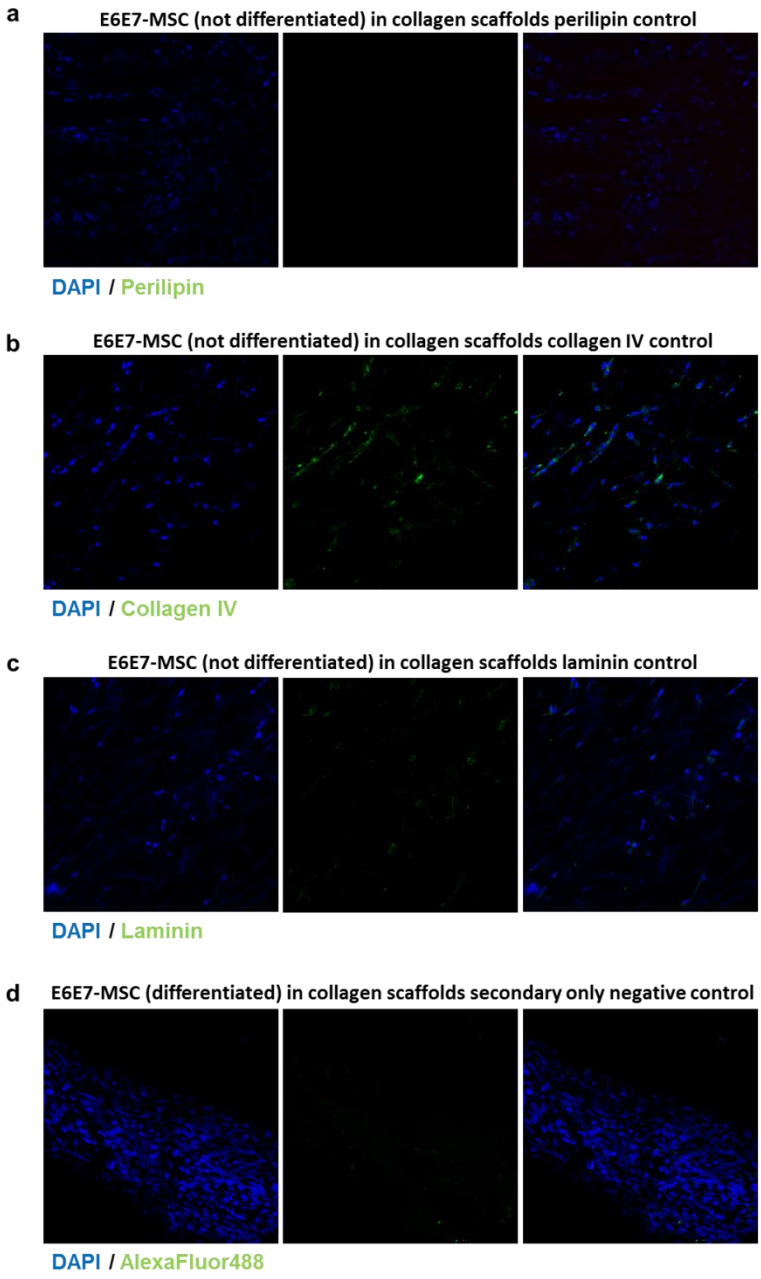


### *Appendix 4: Undifferentiated E6E7-MSC controls for perilipin, laminin and collagen IV and AlexaFluor488 secondary only negative control*

(a-c) E6E7-MSC were seeded into collagen scaffolds and fixed before any adipogenic media was added. Scaffolds were then whole scaffold stained using (a) anti-perilipin, (b) anti-collagen or (c) anti-laminin as a primary antibody. (a) No perilipin observed. (b) Small amounts of collagen IV observed. (c) No laminin observed. (d) E6E7-MSC were seeded into collagen scaffolds and fixed before any adipogenic media was added. Scaffolds were then whole scaffold stained without the use of a primary antibody. (a-d) All samples were stained with AlexaFluor488 secondary antibody. DNA was marked with DAPI dye (blue).

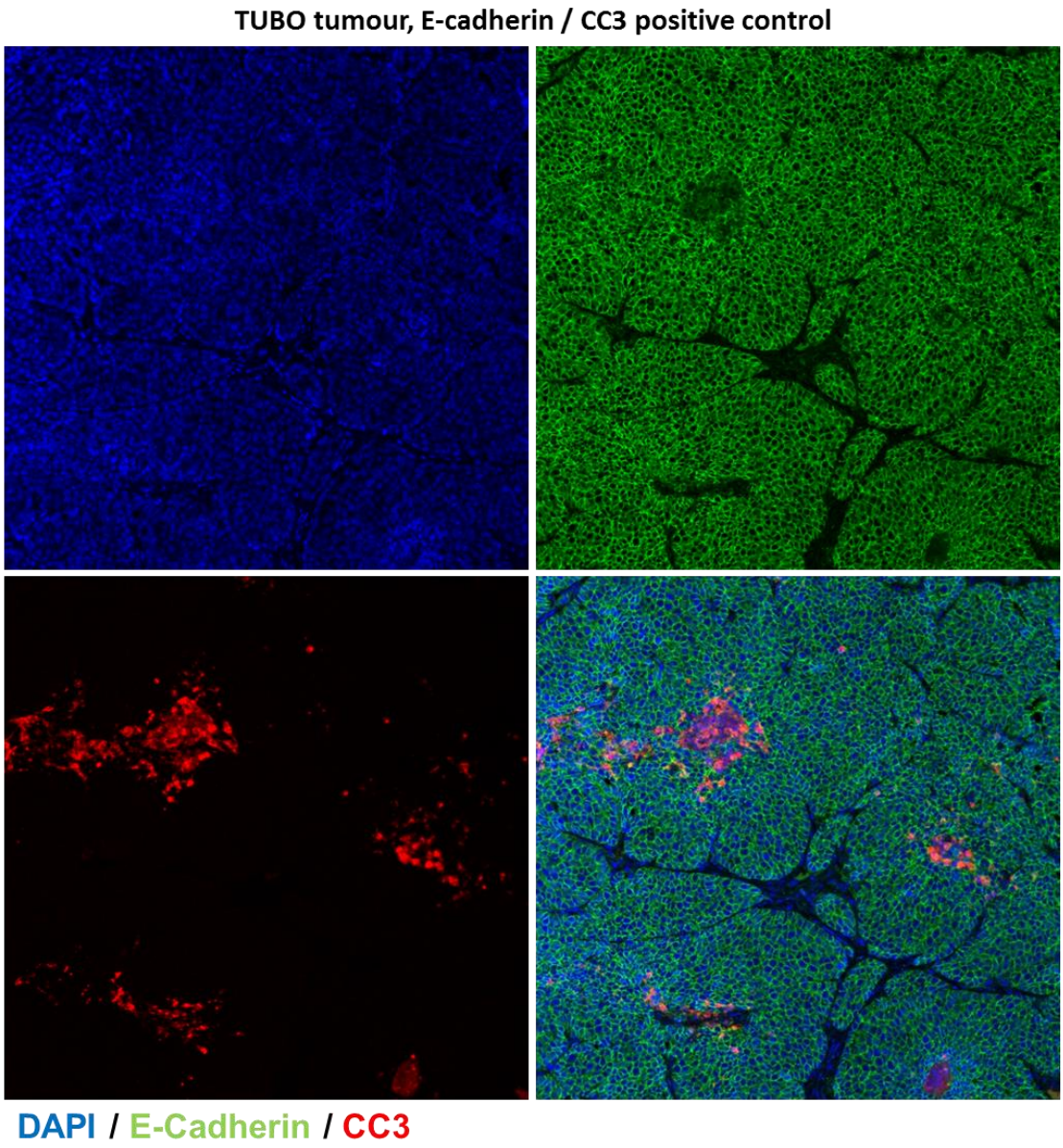


***Appendix 5: Epithelial-cadherin (E-cadherin) and cleaved caspase-3 (CC3) positive controls***

A TUBO tumour was fixed immediately following excision, paraffin embedded and sectioned. This was then stained with E-cadherin (green) and CC3 (red) as a positive control to both markers. As anticipated, membranous E-cadherin can be observed in tumour cells and patches of CC3 can be observed in regions of the tumour without close proximity to blood vessels. DNA was marked with DAPI dye (blue).

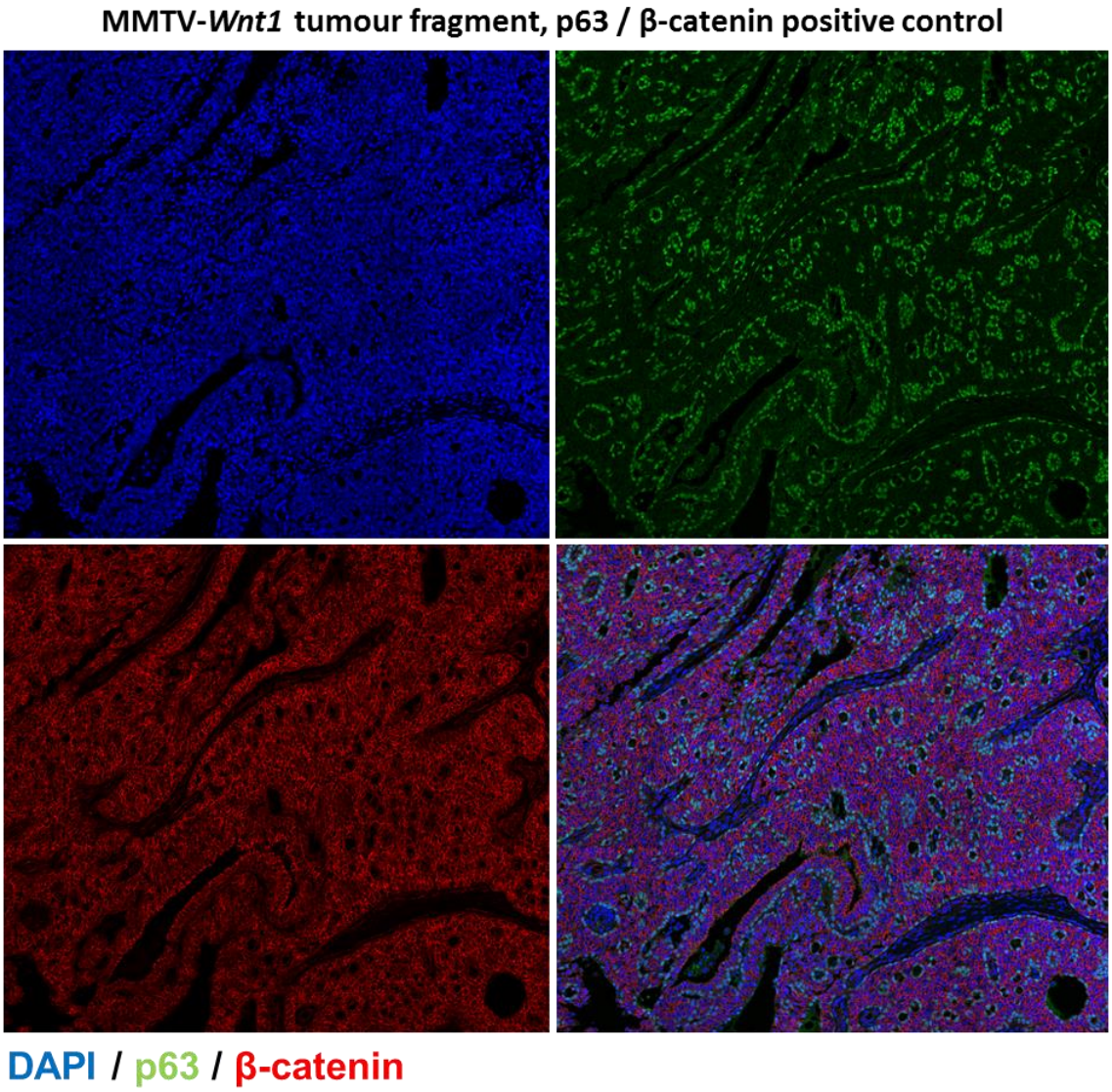


***Appendix 6: p63 and β-catenin positive controls***

An MMTV-*Wnt1* tumour was fixed immediately following excision, paraffin embedded and sectioned. This was then stained with anti-p63 (green) and anti-β-catenin (red) antibodies as positive controls to both markers. As anticipated, nuclear localisation of p63 can be observed in tumour cells with a basal epithelial cell phenotype and membranous β-catenin can be observed in tumour cells with a luminal epithelial cell phenotype. DNA was marked with DAPI dye (blue).

**MMTV-*neu/ErbB2* tumour fragment, Her2 positive control**

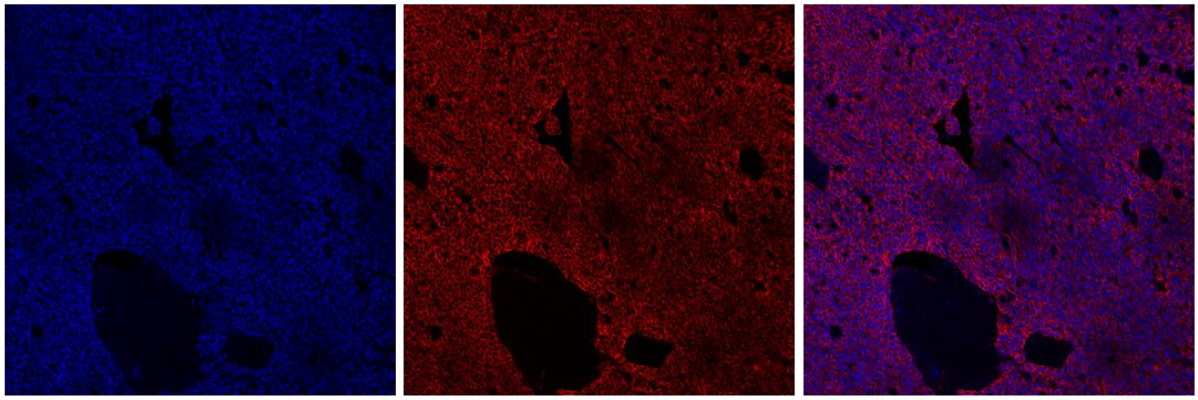

**DAPI / Her2**

### *Appendix 7: Her2 positive control*

An MMTV-*neu/ErbB2* tumour (gift from Dr. Peter Kreuzaler, Department of Biochemistry, University of Cambridge) was fixed immediately following excision, paraffin embedded and sectioned. This was then stained with anti-Her2 (red) antibody as a positive control. As anticipated, membranous Her2 can be observed in all tumour cells. DNA was marked with DAPI dye (blue).

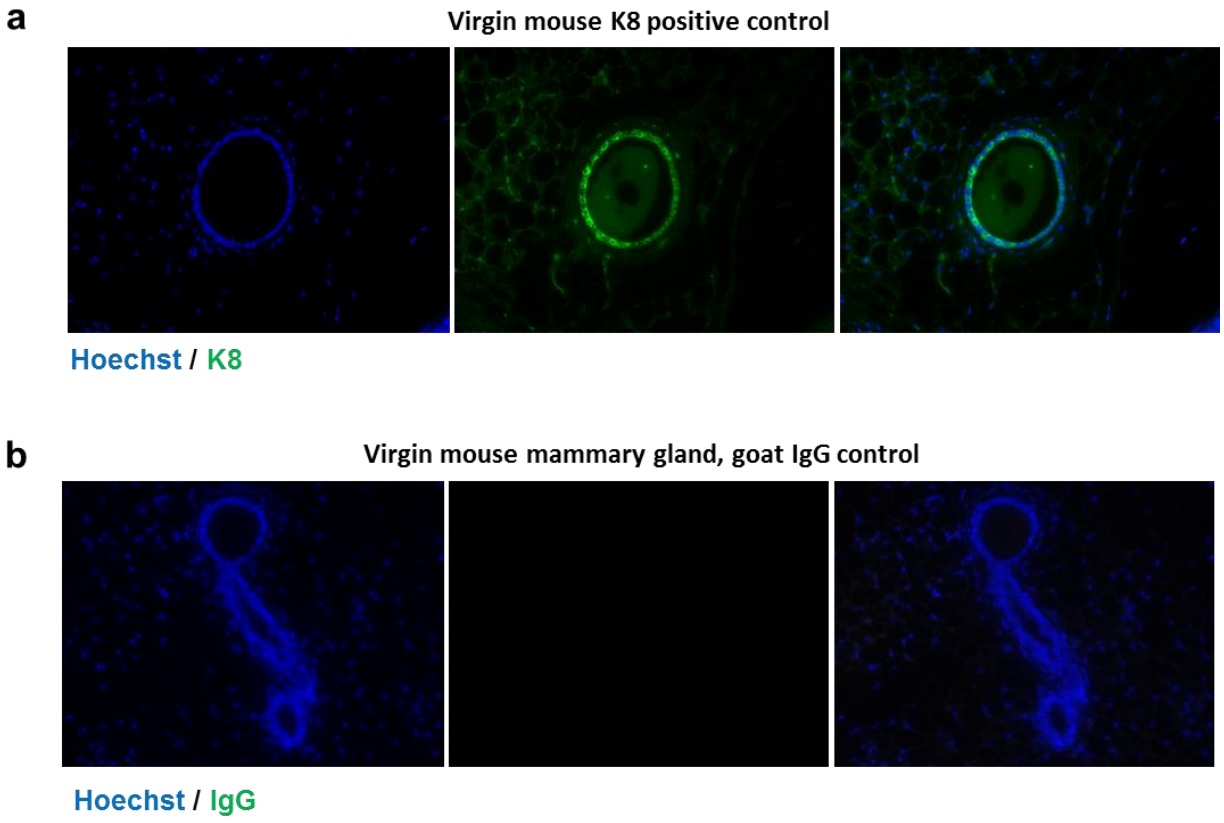


***Appendix 8: Cytokeratin-8 (K8) positive control and Goat immunoglobulin G (IgG) negative control***

A virgin mouse mammary gland was paraffin embedded, sectioned and stained with (a) non-specific goat IgG (green) or (b) anti-K8 (green) antibody. Both were then stained with AlexaFluor488 secondary antibody. (a) Used as a positive control, K8 shows anticipated specificity to luminal cells of the mammary gland with low levels of unspecific stromal staining. (b) Used as a negative control to any anti-rabbit antibodies such as K18, it shows no unspecific binding. DNA was marked with Hoechst dye (blue).

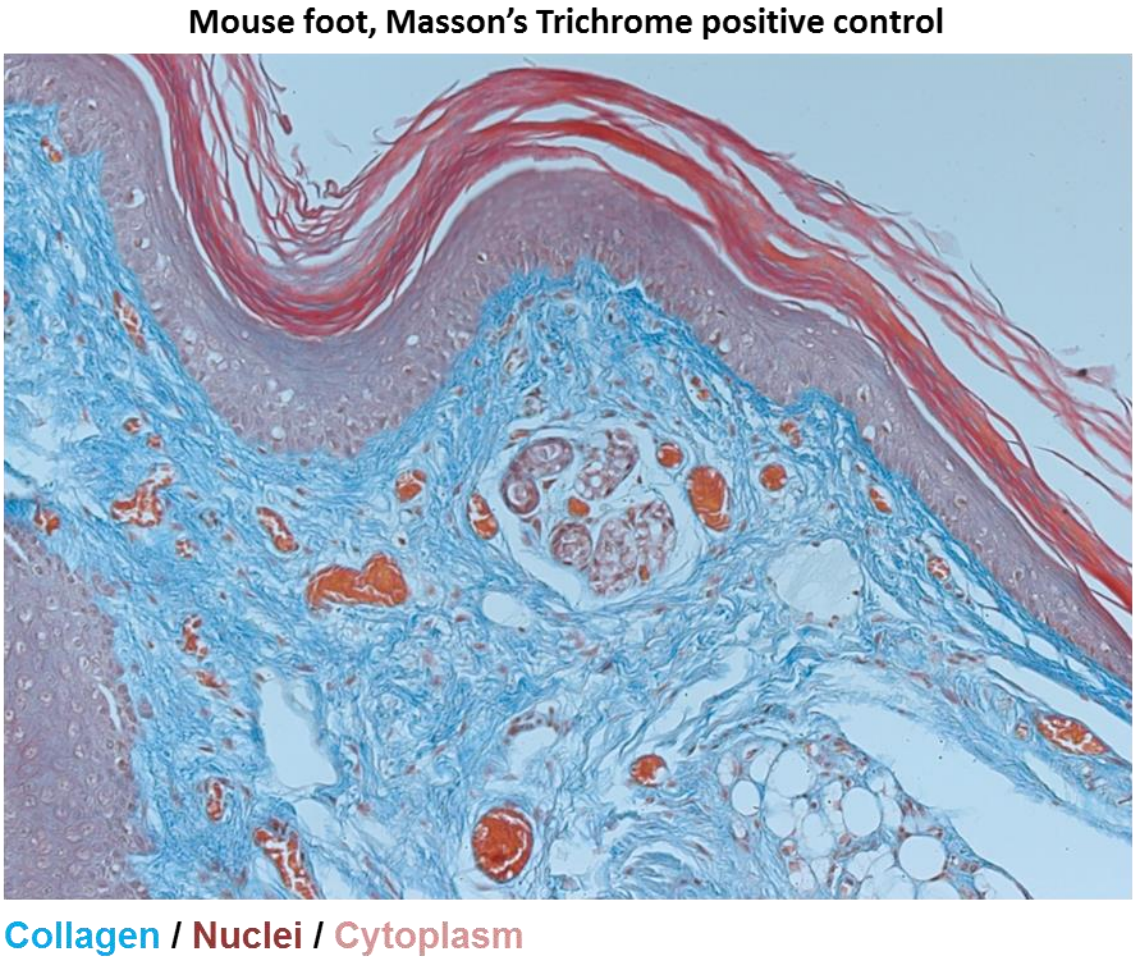


***Appendix 9: Masson's Trichrome positive control***

A mouse foot was fixed, embedded in paraffin, sectioned and stained with Masson's Trichrome stain as a positive control. Large areas of fibrillary collagen (blue) can be observed. Cell nuclei (brown/dark purple) and cytoplasm (pink) can also be observed.

# Appendix B: Publications

# Engineering mammary gland in vitro models for cancer diagnostics and therapy (review article)

During the course of the project a review paper was co-written with Dr. Jonathan Campbell from Prof. Christine Watson's laboratory and was published in the journal Molecular Pharmaceutics in 2014 (Campbell et al., 2014a). Below is the abstract outlining the content of the aforementioned review:

Breast cancer is a complex disease with many distinct subtypes being recognized on the basis of histological features and molecular signatures. It is difficult to predict how cancers will respond to therapy, which results in many women receiving unnecessary or inappropriate treatment. Advances in materials science and tissue engineering are leading the development of complex in vitro 3D breast tissue models that will increase our understanding of normal development and tumorigenic mechanisms. Ultimately, platforms that support primary tissue culture could readily be adapted to form high-throughput drug screening tools for personalized medicine. This review will summarize the control of mammary gland phenotype within in vitro 3D environments, in the context of a detailed analysis of mammary gland development and stem and progenitor cell controlled tumorigenesis.

# Tumour cell invasiveness and response to chemotherapeutics in adipocyte invested 3D engineered anisotropic collagen scaffolds (under peer review)

The results from Chapter 5 have been converted into a manuscript that is currently undergoing the peer review process in the journal *Breast Cancer Research*. I am the first author of this manuscript.

# Development of three-dimensional collagen scaffolds with controlled architecture for cell migration studies using breast cancer cell lines

Following collaboration with Dr. Jonathan Campbell, Dr. Anke Husmann, Prof. Ruth Cameron, Prof. Christine Watson and myself, the results of Chapter 4 were published in the journal *Biomaterials* in 2017. Dr. Jonathan Campbell, Dr. Anke Husmann and I contributed equally to the paper and therefore shared co-first authorship. Following this statement is the completed published version of the aforementioned paper.